Technische Universität München

The Entrepreneurial University.

Dissertation in Pharmaceutical Radiochemistry

Novel ^{18}F-labeled Radiopharmaceuticals comprising Silicon-based Fluoride Acceptors

Daniel Di Carlo

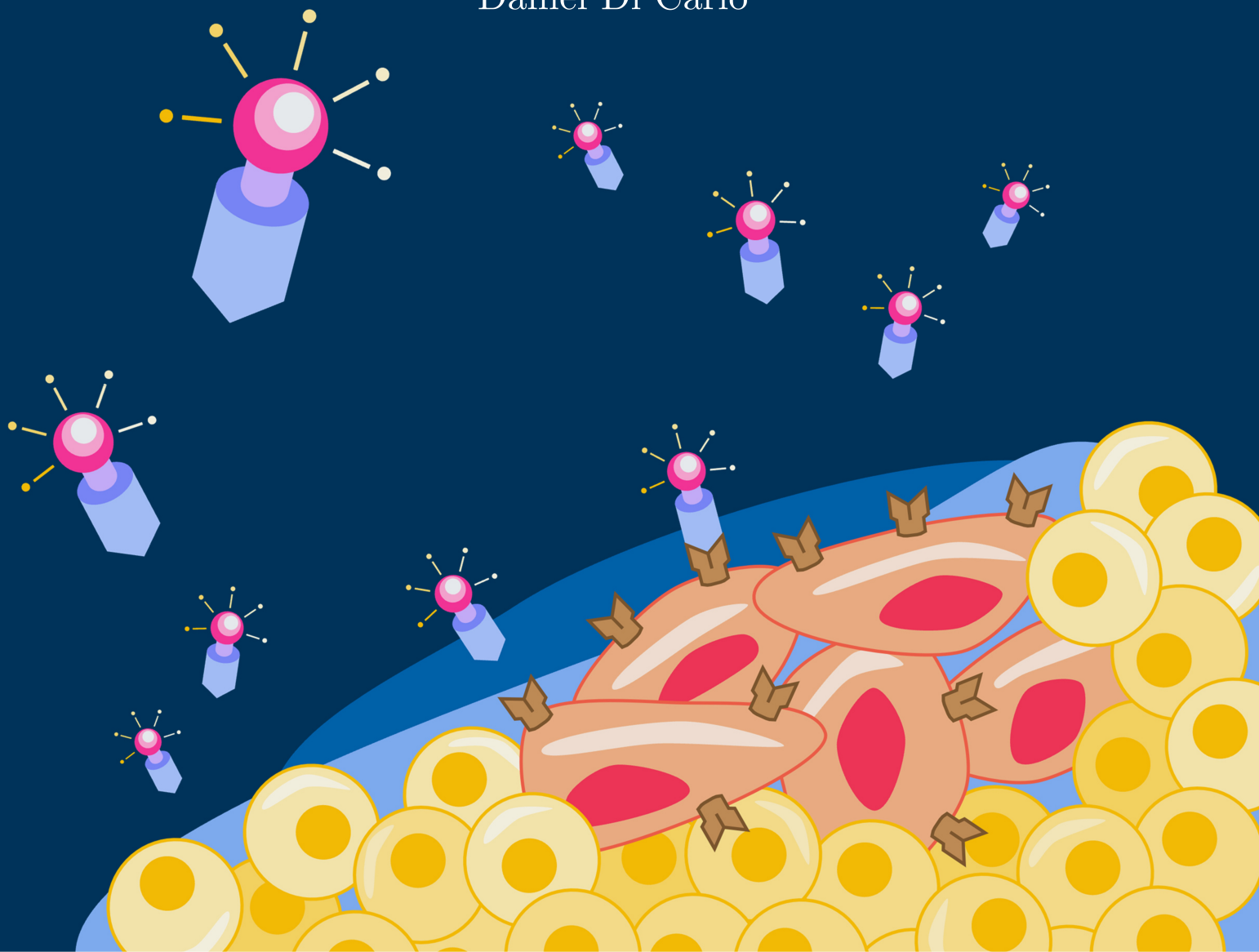

Technische Universität München

TUM School of Natural Sciences

Novel ^{18}F-labeled Radiopharmaceuticals comprising Silicon-based Fluoride Acceptors

Daniel Di Carlo

Vollständiger Abdruck der von der TUM School of Natural Sciences der Technischen Universität München zur Erlangung des akademischen Grades eines

Doktors der Naturwissenschaften (Dr. rer. nat.)

genehmigten Dissertation.

Vorsitz: Prof. Dr. Angela Casini

Prüfer der Dissertation: 1. Priv.-Doz. Dr. Calogero D'Alessandria

2. Prof. Dr. Fritz E. Kühn

Die Dissertation wurde am 04.04.2023 bei der Technischen Universität München eingereicht und durch die TUM School of Natural Sciences am 08.08.2023 angenommen.

Ai Miei Genitori

Alla mia roccia e alla mia luce, che mi hanno insegnato a lottare

e non arrendermi mai di fronte agli imprevisti della vita.

Success is the result of perfection,

hard work, learning from failure,

loyalty, and persistence.

Colin Powell

Abstract

Background: Recently established radiofluorination techniques with simplified labeling chemistry have initiated a new era in the development of ^{18}F-labeled radiotracers and aim to unlock the true potential of high-resolution PET imaging. Among these, radiofluorination by means of Silicon-based Fluoride Acceptors has gained considerable prominence due to its rapid, scalable, and highly efficient incorporation of [^{18}F]fluoride *via* isotopic exchange reaction. However, a major drawback of this approach lies in the inherent lipophilicity of the labeling unit.

Objectives: A first aim of this doctoral thesis was to investigate the ^{18}F-for-^{19}F isotopic exchange with respect to the *Arrhenius parameters* and to further optimize the incorporation reaction by developing an alternative [^{18}F]fluoride preparation procedure. Encouraged by the exceptional radiofluorination performance, a series of ^{18}F-labeled prostate-specific membrane antigen- (PSMA-) and folate receptor- (FR-)targeting ligands exploiting the Silicon-based Fluoride Acceptor technology were developed. As a key component, a pharmacokinetic modifier (PKM) was introduced into the novel radiotracers to counterbalance and fine-tune the elevated lipophilicity induced by the labeling moiety.

Methods: *Arrhenius parameters* were determined *via* kinetic measurements on *N*-benzyl-4-(di-*tert*-butylfluorosilyl)benzamide (**VI**) employing partially neutralized [^{18}F]fluoride obtained by the *Munich Method*. In an optimized alternative preparation procedure (*SiFA-tailored Method*), [^{18}F]fluoride was generated through on-cartridge drying with anhyd. DMSO and subsequent recovery using a solution (1.27 M, 500 µL, 634 µmol) of NH_4HCOO in DMSO. Radiosynthesis on the laboratory scale of novel Silicon-based Fluoride Acceptor-bearing ligands was conducted with [^{18}F]fluoride produced according to both methods, followed by radiotracer purification *via* SPE. Upon preparation by SPPS, newly developed ligands were characterized with respect to their lipophilicity ($\log D_{7.4}$) and HSA binding. For PSMA-targeting inhibitors (siPSMA ligands), *in vitro* properties (IC_{50}, internalization) were determined on LNCaP cells, whereas the *in vivo* performance (biodistribution) was evaluated on LNCaP tumor-bearing CB17-SCID male mice. In the case of FR-targeting compounds (^{nat}Lu-rhFolate ligands), *in*

vitro experiments (IC_{50}) were conducted on KB cells, while the *in vivo* assessment was carried out on KB tumor-bearing CD1-Foxn1^{nu} (biodistribution, µPET/CT imaging) and CB17-SCID (metabolite analysis) female mice. Beyond preclinical testing, [^{18}F]siPSMA-**14** was produced following an established automated synthesis procedure and evaluated in prostate cancer patients.

Results: Based on the constructed *Arrhenius plot*, an activation energy of 46.7 ± 5.7 kJ/mol was calculated for the isotopic exchange reaction on model compound **VI**. This value was found to be considerably lower in direct comparison with the activation energy barriers for conventional radiofluorination reactions relying on carbon-[^{18}F]fluorine bond formation (72–117 kJ/mol).

Further optimization of the labeling reaction with Silicon-based Fluoride Acceptors was achieved through the use of [^{18}F]fluoride generated by the *SiFA-tailored Method*. In this context, the dried activity was efficiently eluted (88 ± 2%, $n = 75$) from the strong anion exchanger and found to be immediately applicable for radiofluorination. By virtue of the mild elution cocktail composition, the recovered eluate turned out to be compatible with base-sensitive precursors as well as with elevated reaction temperatures.

The labeling precursors of novel PSMA ligands were synthesized in high purity (≥95%) and overall yields of 7–59%. Laboratory-scale radiofluorination and formulation was accomplished in 25 min under different labeling conditions (30 nmol, 5 min, rt, or 0.5 nmol, 5–8 min, 65–70°C), leading to [^{18}F]siPSMA ligands with high RCYs (50 ± 15%, $n = 46$) or elevated A_ms (37 ± 12 GBq/µmol, $n = 36$), respectively. The new inhibitors siPSMA-**01** to -**24** revealed variable lipophilicity ($\log D_{7.4} = -4.04$ to -2.30), high PSMA-binding affinity ($IC_{50} = 5.5$–29.4 nM), internalization rates up to 312% of HO-L-Glu-urea-L-Lys(4-[^{125}I]iodobenzoic acid)-OH (**XXV**), and pronounced HSA binding (≥95.7%). Among all candidates, [^{18}F]siPSMA-**14** stood out in biodistribution studies at 1 h p.i., showing excellent tumor uptake (14.30 ± 5.11 %ID/g), low retention in non-target tissue, and a favorable pharmacokinetic profile owing to its convenient lipophilicity ($\log D_{7.4} = -3.28 \pm 0.03$). These promising characteristics were confirmed in first-in-human applications, which have demonstrated the efficacy of [^{18}F]siPSMA-**14** in staging and restaging of prostate cancer. In a dedicated large-scale production ($n = 48$),

starting with 25 ± 4 GBq of [^{18}F]fluoride and 150 nmol of precursor, the novel ligand was prepared with both excellent RCYs (52 ± 16%) and A_ms (87 ± 27 GBq/µmol) in approx. 16 min.

Labeling precursors of new FR ligands were prepared in high purity (≥94%) and acceptable yields (3–10%). Subsequent manual radiofluorination (30 nmol, 10 min, 95°C) resulted in [^{18}F]^{nat}Lu-rhFolate-**01** to -**05** with outstanding RCYs (57 ± 8%, $n = 8$) in about 30 min. Permutation of the PKM within the novel ligands had a major impact on the lipophilicity ($\log D_{7.4}$ = –3.58 to –2.11) and HSA binding (64.7–98.5%). All ^{nat}Lu-rhFolate ligands evidenced high FR-binding affinity (IC_{50} = 10.2–33.1 nM), which was measured according to a newly developed assay using pteroyl-L-Glu(3-[^{125}I]iodo-L-Tyr-OH)-OH (**XXVI**) as a reference. In biodistribution studies at 1 h p.i., [^{18}F]^{nat}Lu-rhFolate-**03** emerged as the most promising candidate due to its good tumor uptake (6.85 ± 0.98 %ID/g) and convenient *in vivo* profile. The FR ligand displayed some metabolic instability in blood and liver samples, but proved to be stable in kidney and urine probes.

Conclusion: The efficient radiofluorination of Silicon-based Fluoride Acceptors *via* isotopic exchange reaction, which was confirmed to be driven by its low activation energy, was further optimized by the novel [^{18}F]fluoride preparation technique following the *SiFA-tailored Method*. Moreover, the introduction of a PKM to adjust the lipophilicity and pharmacokinetic profile of Silicon-based Fluoride Acceptor-bearing compounds proved to be a valuable strategy for tracer modulation, as convincingly illustrated by the promising ligands [^{18}F]siPSMA-**14** and [^{18}F]^{nat}Lu-rhFolate-**03**.

Zusammenfassung

Hintergrund: Die jüngst etablierten Radiofluorierungsverfahren mit vereinfachter Markierungschemie haben eine neue Ära in der Entwicklung ^{18}F-markierter Radiotracer eingeleitet und zielen darauf ab, das volle Potenzial der hochauflösenden PET-Bildgebung zu entfesseln. Unter diesen hat die Radiofluorierung mittels Silicium-basierter Fluoridakzeptoren aufgrund ihrer schnellen, skalierbaren und hocheffizienten Inkorporation von [^{18}F]Fluorid über eine Isotopenaustauschreaktion erhebliche Beachtung gefunden. Ein wesentlicher Nachteil dieses Ansatzes besteht jedoch in der inhärenten Lipophilie der Markierungseinheit.

Ziele: Ein erstes Anliegen dieser Dissertation war die Untersuchung des ^{18}F-für-^{19}F-Isotopenaustauschs hinsichtlich der *Arrhenius-Parameter* sowie die weitere Optimierung der Inkorporationsreaktion durch Erarbeitung eines alternativen Verfahrens zur Präparation von [^{18}F]Fluorid. In Anbetracht der herausragenden Radiofluorierungsergebnisse wurden eine Serie von ^{18}F-markierten Prostataspezifischen Membranantigen- (PSMA-) und Folatrezeptor- (FR-)gerichteten Liganden unter Verwendung Silicium-basierter Fluoridakzeptoren entwickelt. Als Schlüsselkomponente kam in den neuen Radiotracern ein pharmakokinetischer Modifier (PKM) zum Einsatz, um die durch die Markierungseinheit hervorgerufene erhöhte Lipophilie zu kompensieren und präzise einzustellen.

Methoden: Die *Arrhenius-Parameter* wurden durch kinetische Messungen an *N*-Benzyl-4-(di-*tert*-butylfluorsilyl)benzamid (**VI**) unter Verwendung von partiell neutralisiertem [^{18}F]Fluorid nach der *Munich Method* bestimmt. In einem optimierten, alternativen Präparationsverfahren (*SiFA-tailored Method*) wurde [^{18}F]Fluorid über Kartuschen-basierte Trocknung mit wasserfreiem DMSO und anschließender Rückgewinnung unter Verwendung einer Lösung (1.27 M, 500 µL, 634 µmol) aus NH_4HCOO in DMSO erhalten. Die Radiosynthese neuartiger Silicium-basierter Fluoridakzeptor-tragender Liganden im Labormaßstab erfolgte mit [^{18}F]Fluorid, welches gemäß beider Methoden generiert wurde, gefolgt von einer Aufreinigung der Radiotracer mittels Festphasenextraktion. Die neu entwickelten Liganden wurden über Festphasenpeptidsynthese hergestellt und hinsichtlich ihrer Lipophilie ($\log D_{7.4}$) und HSA-Bindung charakterisiert. Für PSMA-gerichtete Inhibitoren (siPSMA-Liganden) wurden die *In-vitro-*

Parameter (IC_{50}, Internalisierung) an LNCaP-Zellen bestimmt, während das *In-vivo*-Verhalten (Biodistribution) in männlichen LNCaP-Tumor-tragenden CB17-SCID-Mäusen untersucht wurde. Im Falle der FR-gerichteten Verbindungen (^{nat}Lu-rhFolate-Liganden) wurden die *In-vitro*-Experimente (IC_{50}) an KB-Zellen durchgeführt, während die *In-vivo*-Evaluierung in weiblichen KB-Tumor-tragenden CD1-Foxn1^{nu}- (Biodistribution, µPET/CT-Bildgebung) und CB17-SCID-Mäusen (Metabolitenanalyse) vorgenommen wurde. Über die präklinische Untersuchung hinaus wurde [^{18}F]siPSMA-**14** nach einem etablierten, automatisierten Syntheseverfahren produziert und an Patienten mit Prostatakrebs untersucht.

Ergebnisse: Auf Grundlage des konstruierten *Arrhenius-Plots* wurde eine Aktivierungsenergie von 46.7 ± 5.7 kJ/mol für die Isotopenaustauschreaktion an Modellverbindung **VI** ermittelt. Im direkten Vergleich mit den Aktivierungsbarrieren konventioneller Radiofluorierungsreaktionen, welche auf einer Kohlenstoff-[^{18}F]Fluor-Bindungsbildung beruhen (72–117 kJ/mol), erwies sich dieser Wert als deutlich niedriger.

Eine weitere Optimierung der Markierungsreaktion Silicium-basierter Fluoridakzeptoren ließ sich durch Verwendung von [^{18}F]Fluorid erreichen, das mit der *SiFA-tailored Method* erzeugt wurde. In diesem Zusammenhang konnte die getrocknete Aktivität mit hoher Effizienz (88 ± 2%, $n = 75$) vom starken Anionenaustauscher eluiert und ohne weitere Zusätze für die Radiofluorierung genutzt werden. Dank der milden Zusammensetzung des Elutionscocktails zeigte sich das erhaltene Eluat sowohl mit basenempfindlichen Präkursoren als auch mit erhöhten Reaktionstemperaturen kompatibel.

Die Markierungsvorläufer der neuen PSMA-Liganden wurden in hoher Reinheit (≥95%) und mit Gesamtausbeuten von 7–59% synthetisiert. Die Radiofluorierung und Formulierung im Labormaßstab erfolgte innerhalb von 25 min unter verschiedenen Markierungsbedingungen (30 nmol, 5 min, Raumtemperatur oder 0.5 nmol, 5–8 min, 65–70°C) und führte zu [^{18}F]siPSMA-Liganden mit ausgezeichneten radiochemischen Ausbeuten (50 ± 15%, $n = 46$) bzw. hohen molaren Aktivitäten (37 ± 12 GBq/µmol, $n = 36$). Die neuen Inhibitoren siPSMA-**01** bis -**24** zeichneten sich durch variable Lipophilie ($\log D_{7.4}$ = –4.04 bis –2.30), hohe PSMA-Bindungsaffinität (IC_{50} = 5.5–29.4 nM), Internalisierungsraten von bis zu 312% gegenüber HO-L-Glu-urea-L-Lys(4-[^{125}I]iodbenzoesäure)-OH (**XXV**) und ausgeprägte HSA-Bindung

(≥95.7%) aus. Unter allen Kandidaten überzeugte [^{18}F]siPSMA-**14** in Biodistributionsstudien (1 h p.i.) mit einer hervorragenden Tumoraufnahme (14.30 ± 5.11 %ID/g), einer geringe Retention in Nicht-Zielgewebe und einem günstigen pharmakokinetischen Profil infolge der vorteilhaften Lipophilie ($\log D_{7.4}$ = –3.28 ± 0.03). Diese vielversprechenden Eigenschaften wurden in ersten Anwendungen am Menschen bestätigt, welche die Wirksamkeit von [^{18}F]siPSMA-**14** beim Staging und Restaging von Prostatakrebs gezeigt haben. In einer hierfür etablierten großtechnischen Produktion (n = 48) wurde der neuartige Ligand ausgehend von 25 ± 4 GBq [^{18}F]Fluorid und 150 nmol Präkursor in circa 16 min mit ausgezeichneten radiochemischen Ausbeuten (52 ± 16%) und molaren Aktivitäten (87 ± 27 GBq/µmol) gewonnen.

Die Markierungsvorläufer der neuen FR-Liganden wurden mit hoher Reinheit (≥94%) und akzeptablen Ausbeuten (3–10%) hergestellt. Nachfolgende manuelle Radiofluorierungsexperimente (30 nmol, 10 min, 95°C) führten zu [^{18}F]^{nat}Lu-rhFolate-**01** bis -**05** mit exzellenten radiochemischen Ausbeuten (57 ± 8%, n = 8) in etwa 30 min. Die Permutation des PKM innerhalb der neuen Liganden hatte einen großen Einfluss auf die Lipophilie ($\log D_{7.4}$ = –3.58 bis –2.11) und die HSA-Bindung (64.7–98.5%). Alle ^{nat}Lu-rhFolate-Liganden zeichneten sich durch eine hohe FR-Bindungsaffinität (IC_{50} = 10.2–33.1 nM) aus, die mit einem neu entwickelten Assay unter Verwendung von Pteroyl-L-Glu(3-[^{125}I]iod-L-Tyr-OH)-OH (**XXVI**) als Referenz bestimmt wurde. In Biodistributionsstudien (1 h p.i.) erwies sich [^{18}F]^{nat}Lu-rhFolate-**03** aufgrund guter Tumoraufnahme (6.85 ± 0.98 %ID/g) und eines günstigen *In-vivo*-Profils als der aussichtsreichste Kandidat. Der FR-Ligand zeigte in Blut- und Leberpräparaten eine gewisse metabolische Instabilität auf, stellte sich aber in Nieren- und Urinproben als stabil heraus.

Schlussfolgerung: Die effiziente Radiofluorierung von Silicium-basierten Fluoridakzeptoren mittels Isotopenaustauschreaktion – bedingt durch dessen bestätigte niedrige Aktivierungsenergie – wurde durch das neuartige Verfahren zur Präparation von [^{18}F]Fluorid nach der *SiFA-tailored Method* weiter optimiert. Darüber hinaus erwies sich die Einführung eines PKM zur Anpassung der Lipophilie und des pharmakokinetischen Profils von Silicium-basierten Fluoridakzeptor-tragenden Verbindungen als wertvolle Strategie zur Tracermodulation. Dies konnte durch die vielversprechenden Liganden [^{18}F]siPSMA-**14** und [^{18}F]^{nat}Lu-rhFolate-**03** überzeugend belegt werden.

Acknowledgments

This thesis would never have been possible in its present form without the constant help, support, and guidance of so many great people.

First and foremost, I would like to express all my gratitude to my supervisor, **Prof. Dr. Hans-Jürgen Wester**, for giving me the opportunity to work on a variety of highly interesting research topics in the radiopharmaceutical field. With your immense knowledge and experience, you have inspired my interest, sharpened my thinking, and encouraged me to pursue my own ideas.

Furthermore, I would like to thank **Prof. Dr. Klemens Scheidhauer** for his mentorship and **Prof. Dr. Margret Schottelius** for her numerous scientific advice.

I sincerely thank the Department of Nuclear Medicine at the *University Hospital Ulm* – **Prof. Dr. Ambros Beer**, **Dr. Christoph Solbach**, **Dr. Vikas Prasad**, **Dr. Gabriel Fischer**, **Dr. Jan Wenz**, **Carmen Hamp**, and **Jonathan Miksch** – for their excellent collaboration throughout the first-in-human applications with [^{18}F]siPSMA-**14**.

Huge thanks go to the previous generation of PhD students – **Dr. Alexander Schmidt**, **Dr. Theresa Osl**, **Dr. Andreas Poschenrieder**, **Dr. Stephanie Robu**, and **Dr. Martina Wirtz**. Thank you for everything you have taught me since my first day at the chair as an undergraduate student and for the great time outside the lab. You all truly inspired me to continue my specialization in the field of radiopharmaceutical sciences.

Sincere thanks also go to **Dr. Roswitha Beck** and **Dr. Nicole Urtz-Urban** for their great expertise and generous support during PET and biodistribution studies. Furthermore, I would like to acknowledge our ever-helpful secretary, **Christine Winkler**, for taking care of all administrative matters during my doctorate.

Many thanks to all my PhD colleagues – **Alexander Wurzer**, **Thomas Günther**, **Veronika Felber**, **Markus Fahnauer**, **Jan-Philip Kunert**, **Sebastian Fischer**, **Matthias Konrad**, and **Mara Parzinger** – for the scientific support and the great time we spent together in and outside the lab. I will particularly miss our legendary after-work foosball tournaments. Special

thanks to **Alexander Wurzer**, for the countless advice on radiofluorination and for the incredible experience we shared in California during the *SNMMI 2019 Annual Meeting*. Moreover, I am especially grateful to **Thomas Günther** and **Veronika Felber** for their friendship and will never forget the awesome time we had together during the *ISRS 2019* in Beijing.

Another big thank you goes to **Jana Herbst** and **Tanja Reichhart** for their amazing help in the lab and for the hilarious moments spent together. You have always made my daily routine more fun and enjoyable.

Furthermore, I would like to acknowledge my former students – **Nadine Holzleitner**, **Christian Gawanda**, **Dominik Dankert**, **Sara Dernoscheck**, and **Sebastian Schleser** – for their outstanding experimental support.

I sincerely want to thank **Felix Reiter**, **Thomas Steiner**, **Hanusch Grab**, **Tobias Bruhm**, **Paul Leidinger**, **Carlos Mejuto-Zaera**, **Matthias Konrad**, and **Lukas Ochmann** for supporting me as true friends since the beginning of my chemistry studies.

To my beloved girlfriend **Stefanie Färber**, I am grateful to have her by my side. Thank you for helping me through all the challenges, for pushing me to keep on going, and for always being there for me.

Finally, the biggest thanks go to my family – my sister **Roberta**, my mom **Raffaella**, my dad **Luciano** and my uncle **Pasquale Di Carlo** – who have always made it possible for me to pursue my passions. Thank you for your unconditional love, your endless support, and your constant encouragement. Without you, I would not be the person I am today.

Table of Contents

1 Introduction

1.1 Fluorine-18 in Nuclear Medicine

1.1.1 General Considerations

In the last few decades, positron emission tomography (PET) has become an established diagnostic procedure with constantly increasing relevance in nuclear medicine. This powerful non-invasive imaging modality allows for the precise detection of pathological processes in the human body, like cancer, metabolic disorders, as well as cardiovascular and neurological diseases[1-2]. Under the common PET radionuclides such as carbon-11, nitrogen-13, oxygen-15, copper-64, and gallium-68, fluorine-18 has always attracted major interest, principally due to its facile large-scale production within a cyclotron and the advantageous physical properties[3-4]. Among them, the convenient half-life (109.8 min) stands out for being long enough to allow for the radiosynthesis of even complex radiotracers and their subsequent distribution to smaller centers without an own production facility[1, 3, 5]. Furthermore, the decay of fluorine-18 occurs predominantly by positron emission (97%) with a relatively low average energy (249.8 keV), rendering this isotope an ideal candidate for high-resolution PET imaging[1, 3]. Despite these exceptional characteristics, the rather challenging radiochemistry of fluorine-18 kept being the crucial limitation to its widespread use, whereas ^{68}Ga-labeled radiopharmaceuticals paved the way with their simple kit-based production technologies[6]. However, a variety of exciting new approaches developed in the recent past have initiated the transition to a broader use of radiofluorinated tracers in nuclear medicine[2].

1.1.2 Conventional Radiofluorination Techniques

Conventional radiofluorination methods rely on the formation of carbon-[^{18}F]fluorine bonds. They historically evolved with the intention to introduce the radiolabel under minimal steric perturbation of a lead structure that is engaged in the metabolic pathway or associated to a specific target[2, 5]. For instance, the most prominent PET tracer 2-deoxy-2-[^{18}F]fluoro-D-glucose, used for imaging of abnormal regional glucose consumption (inflammation, cancer, etc.), was originated by isosteric replacement of a hydroxyl group with fluorine-18[2, 4-5]. Radiolabel linkage

to an aliphatic or aromatic carbon atom is usually performed *via* substitution reactions involving either electrophilic [^{18}F]fluorine species or nucleophilic [^{18}F]fluoride[4]. Unfortunately, both methods pose numerous specific challenges.

By the former, a radiofluorinated tracer can only be obtained with limited molar activity (A_m), since the preparation of [^{18}F]fluorine gas always involves fluorine-19 as contaminant in considerable quantities (so-called *carrier-added* condition)[4-5]. This limitation is particularly disadvantageous as it imposes to increase the amount of administered radiotracer, thus augmenting the risk of pharmacodynamic effects[3]. Moreover, the high reactivity of [^{18}F]fluorine gas during electrophilic substitution reactions leads to the formation of undesired radiolabeled by-products, that often require separation by means of complex and time-consuming high-performance liquid chromatography (HPLC)[1].

In contrast, the use of nucleophilic [^{18}F]fluoride for radiofluorination appears to be more convenient. Its production proceeds by proton bombardment of an H_2[^{18}O]O-enriched water target, resulting in high activities of [^{18}F]fluoride under *non-carrier-added* conditions[1-2, 4]. However, this advantageous production strategy comes with a major drawback hampering the immediate application of [^{18}F]fluoride in a subsequent nucleophilic substitution reaction. Due to the high charge density, a hydrate shell is instantly formed around the [^{18}F]fluoride ion in the aforementioned aqueous (aq.) production environment, which considerably reduces its nucleophilicity and thus reactivity[5]. Therefore, the [^{18}F]fluoride-containing solution has to be reformulated prior to the labeling reaction[5]. This is usually accomplished through laborious repetitive azeotropic distillation involving the use of (i) anhydrous (anhyd.) acetonitrile (MeCN), (ii) a base that avoids the formation of volatile H[^{18}F]F (e.g. K_2CO_3, $KHCO_3$, or $K_2C_2O_4$), and (iii) a phase transfer catalyst that ensures high solubility of [^{18}F]fluoride as counterion in the solvent to be used (e.g. Kryptofix® 222)[2, 4]. Once dried, the "naked" [^{18}F]fluoride is typically redissolved in a dipolar aprotic solvent such as MeCN, dimethyl sulfoxide (DMSO), or *N*,*N*-dimethylformamide (DMF)[2, 4]. Furthermore, in order to achieve a high radiochemical yield (RCY), any substrate intended to be radiofluorinated needs to dispose of a good leaving group (e.g. halides, sulfonate esters, trimethylammonium or nitro groups)[4]. The ^{18}F-labeling reaction itself often has to be carried out at elevated temperatures to promote

the nucleophilic substitution[4]. In most cases, however, these sophisticated conditions imply the formation of unwanted side-products, making complex radiotracer purification procedures inevitable[4]. Radiofluorination with [^{18}F]fluoride *via* nucleophilic substitution becomes even more cumbersome when peptidic precursors rather than small molecules are sought to be labeled[2]. Since these compounds are not compatible with the harsh reaction conditions described above, corresponding radiofluorinated tracers can only be obtained through the use of prosthetic groups in arduous multi-step reaction sequences[2]. All these shortcomings of conventional radiofluorination methods highlight the necessity of finding new approaches to exploit the full potential of ^{18}F-labeled radiopharmaceuticals (*Figure 1*)[7-8].

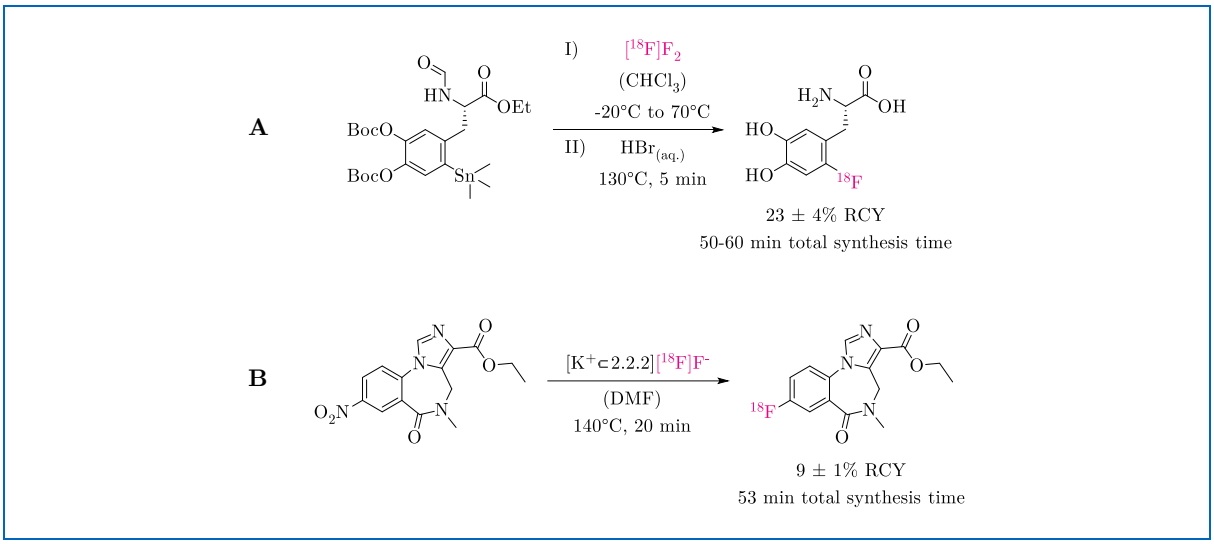

Figure 1. Radiofluorination *via* conventional carbon-[^{18}F]fluorine bond formation exemplified by the **A**) automated radiosynthesis of 6-[^{18}F]fluoro-L-3,4-dihydroxyphenylalanine using electrophilic [^{18}F]fluorine and the **B**) automated radiosynthesis of [^{18}F]flumazenil employing azeotropically dried [^{18}F]fluoride[7-8].

1.1.3 Novel Radiofluorination Techniques

In recent decades, research has focused on the development of novel radiofluorination techniques to overcome the constraints of conventional carbon-[^{18}F]fluorine chemistry. Special interest has been devoted to the elements of group 13 (boron, aluminum) and group 14 (silicon), due to their strong bond formation with fluorine, as evidenced by the particularly high dissociation energies[9].

The idea of using boron as a reaction center to bind fluorine-18 was proposed about 60 years ago with the investigation of [^{18}F]tetrafluoroborate as a potential PET tracer for the detection

of intracranial tumors[10]. However, this approach did not receive notable attention until 2005, when *Perrin* and colleagues surprisingly reported that a biotinylated aryl[^{18}F]trifluoroborate had been generated with high efficiency by nucleophilic substitution under aq. conditions[11]. After significantly improving the hydrolytic stability of the boron-[^{18}F]fluorine bond by integrating electron-withdrawing substituents, the applicability of optimized aryl[^{18}F]trifluoroborate functionalities was successfully demonstrated with the development of several radiofluorinated tracers targeting matrix metalloproteinases, the gastrin-releasing peptide receptor (GRPR), or integrins[12-16]. The potential of ^{18}F-labeled organotrifluoroborates was further amplified upon recognizing that radiofluorination could be accomplished by simple isotopic exchange reaction[17]. In the presence of a pyridazine-HCl buffered mixture (pH 2), low nanomolar amounts of precursors were efficiently labeled (45°C, 20 min) to yield the corresponding radiotracers with impressively high RCYs and A_ms[18-19]. However, time-consuming HPLC purification of the final products proved to be indispensable, since aryltrifluoroborates tend to form the respective boronic esters due to their susceptibility towards hydrolysis[18-19]. Aiming to overcome this limitation, *Perrin* and co-workers designed a zwitterionic *N,N*-dimethyl-ammoniomethyltrifluoroborate ($AMBF_3$) moiety with high hydrolytic stability[20]. As a result, the purification effort for the corresponding radiofluorinated tracers was simplified to solid-phase extraction (SPE), since only unincorporated [^{18}F]fluoride required separation as interfering component[20-21]. These characteristics combined with the efficient labeling capability, made the $AMBF_3$ group become the organotrifluoroborate of choice for this new radiofluorination method[22]. Moreover, the moiety revealed to be particularly useful for the two-step radiofluorination of sensitive biomolecules that are incompatible with the general labeling conditions imposing acidic pH and elevated temperatures[23]. For the most promising radiotracer in this regard, namely the somatostatin receptor (SSTR) ligand [^{18}F]$AMBF_3$-TATE, an automated synthesis procedure was recently established (*Figure 2*)[24]. Based on the encouraging results observed in first-in-human applications, high hopes are pinned on this novel SSTR ligand and the entire organotrifluoroborate radiofluorination technology[25].

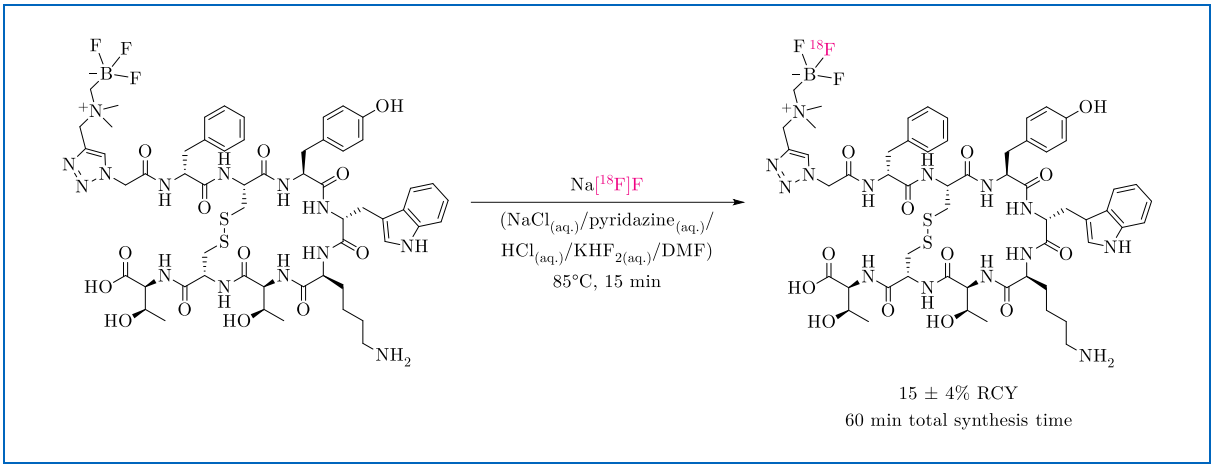

Figure 2. Radiofluorination *via* the organotrifluoroborate approach exemplified by the automated radiosynthesis of [^{18}F]AMBF$_3$-TATE[24].

A further promising method for the introduction of fluorine-18 into organic compounds relies on the usage of aluminum, the next homologous element to boron in group 13. This radiofluorination strategy was first reported by *McBride et al.* in 2009 and combines the advantages of metal-based radiochemistry along with the exceptional radionuclide properties of fluorine-18[26]. Accordingly, the labeling reaction proceeds by a two-step one-pot process involving the formation of an [Al[^{18}F]F]$^{2+}$-complex and its subsequent chelation[26-28]. Considerable efforts were devoted to the development of appropriate chelators for stable and efficient complexation of the [Al[^{18}F]F]$^{2+}$-species, since widely-used agents such as ethylenediaminetetraacetic acid (EDTA), diethylenetriaminepentaacetic acid (DTPA), and 1,4,7,10-tetraazacyclododecane-1,4,7,10-tetraacetic acid (DOTA) turned out to be unsuitable[26]. The breakthrough came with the finding that 1,4,7-triazacyclononane-1,4,7-triacetic acid (NOTA) and 1,4,7-triazacyclononane-1,4-diacetic acid (NODA) derivatives efficiently form stable [Al[^{18}F]F]$^{2+}$-complexes upon heating by means of their pentadentate N_3O_2 configuration[29-31]. This prompted *McBride* and colleagues to develop a lyophilized formulation for a simple, kit-like labeling procedure[32]. Based on their protocol, nanomolar amounts of the chelator-conjugated compound, $AlCl_3$, and a buffering agent were mixed with aq. [^{18}F]fluoride and reacted at elevated temperatures (pH ~4, 100–110°C, 15 min)[32]. Subsequent radiotracer workup was performed analogously to ^{68}Ga-labeled radiopharmaceuticals *via* SPE, since unbound [Al[^{18}F]F]$^{2+}$ constitutes the only undesired species that has to be separated from the reaction mixture[32]. Owing to the rapid, facile, and efficient ^{18}F-labeling by [Al[^{18}F]F]$^{2+}$-

chelation, corresponding radiofluorinated compounds were obtained with generally good RCYs and high A_ms (*Figure 3*)[32-33].

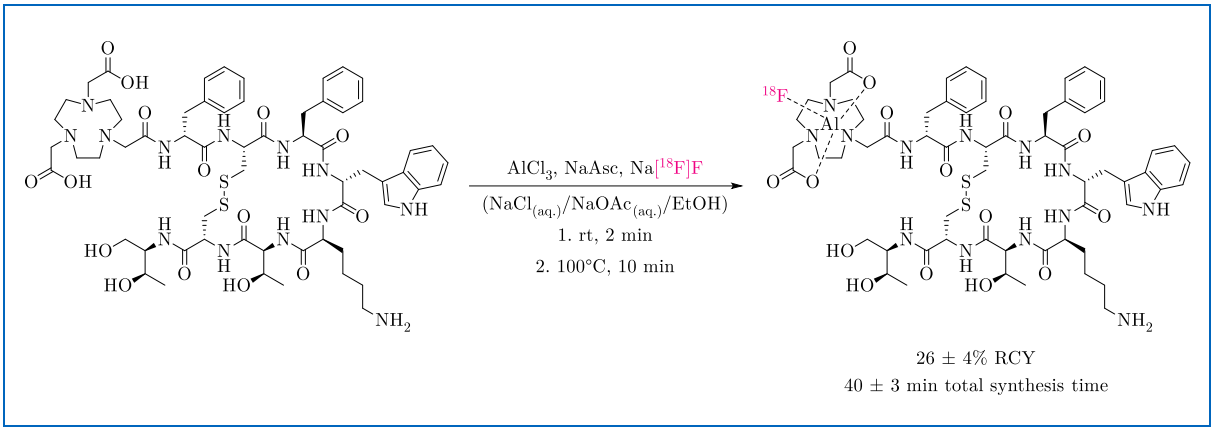

Figure 3. Radiofluorination *via* $[Al[^{18}F]F]^{2+}$-complexation exemplified by the automated radiosynthesis of $[^{18}F]$AlF-NOTA-octreotide[33].

However, broad applicability of this labeling strategy is restricted by the required reaction temperatures, which hinder the direct radiofluorination of heat-sensitive biomolecules[34-36]. Further investigations have therefore aimed at developing novel chelating agents capable of incorporating $[Al[^{18}F]F]^{2+}$ at significantly lower temperatures[34-36]. The great expectations placed on this novel radiofluorination technique are reflected by the large number of related radiofluorinated tracers developed to date[28, 37-40]. Some of these candidates have even been evaluated in first proof-of-concept studies in patients or are subject to ongoing clinical trials[41-44].

Last but not least, the use of silicon for binding fluorine-18 in radiotracers has witnessed an impressive development over the past 15 years, advancing from an unconventional idea to a well-established labeling approach in ^{18}F-radiochemistry[45]. Due to its great potential, radiofluorination by means of Silicon-based Fluoride Acceptors was chosen for the development of novel ^{18}F-labeled radiopharmaceuticals summarized in the present doctoral thesis. In this context, a detailed introduction is provided in the next chapter (*Section 1.2*), covering the historical background, labeling principles, limitations, and clinical relevance of this promising radiofluorination strategy.

1.2 Silicon-based Fluoride Acceptors

1.2.1 Early Development

Although exhibiting a rather high dissociation energy (540 kJ/mol), the silicon-fluorine bond is characterized by particularly strong polarization[9]. This circumstance implies a high susceptibility towards hydrolysis and has posed a long-standing challenge in the development of *in vivo* stable radiopharmaceuticals[46]. As a result, only few studies related to radiofluorinated silicon compounds were published in the past century[47-49]. In 1958, *Gens et al.* described that SiF_4 rapidly incorporates [^{18}F]fluoride by isotopic exchange reaction when passed over ^{18}F-enriched LiF, and hypothesized a potential future application[47]. Decades later, in 1985, *Rosenthal* and co-workers reported preparation of the first radiofluorinated organosilicon compound[48]. The group successfully synthesized [^{18}F]fluorotrimethylsilane with 80% RCY by substitution reaction on chlorotrimethylsilane with *non-carrier-added* tetramethylammonium [^{18}F]fluoride[48]. However, subsequent biodistribution experiments in rats evidenced the *in vivo* instability of this simple organosilane, leading the authors to speculate that compounds with higher steric hindrance would be less prone to hydrolysis[48]. Nevertheless, the researchers took advantage of the observed hydrolytic degradation of [^{18}F]fluorotrimethylsilane and developed a thereupon based preparation protocol for highly nucleophilic tetraethylammonium [^{18}F]fluoride[49]. More than 20 years later, *Ting et al.* demonstrated the rapid and efficient radiofluorination of a biotinylated alkyltriethoxysilane to the respective [^{18}F]tetrafluorosilicate salt, which proceeded under mild reaction conditions[11]. Unfortunately, the ^{18}F-labeled biotin conjugate turned out to decompose in aq. solvents and thus to be unsuitable for *in vivo* application[11]. The breakthrough finally came in 2006, when two research groups independently published the preparation of sufficiently stable radiofluorinated organosilicon compounds[46, 50].

1.2.2 Labeling Principles

Important pioneering work was accomplished by *Schirrmacher* and colleagues, who reported the highly efficient radiosynthesis of di-*tert*-butylphenyl[^{18}F]fluorosilane by means of isotopic exchange reaction[46]. Since this model compound proved to be stable under physiological conditions, the research group developed 4-(di-*tert*-butylfluorosilyl)benzaldehyde as a broadly applicable prosthetic moiety for ligation to aminooxy-derivatized compounds[46]. An exemplary synthesized Tyr^3-octreotate derivative was successfully radiofluorinated (55–65% RCY) in a single step with azeotropically dried [K^+⊂2.2.2][^{18}F]F^- under mild reaction conditions (room temperature (rt), 10–15 min)[46]. Although only low A_ms (3–5 GBq/µmol) were obtained for the resulting ^{18}F-labeled SSTR ligand, the group firmly believed in the potential of organosilicon radiolabeling by the isotopic exchange methodology[46]. In parallel, *Choudhry et al.* presented a study hypothesizing that *tert*-butyldiphenyl[^{18}F]fluorosilane might exhibit reasonable stability for *in vivo* application[50]. Notably, rapid and high-yielding radiosynthesis of this model compound had been achieved *via* bimolecular nucleophilic substitution (S_N2) on the corresponding alkoxytrialkylsilane precursor using [K^+⊂2.2.2][^{18}F]F^- without prior drying[51]. Based on this more conventional ^{18}F-labeling approach, organosilicons with further leaving groups including ethoxy, hydroxyl, and hydride were subsequently investigated by *Höhne*, *Mu*, and co-workers[52-53]. In contrast to the initial finding, it became evident that such displacement reactions required azeotropically dried [K^+⊂2.2.2][^{18}F]F^- as well as elevated temperatures to proceed with high efficiency[52-53]. Moreover, time-consuming purification by HPLC was found to be mandatory in order to separate the micromolar amounts of precursor and undesired by-products from the final radiotracer[52]. Concurrently, *Schirrmacher et al.* surprisingly reported that the A_ms of 4-(di-*tert*-butyl[^{18}F]fluorosilyl)benzaldehyde prepared *via* isotopic exchange reaction could be increased to 225–680 GBq/µmol by reducing the amount of precursor to a nanomolar scale[54]. This finding represented a game changer in ^{18}F-radiochemistry, as it demonstrated – contrary to the prevailing assumption – that competitive A_ms were obtainable through simple ^{18}F-for-^{19}F exchange[54]. An explanation for the unexpectedly high efficiency was identified in the rapid formation of the penta-coordinated siliconate intermediate and its instant dissociation[54]. This exchange appears to be statistically irreversible, as the concentrations of

liberated [^{19}F]fluoride and organo[^{18}F]fluorosilane are orders of magnitude lower than those of the non-radioactive precursor, thus hindering the reverse reaction (*Figure 4*)[54].

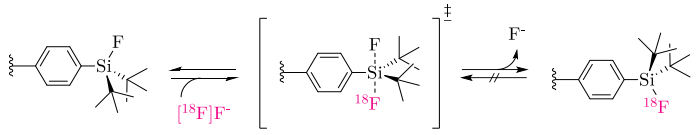

Figure 4. Radiofluorination of an organofluorosilane moiety *via* isotopic exchange reaction involving the formation of a penta-coordinated siliconate transition state[54-55]. Thereby, the reverse reaction is statistically disfavored[55].

1.2.3 Hydrolytic Stability

Thrilled by the potential of this new radiofluorination method, extensive investigations were undertaken to elucidate the stability-determining aspects in organofluorosilanes, also referred to as Silicon-based Fluoride Acceptors. In their first report, *Schirrmacher et al.* had already highlighted that both triphenyl[^{18}F]fluorosilane and *tert*-butyldiphenyl[^{18}F]fluorosilane are prone to hydrolysis under physiological conditions[46]. As shown with di-*tert*-butylphenyl-[^{18}F]fluorosilane, the presence of two *tert*-butyl groups surrounding the silicon atom proved to be crucial for ensuring sufficient stability *in vivo*[46]. Subsequent in-depth studies by several research groups confirmed a correlation between the hydrolytic half-life of organofluorosilanes and the degree of steric hindrance around the silicon-fluorine bond (*Figure 5*), as previously suspected by *Rosenthal et al.* back in 1985[48, 56-60].

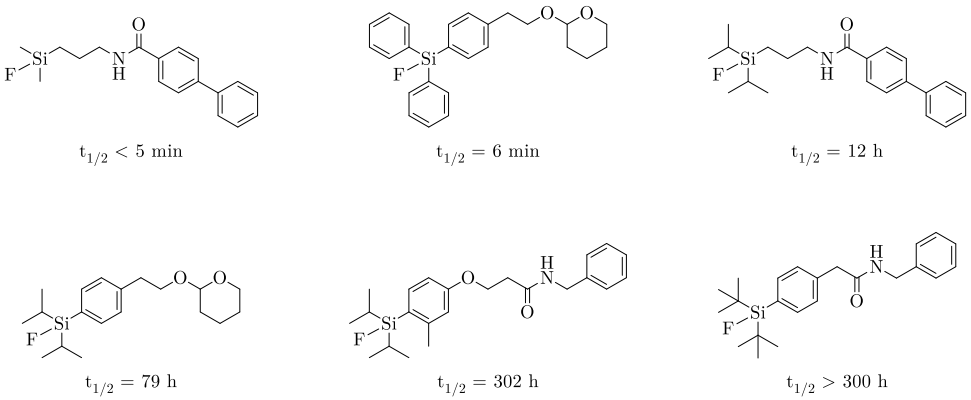

Figure 5. Hydrolytic half-lives ($t_{1/2}$) of selected Silicon-based Fluoride Acceptor model compounds determined in a mixture (2:1, *v/v*, pH 7) of MeCN/water at rt[56].

Indeed, during the development of radiofluorinated nitroimidazole derivatives, it was observed that the structurally less demanding dimethyl-, diphenyl- and di-*iso*propyl-substituted alkylfluorosilanes were highly susceptible to hydrolysis[57]. The introduction of bulkier dinaphtyl substituents decreased the defluorination tendency, although not to an extent suitable for *in vivo* application[57, 59]. Improved shielding of the silicon-fluorine bond was reported in the case of dialkylphenylfluorosilanes, especially for the di-*iso*propyl- and di-*tert*-butyl-bearing compounds[56]. Notably, the hydrolytic half-lives of such Silicon-based Fluoride Acceptors could be prolonged even further by the introduction of *ortho*-methyl-substituted phenyl groups[56]. Since the di-*tert*-butylphenylfluorosilane moiety emerged to satisfactorily meet the stability requirements for use in PET tracers, a variety of *para*-functionalized building blocks were developed[46]. These included, on the one hand, aldehyde, thiol, tetrazine, and isothiocyanate derivatives, which were intended as prosthetic groups for the two-step radiofluorination of complex biomolecules[54, 61-64]. On the other hand, carboxyl-, active ester-, azide-, alkyne-, maleimide-, and even amino acid-functionalized di-*tert*-butylphenylfluorosilanes were designed for the synthesis of precursor ligands to be directly radiolabeled in a single step[65-70].

1.2.4 Lipophilicity Issue

A major shortcoming of Silicon-based Fluoride Acceptors resides in their inherently pronounced lipophilicity, which results from the sterically demanding residues required for sufficient *in vivo* stabilization of the silicon-[^{18}F]fluorine bond[71]. Unfortunately, this characteristic has significant implications on the overall pharmacokinetics of corresponding radiotracers, as reported during the development of early Silicon-based Fluoride Acceptor-bearing ligands targeting the SSTR and GRPR[52, 71]. These first ^{18}F-labeled compounds suffered from low tumor uptake, high unspecific binding, and substantial accumulation in organs of the hepatobiliary system[52, 71]. The reason for this observation was ascribed to the first-pass effect, meaning an accumulation and metabolization of the highly lipophilic radiotracer during its first passage through the liver[55]. Under such conditions, the radiolabeled compound is rapidly cleared from the blood pool and becomes no longer available for addressing the target tissue[55]. To overcome this problem, the research groups of *Schirrmacher*, *Wängler,* and *Wester* pursued the strategy of incorporating hydrophilic building blocks in close proximity to the Silicon-based Fluoride

Acceptor moiety[71-77]. In this context, poly(ethylene glycol) (PEG) linkers, carbohydrate moieties, amino acids, metal chelates, and permanent charges were considered in ligand design to compensate for the lipophilic nature of the labeling unit[71-77]. The utility of this kind of approach was impressively demonstrated during the development of novel radiofluorinated SSTR ligands (*Figure 6*)[71, 73-74].

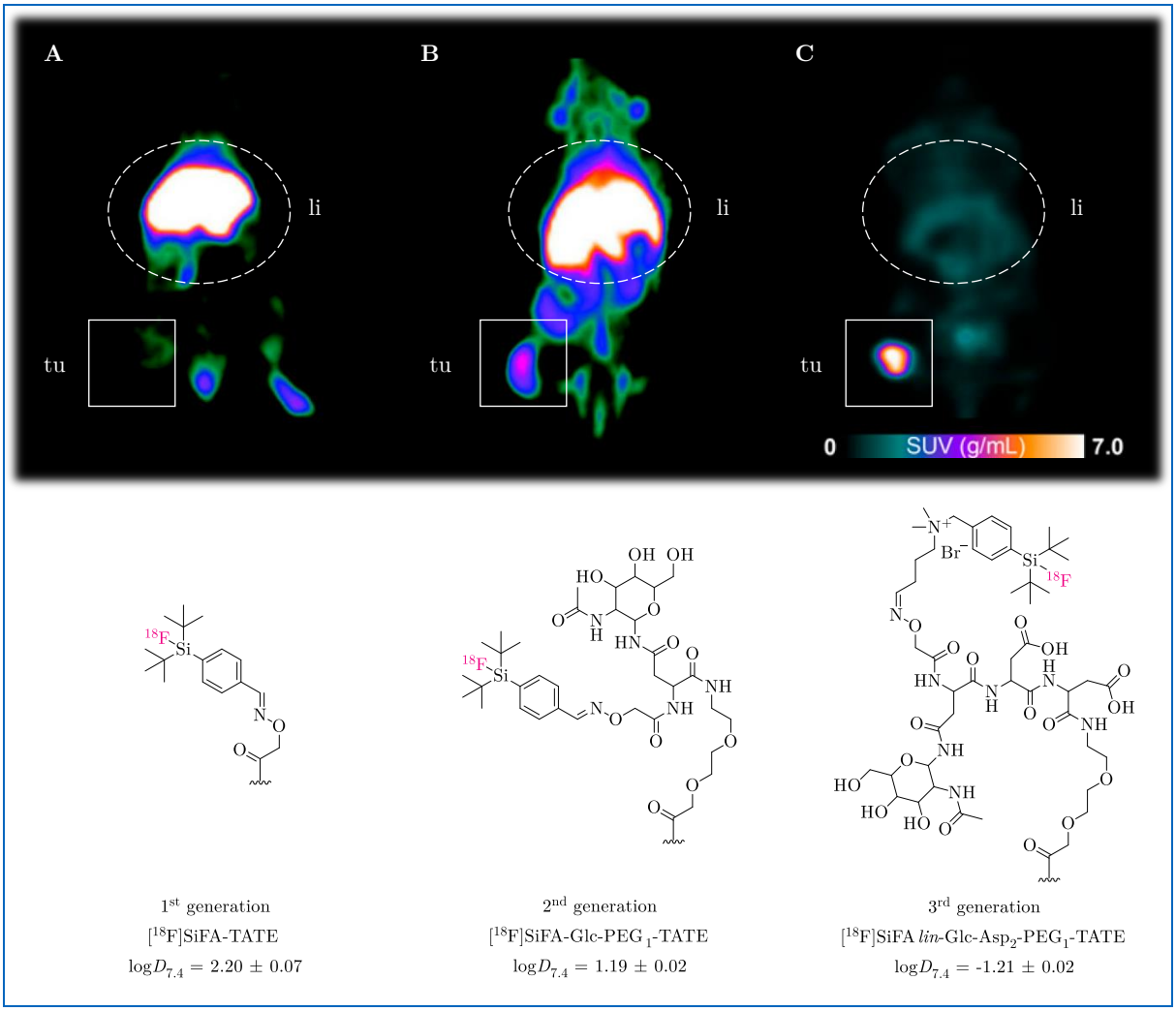

Figure 6. Coronal PET images of AR42J tumor-bearing CD1-Foxn1^{nu} mice acquired at 50–90 min post-injection (p.i.) with three generations of SSTR ligands, including **A**) [^{18}F]SiFA-TATE, **B**) [^{18}F]SiFA-Glc-PEG$_1$-TATE, and **C**) [^{18}F]SiFA*lin*-Glc-Asp$_2$-PEG$_1$-TATE (modified from the source)[73]. Activity accumulation in liver (li, dashed white circle) and AR42J tumor (tu, white box) is additionally indicated[73]. The respective structural differences in the Silicon-based Fluoride Acceptor-bearing side chain are shown below together with the ligand lipophilicity expressed as log$D_{7.4}$ value[73].

The first SSTR ligand, SiFA-TATE, was prepared by simple elongation of the binding motif structure with 4-(di-*tert*-butylfluorosilyl)benzaldehyde *via* oxime ligation[71]. Unfortunately, biodistribution studies of the respective radiofluorinated compound revealed only marginal

tumor uptake (*Figure 6A*)[71]. Instead, massive accumulation of the radiotracer occurred in the liver and gallbladder, which was assumed to be a result of the marked lipophilicity ($\log D_{7.4} = 2.20 \pm 0.07$)[71, 73]. To compensate for the latter, a second generation SSTR ligand was designed with an additional ethylene glycol spacer and a glucose moiety prior to the Silicon-based Fluoride Acceptor[71]. The introduction of such hydrophilic building blocks contributed to the reduction in lipophilicity ($\log D_{7.4} = 1.19 \pm 0.02$) and to a significantly improved pharmacokinetic profile of the radioligand with satisfactory accumulation in tumor tissue and slightly lower hepatic uptake (*Figure 6B*)[71, 73]. With the aim of further improving the *in vivo* distribution, especially regarding the excretion pathway, a third series of SSTR ligands was developed[73]. In addition to the hydrophilic moieties of the second generation, these ligands were designed to also comprise several charged amino acids as well as a permanent positive charge in proximity to the Silicon-based Fluoride Acceptor[73]. The most promising radiotracer, [^{18}F]SiFA*lin*-Glc-Asp$_2$-PEG$_1$-TATE, displayed a further decreased lipophilic character ($\log D_{7.4} = -1.21 \pm 0.02$) and an impressive pharmacokinetic profile (*Figure 6C*)[73]. Indeed, the radioligand exhibited high tumor uptake, excellent tumor-to-organ ratios, and exclusive renal excretion[73]. With these results in hand, *Wängler* and co-workers were able to convincingly demonstrate that the lipophilicity issue of Silicon-based Fluoride Acceptors could be solved by an adequate introduction of hydrophilic auxiliaries[73].

1.2.5 Clinical Relevance

Since first investigations in the early 2000s, radiofluorination by Silicon-based Fluoride Acceptors has undergone tremendous development and has evolved into an established technology for ^{18}F-labeling[46, 50]. To date, a variety of thereupon based radiotracers against different oncological targets have been reported, including ligands addressing the prostate-specific membrane antigen (PSMA), SSTR, GRPR, dopamine receptor D$_2$, cholecystokinin-2 receptor, and integrins[71-73, 76, 78-79]. Widespread application of this novel radiofluorination strategy is owed to the advantageous labeling procedure *via* isotopic exchange reaction, which has been proven to be exceptionally efficient, simple, and easily reproducible on a large-scale (*Figure 7*)[80-83].

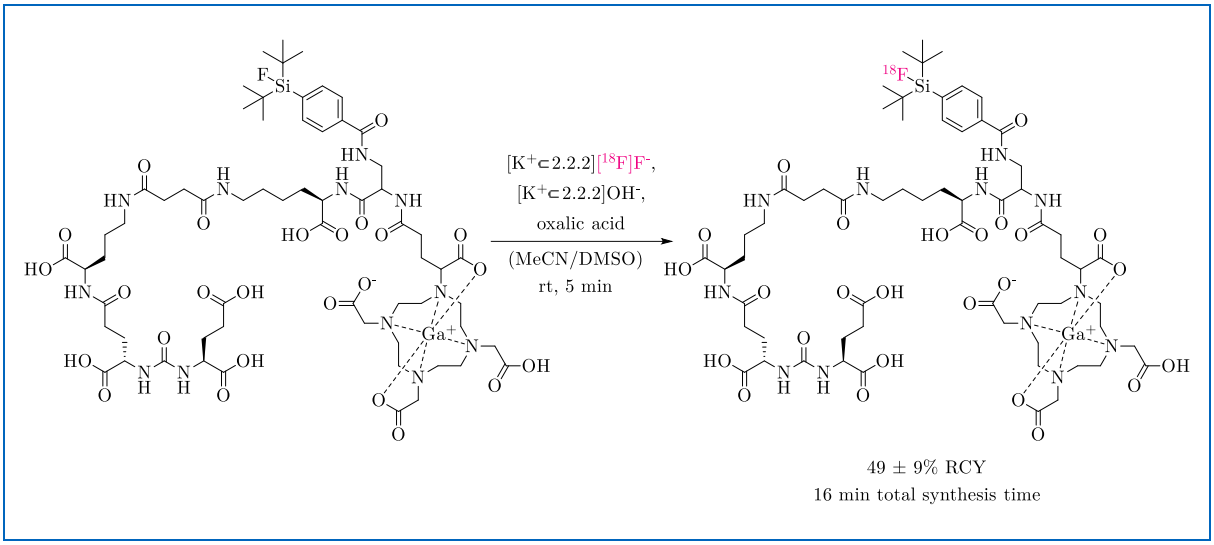

Figure 7. Radiofluorination *via* Silicon-based Fluoride Acceptors exemplified by the automated radiosynthesis of [^{18}F]^{nat}Ga-rhPSMA-7/7.3[82].

Among the most promising preclinical candidates, a handful of radiotracers have made it into human application so far, including the SSTR ligand [^{18}F]SiFA*lin*-Glc-Asp$_2$-PEG$_1$-TATE (also referred to as [^{18}F]siTATE) as well as the PSMA inhibitors [^{18}F]^{nat}Ga-rhPSMA-7/7.3 and [^{18}F]siPSMA-**14**[83-87]. The latter ligand mentioned in this context was developed as part of the present doctoral thesis. Superior imaging properties were reported for all of these radiofluorinated ligands, evidencing the *in vivo* applicability and safety of ^{18}F-labeled Silicon-based Fluoride Acceptors[86-88]. This radiofluorination strategy therefore holds the potential to revolutionize ^{18}F-labeling and to significantly increase the relevance of radiofluorinated tracers in PET diagnostics.

1.3 Radiofluorinated PSMA Inhibitors for PET Imaging

1.3.1 Prostate Cancer in Germany

According to the latest data on population-based cancer occurrence published by the *Robert Koch Institute*, prostate carcinoma was again the most common tumor malignancy (65˙200 cases) and the second cancer-associated cause of death (14˙963 cases) among German men in 2018[89]. For 2022, an even higher number of new cases (about 70˙100) was projected to occur[89]. The risk of developing prostate cancer appears to be negligible in men up to the age of 35, but increases rapidly in the 50–80 age group[89]. Statistically, one in eighteen 65-year-old German men will be diagnosed with prostate carcinoma in the next ten years[89]. Although the five-year relative survival rate of patients with prostate cancer in local or regional stages approaches 100%, a strikingly higher mortality is observed for the distant-stage disease[89]. It is hence of utmost importance to develop efficient methods for early and sensitive diagnosis of prostate carcinoma.

1.3.2 PSMA as Target Structure for Prostate Cancer

Although well-established and widely used for the detection of various cancer types, conventional non-invasive imaging modalities often suffer from significant limitations when it comes to prostate cancer visualization. In this context, transrectal ultrasonography, X-ray computed tomography (CT), magnetic resonance imaging, as well as bone scintigraphy lack sensitivity and specificity in differentiating benign hyperplasia, localizing the primary tumor, or detecting metastases and recurrences[90-91]. The same shortcomings prevail when using common PET radiotracers aiming to detect malignancies through upregulated cancer metabolism or proliferation[92]. For instance, 2-deoxy-2-[^{18}F]fluoro-D-glucose as well as various ^{11}C- or ^{18}F-labeled choline and acetate derivatives fail to image prostate carcinoma with adequate specificity and sensitivity[92]. An alternative consists in addressing specific marker structures prevalently present in tumor cells. In this regard, PSMA has emerged as a promising target over the last decades, leading to the development of several clinically established ligands for imaging and therapy of prostate cancer[93].

PSMA was originally identified by *Horoszewicz et al.* in 1987[94]. It was discovered using the monoclonal antibody 7E11-C5, previously obtained through immunization of mice with the human LNCaP prostate cancer cell line[94]. Subsequent characterizations revealed that PSMA represents a homodimeric type II transmembrane glycoprotein with a molecular weight of about 100 kDa[95-96]. The protein structure, which shares great homology with the transferrin receptor, consists of 750 amino acids and includes a zinc(II)-dependent metallopeptidase domain in the extracellular part[96-97]. On its surface, PSMA exhibits multiple mostly *N*-linked oligosaccharides that are essential for both enzyme function and stability (*Figure 8*)[98-100].

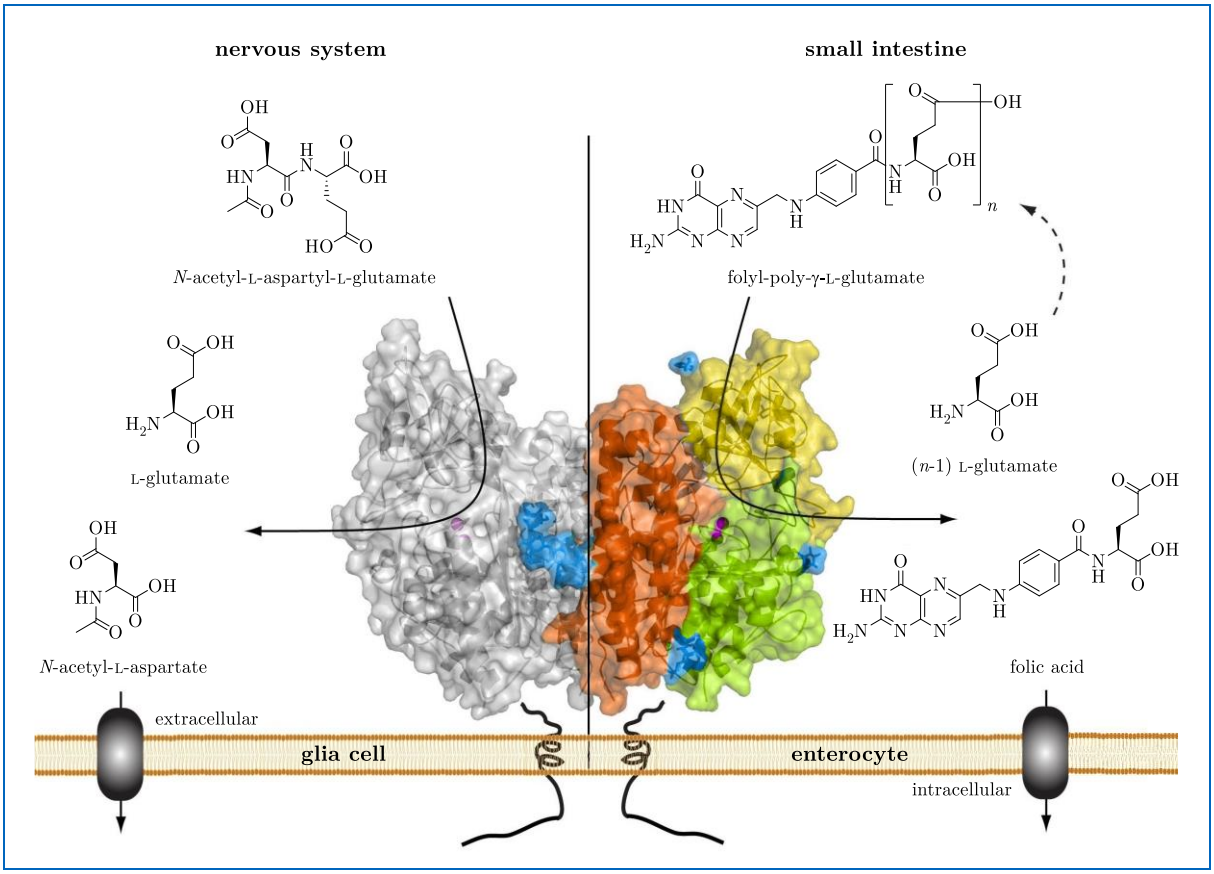

Figure 8. Crystal structure of the extracellular PSMA domain and representation of its enzymatic function in the nervous system and small intestine (modified from the source)[101]. The extracellular part comprises the protease domain (green), the apical domain (yellow), the C-terminal domain (orange), as well as several glycosylation sites (blue)[101]. The zinc(II) ions occupying the active site of PSMA are highlighted in purple[101].

The enzymatic activity consists of cleaving C-terminal L-glutamate from different substrates in various tissues[102]. For this reason, PSMA was initially referred under distinct names characterizing the substrate-specific function. The catalytic activity was first described by

Robinson et al. observing the cleavage of *N*-acetyl-L-aspartyl-L-glutamate to *N*-acetyl-L-aspartate and L-glutamate in brain cells[103-104]. It was subsequently ascertained that this *N*-acetylated α-linked acidic dipeptidase (NAALADase) was identical to both PSMA and folate hydrolase I (FOLH1), the latter having been previously identified as responsible for the degradation of folyl-poly-γ-L-glutamate in the small intestine[105-108]. In order to introduce a clear designation, the enzyme is nowadays also denominated as glutamate carboxypeptidase II (GCPII)[102].

Physiological expression of PSMA has been reported in several tissues, including prostatic epithelium, glomeruli and proximal tubules of the kidney, jejunal brush border, as well as astrocytes and non-myelinating Schwann cells of the nervous system[109-114]. Some other organs such as adrenal glands, salivary glands, breast, liver, spleen, bladder, and ovaries have also been identified in expressing PSMA, although commonly to a weaker extent[115-117]. In contrast to the occurrence in healthy tissue, PSMA overexpression was reported in primary as well as metastatic prostate cancer, including lymph node and bone metastases[109-110, 116, 118]. Elevated levels of the enzyme were also detected in the neovasculature of certain non-prostatic tumor types, like neuroendocrine, colon, as well as renal cell and transitional cell carcinomas[109, 119]. Notably, upregulation of PSMA in prostate cancer was found to correlate with tumor grade and stage, as well as aneuploidy and biochemical recurrence[116, 118, 120]. These characteristics, along with its restricted physiological presence, render PSMA a sensitive and specific biomarker for the development of radiopharmaceuticals targeting prostate carcinoma[119, 121].

1.3.3 General Design of PSMA-targeting Inhibitors

Extensive X-ray crystallographic studies of PSMA interacting with ligands developed over the last years have been crucial for understanding the substrate binding cavity and paved the way for a general inhibitor design (*Figure 9*)[122-127].

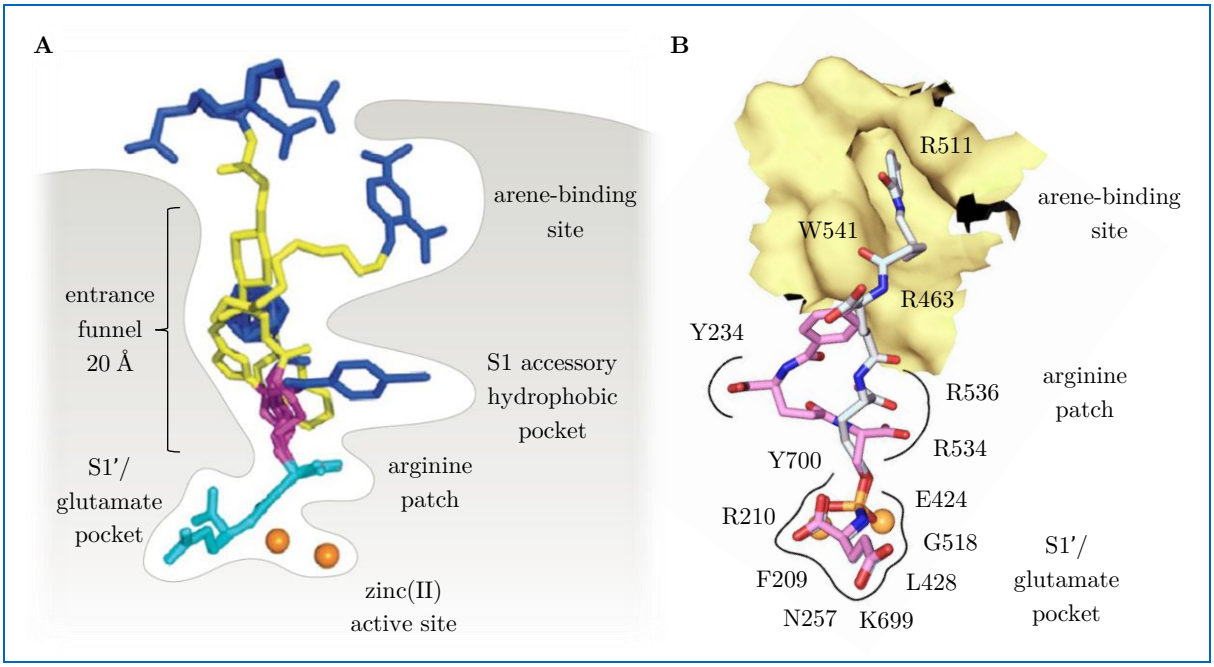

Figure 9. Interaction of superimposed exemplary PSMA inhibitors with **A**) various regions and **B**) respectively involved amino acid side chains of the binding pocket cavity (modified from sources)[128-129].

Potent PSMA ligands typically address multiple regions within the binding pocket, which includes the pharmacophore S1' cavity, the binuclear zinc(II) active site, and the S1 pocket leading to the enzyme surface (*Figure 9A*)[123, 127-129]. The former cavity is shaped by various amino acid side chains (R210, Y552, Y700, N257, K699) that are responsible for recognition of the C-terminal L-glutamate in endogenous substrates (*Figure 9B*)[123]. Due to its poor tolerance to structural modifications, the pharmacophore S1' pocket is generally accommodated with L-glutamate or L-glutamate-like residues in PSMA ligands[123]. The active site of the enzyme comprises two zinc(II) ions with a coordinated water molecule, which participate in the hydrolytic cleavage of the amide bond within endogenous ligands[122]. In order to block the catalytic center, zinc-binding moieties such as thiol, phosphonate, phosphinate, urea, or phosphoramidate are utilized as inhibitor component[130-134]. Among these, a great variety of urea-based ligands have been reported so far, most notably by the groups of *Pomper* and *Wester*[135-137]. While the structural requirements to address the S1' (glutamate) cavity and the active site of PSMA are relatively stringent, greater flexibility is allowed in occupying the S1 pocket[126]. Noteworthy, this 20 Å long funnel to the enzyme surface features specific sites which can be exploited to further increase the inhibitor's affinity[123]. A first reported region accommodates negatively charged P1 substrate moieties through interaction with the amino

acids R463, R534, and R536[125]. Due to the presence of such guanidinium-rich residues, this site was denominated as arginine patch[122, 125]. Shortly thereafter, the existence of a further cavity was identified in the S1 region[126]. The recognized S1 accessory hydrophobic pocket strongly interacts with an aromatic functionality of PSMA inhibitors if adequately spaced from the zinc-binding group[126]. Another site for hydrophobic interactions was discovered near the entrance of the PSMA cavity[127]. Access to the binding pocket is regulated by an entrance lid that can assume an open and a closed conformation[127]. When the entrance lid adopts the open conformation, a so-called arene-binding site is shaped by the amino acid side chain functionalities of W541, R511, and R463[127]. If appropriately placed in the inhibitor structure, aromatic moieties are able to accommodate this region and thus enhance binding affinity, presumably through simultaneous formation of π-cation and π-stacking interactions[127, 138]. All these insights gained into the structure of PSMA have contributed to the development of sophisticated inhibitors that fit precisely within the enzyme pocket and therefore exhibit remarkably high binding affinity in the low nanomolar range[136].

1.3.4 Clinically relevant ^{18}F-labeled PSMA Inhibitors

The approach of visualizing prostate cancer through radiofluorinated PSMA-targeting PET probes has witnessed an impressive development in the last decade. In this context, various ^{18}F-labeled ligands made it into first proof-of-concept studies in patients, some of which have even become established in routine clinical practice.

[^{18}F]DCFBC

N-[*N*-[(*S*)-1,3-dicarboxypropyl]carbamoyl]-4-[^{18}F]fluorobenzyl-L-cysteine, also referred to as [^{18}F]DCFBC (*Figure 10*) and developed by *Mease et al.*, represented the first radiofluorinated PSMA tracer to enter clinical trials[139-143].

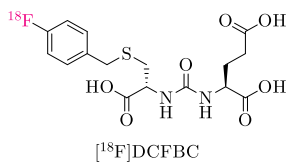

[^{18}F]DCFBC

Figure 10. Chemical structure of the radiofluorinated PSMA ligand [^{18}F]DCFBC[139].

Despite its high tumor specificity, a considerable limitation was seen in the pronounced plasma protein binding[141]. The associated delay in blood clearance resulted in a reduced tumor-to-background ratio, particularly compromising the detection of small metastases[141].

[^{18}F]DCFPyL

With the aim to improve the pharmacokinetic profile of [^{18}F]DCFBC, the same research group designed a second-generation ligand consisting of an L-glutamate-urea-L-lysine binding motif elongated by a 6-[^{18}F]fluoronicotinic acid moiety[144]. This PSMA inhibitor, designated [^{18}F]DCFPyL (*Figure 11*), demonstrated superior tumor uptake and rapid excretion from non-target tissue in preclinical studies[144].

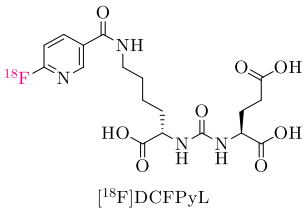

[^{18}F]DCFPyL

Figure 11. Chemical structure of the radiofluorinated PSMA inhibitor [^{18}F]DCFPyL[144].

Subsequent investigations in patients confirmed the safety of [^{18}F]DCFPyL and evidenced a favorable distribution pattern with high and specific radiotracer uptake in tumor lesions[145-147]. Most notably, metastatic lymph nodes close to vessels were better visualized due to the rapid clearance of the radiotracer from the blood pool[145]. Considerable accumulation of [^{18}F]DCFPyL was also observed in kidney and bladder, indicating predominant excretion *via* the urinary system[145, 148]. This characteristic, however, revealed to be disadvantageous for the detection of lesions in the vicinity of the bladder[145, 148]. Nonetheless, the overall encouraging results obtained with [^{18}F]DCFPyL prompted the development of various automated synthesis procedures for its large-scale production, which contributed to the widespread availability of this ^{18}F-labeled PSMA inhibitor in clinical routine[149-150]. In 2021, [^{18}F]DCFPyL (Pylarify®) became the first commercially available radiofluorinated PSMA ligand to be approved by the Food and Drug Administration in the United States[151].

[^{18}F]AlF-PSMA-11

Malik et al. and *Boschi et al.* were the first to report the radiofluorination of PSMA-11 by means of Al[^{18}F]F^{2+}-complexation through a simple and high-yielding one-pot approach[40, 152]. In preclinical comparison with the previously published and extensively studied ^{68}Ga-labeled counterpart, [^{18}F]AlF-PSMA-11 (*Figure 12*) revealed similar tumor uptake and blood clearance in biodistribution studies[153].

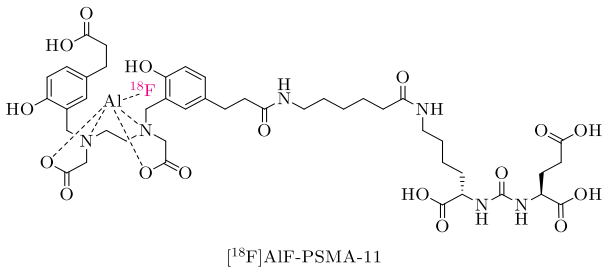

Figure 12. Chemical structure of the radiofluorinated ligand [^{18}F]AlF-PSMA-11[154].

However, mice experiments also highlighted significant bone accumulation and thus instability of the tracer over time[153]. In a subsequent study, it was found that the addition of ethanol (EtOH) to the reconstituted radiotracer prevented its degradation, paving the way for the clinical application of [^{18}F]AlF-PSMA-11[155]. After implementing an automated synthesis procedure for large-scale production, [^{18}F]AlF-PSMA-11 was successfully tested in an initial proof-of-concept study in men[154, 156-157]. In a head-to-head comparison involving prostate cancer patients administered with both [^{68}Ga]Ga-PSMA-11 and [^{18}F]AlF-PSMA-11, the radiofluorinated tracer was able to visualize all abnormal findings as well as some bone lesions that were undetectable with the ^{68}Ga-labeled counterpart[158].

[^{18}F]FSU-880

Although [^{18}F]DCFPyL had proven to be a promising PET probe in clinical studies, production at that time suffered from low RCYs[159]. To address this issue, *Harada et al.* developed a radiofluorinated PSMA ligand based on a two-step coupling approach with *N*-succinimidyl 4-[^{18}F]fluorobenzoate, which had earlier been established in an efficient automated synthesis

procedure[159-160]. The design of this novel asymmetric urea ligand, designated [^{18}F]FSU-880 (*Figure 13*), was inspired by a previously developed ^{123}I-labeled PSMA inhibitor[161].

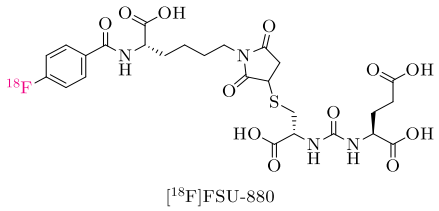

Figure 13. Chemical structure of the radiofluorinated PSMA inhibitor [^{18}F]FSU-880[159].

Since [^{18}F]FSU-880 showed high PSMA-binding affinity, a favorable biodistribution pattern in mice, and was also accessible in high RCYs (30–50%), the ligand advanced to a potential candidate for clinical application[159]. In a first-in-men study with metastatic prostate cancer patients, lesions were successfully visualized with high contrast and precision, thereby demonstrating the safety and efficacy of [^{18}F]FSU-880[162].

[^{18}F]PSMA-1007

Inspired by the scaffold of PSMA-617, one of the gold standards for radiometal labeling, *Cardinale et al.* designed a resembling radiofluorinated ligand termed [^{18}F]PSMA-1007 (*Figure 14*)[163].

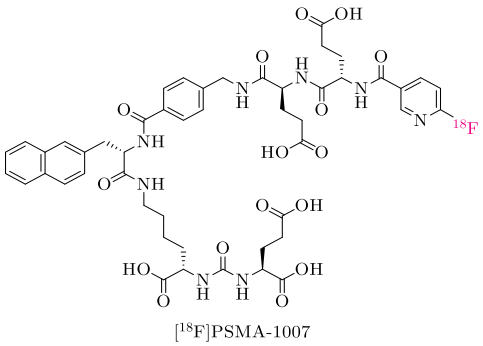

Figure 14. Chemical structure of the radiofluorinated ligand [^{18}F]PSMA-1007[164].

As the preclinical evaluation demonstrated nanomolar binding affinity to PSMA, elevated internalization rate, as well as high and specific tumor accumulation in xenograft models, [^{18}F]PSMA-1007 was considered for first-in-human studies[163]. Thereby, the radiotracer proved

to detect tumor lesions with high sensitivity and contrast, comparable to ^{68}Ga-labeled PSMA inhibitors[165]. In addition, tumor uptake of [^{18}F]PSMA-1007 and [^{177}Lu]Lu-PSMA-617 appeared to be similar, allowing for the use of both ligands as theragnostic pair[164]. Excretion of the rather lipophilic [^{18}F]PSMA-1007 was reported to occur primarily through the liver and only to a minor extent *via* the urinary tract[165-166]. This condition turned out to be particularly advantageous for visualization of malignancies located in the prostate bed since uptake was not obscured by activity in the bladder[165-166]. At the same time, however, the hepatobiliary elimination of [^{18}F]PSMA-1007 complicated the detection of potential liver and visceral metastases, as signal interference allowed false-negative findings[167].

[^{18}F]^{nat}Ga-rhPSMA-7.3

In 2019, a novel class of so-called *radiohybrid* PSMA inhibitors was presented by *Wurzer et al.* and received particular attention[76]. Contrary to previously introduced ^{18}F-labeled ligands relying on conventional carbon-[^{18}F]fluorine chemistry, the newly developed rhPSMA inhibitors incorporate the ^{18}F-label *via* isotopic exchange reaction on a Silicon-based Fluoride Acceptor[76]. To compensate for the inherent lipophilicity of the labeling moiety, rhPSMA ligands feature a hydrophilic chelator offering an additional degree of freedom with respect to radiometal labeling[76]. Thus, chemically identical twins can be employed for either diagnostic ([^{18}F]^{nat}Ga-rhPSMA and [^{68}Ga]Ga-rhPSMA) or theragnostic ([^{18}F]^{nat}Lu-rhPSMA and [^{177}Lu]Lu-rhPSMA) purposes[76]. Among the purely diagnostic ligands, [^{18}F]^{nat}Ga-rhPSMA-7.3 (*Figure 15*) showed the most promising preclinical results and advanced to first-in-human studies[85, 168].

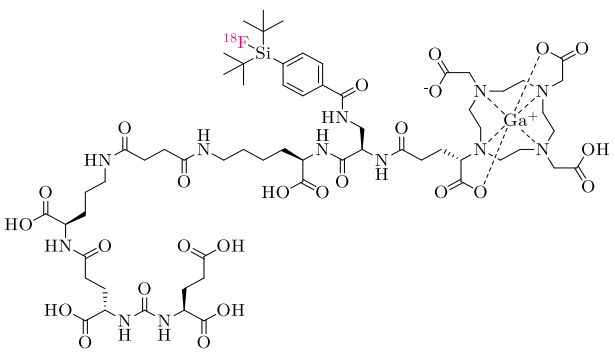

[^{18}F]^{nat}Ga-rhPSMA-7.3

Figure 15. Chemical structure of the radiofluorinated ligand [^{18}F]^{nat}Ga-rhPSMA-7.3[168].

Application of [^{18}F]^{nat}Ga-rhPSMA-7.3 in patients revealed high radiotracer accumulation in primary as well as metastatic prostate cancer lesions[169-171]. Most notably, the advantageous pharmacokinetic behavior resulted in clear visualization of malignancies within the prostate bed[172]. A further strength of [^{18}F]^{nat}Ga-rhPSMA-7.3 resides in its automated radiosynthesis, which was reported to proceed in an exceptionally simple, fast, and highly efficient manner[82].

1.4 Radiofluorinated FR Ligands for PET Imaging

1.4.1 Folic Acid and Folates

Folates are a family of heterocyclic compounds derived from folic acid, a water-soluble vitamin belonging to the B-complex[173]. The term "folate" refers to the Latin word for leaf (*folium*), since folic acid was first isolated from spinach in 1941 and abundantly occurs in green leafy vegetables[173-175]. With respect to the chemical structure, folic acid and folates are composed of three building blocks: L-glutamic acid, 4-aminobenzoic acid, and 2-amino-4-oxopteridine or derivatives thereof (*Figure 16*)[173].

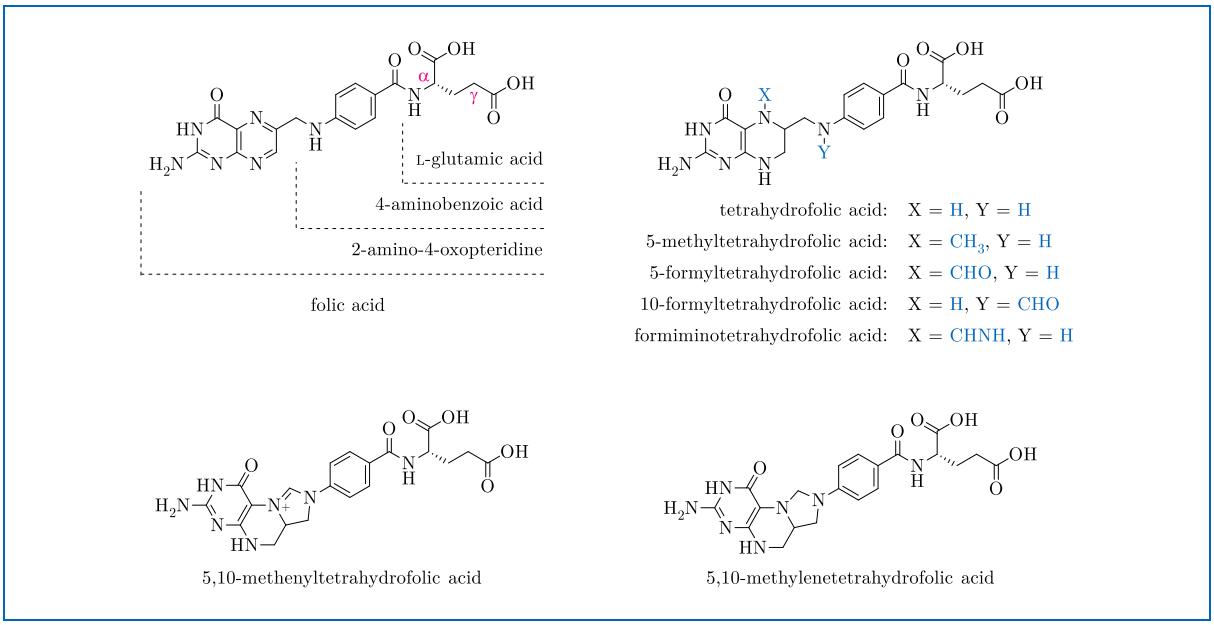

Figure 16. Chemical structures of folic acid and naturally occurring folates[173].

Like other mammals, humans are unable to endogenously generate folic acid and therefore depend on the dietary intake of this essential nutrient[173]. The body requires folic acid for the biosynthesis of certain cofactors[173]. These function as both donors and acceptors in relevant one-carbon transfer reactions that occur during regulation of gene expression, *de novo* synthesis of DNA nucleotides, and DNA repair pathways[173]. Hence, folates assume a key role in processes related to cell growth and proliferation. As a result, folate deficiency is associated with some serious pathologies, including megaloblastic anemia, vascular diseases, and neurological conditions[176-178]. Especially in pregnant women, it is well known that deficiency symptoms can lead to congenital malformations, like neural-tube defects in the unborn child[179].

1.4.2 FR as Target Structure for various types of Cancer

Due to their negatively charged nature under physiological conditions, folates are unable to cross the cell membrane by passive diffusion[180]. As a consequence, cellular uptake of folates is mediated *via* specific transport proteins[180]. Among these, the reduced folate carrier (RFC) and the proton-coupled folate transporter (PCFT) represent the most important transport systems, whereas a minor role can be attributed to the folate receptor (FR)[180]. The discovery of the latter occurred more than 50 years ago when a protein with folate-binding ability was identified in bovine milk[181-182]. It was later on recognized, that the FR constitutes a family of glycoproteins present in four isoforms (FRα, FRβ, FRγ, and FRδ) with molecular weights between 38–45 kDa[182-186]. The subtypes share a sequence identity of 54–82%, but display some differences in terms of linkage and expression pattern[185]. Hence, FRα has been characterized as a glycosylphosphatidylinositol- (GPI-)anchored protein that displays high affinity to folic acid (K_d = 0.1–1 nM) and reduced derivatives (K_d = 1–10 nM), which are internalized upon binding through receptor-mediated endocytosis[187-189]. Its physiological expression is restricted to a few organs, including the proximal and distal tubules of the kidney, choroid plexus, salivary glands, thyroid, esophagus, lung, breast, fallopian tubes, pancreas, and placenta[190-193]. The other three isoforms are expressed in hematopoietic cells, with FRβ and FRδ also representing GPI-anchored receptors, whereas FRγ exists as a secreted protein[184, 194-197]. Within these isoforms, FRα has attracted considerable interest as oncological biomarker due to the high-level expression in different tumors[198-199]. An immunohistochemical study by *Garin-Chesa et al.* revealed upregulation of FRα in a multitude of epithelial cancer types with particular prevalence in ovarian (52/56), endometrial (10/11), renal (10/20), gastric (3/8), non-small-cell lung (6/18), colorectal (6/27), and breast (11/53) carcinomas[198]. In another investigation published by *Parker et al.*, FRα expression for the aforementioned malignancies was reported to be up to 30-fold higher when compared to the physiological distribution[200]. As demonstrated for breast and ovarian carcinoma, upregulation of the receptor confers a growth advantage to cancer cells and is directly correlated with tumor aggressiveness and progression[201-203]. Due to these characteristics, FRα advanced to a promising target structure for the development of diagnostic and therapeutic agents against FR-positive carcinomas[204-205]. Over the past two

decades, a plethora of radiolabeled folate conjugates have been published, reflecting the great interest and high expectations placed on FR-targeting ligands[204-205].

1.4.3 General Design of FR-targeting Ligands

Important insights for the structural design of FR ligands were obtained with the aid of X-ray crystallography[206]. In this context, *Chen et al.* were the first to disclose the structure of human FRα in co-crystallization with folic acid (*Figure 17*)[206].

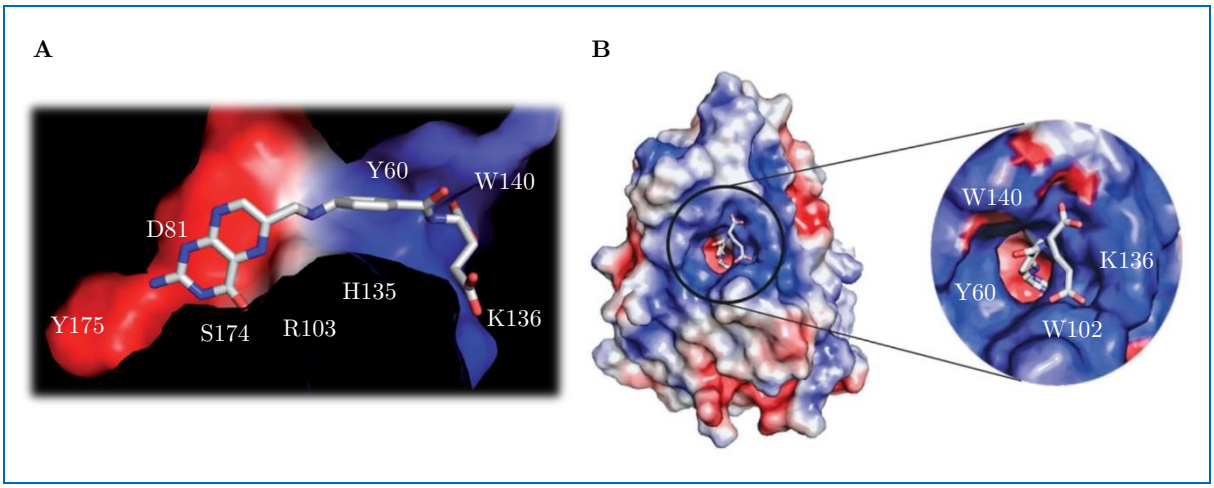

Figure 17. Interaction of folic acid with human FRα illustrated by **A**) an internal view of the binding cavity showing the amino acid side chains involved in substrate binding and **B**) a side view with close-up on the pocket entrance (modified from the source)[206]. The color of the receptor surface reflects its charge distribution with negatively charged regions depicted in red and positively charged areas in blue[206].

The researchers discovered that the 2-amino-4-oxopteridine moiety is deeply embedded in the binding pocket, undergoing hydrogen bonds (D81, S174, R103, R106, H135) and hydrophobic interactions (Y85, W171, Y175) with the amino acid residues of the receptor (*Figure 17A*)[206]. Especially the hydrogen bond formation with the carboxylate functionality of D81 proved to be crucial for strong binding[206]. Due to these specific interactions, only structurally similar substrates to folic acid, e.g. 5-methyltetrahydrofolate, can be accommodated in the binding cavity and therefore be considered as targeting agents for the development of FR ligands[206]. In contrast, the L-glutamate functionality of folic acid was found to protrude from the binding pocket (*Figure 17B*) and to exhibit extensive hydrogen bonding with the positively charged amino acid side chains (W102, K136, W140, H135, G137, W138) at the pocket entrance[206].

Based on these results, two distinct strategies for the development of FR-targeting ligands emerged, namely *pendant* and *integrated approach*.

1.4.4 Selected ^{18}F-labeled FR Ligands according to the *Pendant Approach*

Since the L-glutamate moiety of folic acid remains exposed on the FR surface upon binding, structural modifications at the respective α- or γ-carboxylate groups are well tolerated without compromising affinity to the receptor[206]. Hence, FR ligands can be conveniently designed by elongating these functionalities with the intended conjugate[206]. This so-called *pendant approach* has led to the rapid development of a large number of FR-targeting compounds[207-215].

[^{18}F]Fluorobenzylamine-folates

In 2006, *Bettio et al.* were the first to develop a radiofluorinated FR-targeting tracer by linking 4-[^{18}F]fluorobenzylamine to unprotected folic acid[207]. As a result, a regioisomeric mixture of α- and γ-4-[^{18}F]fluorobenzylamine-folate (*Figure 18*) was obtained[207].

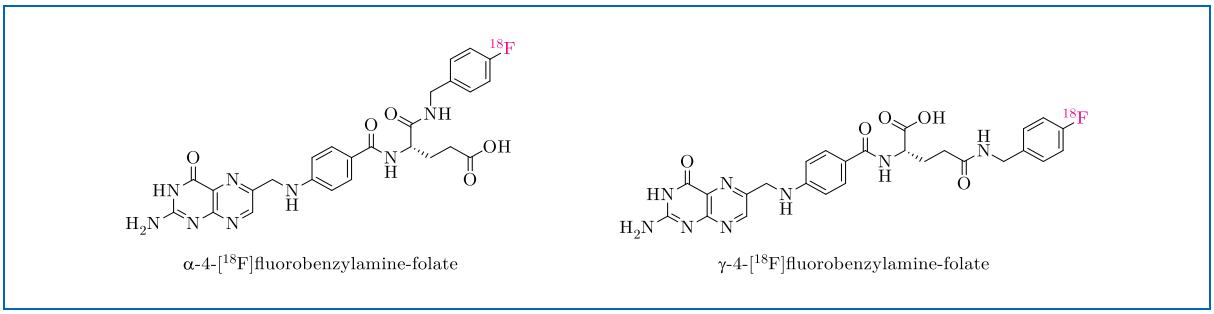

Figure 18. Chemical structures of the radiofluorinated FR ligands α- and γ-4-[^{18}F]fluorobenzylamine-folate[207].

The determined FR affinities for the α- and γ-regioisomer were only 1.7- and 1.5-fold lower when compared to folic acid, indicating pronounced binding to the receptor regardless of the prosthetic group linkage[207]. PET imaging studies in KB tumor-bearing mice with α/γ-4-[^{18}F]fluorobenzylamine-folate revealed clear tumor visualization and additional biodistribution studies at 125 min p.i. confirmed high and specific tumor uptake with 6.56% injected dose per gram of tissue (%ID/g)[207]. Despite these encouraging results, the low-yielding four-step radiosynthesis as well as the substantial hepatobiliary excretion posed significant limitations that hindered further tracer development[207].

[^{18}F]Fluorobenzene- and [^{18}F]fluoropyridine-carbohydrazide-folates/methotrexates

With the aim to prepare radiofluorinated FR-targeting ligands in an easier and more efficient manner, *Al Jammaz et al.* applied 4-[^{18}F]fluorobenzene-carbohydrazide and 2-[^{18}F]fluoropyridine-4-carbohydrazide as prosthetic groups for conjugation to the binding motifs folate and methotrexate (*Figure 19*)[208-209].

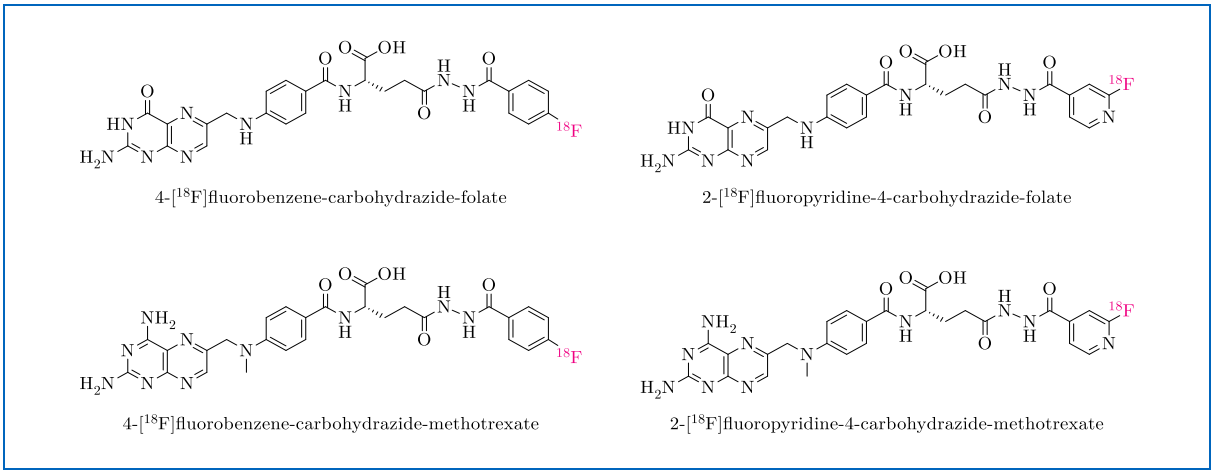

Figure 19. Chemical structures of the radiofluorinated FR ligands 4-[^{18}F]fluorobenzene-carbohydrazide-folate/methotrexate and 2-[^{18}F]fluoropyridine-4-carbohydrazide-folate/methotrexate[208-209].

Radiolabeling was accomplished with remarkably high RCYs (>80%) and in a relatively short synthesis time (40–45 min)[209]. Subsequent cell binding studies revealed a 2-fold higher affinity for the folate conjugates over the methotrexate analogs[209]. Moreover, lipophilicity was found to be generally high for both 4-[^{18}F]fluorobenzene-carbohydrazide-bearing ligands ($\log_{10}$ = 0.38–0.43) and 2-[^{18}F]fluoropyridine-4-carbohydrazide conjugates ($\log_{10}$ = 0.14–0.16)[208-209]. Distinct differences were observed in biodistribution studies at 1 h p.i. with KB tumor-bearing mice[209]. While folate conjugates demonstrated good tumor accumulation (5.74–5.94 %ID/g), methotrexate counterparts exhibited more than 5-fold lower uptake, which rendered the latter unsuitable as radiotracers[209]. Besides, with the only exception of 2-[^{18}F]fluoropyridine-4-carbohydrazide-folate, the developed ligands evidenced an unfavorable pharmacokinetic profile with particularly high activity retention in liver and intestine[209].

Clicked [^{18}F]fluoro-folates and -5-methyltetrahydrofolates

Another pursued approach to facilitate the synthesis of ^{18}F-labeled FR ligands consisted in the development of radiotracers relying on *click chemistry*[210-213]. The first compound according to this strategy, namely [^{18}F]click-folate (*Figure 20*), was prepared by the group of *Ametamey* with acceptable RCYs (25–35%) in less than 90 min[210]. Despite good *in vitro* characteristics, biodistribution and PET studies in KB tumor-bearing mice revealed unfavorable tracer accumulation in the liver as well as excessive hepatobiliary excretion[210].

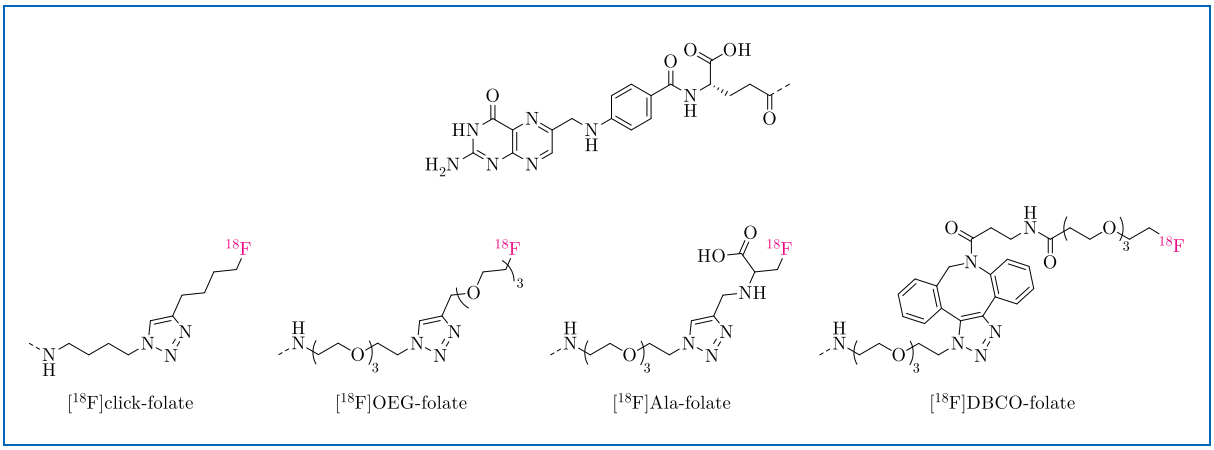

Figure 20. Chemical structures of the radiofluorinated FR ligands [^{18}F]click-folate, [^{18}F]OEG-folate, [^{18}F]Ala-folate, and [^{18}F]DBCO-folate[210-212].

Since the pronounced lipophilicity of [^{18}F]click-folate was assumed to be responsible for its inconvenient pharmacokinetic profile, the group of *Ross* designed an optimized [^{18}F]OEG-folate (*Figure 20*) by replacing both *n*-butyl spacers with oligo(ethylene glycol) (OEG) linkers[211]. *In vivo* investigations with this more hydrophilic FR ligand showed similar tumor uptake (3.39 ± 0.44 %ID/g, 1 h p.i.), reduced hepatobiliary elimination, and enhanced renal excretion when compared to [^{18}F]click-folate[211]. In spite of these improvements, significant accumulation of [^{18}F]OEG-folate was still observed in liver, gallbladder, and intestine, leading the authors to conclude that further optimization of ligand polarity was required[211].

Subsequent investigations by *Ross* and co-workers focused on the development of two novel FR ligands, [^{18}F]Ala-folate and [^{18}F]DBCO-folate (*Figure 20*), employing different *click* strategies[212]. While preparation of the former through copper-catalyzed azide-alkyne cyclo-addition was accomplished with acceptable RCYs, radiosynthesis of [^{18}F]DBCO-folate by the

strain-promoted approach turned out to be very inefficient[212]. Unfortunately, biodistribution studies with [^{18}F]DBCO-folate evidenced negligible tumor uptake and elevated unspecific binding as a result of its marked lipophilicity ($\log D = 0.6 \pm 0.1$), rendering the tracer unsuitable for imaging[212]. The same fate occurred to the more hydrophilic [^{18}F]Ala-folate ($\log D = -1.4 \pm 0.1$), which showed a better pharmacokinetic profile but very limited KB tumor accumulation (1.68 ± 0.13 %ID/g, 1 h p.i.)[212].

Further radiofluorinated FR ligands exploiting *click chemistry* were presented in 2018 by *Boss et al.*[213]. The group was the first to investigate (6*R*)- and (6*S*)-5-methyltetrahydrofolate as alternatives to the commonly used folic acid binding motif by preparing four different click-[^{18}F]fluoroethyl-5-methyltetrahydrofolates (*Figure 21*)[213].

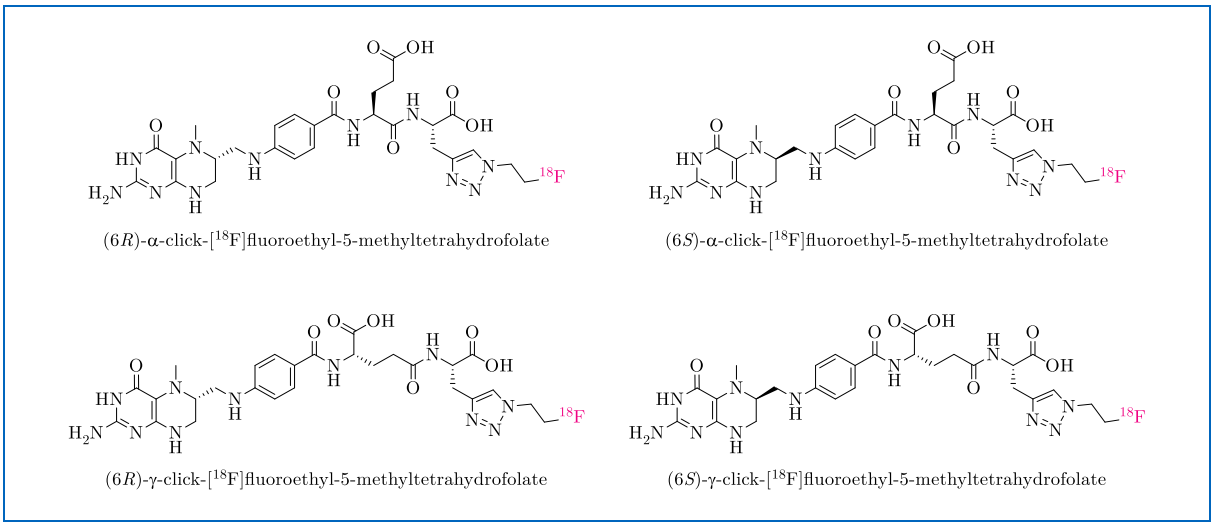

Figure 21. Chemical structures of different click-[^{18}F]fluoroethyl-5-methyltetrahydrofolates[213].

Although these novel ligands displayed significantly lower (29- to 40-fold) binding affinity when compared to folic acid, encouraging results were reported with respect to their *in vivo* behavior[213]. In fact, all four FR ligands showed surprisingly high KB tumor uptake with 8.2–10.6% injected activity per gram of tissue (%IA/g) in 1 h p.i. biodistribution studies[213]. Marked differences were found in renal and hepatic accumulation depending on the isomeric configuration of 5-methyltetrahydrofolate[213]. While the (6*S*)-derivatives exhibited high uptake in the liver and low kidney accumulation, an inverse distribution pattern was observed for the (6*R*)-conjugates[213]. Notwithstanding the promising results, radiosynthesis of these sensitive conjugates proved to be challenging and resulted in very low RCYs (1–7%)[213].

[^{18}F]NOTA(AlF)-folates

In 2016, *Chen et al.* reported an ^{18}F-labeled FR ligand using the principle of [Al[^{18}F]F]$^{2+}$-complexation through an appropriate chelator[214]. The developed [^{18}F]NOTA(AlF)-folate (*Figure 22*) was prepared in a one-pot strategy with reasonably good RCYs (19 ± 5%) and short synthesis time (37 min)[214]. *In vitro* evaluation of the ligand evidenced its high binding affinity to the FR, which was only 4.1-fold lower when compared to folic acid[214]. Unfortunately, the pharmacokinetic profile of [^{18}F]NOTA(AlF)-folate revealed moderate accumulation in the liver, associated with unfavorable elimination *via* the hepatobiliary pathway[214].

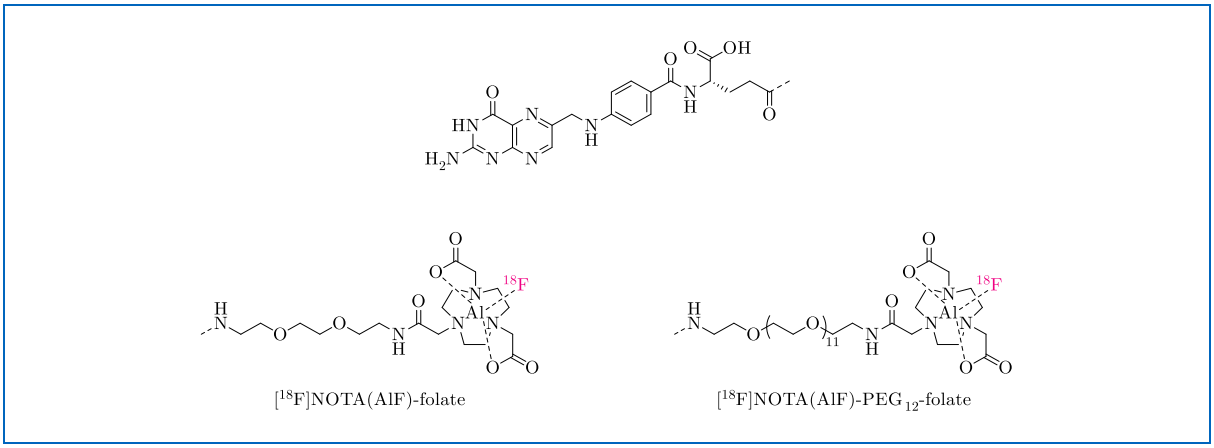

Figure 22. Chemical structures of the radiofluorinated FR ligands [^{18}F]NOTA(AlF)-folate and [^{18}F]NOTA(AlF)-PEG$_{12}$-folate[214-215].

Aiming to improve the *in vivo* distribution pattern, the research group designed a further ligand with enhanced hydrophilicity by elongating the ethylene glycol spacer unit[215]. Radiosynthesis of this novel [^{18}F]NOTA(AlF)-PEG$_{12}$-folate (*Figure 22*) was performed in analogy to the aforementioned approach and resulted in slightly lower RCYs (8 ± 1%)[215]. Introduction of the additional PEG$_{10}$ entity had just a minor impact on the FR-binding affinity, which was found to be 7.3-fold lower in direct comparison with folic acid[215]. The increased hydrophilicity provided by the extended spacer led to a significantly improved *in vivo* behavior[215]. When compared with the biodistribution performance of the first ligand, [^{18}F]NOTA(AlF)-PEG$_{12}$-folate showed reduced uptake by half in the liver, while accumulation in KB tumor xenografts (9.20 ± 0.62 %IA/g, 90 min p.i.) was similarly high and specific[215].

1.4.5 Selected ^{18}F-labeled FR Ligands following the *Integrated Approach*

In 2010, *Ross et al.* sought to develop ^{18}F-labeled FR ligands using a simplified radiolabeling strategy[216]. According to the *integrated approach*, ligand precursors are designed for direct radiofluorination to circumvent the time-consuming and challenging multi-step radiosynthesis with prosthetic groups[216]. In such radiotracers, which typically comprise scaffolds that closely resemble endogenous FR-binding motifs, introduction of fluorine-18 is accomplished under minimal structural perturbation *via* nucleophilic aromatic substitution (S_NAr)[216-218].

2'-[^{18}F]Fluorofolic acid and [^{18}F]AzaFol

2'-[^{18}F]Fluorofolic acid (*Figure 23*) represented the first radiotracer developed by means of the *integrated approach*[216]. Because of its structural similarity, the FR affinity was found to be only 3.1-fold lower when compared to folic acid[216]. Subsequent analysis of the *in vivo* behavior confirmed the favorable binding properties, as high and specific radiotracer accumulation was observed in KB tumor xenografts[216]. In addition, 2'-[^{18}F]fluorofolic acid revealed to exhibit an advantageous pharmacokinetic profile, including rapid elimination through the kidney and moderate uptake within organs of the hepatobiliary system[216]. However, radiofluorination of the respective precursor *via* ^{18}F-for-NO_2 substitution proved to be highly inefficient, resulting in poor overall RCYs of about 4%[216].

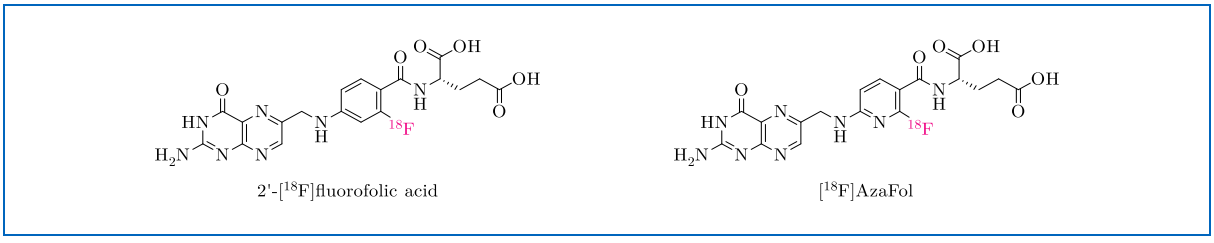

Figure 23. Chemical structures of the radiofluorinated FR ligands 2'-[^{18}F]fluorofolic acid and [^{18}F]AzaFol[216-217].

With the goal of improving the SNAr reaction, an optimized variant of 2'-[^{18}F]fluorofolic acid was designed by replacing the phenyl ring with a more electron-deficient pyridine moiety[217]. Radiofluorination of the corresponding precursor afforded the novel FR ligand 3'-aza-2'-[^{18}F]fluorofolic acid with slightly higher RCYs (3–9%)[217]. The introduction of the pyridine ring had no impact on the *in vitro* characteristics, as 3'-aza-2'-[^{18}F]fluorofolic acid was found to possess specific internalization and potent binding affinity to the FR[217]. Follow-up *in vivo*

investigations demonstrated high radiotracer accumulation in KB tumor xenografts (11.86 ± 1.73 %ID/g, 1 h p.i.) and favorable pharmacokinetics[217]. Based on these promising results, 3'-aza-2'-[^{18}F]fluorofolic acid, later renamed as [^{18}F]AzaFol (*Figure 23*), became the first radiofluorinated FR ligand to enter clinical trials[219].

3'-Aza-2'-[^{18}F]fluoro-5-methyltetrahydrofolates

After gaining experience with 5-methyltetrahydrofolate-based ligands using the *pendant approach*, *Boss et al.* applied the same binding motif in its (6*R*)- and (6*S*)-diastereomers to develop analogs of the highly promising [^{18}F]AzaFol[218]. Although the exhibited FR-binding affinities of (6*R*)-3'-aza-2'-[^{18}F]fluoro-5-methyltetrahydrofolate and (6*S*)-3'-aza-2'-[^{18}F]fluoro-5-methyltetrahydrofolate (*Figure 24*) were found to be significantly lower (17- to 19-fold) when compared to [^{18}F]AzaFol, subsequent evaluation of the *in vivo* behavior revealed excellent results[218].

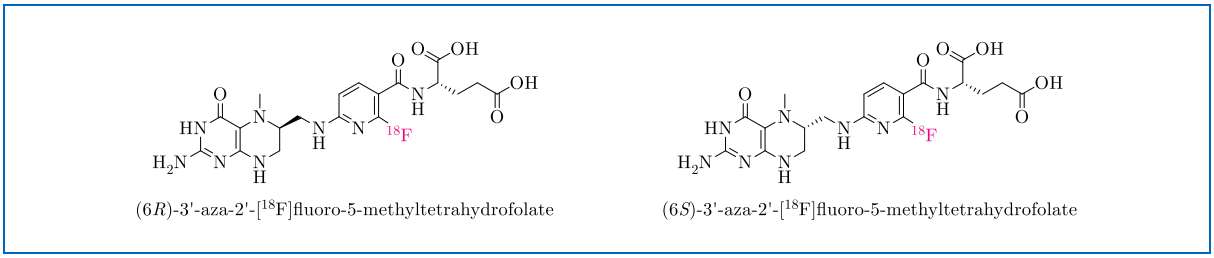

Figure 24. Chemical structures of the radiofluorinated FR ligands (6*R*)- and (6*S*)-3'-aza-2'-[^{18}F]fluoro-5-methyltetrahydrofolate[218].

For both 3'-aza-2'-[^{18}F]fluoro-5-methyltetrahydrofolates, biodistribution studies in mice at 3 h p.i. demonstrated remarkably high accumulation in KB tumor xenografts (32.3–34.8 %ID/g), which exceeded the uptake of [^{18}F]AzaFol (15.0 ± 2.3 %ID/g) determined under identical conditions and set new benchmarks for ^{18}F-labeled FR ligands[218]. Furthermore, PET/CT studies confirmed the exceptional KB tumor accumulation and evidenced relatively low background activity[218]. Despite these impressive tracer characteristics, production of both ^{18}F-labeled conjugates proved to be highly unfavorable (1–5% RCY) and further optimization work was recognized to be necessary for the establishment of a clinically applicable radiosynthesis protocol[218].

1.5 Objectives

Fluorine-18 has always attracted major interest in nuclear medicine due to the outstanding radionuclide properties that enable high-resolution PET imaging. However, its widespread use in radiotracers has ever since been hampered by significant limitations related to the ^{18}F-labeling chemistry. Therefore, considerable efforts have been dedicated to the development of novel radiofluorination techniques. The decisive breakthrough in simplifying ^{18}F-labeling seems to have been achieved in the last decade by several research groups thinking outside the box and focusing on radiofluorination methods beyond classical carbon-[^{18}F]fluorine chemistry.

In this regard, the promising strategy followed by *Schirrmacher*, *Jurkschat*, and colleagues of incorporating [^{18}F]fluoride into Silicon-based Fluoride Acceptors *via* isotopic exchange reaction has received particular attention. A major shortcoming, however, remains the marked lipophilic character of the labeling moiety, which results from the *tert*-butyl groups required to adequately stabilize the silicon-[^{18}F]fluorine bond against hydrolysis. Since this circumstance strongly affects the overall lipophilicity and thus the pharmacokinetic profile of respective radiotracers, the additional introduction of hydrophilic building blocks has proven to be mandatory. Within this context, it is of utmost importance to precisely adjust the tracer's lipophilicity in order to achieve an optimal distribution behavior *in vivo*. On the one hand, the lipophilic character should not be overly pronounced, as this would increase unspecific tracer binding and consequently reduce the imaging contrast. On the other hand, excessively high hydrophilicity would result in decreased specific uptake and rapid radiotracer elimination *via* the urinary tract, leading to substantial activity accumulation in the bladder. Such a premature excretion particularly compromises the detection of common gender-specific tumors in the pelvic region, including prostate cancer in men and ovarian carcinoma in women.

An initial goal of the present doctoral thesis was to optimize the radiofluorination of Silicon-based Fluoride Acceptors *via* isotopic exchange reaction. For this purpose, the labeling procedure describing the state of the art was first investigated and additionally characterized by kinetic measurements to determine the *Arrhenius parameters*. Striving to overcome various drawbacks in this regard, a novel [^{18}F]fluoride preparation technique was subsequently

elaborated and applied for the radiofluorination of novel Silicon-based Fluoride Acceptor-bearing radiopharmaceuticals developed in the second part of this work. A key feature of these newly designed ligands was the pharmacokinetic modifier (PKM), which was introduced to address the lipophilicity issue associated with the use of Silicon-based Fluoride Acceptors. In detail, the PKM structure was conceived of linked amino acids that were individually varied, with the further goal of fine-tuning the tracer's lipophilicity degree. Following this strategy, a balanced pharmacokinetic profile in terms of target accumulation and excretion was intended to be achieved. Since imaging of the aforementioned cancer types in the pelvic region would have particularly profited from such an approach, PSMA and FR were selected as target structures for the newly developed radiopharmaceuticals, namely siPSMA and ^{nat}Lu-rhFolate ligands. An overview of the objectives and strategies pursued in the present work is provided below (*Figure 25*).

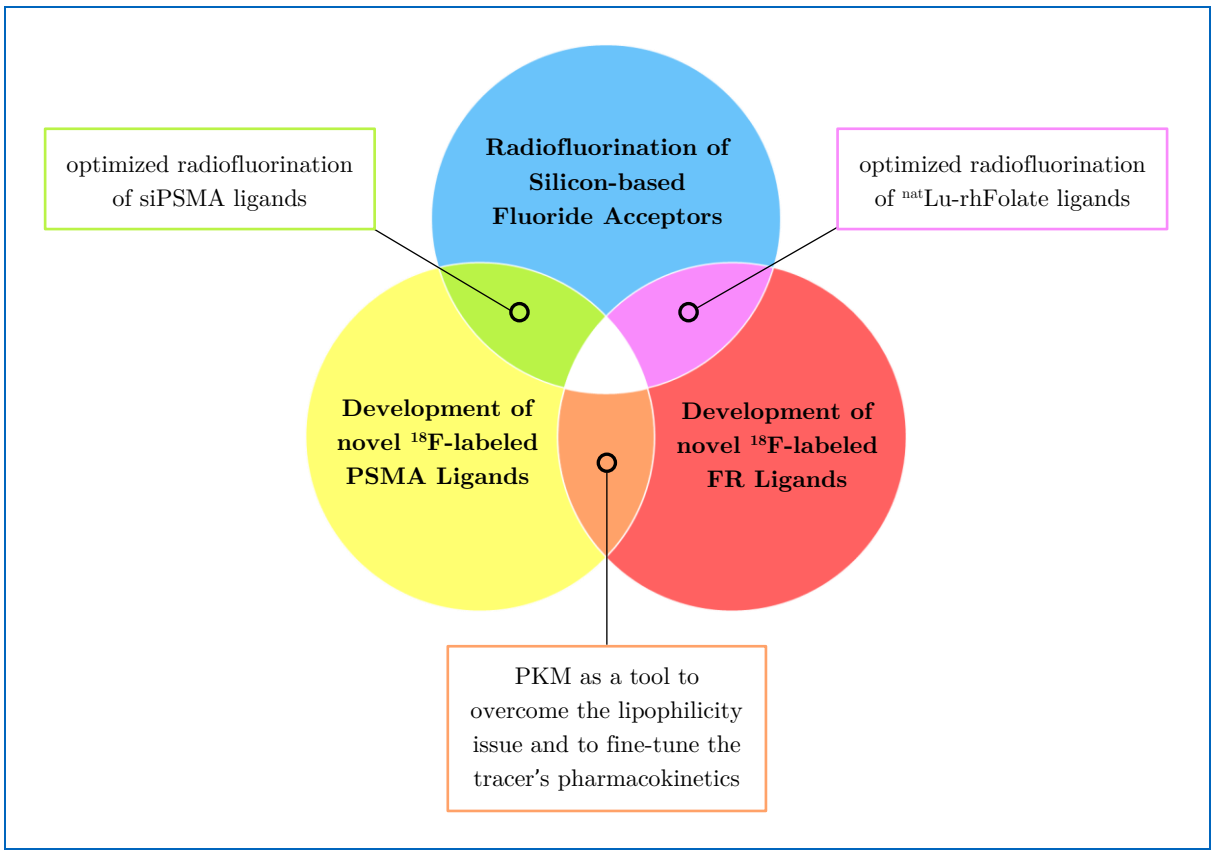

Figure 25. Objectives and strategies pursued in the present doctoral thesis for the development of novel ^{18}F-labeled radiopharmaceuticals comprising Silicon-based Fluoride Acceptors.

2 Experimental Section

2.1 Preparation of Building Blocks

2.1.1 Synthesis Equipment for Building Blocks

Reagents and solvents for the synthesis of building blocks were used in laboratory or reagent grade and purchased from either *Sigma-Aldrich Chemie GmbH* (Steinheim, Germany), *VWR International GmbH* (Darmstadt, Germany), *Alfa Aesar GmbH & Co. KG* (Karlsruhe, Germany), *Merck KGaA* (Darmstadt, Germany), or *ACROS Organics BVBA* (Geel, Belgium). In particular, di-*tert*-butyldifluorosilane as starting material for the preparation of Silicon-based Fluoride Acceptors was delivered by *Fluorochem Ltd.* (Hadfield, United Kingdom). Benzyl- (Bn-), *tert*-butyl- (*t*Bu-), and benzyloxycarbonyl- (Cbz-)protected amino acids (aspartic acid (Asp), glutamic acid (Glu), lysine (Lys)) for the synthesis of urea-based PSMA-binding motifs and building blocks, as well as preloaded 2-chlorotrityl (2-CT) resin were obtained from *Iris Biotech GmbH* (Marktredwitz, Germany). Pteroic acid and 2-(trimethylsilyl)ethanol for preparation of the 2-(trimethylsilyl)ethoxycarbonyl- (Teoc-)protected FR-binding motif were provided by *abcr GmbH* (Karlsruhe, Germany) and *TCI Deutschland GmbH* (Eschborn, Germany), respectively.

Precipitates were sedimented by ultracentrifugation using a Heraeus™ Megafuge™ 16R (*Fisher Scientific GmbH*, Schwerte, Germany).

For analytical (anal.) thin-layer chromatography (TLC) of reaction mixtures, a sample was chromatographed on a silica gel 60 F_{254} plate (*Merck KGaA*). Thereafter, the plate was analyzed under ultraviolet (UV) light at a wavelength (λ) of 254 nm or exposed to basic $KMnO_4$ in order to determine the retention factor (R_f).

Solvents for chromatography, including ethyl acetate (EtOAc, quality grade "≥99.5%, AnalaR NORMAPUR®"), petroleum ether (PE, quality grade "40/60"), *n*-hexane (quality grade "≥97%, HiPerSolv CHROMANORM®"), MeCN (quality grade "≥99.9%, HiPerSolv CHROMANORM®"), and trifluoroacetic acid (TFA, quality grade "≥99%, for synthesis") were supplied by *VWR International GmbH*, *Alfa Aesar GmbH & Co. KG*, and *Sigma-Aldrich*

Chemie GmbH. Water was obtained from a Barnstead™ MicroPure™ purification system (*Fisher Scientific GmbH*).

Manual flash column chromatography was carried out using silica gel (60 Å pore size, 40–63 µm particle size) obtained from *Sigma-Aldrich Chemie GmbH*, while automated flash chromatography was performed on a Biotage® SP1 HPFC system (*Biotage AB*, Uppsala, Sweden) equipped with a Biotage® SNAP KPC18-HS column (12 g weight, 93 Å pore size, 382 m^2/g surface area, 12 mL/min flow rate).

Preparative (prep.) purification and anal. characterization of building blocks was performed on HPLC systems from *Shimadzu Deutschland GmbH* (Neufahrn bei Freising, Germany), consisting of gradient pumps (two LC-20AD or an LC-20AT), a system controller (CBM-20A), a column oven (CTO-20A), and an UV-visible detector (SPD-20A). Employed columns for reversed-phase- (RP-)HPLC, including column I (Nucleosil® 100-5 C18, 125 × 4.6 mm dimension, 5 µm particle size, 1 mL/min flow rate), column III (MultoKrom® 100-5 C18, 125 × 4.6 mm dimension, 5 µm particle size, 1 mL/min flow rate), column IV (MultoKrom® 100-5 C18, 150 × 4.6 mm dimension, 5 µm particle size, 1 mL/min flow rate), and column V (MultoHigh® 100 RP 18-5µ, 250 × 10 mm dimension, 5 µm particle size, 5 mL/min flow rate) were purchased from *Macherey-Nagel GmbH & Co. KG* (Düren, Germany) and *CS-Chromatographie Service GmbH* (Langerwehe, Germany). Building blocks were eluted by applying different gradients of solvent A (water, additional (add.) 0.1% TFA, *v/v*) and solvent B (MeCN, add. 0.1% TFA, add. 2% water, *v/v/v*) or solvent C (MeCN, add. 0.1% TFA, add. 5% water, *v/v/v*) at a constant flow. LabSolutions 5.92 software by *Shimadzu Deutschland GmbH* was used for analysis of chromatograms, including retention time (t_R) and capacity factor (*K'*) determination.

Electrospray ionization (ESI) mass spectrometry (MS) characterization of synthesized compounds was conducted on an expression^L CMS mass spectrometer (*Advion Inc.*, Ithaca, NY, United States). Observed mass-to-charge ratios (*m/z*) were assigned to the calculated (calc.) molecular weight of ions based on the monoisotopic (m.i.) mass.

Nuclear magnetic resonance (NMR) spectra were recorded at 25°C on an AVANCE™III HD 300 (^{1}H: 300.13 MHz) or an AVANCE™III HD 500 (^{1}H: 500.13 MHz) spectrometer from *Bruker Inc.* (Billerica, MA, United States) and evaluated using MestReNova 14.1.1 software (*Mestrelab Research S.L.*, Santiago de Compostela, Spain). The chemical shifts (δ) were specified in parts per million (ppm) relative to the external standard tetramethylsilane. Signals in the NMR spectra were calibrated to the residual proton signal of the reference $CDCl_3$ (δ(^{1}H) = 7.26 ppm) and characterized in terms of multiplicity as singlet (s) or doublet (d). The coupling constants (*J*) were reported as averaged values and referred to couplings between two protons.

2.1.2 Synthesis of Silicon-based Fluoride Acceptor-bearing Building Blocks

The preparation of Silicon-based Fluoride Acceptor-bearing building blocks was carried out following previously published protocols[65, 77, 220]. Minor modifications were applied for the preparation of 4-(di-*tert*-butylfluorosilyl)benzoic acid (SiFA-BzA, **V**). In order to avoid the stepwise oxidation route, alcohol **III** was directly converted to the respective acid **V**. All spectroscopic data were consistent with those reported in the literature[65, 77, 220].

((4-Bromobenzyl)oxy)(*tert*-butyl)dimethylsilane (**I**)

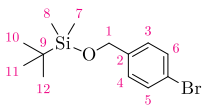

I

Chemical Formula: $C_{13}H_{21}BrOSi$
Molecular Weight: 301.30 g/mol

Imidazole (2.04 g, 30.0 mmol, 1.2 eq.) and *tert*-butyldimethylsilyl (TBDMS) chloride (4.52 g, 30.0 mmol, 1.2 eq.) were added to a solution of 4-bromobenzylalcohol (4.68 g, 25.0 mmol, 1.0 eq.) in anhyd. DMF (70 mL). The resulting mixture was stirred for 16 h at rt, subsequently poured into ice-cold water (250 mL) and extracted with diethyl ether (Et_2O, 5 × 50 mL). The combined organic layers were washed with saturated (sat.) aq. $NaHCO_3$ (2 × 100 mL) and sat. aq. NaCl (100 mL), dried over $MgSO_4$, filtered, and concentrated *in vacuo*. The resulting crude product was purified *via* flash column chromatography (silica gel, 5% EtOAc in PE, *v/v*), yielding **I** as a colorless oil (7.27 g, 24.1 mmol, 97%).

TLC: R_f (silica gel 60 F_{254}; 5% EtOAc in PE, *v/v*) = 0.87 [UV].

Anal. RP-HPLC (column I, 50→100% B in A, 15 min, λ = 220 nm): t_R = 14.0 min, *K'* = 8.9; MS (ESI, positive): *m/z* calc. m.i. mass ($C_{13}H_{21}BrOSi$): 300.1, *m/z* found: not detectable.

^{1}H-NMR (300.13 MHz, $CDCl_3$): δ [ppm] = 0.11 (s, 6 H, C7-H_3, C8-H_3), 0.96 (s, 9 H, C10-H_3, C11-H_3, C12-H_3), 4.77 (s, 2 H, C1-H_2), 7.34 (d, *J* = 7.9 Hz, 2 H, C3-H, C4-H), 7.57 (d, *J* = 8.0 Hz, 2 H, C5-H, C6-H).

Di-*tert*-butyl(4-(((*tert*-butyldimethylsilyl)oxy)methyl)phenyl)fluorosilane (**II**)

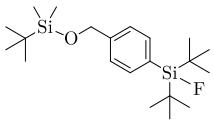

II

Chemical Formula: $C_{21}H_{39}FOSi_2$
Molecular Weight: 382.71 g/mol

A solution of 1.7 M *tert*-butyllithium (*t*BuLi) in *n*-pentane (9.37 mL, 15.9 mmol, 2.4 eq.) was added to a solution of ((4-bromobenzyl)oxy)(*tert*-butyl)dimethylsilane (**I**, 2.00 g, 6.64 mmol, 1.0 eq.) in anhyd. tetrahydrofuran (THF, 20 mL) at –78°C. The resulting yellow reaction mixture was stirred for 30 min at –78°C and then added dropwise to a stirred solution of di-*tert*-butyldifluorosilane (1.61 mL, 7.97 mmol, 1.2 eq.) in anhyd. THF (15 mL) at –78°C. Subsequently, the mixture was allowed to warm up to rt for 18 h, hydrolyzed with sat. aq. NaCl (120 mL), and extracted with Et_2O (4 × 100 mL). The combined organic phases were dried over $MgSO_4$, filtered, and concentrated *in vacuo*, affording **II** as a pale-yellow oil (2.77 g). The crude product was used for the next reaction step without further purification.

Anal. RP-HPLC (column I, 80→100% B in A, 20 min, λ = 220 nm): t_R = 16.9 min, *K'* = 11.0; MS (ESI, positive): *m/z* calc. m.i. mass ($C_{21}H_{39}FOSi_2$): 382.3, *m/z* found: not detectable.

(4-(Di-*tert*-butylfluorosilyl)phenyl)methanol (**III**)

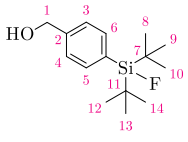

III

Chemical Formula: $C_{15}H_{25}FOSi$
Molecular Weight: 268.45 g/mol

A catalytic amount of aq. HCl (37%, *w/w*, 0.8 mL) was added to a solution of di-*tert*-butyl(4-(((*tert*-butyldimethylsilyl)oxy)methyl)phenyl)fluorosilane (**II**, 1.88 g, 4.91 mmol, 1.0 eq.) in

methanol (MeOH, 75 mL). The reaction mixture was stirred for 20 h at rt and subsequently concentrated *in vacuo*. Thereafter, the residue was redissolved in Et_2O (50 mL), washed with sat. aq. $NaHCO_3$ (50 mL), and extracted with Et_2O (3 × 50 mL). The combined organic fractions were dried over $MgSO_4$, filtered, and concentrated *in vacuo*, giving **III** as a yellowish oil (1.96 g). The crude product was used for the next reaction step without further purification.

Anal. RP-HPLC (column I, 50→100% B in A, 15 min, λ = 220 nm): t_R = 9.3 min, *K'* = 5.6; MS (ESI, positive): *m/z* calc. m.i. mass ($C_{15}H_{25}FOSi$): 268.2, *m/z* found: not detectable.

^{1}H-NMR (300.13 MHz, $CDCl_3$): δ [ppm] = 1.06 (s, 18 H, C8-H_3, C9-H_3, C10-H_3, C12-H_3, C13-H_3, C14-H_3), 4.71 (s, 2 H, C1-H_2), 7.38 (d, 2 H, *J* = 7.8 Hz, C5-H, C6-H), 7.61 (d, 2 H, *J* = 8.0 Hz, C3-H, C4-H).

(4-(Bromomethyl)phenyl)di-*tert*-butylfluorosilane (SiFA-BnBr, **IV**)

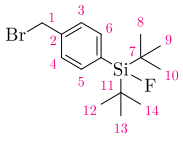

IV

Chemical Formula: $C_{15}H_{24}BrFSi$
Molecular Weight: 331.34 g/mol

Triphenylphosphine (1.88 g, 7.17 mmol, 1.1 eq.) was added in small portions over 1 h to an ice-cold solution of (4-(di-*tert*-butylfluorosilyl)phenyl)methanol (**III**, 1.75 g, 6.52 mmol, 1.0 eq.) and tetrabromomethane (2.38 g, 7.17 mmol, 1.1 eq.) in dichloromethane (DCM, 50 mL). The reaction mixture was stirred for 2 h at rt and subsequently concentrated *in vacuo*. Thereafter, the residue was washed with ice-cold *n*-hexane (75 mL) and the resulting mixture was filtered to remove the white precipitate. Finally, the clear solution was concentrated *in vacuo* and the crude product was purified *via* flash column chromatography (silica gel, 100% PE), yielding **IV** as a colorless solid (1.06 g, 3.20 mmol, 49%).

TLC: R_f (silica gel 60 F_{254}; 100% PE) = 0.51 [UV].

Anal. RP-HPLC (column I, 50→100% B in A, 15 min, λ = 220 nm): t_R = 11.2 min, *K'* = 6.9; MS (ESI, positive): *m/z* calc. m.i. mass ($C_{15}H_{24}BrFSi$): 330.1, *m/z* found: not detectable.

^{1}H-NMR (300.13 MHz, $CDCl_3$): δ [ppm] = 1.00 (s, 18 H, C8-H_3, C9-H_3, C10-H_3, C12-H_3, C13-H_3, C14-H_3), 4.71 (s, 2 H, C1-H_2), 7.28 (d, J = 7.8 Hz, 2 H, C5-H, C6-H), 7.51 (d, J = 8.0 Hz, 2 H, C3-H, C4-H).

4-(Di-*tert*-butylfluorosilyl)benzoic acid (SiFA-BzA, **V**)

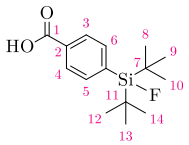

V

Chemical Formula: $C_{15}H_{23}FO_2Si$
Molecular Weight: 282.43 g/mol

(4-(Di-*tert*-butylfluorosilyl)phenyl)methanol (**III**, 6.61 g, 24.6 mmol, 1.0 eq.) was dissolved in a mixture of 1 M aq. $KMnO_4$ (37 mL, 36.9 mmol, 1.5 eq.), *tert*-butanol (*t*BuOH, 65 mL), DCM (9 mL), and 1.25 M aq. NaH_2PO_4 (65 mL, 81.3 mmol, 3.3 eq.). After stirring the reaction for 45 min at rt and cooling to 0°C, an excess of $KMnO_4$ (7.78 g, 49.2 mmol, 2.0 eq.) was added and the mixture was stirred for another 2 h at 0°C. The reaction was subsequently quenched by the addition of sat. aq. Na_2SO_3 (150 mL). Precipitated MnO_2 was dissolved with aq. HCl (37%, *w/w*, 20 mL) and the resulting solution was extracted with Et_2O (3 × 300 mL). The combined organic fractions were washed with sat. aq. $NaHCO_3$ (300 mL), dried over $MgSO_4$, filtered, and concentrated *in vacuo* to give a beige residue. The crude product was purified *via* recrystallization from a mixture (1:3, *v/v*, 10 mL) of Et_2O and *n*-hexane, affording **V** as a colorless solid (2.57 g, 9.10 mmol, 37%).

Anal. RP-HPLC (column I, 50→100% B in A, 15 min, λ = 220 nm): t_R = 8.5 min, K' = 5.0; MS (ESI, positive): *m/z* calc. m.i. mass ($C_{15}H_{23}FO_2Si$): 282.2, *m/z* found: not detectable.

^{1}H-NMR (500.13 MHz, $CDCl_3$): δ [ppm] = 1.07 (s, 18 H, C8-H_3, C9-H_3, C10-H_3, C12-H_3, C13-H_3, C14-H_3), 7.74 (d, J = 8.2 Hz, 2 H, C5-H, C6-H), 8.10 (d, J = 8.2 Hz, 2 H, C3-H, C4-H).

2.1.3 Synthesis of the Silicon-based Fluoride Acceptor Model Compound

N-Benzyl-4-(di-*tert*-butylfluorosilyl)benzamide (**VI**)

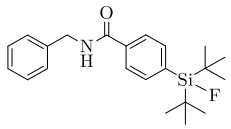

VI

Chemical Formula: $C_{22}H_{30}FNOSi$
Molecular Weight: 371.57 g/mol

A solution of SiFA-BzA (**V**, 10.0 mg, 35.4 µmol, 1.0 eq.), hydroxybenzotriazole (HOBt, 7.17 mg, 53.1 µmol, 1.5 eq.), *N,N,N',N'*-tetramethyl-*O*-(benzotriazol-1-yl)uronium tetrafluoroborate (TBTU, 17.0 mg, 53.1 µmol, 1.5 eq.), and *N,N*-diisopropylethylamine (DIPEA, 27.8 µL, 159 µmol, 4.5 eq.) in DMF (2 mL) was treated with benzylamine (3.87 µL, 35.4 µmol, 1.0 eq.). The mixture was stirred for 19 h at rt, concentrated *in vacuo*, and the resulting residue was finally purified *via* prep. RP-HPLC. *N*-Benzyl-4-(di-*tert*-butylfluorosilyl)benzamide (**VI**) was obtained as a colorless solid (5.56 mg, 15.0 µmol, 42%).

Prep. RP-HPLC (column V, 75→95% C in A, 20 min, λ = 220 nm): t_R = 11.7 min, *K'* = 5.3; anal. RP-HPLC (column I, 40→90% B in A, 15 min, λ = 220 nm): t_R = 12.9 min, *K'* = 8.1, purity: >99%; MS (ESI, positive): *m/z* calc. m.i. mass ($C_{22}H_{30}FNOSi$): 371.2, *m/z* found: 372.1 $[M+H]^+$, 743.2 $[2M+H]^+$.

2.1.4 Synthesis of protected PSMA-binding Motifs

The protected PSMA-binding motifs **X** and **XI** as well as precursor **VII** were prepared according to a literature procedure with slight modifications[221]. Synthesis of protected binding motifs **VIII** and **IX** was carried out analogously using H-L-Glu(OBn)-O*t*Bu · HCl instead of H-L-Lys(Cbz)-O*t*Bu · HCl as starting material[221].

(*S*)-di-*tert*-butyl 2-(1*H*-imidazole-1-carboxamido)pentanedioate (**VII**)

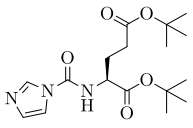

VII

Chemical Formula: $C_{17}H_{27}N_3O_5$
Molecular Weight: 353.42 g/mol

Under argon atmosphere, triethylamine (TEA, 3.90 mL, 28.0 mmol, 2.5 eq.) was added dropwise at rt to a solution of H-L-Glu(O*t*Bu)-O*t*Bu · HCl (3.31 g, 11.2 mmol, 1.0 eq.) and 4-dimethylaminopyridine (54.7 mg, 448 µmol, 0.04 eq.) in anhyd. DCM (25 mL), generating a white precipitate. The suspension was cooled to 0°C and added dropwise to an ice-cold solution of *N,N'*-carbonyldiimidazole (CDI, 2.00 g, 12.3 mmol, 1.1 eq.) in anhyd. DCM (25 mL). After stirring the resulting colorless solution overnight at rt, DCM (25 mL) was added and the organic phase was extracted with sat. aq. $NaHCO_3$ (30 mL), water (2 × 30 mL), and sat. aq. NaCl (30 mL). The organic fraction was finally concentrated *in vacuo*, giving **VII** as a yellowish gel (4.05 g). The crude product was used for the next reaction step without further purification.

Anal. RP-HPLC (column I, 10→90% B in A, 15 min, λ = 220 nm): t_R = 14.5 min, *K'* = 9.3; MS (ESI, positive): *m/z* calc. m.i. mass ($C_{17}H_{27}N_3O_5$): 353.2, *m/z* found: 376.3 $[M+Na]^+$.

*t*BuO-L-Glu(O*t*Bu)-urea-L-Glu(OBn)-O*t*Bu (**VIII**)

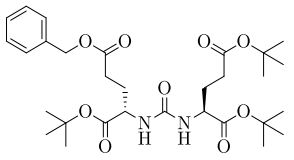

VIII

Chemical Formula: $C_{30}H_{46}N_2O_9$
Molecular Weight: 578.70 g/mol

A solution of (*S*)-di-*tert*-butyl 2-(1*H*-imidazole-1-carboxamido)pentanedioate (**VII**, 2.73 g, 7.73 mmol, 1.0 eq.) and H-L-Glu(OBn)-O*t*Bu · HCl (2.55 g, 7.73 mmol, 1.0 eq.) in 1,2-dichloroethane (DCE, 25 mL) was cooled to 0°C and treated dropwise with TEA (2.16 mL, 15.5 mmol, 2.0 eq.). The resulting reaction mixture was initially stirred for 1 h at 0°C, then for 5 h at rt, and finally overnight at 40°C. After concentrating the mixture *in vacuo*, the residue was redissolved in MeOH (5 mL) and purified *via* flash column chromatography (silica gel, 40→50% EtOAc in *n*-hexane, *v/v*) to yield **VIII** as a yellowish, viscous oil (3.89 g, 6.72 mmol, 87%).

Anal. RP-HPLC (column I, 10→90% B in A, 15 min, λ = 220 nm): t_R = 17.4 min, *K'* = 11.3; MS (ESI, positive): *m/z* calc. m.i. mass ($C_{30}H_{46}N_2O_9$): 578.3, *m/z* found: 411.3 $[M–3t\text{Bu}+H]^+$, 467.3 $[M–2t\text{Bu}+H]^+$, 523.3 $[M–t\text{Bu}+H]^+$, 601.5 $[M+Na]^+$.

*t*BuO-L-Glu(O*t*Bu)-urea-L-Glu-O*t*Bu (**IX**)

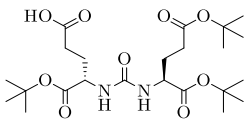

IX

Chemical Formula: $C_{23}H_{40}N_2O_9$
Molecular Weight: 488.58 g/mol

A solution of *t*BuO-L-Glu(O*t*Bu)-urea-L-Glu(OBn)-O*t*Bu (**VIII**, 3.89 g, 6.72 mmol, 1.0 eq.) in absolute (abs.) EtOH (35 mL) was treated with palladium on carbon (10%, *w/w*, 390 mg, 366 µmol, 0.05 eq.) and stirred overnight at rt under hydrogen atmosphere. The mixture was subsequently filtered through Celite® and concentrated *in vacuo*, affording **IX** as a colorless, hygroscopic solid (3.00 g, 6.14 mmol, 91%). The PSMA-binding motif was used for subsequent coupling reactions without further purification.

Anal. RP-HPLC (column I, 10→90% B in A, 15 min, λ = 220 nm): t_R = 11.3 min, *K'* = 7.0; MS (ESI, positive): *m/z* calc. m.i. mass ($C_{23}H_{40}N_2O_9$): 488.3, *m/z* found: 321.2 $[M–3tBu+H]^+$, 489.1 $[M+H]^+$, 511.4 $[M+Na]^+$.

*t*BuO-L-Glu(O*t*Bu)-urea-L-Lys(Cbz)-O*t*Bu (**X**)

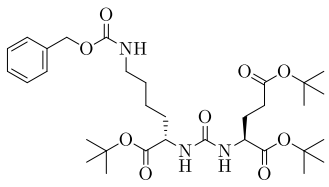

X

Chemical Formula: $C_{32}H_{51}N_3O_9$
Molecular Weight: 621.77 g/mol

A solution of (*S*)-di-*tert*-butyl 2-(1*H*-imidazole-1-carboxamido)pentanedioate (**VII**, 3.57 g, 10.1 mmol, 1.0 eq.) in DCE (45 mL) was cooled to 0°C and treated successively with TEA (2.82 mL, 20.2 mmol, 2.0 eq.) and H-L-Lys(Cbz)-O*t*Bu · HCl (4.14 g, 11.1 mmol, 1.1 eq.). The reaction mixture was stirred overnight at 40°C, subsequently washed with water (45 mL) and sat. aq. NaCl (45 mL), dried over $MgSO_4$, filtered, and concentrated *in vacuo*. The resulting crude product was purified *via* flash column chromatography (silica gel, 40% EtOAc in *n*-hexane, *v/v*) to give **X** as a colorless oil (5.04 g, 8.11 mmol, 80%).

TLC: R_f (silica gel 60 F_{254}; 5% EtOAc in *n*-hexane, *v/v*) = 0.45 [$KMnO_4$].

Anal. RP-HPLC (column III, 10→90% B in A, 15 min, λ = 220 nm): t_R = 14.9 min, *K'* = 6.9; MS (ESI, positive): *m/z* calc. m.i. mass ($C_{32}H_{51}N_3O_9$): 621.4, *m/z* found: 621.5 $[M+H]^+$, 1242.9 $[2M+H]^+$, 1264.8 $[2M+Na]^+$.

*t*BuO-L-Glu(O*t*Bu)-urea-L-Lys-O*t*Bu (**XI**)

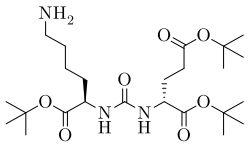

XI

Chemical Formula: $C_{24}H_{45}N_3O_7$
Molecular Weight: 487.64 g/mol

A solution of *t*BuO-L-Glu(O*t*Bu)-urea-L-Lys(Cbz)-O*t*Bu (**X**, 6.03 g, 9.70 mmol, 1.0 eq.) in abs. EtOH (150 mL) was treated with palladium on carbon (10%, *w/w*, 600 mg, 564 µmol, 0.06 eq.) and stirred overnight at rt under hydrogen atmosphere. Thereafter, the mixture was filtered through Celite® and concentrated *in vacuo*, yielding **XI** as a colorless, waxy solid (4.33 g, 8.88 mmol, 92%). The PSMA-binding motif was used for the subsequent coupling reaction without further purification.

Anal. RP-HPLC (column I, 10→90% B in A, 15 min, λ = 220 nm): t_R = 12.6 min, *K'* = 7.9; MS (ESI, positive): *m/z* calc. m.i. mass ($C_{24}H_{45}N_3O_7$): 487.3, *m/z* found: 488.3 $[M+H]^+$, 510.3 $[M+Na]^+$.

2.1.5 Synthesis of the protected FR-binding Motif

1-(2-*N*-Teoc-pteroyl)imidazole (**XII**)

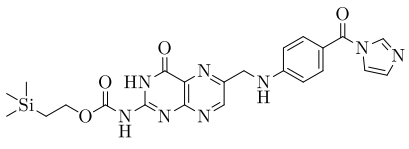

XII

Chemical Formula: $C_{23}H_{26}N_8O_4Si$
Molecular Weight: 506.60 g/mol

The Teoc-protected and imidazole-activated pteroic acid derivative **XII** was synthesized according to a reported protocol with some modifications[222]. A suspension of pteroic acid (400 mg, 1.28 mmol, 1.0 eq.) and CDI (831 mg, 5.13 mmol, 4.0 eq.) in DMSO (6 mL) was treated with TEA (715 µL, 5.13 mmol, 4.0 eq.) and stirred for 3 h at rt. Afterwards, 2-(trimethylsilyl)ethanol (1.47 mL, 10.3 mmol, 8.0 eq.) was added and the brownish solution

was stirred for another 4 h at rt. The reaction was subsequently poured into a mixture (1:1, *v/v*, 50 mL) of Et_2O and water, stirred for 15 min at rt, and ultracentrifuged (5˙300 revolutions per minute (rpm), 5 × 4 min). The collected yellow precipitate was washed with water (2 × 50 mL) and Et_2O (2 × 50 mL). Final drying *in vacuo* provided **XII** as a yellow solid (202 mg, 398 µmol, 31%). The protected FR-binding motif was used for subsequent coupling reactions without further purification.

Anal. RP-HPLC (column III, 10→90% B in A, 15 min, λ = 220 nm): t_R = 9.4 min, *K'* = 4.0; MS (ESI, positive): *m/z* calc. m.i. mass ($C_{23}H_{26}N_8O_4Si$): 506.2, *m/z* found: 506.6 $[M+H]^+$, 1012.9 $[2M+H]^+$.

2.1.6 Synthesis of further Building Blocks

*t*BuO-D-Glu(O*t*Bu)-urea-D-Glu-O*t*Bu (**XIII**)

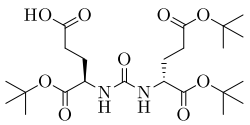

XIII

Chemical Formula: $C_{23}H_{40}N_2O_9$
Molecular Weight: 488.58 g/mol

*t*BuO-D-Glu(O*t*Bu)-urea-D-Glu-O*t*Bu (**XIII**) was synthesized in analogy to the previously described protected PSMA-binding motif **IX**[221]. By using H-D-Glu(O*t*Bu)-O*t*Bu · HCl as starting material, (*R*)-di-*tert*-butyl 2-(1*H*-imidazole-1-carboxamido)pentanedioate (1.48 g, 4.19 mmol, 91%) was prepared in a first reaction step. The subsequent coupling reaction with H-D-Glu(OBn)-O*t*Bu · HCl resulted in the formation of *t*BuO-D-Glu(O*t*Bu)-urea-D-Glu(OBn)-O*t*Bu (2.05 g, 3.54 mmol, 84%). After final Bn-deprotection, compound **XIII** was obtained as a colorless, hygroscopic solid (1.42 g, 2.91 mmol, 82%).

Anal. RP-HPLC (column I, 10→90% B in A, 15 min, λ = 220 nm): t_R = 12.0 min, *K'* = 7.5; MS (ESI, positive): *m/z* calc. m.i. mass ($C_{23}H_{40}N_2O_9$): 488.3, *m/z* found: 489.5 $[M+H]^+$.

3,5-Bis(*tert*-butoxycarbonyl)benzoic acid **(XIV)**

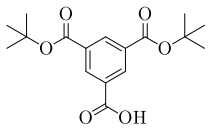

XIV

Chemical Formula: $C_{17}H_{22}O_6$
Molecular Weight: 322.36 g/mol

Trimesic acid (500 mg, 2.38 mmol, 1.0 eq.) and CDI (769 mg, 4.76 mmol, 2.0 eq.) were dissolved in DMF (10 mL) and the resulting solution was stirred for 1 h at 40°C. Afterwards, *t*BuOH (667 µL, 7.14 mmol, 3.0 eq.) as well as 1,8-diazabicyclo[5.4.0]undec-7-ene (707 µL, 4.76 mmol, 2.0 eq.) were added and the reaction mixture was stirred for another 24 h at 40°C. The mixture was finally concentrated *in vacuo* and the crude product was purified *via* automated flash chromatography, giving **XIV** as a colorless solid (310 mg, 962 µmol, 40%).

Automated flash chromatography (Biotage® SNAP KPC18-HS column, 30→80% C in A, 20 min, $\lambda = 220$ nm): $t_R = 15.5$ min; MS (ESI, negative): *m/z* calc. m.i. mass ($C_{17}H_{22}O_6$): 322.1, *m/z* found: 320.9 $[M–H]^-$.

SiFA-BzA-D-Asp-OH (**XV**)

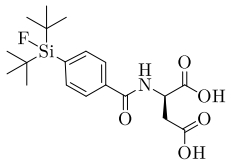

XV

Chemical Formula: $C_{19}H_{28}FNO_5Si$
Molecular Weight: 397.52 g/mol

A solution of SiFA-BzA (**V**, 79.0 mg, 280 µmol, 1.5 eq.), 1-hydroxy-7-azabenzotriazole (HOAt, 38.1 mg, 280 µmol, 1.5 eq.), and TBTU (89.8 mg, 280 µmol, 1.5 eq.) in DMF (5 mL) was treated with 2,4,6-collidine (111 µL, 839 µmol, 4.5 eq.) and pre-activated for 10 min at rt. Afterwards, the solution was added to a suspension of H-D-Asp(O*t*Bu)-2-CT resin (373 mg, 186 µmol, 1.0 eq.) in DMF (5 mL) and the mixture was stirred for 2 h at rt. The resin was subsequently filtered, washed with DCM (3 × 15 mL), and treated for 2 h at rt with a solution (95:2.5:2.5, *v/v/v*, 5 mL) of TFA, triisopropylsilane (TIPS), and water. The resin was separated by filtration and the solution was evaporated under a stream of nitrogen, yielding **XV** as a

colorless oil (126 mg). The building block was used for subsequent coupling reactions without further purification.

Anal. RP-HPLC (column IV, 10→90% B in A, 15 min, λ = 220 nm): t_R = 13.0 min, *K'* = 4.9; MS (ESI, positive): *m/z* calc. m.i. mass ($C_{19}H_{28}FNO_5Si$): 397.2, *m/z* found: 398.2 $[M+H]^+$.

2.2 Preparation of Compounds and Ligands

2.2.1 Synthesis Equipment for Compounds and Ligands

For solid-phase peptide synthesis (SPPS), 2-chlorotrityl chloride (2-CTC) resin was obtained from *Sigma-Aldrich Chemie GmbH*, while 9-fluorenylmethoxycarbonyl- (Fmoc-), 1-(4,4-dimethyl-2,6-dioxocyclohex-1-ylidene)ethyl- (Dde-), *tert*-butyloxycarbonyl- (Boc-), and *t*Bu-protected amino acids (8-amino-octanoic acid (8-Aoc), 8-amino-3,6-dioxaoctanoic acid (AEEAc), 6-aminohexanoic acid (Ahx), β-alanine (β-Ala), Asp, citrulline (Cit), 2,3-diaminopropionic acid (Dap), Glu, glycine (Gly), Lys, ornithine (Orn), phenylalanine (Phe), threonine (Thr), tyrosine (Tyr)) were delivered by *Iris Biotech GmbH*, *Carbolution Chemicals GmbH* (St. Ingbert, Germany), or *Bachem AG* (Bubendorf, Switzerland). Further reagents and solvents were used in laboratory or reagent grade and purchased from either *Sigma-Aldrich Chemie GmbH*, *VWR International GmbH*, *Alfa Aesar GmbH & Co. KG*, *Merck KGaA*, or *ACROS Organics BVBA*. In particular, *CheMatech SAS* (Dijon, France) supplied the macrocyclic chelator DOTA(O*t*Bu)$_3$. Water was obtained from a Barnstead™ MicroPure™ purification system (*Fisher Scientific GmbH*), while pure water (quality grade "Tracepur®") was delivered by *Merck KGaA*.

Synthesis of compounds and ligands was carried out manually *via* SPPS using the IntelliMixer™ RM-2 from *neoLab Migge GmbH* (Heidelberg, Germany).

Anal. characterization and prep. purification of compounds and ligands was performed on the aforementioned (*Section 2.1.1*) HPLC systems (*Shimadzu Deutschland GmbH*). Employed columns for RP-HPLC, including column II (Multospher® 100 RP 18-5µ, 125 × 4.6 mm dimension, 5 µm particle size, 1 mL/min flow rate), column III (MultoKrom® 100-5 C18, 125 × 4.6 mm dimension, 5 µm particle size, 1 mL/min flow rate), column IV (MultoKrom® 100-5 C18, 150 × 4.6 mm dimension, 5 µm particle size, 1 mL/min flow rate), column V (MultoHigh® 100 RP 18-5µ, 250 × 10 mm dimension, 5 µm particle size, 5 mL/min flow rate), column VI (Multospher® 100 RP 18-5µ, 250 × 10 mm dimension, 5 µm particle size, 5 mL/min flow rate), column VII (MultoKrom® 100-5 C18, 150 × 10 mm dimension, 5 µm particle size, 5 mL/min flow rate), column VIII (MultoKrom® 100-5 C18, 150 × 20 mm

dimension, 5 µm particle size, 5 mL/min flow rate), column IX (MultoKrom® 100-5 C18, 250 × 10 mm dimension, 5 µm particle size, 5 mL/min flow rate), and column X (MultoKrom® 100-5 C18, 250 × 20 mm dimension, 5 µm particle size, 8 mL/min flow rate) were delivered by *CS-Chromatographie Service GmbH*. Compounds and ligands were eluted by applying different gradients of the previously described (*Section 2.1.1*) solvent A and solvent B or solvent C at a constant flow. LabSolutions 5.92 software (*Shimadzu Deutschland GmbH*) was again used for analysis of chromatograms, while the expression^{L} CMS mass spectrometer (*Advion Inc.*) was employed for ESI-MS characterization.

Purified compounds and ligands were obtained as fluffy powders by lyophilization using the Christ Martin™ freeze dryer Alpha 1-4 LSC (*Martin Christ Gefriertrocknungsanlagen GmbH*, Osterode am Harz, Germany).

2.2.2 General Synthesis Procedures

Compounds and ligands were prepared *via* Fmoc-based SPPS following various literature protocols with minor changes[223-226]. Prior to a deprotection or coupling reaction according to GSP2, GSP3, and GSP4, the loaded resin was swollen for at least 30 min at rt in *N*-methyl-2-pyrrolidone (NMP). This procedure was omitted in the case of resin loading (GSP1) or final cleavage from the resin (GSP5). For coupling reaction control, a small amount of peptide-loaded resin was treated for 10 min at rt with either TFA (200 µL, method A) or a mixture (1:4, *v/v*, 200 µL, method B) of 1,1,1,3,3,3-hexafluoropropan-2-ol in DCM[223, 227]. After separation from the resin, the solution was evaporated under a stream of nitrogen. The residue was subsequently redissolved in a mixture (1:1, *v/v*, 100 µL) of MeCN/water and a sample thereof was analyzed by RP-HPLC. ^{nat}Lu-complexation of chelator-bearing compounds (GSP6) was accomplished in accordance with a modified literature procedure[228].

GSP1 Resin Loading

2-CTC resin (1.60 mmol/g, 1.0 eq.) was transferred into a syringe and swollen for 5 min at rt with the dissolved Fmoc-protected amino acid (1.5 eq.) in a mixture (10 mL/g of resin) of DIPEA (1.3 eq.) in DMF. Afterwards, the solution was treated with a second portion of DIPEA (2.6 eq.) and shaken with the resin for another 1.5 h at rt. For end-capping, MeOH (1 mL/g

of resin) was added to the solution and shaken with the resin for 15 min at rt. The resin was filtered, washed successively with DMF (3 × 15 mL/g of resin), MeOH (3 × 15 mL/g of resin), DCM (3 × 15 mL/g of resin), and finally dried *in vacuo*. The resin loading was calculated according to the following equation (*Formula 1*)[136].

$$\rho = \frac{(m_2 - m_1)}{(MW - 36.46\ \text{g/mol}) \cdot m_2}$$

ρ = resin loading [mol/g]
MW = molecular weight of coupled amino acid [g/mol]
m_1 = mass of dry resin before loading [g]
m_2 = mass of dry resin after loading [g]

Formula 1. Calculation of the resin loading[136].

GSP2 On-resin Fmoc-Deprotection

Cleavage of an Fmoc-protected amine functionality was achieved by treating the swollen resin twice with a solution (1:4, *v/v*, 15 mL/g of resin) of piperidine (Pip) in DMF for 5 min and 15 min at rt, respectively. For resin-bound compounds bearing a Dde-protecting group besides Fmoc, the deprotection was performed twice for 5 min at rt. The resin was subsequently filtered and washed thoroughly with DMF (7 × 15 mL/g of resin).

GSP3 On-resin Coupling Reaction

a) Coupling reaction with amino acids or carboxyl-bearing compounds

The amino acid or the carboxyl-bearing compound (1.5–3.0 eq.), HOAt (1.5–3.0 eq.), and TBTU (1.5–3.0 eq.) were dissolved in DMF (10 mL/g of resin), and 2,4,6-collidine (4.5–9.0 eq.) was added. The solution was pre-activated for 10 min at rt, transferred into the syringe containing the swollen resin (1.0 eq.), and shaken for 1.5 h at rt. Finally, the resin was filtered, followed by washing with DMF (3 × 15 mL/g of resin) and DCM (3 × 15 mL/g of resin).

b) Coupling reaction with succinic anhydride

A solution of succinic anhydride (7.0 eq.) and DIPEA (7.0 eq.) in DMF (10 mL/g of resin) was transferred into the syringe containing the swollen resin (1.0 eq.) and shaken for 12 h at rt.

The resin was subsequently filtered, followed by washing with DMF (3 × 15 mL/g of resin) and DCM (3 × 15 mL/g of resin).

c) Coupling reaction with SiFA-BzA

SiFA-BzA (**V**, 2.0 eq.), HOAt (2.0 eq.), and TBTU (2.0 eq.) were dissolved in DMF (10 mL/g of resin), and 2,4,6-collidine (6.0 eq.) was added. After pre-activation for 10 min at rt, the mixture was transferred into the syringe containing the swollen resin (1.0 eq.) and shaken for 2 h at rt. The resin was finally filtered, followed by washing with DMF (3 × 15 mL/g of resin) and DCM (3 × 15 mL/g of resin).

d) Coupling reaction with SiFA-BnBr

A solution of SiFA-BnBr (**IV**, 3.0 eq.) and 2,4,6-collidine (6.0 eq.) in DCM (10 mL/g of resin) was shaken with the swollen resin (1.0 eq.) for 16 h at rt. The resin was subsequently filtered and washed with DCM (3 × 15 mL/g of resin).

e) Coupling reaction with DOTA(OtBu)$_3$

DOTA(O*t*Bu)$_3$ (2.0 eq.), HOAt (2.0 eq.), and TBTU (2.0 eq.) were dissolved in DMF (10 mL/g of resin), and 2,4,6-collidine (6.0 eq.) was added. After pre-activation for 10 min at rt, the mixture was transferred into the syringe containing the swollen resin (1.0 eq.) and shaken for 2 h at rt. The resin was subsequently filtered, followed by washing with DMF (3 × 15 mL/g of resin) and DCM (3 × 15 mL/g of resin).

f) Coupling reaction with 1-(2-N-Teoc-pteroyl)imidazole

1-(2-*N*-Teoc-pteroyl)imidazole (**XII**, 3.0 eq.), HOAt (3.0 eq.), and benzotriazol-1-yl-oxytri-pyrrolidinophosphonium hexafluorophosphate (PyBOP, 3.0 eq.) were dissolved in DMSO (10 mL/g of resin), and DIPEA (9.0 eq.) was added. The mixture was transferred into the syringe containing the swollen resin (1.0 eq.) and shaken for 3 h at rt. Afterwards, the resin was filtered and washed successively with DMSO (3 × 15 mL/g of resin), DMF (3 × 15 mL/g of resin), and DCM (3 × 15 mL/g of resin).

GSP4 On-resin Dde-Deprotection

a) Dde-deprotection in absence of an Fmoc-protecting group

In absence of an Fmoc-protecting group, Dde-deprotection of amino acids was carried out by treating the swollen resin with a solution (1:50, *v/v*, 15 mL/g of resin) of hydrazine monohydrate in DMF for 20 min at rt. The resin was subsequently filtered and washed thoroughly with DMF (7 × 15 mL/g of resin) and DCM (3 × 15 mL/g of resin).

b) Selective Dde-deprotection in presence of an Fmoc-protecting group

In presence of an Fmoc-protecting group, Dde-deprotection of amino acids was performed by treating the swollen resin (1.0 eq.) twice with a solution of imidazole (90 eq.) and hydroxylamine hydrochloride (120 eq.) in a mixture (1:5, *v/v*, 15 mL/g of resin) of DCM in NMP for 1.5 h at rt. Thereafter, the resin was filtered and washed thoroughly with DMF (7 × 15 mL/g of resin) and DCM (3 × 15 mL/g of resin).

GSP5 Cleavage of resin-bound Compounds and Final Deprotection

a) Cleavage from the resin and final deprotection in absence of DOTA(OtBu)$_3$

The resin-bound compound with acid-labile protecting groups was treated twice with a solution (95:2.5:2.5, *v/v/v*, 10 mL/g of resin) of TFA, TIPS, and water for respectively 1 h at rt and subsequently washed with the cleavage cocktail (10 mL/g of resin). Thereafter, the combined acidic fractions were concentrated under a stream of nitrogen, and the residue was redissolved in an appropriate solvent for prep. RP-HPLC purification.

b) Cleavage from the resin and final deprotection in presence of DOTA(OtBu)$_3$

The resin-bound compound containing acid-labile protecting groups was treated twice with a solution (95:2.5:2.5, *v/v/v*, 10 mL/g of resin) of TFA, TIPS, and water for respectively 1 h at rt and subsequently washed with the cleavage cocktail (10 mL/g of resin). Thereafter, the combined acidic fractions were stirred for 6 h at rt to ensure quantitative deprotection of the chelator. The solution was finally concentrated under a stream of nitrogen, and the residue was redissolved in an appropriate solvent for prep. RP-HPLC purification.

GSP6 ^{nat}Lu-Complexation of DOTA

For ^{nat}Lu-complexation of DOTA, a solution of the chelator-bearing compound (4 mM, 1.0 eq.) in DMSO was combined with a solution of $LuCl_3$ (20 mM, 5.0 eq.) in pure water, and the mixture was heated at 95°C for 30 min. The solution as a whole was subjected to subsequent prep. RP-HPLC purification.

2.2.3 Synthesis of siPSMA Ligands

*t*BuO-L-Glu(O*t*Bu)-urea-L-Glu(D-Orn-2-CT resin)-O*t*Bu (**XVI**)

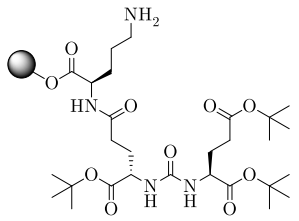

XVI

Chemical Formula: $C_{28}H_{50}N_4O_{10}$
Molecular Weight: 602.73 g/mol

2-CTC resin was loaded with Fmoc-D-Orn(Dde)-OH (GSP1). The amino acid was subsequently Fmoc-deprotected (GSP2) and the resulting N^{α}-amine was coupled to *t*BuO-L-Glu(O*t*Bu)-urea-L-Glu-O*t*Bu (**IX**) according to GSP3a. The resin-bound peptide was finally Dde-deprotected (GSP4a), yielding the PSMA ligand precursor **XVI**.

Coupling reaction control: method B; anal. RP-HPLC (column III, 10→90% B in A, 15 min, λ = 220 nm): t_R = 9.3 min, K' = 3.9; MS (ESI, positive): *m/z* calc. m.i. mass ($C_{28}H_{50}N_4O_{10}$): 602.4, *m/z* found: 602.5 $[M+H]^+$, 1204.7 $[2M+H]^+$.

*t*BuO-L-Glu(O*t*Bu)-urea-L-Glu(D-Orn(Suc(H-D-Lys-O*t*Bu))-2-CT resin)-O*t*Bu (**XVII**)

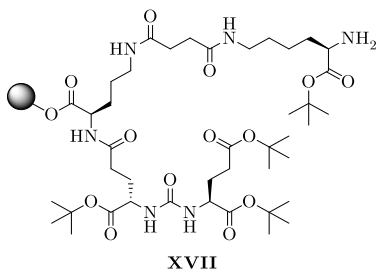

XVII

Chemical Formula: $C_{42}H_{74}N_6O_{14}$
Molecular Weight: 887.08 g/mol

The N^{δ}-amine of the resin-bound precursor **XVI** was reacted with succinic anhydride (GSP3b). Afterwards, Fmoc-D-Lys-O*t*Bu was coupled to the carboxylate functionality resulting from the

anhydride opening (GSP3a). The resin-bound peptide was finally Fmoc-deprotected (GSP2), affording the PSMA ligand precursor **XVII**.

Coupling reaction control: method B; anal. RP-HPLC (column III, 10→90% B in A, 15 min, λ = 220 nm): t_R = 10.0 min, *K'* = 4.3; MS (ESI, positive): *m/z* calc. m.i. mass ($C_{42}H_{74}N_6O_{14}$): 886.5, *m/z* found: 443.7 $[M+2H]^{2+}$, 886.6 $[M+H]^+$.

*t*BuO-L-Glu(O*t*Bu)-urea-L-Glu(D-Orn(Suc(H-D-Dap(SiFA-BzA)-D-Lys-O*t*Bu))-2-CT resin)-O*t*Bu (**XVIII**)

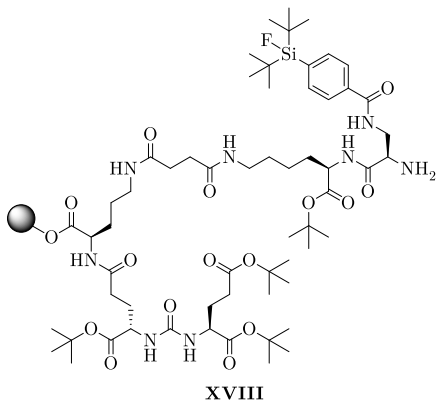

XVIII

Chemical Formula: $C_{60}H_{101}FN_8O_{16}Si$
Molecular Weight: 1237.59 g/mol

The N^{α}-amine of the resin-bound precursor **XVII** was coupled to Fmoc-D-Dap(Dde)-OH (GSP3a) and the peptide was subsequently Dde-deprotected (GSP4b). The resulting N^{β}-amine was coupled to SiFA-BzA (**V**) following GSP3c. The Fmoc-protecting group was finally cleaved (GSP2), giving the PSMA ligand precursor **XVIII**.

Coupling reaction control: method A; anal. RP-HPLC (column IV, 10→70% B in A, 15 min, λ = 220 nm): t_R = 11.4 min, *K'* = 4.2; MS (ESI, positive): *m/z* calc. m.i. mass ($C_{60}H_{101}FN_8O_{16}Si$): 1236.7, *m/z* found: 507.6 $[M–4t\text{Bu}+2H]^{2+}$, 1014.1 $[M–4t\text{Bu}+H]^+$.

*t*BuO-L-Glu(O*t*Bu)-urea-L-Glu(D-Lys(H-D-Orn(Dde))-2-CT resin)-O*t*Bu (**XIX**)

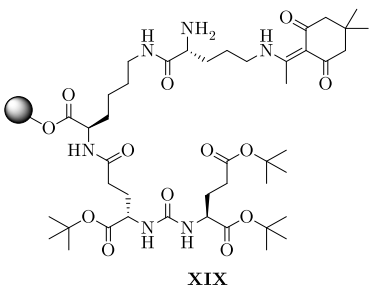

XIX

Chemical Formula: $C_{44}H_{74}N_6O_{13}$
Molecular Weight: 895.11 g/mol

2-CTC resin was loaded with Fmoc-D-Lys(Dde)-OH (GSP1). The amino acid was subsequently Fmoc-deprotected (GSP2) and the resulting N^{α}-amine was coupled to *t*BuO-L-Glu(O*t*Bu)-urea-L-Glu-O*t*Bu (**IX**) according to GSP3a. After cleavage of the Dde-protecting group (GSP4a), the resulting N^{ε}-amine was coupled to Fmoc-D-Orn(Dde)-OH (GSP3a). The resin-bound peptide was finally Fmoc-deprotected (GSP2), yielding the PSMA ligand precursor **XIX**.

Coupling reaction control: method A; anal. RP-HPLC (column III, 10→90% B in A, 15 min, λ = 220 nm): t_R = 5.0 min, *K'* = 1.7; MS (ESI, positive): *m/z* calc. m.i. mass ($C_{44}H_{74}N_6O_{13}$): 894.5, *m/z* found: 726.4 $[M–3tBu+H]^+$, 1453.0 $[2M–6tBu+H]^+$.

siPSMA-**0a**

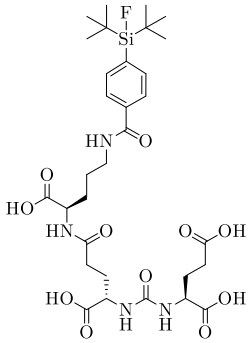

siPSMA-**0a**
Chemical Formula: $C_{31}H_{47}FN_4O_{11}Si$
Molecular Weight: 698.82 g/mol

Resin-bound ligand precursor **XVI** was coupled with SiFA-BzA (**V**) according to GSP3c. The ligand was subsequently cleaved from the resin under removal of acid-labile *t*Bu-protecting groups (GSP5a), followed by purification *via* prep. RP-HPLC. siPSMA-**0a** was afforded as a colorless solid.

siPSMA-**0a**: Prep. RP-HPLC (column IX, 45→55% C in A, 20 min, λ = 220 nm): t_R = 14.3 min, *K'* = 7.2; yield: 2.68 mg (3.84 µmol, 39%); anal. RP-HPLC (column IV, 10→70% B in A, 15 min, λ = 220 nm): t_R = 13.9 min, *K'* = 5.3, purity: >99%; MS (ESI, positive): *m/z* calc. m.i. mass ($C_{31}H_{47}FN_4O_{11}Si$): 698.3, *m/z* found: 699.1 $[M+H]^+$, 1397.4 $[2M+H]^+$.

siPSMA-**0b**

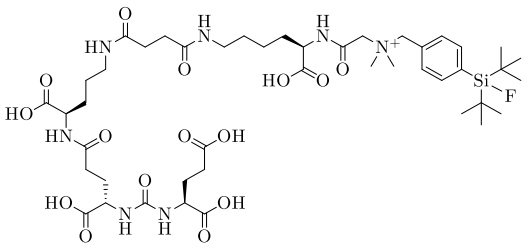

siPSMA-**0b**
Chemical Formula: $C_{45}H_{73}FN_7O_{15}Si^+$
Molecular Weight: 999.20 g/mol

Resin-bound ligand precursor **XVII** was coupled with *N,N*-dimethyl-Gly-OH following GSP3a. Afterwards, SiFA-BnBr (**IV**) was coupled to the dimethylated amine according to GSP3d. The ligand was finally cleaved from the resin under removal of acid-labile *t*Bu-protecting groups (GSP5a), followed by purification *via* prep. RP-HPLC. siPSMA-**0b** was obtained as a colorless solid.

siPSMA-**0b**: Prep. RP-HPLC (column IX, 40→50% C in A, 20 min, λ = 220 nm): t_R = 12.5 min, *K'* = 6.1; yield: 2.15 mg (1.93 µmol, 12%); anal. RP-HPLC (column IV, 10→70% B in A, 15 min, λ = 220 nm): t_R = 11.5 min, *K'* = 4.2, purity: >99%; MS (ESI, positive): *m/z* calc. m.i. mass ($C_{45}H_{73}FN_7O_{15}Si^+$): 998.5, *m/z* found: 500.0 $[M+H]^{2+}$, 998.9 $[M]^+$.

siPSMA-**01** to **-06α** and siPSMA-**07** to **-09**

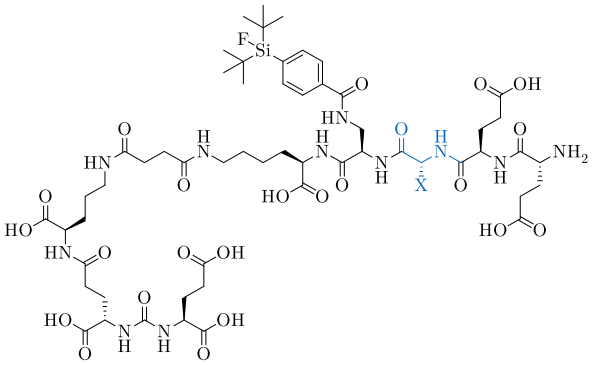

siPSMA-**01** to **-06α** and siPSMA-**07** to **-09**

siPSMA-**01**
X = CH_2COOH: D-Asp
Chemical Formula: $C_{58}H_{88}FN_{11}O_{25}Si$
Molecular Weight: 1386.48 g/mol

siPSMA-**02**
X = $(CH_2)_2COOH$: D-Glu
Chemical Formula: $C_{59}H_{90}FN_{11}O_{25}Si$
Molecular Weight: 1400.50 g/mol

siPSMA-**03**
X = $CH(OH)CH_3$: D-Thr
Chemical Formula: $C_{58}H_{90}FN_{11}O_{24}Si$
Molecular Weight: 1372.49 g/mol

siPSMA-**04**
X = $(CH_2)_3NHCONH_2$: D-Cit
Chemical Formula: $C_{60}H_{94}FN_{13}O_{24}Si$
Molecular Weight: 1428.56 g/mol

siPSMA-**05**
X = $CH_2C_6H_5$: D-Phe
Chemical Formula: $C_{63}H_{92}FN_{11}O_{23}Si$
Molecular Weight: 1418.57 g/mol

siPSMA-**06α**
X = CH_2NH_2: D-Dap
Chemical Formula: $C_{57}H_{89}FN_{12}O_{23}Si$
Molecular Weight: 1357.48 g/mol

siPSMA-**07**
X = $(CH_2)_3NH_2$: D-Orn
Chemical Formula: $C_{59}H_{93}FN_{12}O_{23}Si$
Molecular Weight: 1385.54 g/mol

siPSMA-**08**
X = $(CH_2)_4NH_2$: D-Lys
Chemical Formula: $C_{60}H_{95}FN_{12}O_{23}Si$
Molecular Weight: 1399.56 g/mol

siPSMA-**09**
X = H: Gly
Chemical Formula: $C_{56}H_{86}FN_{11}O_{23}Si$
Molecular Weight: 1328.44 g/mol

Resin-bound ligand precursor **XVIII** was coupled with the respective Fmoc-protected amino acid (Fmoc-D-Asp(O*t*Bu)-OH, Fmoc-D-Glu(O*t*Bu)-OH, Fmoc-D-Thr(*t*Bu)-OH, Fmoc-D-Cit-OH, Fmoc-D-Phe-OH, Fmoc-D-Dap(Boc)-OH, Fmoc-D-Orn(Boc)-OH, Fmoc-D-Lys(Boc)-OH, or Fmoc-Gly-OH) according to GSP3a. After cleavage of the Fmoc-protecting group (GSP2), the resulting N^{α}-amine was coupled to Fmoc-D-Glu(O*t*Bu)-OH (GSP3a) and the peptide was again Fmoc-deprotected (GSP2). This procedure was repeated one more time. The ligands were finally cleaved from the resin under removal of acid-labile protecting groups (GSP5a), followed by purification *via* prep. RP-HPLC. siPSMA-**01** to **-06α** and siPSMA-**07** to **-09** were isolated as colorless solids.

siPSMA-**01**: Prep. RP-HPLC (column IX, 38→45% C in A, 20 min, λ = 220 nm): t_R = 13.6 min, *K'* = 6.8; yield: 5.06 mg (3.37 µmol, 25%); anal. RP-HPLC (column II, 10→70% B in A, 15 min, λ = 220 nm): t_R = 11.3 min, *K'* = 7.1,

purity: 96%; MS (ESI, positive): *m/z* calc. m.i. mass ($C_{58}H_{88}FN_{11}O_{25}Si$): 1385.6, *m/z* found: 694.1 $[M+2H]^{2+}$, 1387.0 $[M+H]^{+}$.

siPSMA-**02**: Prep. RP-HPLC (column IX, 38→45% C in A, 20 min, λ = 220 nm): t_R = 7.8 min, *K'* = 3.5; yield: 5.10 mg (3.37 µmol, 25%); anal. RP-HPLC (column II, 10→70% B in A, 15 min, λ = 220 nm): t_R = 11.4 min, *K'* = 7.2, purity: 98%; MS (ESI, positive): *m/z* calc. m.i. mass ($C_{59}H_{90}FN_{11}O_{25}Si$): 1399.6, *m/z* found: 701.2 $[M+2H]^{2+}$, 1401.0 $[M+H]^{+}$.

siPSMA-**03**: Prep. RP-HPLC (column IX, 38→45% C in A, 20 min, λ = 220 nm): t_R = 9.5 min, *K'* = 4.4; yield: 4.38 mg (2.95 µmol, 28%); anal. RP-HPLC (column IV, 10→70% B in A, 15 min, λ = 220 nm): t_R = 10.2 min, *K'* = 3.6, purity: >99%; MS (ESI, positive): *m/z* calc. m.i. mass ($C_{58}H_{90}FN_{11}O_{24}Si$): 1371.6, *m/z* found: 687.1 $[M+2H]^{2+}$, 1372.8 $[M+H]^{+}$.

siPSMA-**04**: Prep. RP-HPLC (column IX, 38→45% C in A, 20 min, λ = 220 nm): t_R = 7.0 min, *K'* = 3.0; yield: 5.40 mg (3.50 µmol, 31%); anal. RP-HPLC (column II, 10→70% B in A, 15 min, λ = 220 nm): t_R = 11.0 min, *K'* = 6.9, purity: 98%; MS (ESI, positive): *m/z* calc. m.i. mass ($C_{60}H_{94}FN_{13}O_{24}Si$): 1427.6, *m/z* found: 715.2 $[M+2H]^{2+}$, 1428.8 $[M+H]^{+}$.

siPSMA-**05**: Prep. RP-HPLC (column IX, 40→50% C in A, 20 min, λ = 220 nm): t_R = 12.4 min, *K'* = 6.1; yield: 5.35 mg (3.49 µmol, 31%); anal. RP-HPLC (column IV, 10→70% B in A, 15 min, λ = 220 nm): t_R = 11.3 min, *K'* = 4.1, purity: 99%; MS (ESI, positive): *m/z* calc. m.i. mass ($C_{63}H_{92}FN_{11}O_{23}Si$): 1417.6, *m/z* found: 710.1 $[M+2H]^{2+}$, 1418.9 $[M+H]^{+}$.

siPSMA-**06α**: Prep. RP-HPLC (column IX, 38→45% C in A, 20 min, λ = 220 nm): t_R = 5.4 min, *K'* = 2.1; yield: 4.65 mg (3.16 µmol, 46%); anal. RP-HPLC (column II, 10→70% B in A, 15 min, λ = 220 nm): t_R = 10.8 min, *K'* = 6.8, purity: 97%; MS (ESI, positive): *m/z* calc. m.i. mass ($C_{57}H_{89}FN_{12}O_{23}Si$): 1356.6, *m/z* found: 679.7 $[M+2H]^{2+}$, 1358.0 $[M+H]^{+}$.

siPSMA-**07**: Prep. RP-HPLC (column IX, 35→40% C in A, 20 min, λ = 220 nm): t_R = 10.2 min, *K'* = 4.8; yield: 4.51 mg (2.80 µmol, 25%); anal. RP-HPLC (column IV, 10→70% B in A, 15 min, λ = 220 nm): t_R = 9.6 min, *K'* = 3.4, purity: 98%; MS (ESI, positive): *m/z* calc. m.i. mass ($C_{59}H_{93}FN_{12}O_{23}Si$): 1384.6, *m/z* found: 693.8 $[M+2H]^{2+}$, 1386.7 $[M+H]^{+}$.

siPSMA-**08**: Prep. RP-HPLC (column IX, 35→45% C in A, 20 min, λ = 220 nm): t_R = 7.5 min, *K'* = 3.3; yield: 7.44 mg (4.57 µmol, 40%); anal. RP-HPLC (column IV, 10→70% B in A, 15 min, λ = 220 nm): t_R = 9.9 min, *K'* = 3.5, purity: 95%; MS (ESI, positive): *m/z* calc. m.i. mass ($C_{60}H_{95}FN_{12}O_{23}Si$): 1398.6, *m/z* found: 700.9 $[M+2H]^{2+}$, 1400.8 $[M+H]^{+}$.

siPSMA-**09**: Prep. RP-HPLC (column IX, 38→45% C in A, 20 min, λ = 220 nm): t_R = 9.5 min, *K'* = 4.4; yield: 2.50 mg (1.73 µmol, 17%); anal. RP-HPLC (column IV, 10→70% B in A, 15 min, λ = 220 nm): t_R = 10.3 min, *K'* = 3.7, purity: 98%; MS (ESI, positive): *m/z* calc. m.i. mass ($C_{56}H_{86}FN_{11}O_{23}Si$): 1327.6, *m/z* found: 665.0 $[M+2H]^{2+}$, 1328.7 $[M+H]^{+}$.

siPSMA-**06β**

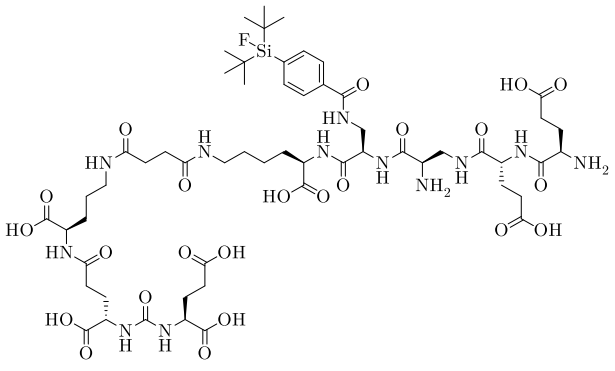

siPSMA-**06β**
Chemical Formula: $C_{57}H_{89}FN_{12}O_{23}Si$
Molecular Weight: 1357.48 g/mol

Resin-bound ligand precursor **XVIII** was coupled with Boc-D-Dap(Fmoc)-OH (GSP3a) and the peptide was Fmoc-deprotected (GSP2). Thereafter, the resulting N^{β}-amine was coupled to Fmoc-D-Glu(O*t*Bu)-OH (GSP3a) and the peptide was again Fmoc-deprotected (GSP2). This procedure was repeated one more time. The ligand was finally cleaved from the resin under

removal of acid-labile protecting groups (GSP5a), followed by purification *via* prep. RP-HPLC. siPSMA-**06β** was afforded as a colorless solid.

siPSMA-**06β**: Prep. RP-HPLC (column IX, 32→40% C in A, 20 min, λ = 220 nm): t_R = 13.2 min, *K'* = 6.5; yield: 4.87 mg (3.07 µmol, 27%); anal. RP-HPLC (column IV, 10→70% B in A, 15 min, λ = 220 nm): t_R = 9.8 min, *K'* = 3.5, purity: 98%; MS (ESI, positive): *m/z* calc. m.i. mass ($C_{57}H_{89}FN_{12}O_{23}Si$): 1356.6, *m/z* found: 679.5 $[M+2H]^{2+}$, 1357.8 $[M+H]^{+}$.

siPSMA-**10**

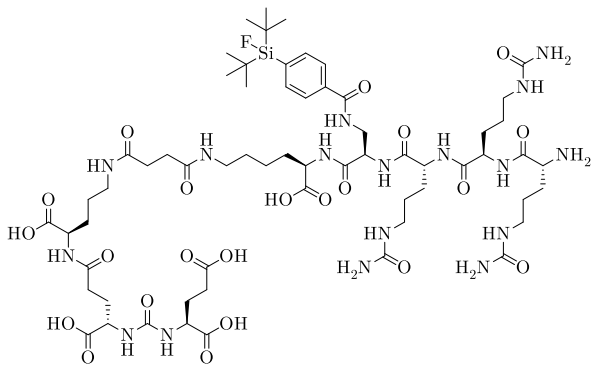

siPSMA-**10**
Chemical Formula: $C_{62}H_{102}FN_{17}O_{22}Si$
Molecular Weight: 1484.68 g/mol

Resin-bound ligand precursor **XVIII** was coupled with Fmoc-D-Cit-OH (GSP3a) and the peptide was Fmoc-deprotected according to GSP2. This procedure was repeated two more times. The ligand was finally cleaved from the resin under removal of acid-labile *t*Bu-protecting groups (GSP5a), followed by purification *via* prep. RP-HPLC. siPSMA-**10** was obtained as a colorless solid.

siPSMA-**10**: Prep. RP-HPLC (column IX, 35→45% C in A, 20 min, λ = 220 nm): t_R = 8.3 min, *K'* = 3.7; yield: 7.56 mg (4.73 µmol, 36%); anal. RP-HPLC (column IV, 10→70% B in A, 15 min, λ = 220 nm): t_R = 10.0 min, *K'* = 3.6, purity: 97%; MS (ESI, positive): *m/z* calc. m.i. mass ($C_{62}H_{102}FN_{17}O_{22}Si$): 1483.7, *m/z* found: 743.4 $[M+2H]^{2+}$, 1486.5 $[M+H]^{+}$.

siPSMA-**11** to -**16α** and siPSMA-**17** to -**18L**

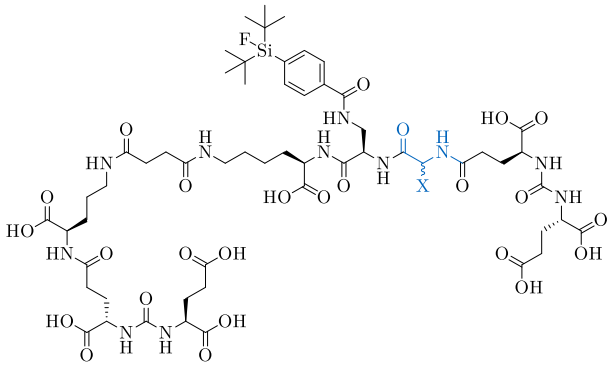

siPSMA-**11** to -**16α** and siPSMA-**17** to -**18L**

siPSMA-**11**
X = CH_2COOH: D-Asp
Chemical Formula: $C_{59}H_{88}FN_{11}O_{27}Si$
Molecular Weight: 1430.49 g/mol

siPSMA-**12D**
X = $(CH_2)_2COOH$: D-Glu
Chemical Formula: $C_{60}H_{90}FN_{11}O_{27}Si$
Molecular Weight: 1444.51 g/mol

siPSMA-**12L**
X = $(CH_2)_2COOH$: L-Glu
Chemical Formula: $C_{60}H_{90}FN_{11}O_{27}Si$
Molecular Weight: 1444.51 g/mol

siPSMA-**13**
X = $CH(OH)CH_3$: D-Thr
Chemical Formula: $C_{59}H_{90}FN_{11}O_{26}Si$
Molecular Weight: 1416.50 g/mol

siPSMA-**14**
X = $(CH_2)_3NHCONH_2$: D-Cit
Chemical Formula: $C_{61}H_{94}FN_{13}O_{26}Si$
Molecular Weight: 1472.57 g/mol

siPSMA-**15**
X = $CH_2C_6H_5$: D-Phe
Chemical Formula: $C_{64}H_{92}FN_{11}O_{25}Si$
Molecular Weight: 1462.58 g/mol

siPSMA-**16α**
X = CH_2NH_2: D-Dap
Chemical Formula: $C_{58}H_{89}FN_{12}O_{25}Si$
Molecular Weight: 1401.49 g/mol

siPSMA-**17**
X = $(CH_2)_3NH_2$: D-Orn
Chemical Formula: $C_{60}H_{93}FN_{12}O_{25}Si$
Molecular Weight: 1429.55 g/mol

siPSMA-**18D**
X = $(CH_2)_4NH_2$: D-Lys
Chemical Formula: $C_{61}H_{95}FN_{12}O_{25}Si$
Molecular Weight: 1443.57 g/mol

siPSMA-**18L**
X = $(CH_2)_4NH_2$: L-Lys
Chemical Formula: $C_{61}H_{95}FN_{12}O_{25}Si$
Molecular Weight: 1443.57 g/mol

Resin-bound ligand precursor **XVIII** was coupled with the respective Fmoc-protected amino acid (Fmoc-D-Asp(O*t*Bu)-OH, Fmoc-D-Glu(O*t*Bu)-OH, Fmoc-L-Glu(O*t*Bu)-OH, Fmoc-D-Thr(*t*Bu)-OH, Fmoc-D-Cit-OH, Fmoc-D-Phe-OH, Fmoc-D-Dap(Boc)-OH, Fmoc-D-Orn(Boc)-OH, Fmoc-D-Lys(Boc)-OH, or Fmoc-L-Lys(Boc)-OH) according to GSP3a. After cleavage of the Fmoc-protecting group (GSP2), the resulting N^{α}-amine was coupled to *t*BuO-L-Glu(O*t*Bu)-urea-L-Glu-O*t*Bu (**IX**) according to GSP3a. Finally, the ligands were cleaved from the resin under removal of acid-labile protecting groups (GSP5a), followed by purification *via* prep. RP-HPLC. siPSMA-**11** to -**16α** and siPSMA-**17** to -**18L** were isolated as colorless solids.

siPSMA-**11**: Prep. RP-HPLC (column IX, 38→45% C in A, 20 min, λ = 220 nm): t_R = 9.4 min, K' = 4.4; yield: 6.40 mg (4.47 µmol, 36%); anal. RP-HPLC

(column II, 10→70% B in A, 15 min, λ = 220 nm): t_R = 11.2 min, *K'* = 7.1, purity: 96%; MS (ESI, positive): *m/z* calc. m.i. mass ($C_{59}H_{88}FN_{11}O_{27}Si$): 1429.6, *m/z* found: 716.2 $[M+2H]^{2+}$, 1430.9 $[M+H]^{+}$.

siPSMA-**12D**: Prep. RP-HPLC (column IX, 38→45% C in A, 20 min, λ = 220 nm): t_R = 9.6 min, *K'* = 4.5; yield: 4.70 mg (3.25 µmol, 40%); anal. RP-HPLC (column II, 10→70% B in A, 15 min, λ = 220 nm): t_R = 11.5 min, *K'* = 7.3, purity: 95%; MS (ESI, positive): *m/z* calc. m.i. mass ($C_{60}H_{90}FN_{11}O_{27}Si$): 1443.6, *m/z* found: 723.1 $[M+2H]^{2+}$, 1445.0 $[M+H]^{+}$.

siPSMA-**12L**: Prep. RP-HPLC (column IX, 38→45% C in A, 20 min, λ = 220 nm): t_R = 11.0 min, *K'* = 5.3; yield: 4.34 mg (3.00 µmol, 49%); anal. RP-HPLC (column II, 10→70% B in A, 15 min, λ = 220 nm): t_R = 11.4 min, *K'* = 7.2, purity: 98%; MS (ESI, positive): *m/z* calc. m.i. mass ($C_{60}H_{90}FN_{11}O_{27}Si$): 1443.6, *m/z* found: 723.2 $[M+2H]^{2+}$, 1444.7 $[M+H]^{+}$.

siPSMA-**13**: Prep. RP-HPLC (column IX, 35→45% C in A, 20 min, λ = 220 nm): t_R = 13.9 min, *K'* = 6.9; yield: 5.56 mg (3.93 µmol, 36%); anal. RP-HPLC (column IV, 10→70% B in A, 15 min, λ = 220 nm): t_R = 11.0 min, *K'* = 4.0, purity: 97%; MS (ESI, positive): *m/z* calc. m.i. mass ($C_{59}H_{90}FN_{11}O_{26}Si$): 1415.6, *m/z* found: 709.1 $[M+2H]^{2+}$, 1417.0 $[M+H]^{+}$.

siPSMA-**14**: Prep. RP-HPLC (column IX, 38→45% C in A, 20 min, λ = 220 nm): t_R = 8.2 min, *K'* = 3.7; yield: 4.01 mg (2.72 µmol, 56%); anal. RP-HPLC (column II, 10→70% B in A, 15 min, λ = 220 nm): t_R = 11.0 min, *K'* = 6.9, purity: 99%; MS (ESI, positive): *m/z* calc. m.i. mass ($C_{61}H_{94}FN_{13}O_{26}Si$): 1471.6, *m/z* found: 737.2 $[M+2H]^{2+}$, 1473.0 $[M+H]^{+}$.

siPSMA-**15**: Prep. RP-HPLC (column IX, 40→60% C in A, 20 min, λ = 220 nm): t_R = 11.2 min, *K'* = 5.4; yield: 7.06 mg (4.83 µmol, 47%); anal. RP-HPLC (column IV, 10→70% B in A, 15 min, λ = 220 nm): t_R = 12.5 min, *K'* = 4.7, purity: 98%; MS (ESI, positive): *m/z* calc. m.i. mass ($C_{64}H_{92}FN_{11}O_{25}Si$): 1461.6, *m/z* found: 732.5 $[M+2H]^{2+}$, 1464.0 $[M+H]^{+}$.

siPSMA-**16α**: Prep. RP-HPLC (column IX, 38→45% C in A, 20 min, λ = 220 nm): t_R = 6.7 min, *K'* = 2.8; yield: 2.00 mg (1.32 µmol, 15%); anal. RP-HPLC (column IV, 10→70% B in A, 15 min, λ = 220 nm): t_R = 10.3 min, *K'* = 3.7, purity: 98%; MS (ESI, positive): *m/z* calc. m.i. mass ($C_{58}H_{89}FN_{12}O_{25}Si$): 1400.6, *m/z* found: 701.9 $[M+2H]^{2+}$, 1403.4 $[M+H]^{+}$.

siPSMA-**17**: Prep. RP-HPLC (column IX, 38→45% C in A, 20 min, λ = 220 nm): t_R = 6.4 min, *K'* = 2.7; yield: 3.82 mg (2.47 µmol, 59%); anal. RP-HPLC (column II, 10→70% B in A, 15 min, λ = 220 nm): t_R = 10.8 min, *K'* = 6.8, purity: 98%; MS (ESI, positive): *m/z* calc. m.i. mass ($C_{60}H_{93}FN_{12}O_{25}Si$): 1428.6, *m/z* found: 715.7 $[M+2H]^{2+}$, 1429.8 $[M+H]^{+}$.

siPSMA-**18D**: Prep. RP-HPLC (column VI, 40→70% C in A, 20 min, λ = 220 nm): t_R = 6.3 min, *K'* = 1.9; yield: 7.96 mg (5.11 µmol, 49%); anal. RP-HPLC (column II, 10→70% B in A, 15 min, λ = 220 nm): t_R = 10.9 min, *K'* = 6.9, purity: 99%; MS (ESI, positive): *m/z* calc. m.i. mass ($C_{61}H_{95}FN_{12}O_{25}Si$): 1442.6, *m/z* found: 722.8 $[M+2H]^{2+}$, 1444.7 $[M+H]^{+}$.

siPSMA-**18L**: Prep. RP-HPLC (column VII, 35→40% C in A, 20 min, λ = 220 nm): t_R = 7.7 min, *K'* = 3.3; yield: 4.96 mg (3.18 µmol, 37%); anal. RP-HPLC (column IV, 10→70% B in A, 15 min, λ = 220 nm): t_R = 10.1 min, *K'* = 3.6, purity: 98%; MS (ESI, positive): *m/z* calc. m.i. mass ($C_{61}H_{95}FN_{12}O_{25}Si$): 1442.6, *m/z* found: 722.8 $[M+2H]^{2+}$, 1443.8 $[M+H]^{+}$.

siPSMA-**16β**

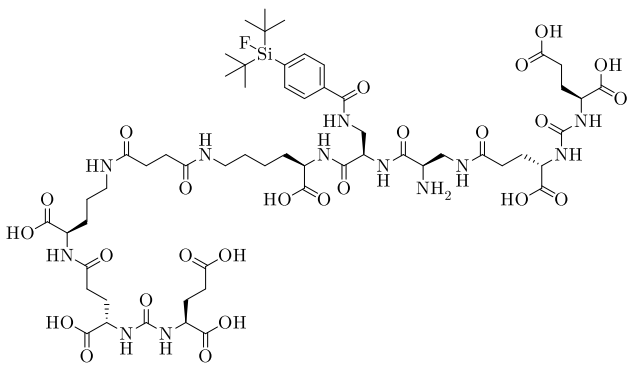

siPSMA-**16β**
Chemical Formula: $C_{58}H_{89}FN_{12}O_{25}Si$
Molecular Weight: 1401.49 g/mol

Resin-bound ligand precursor **XVIII** was coupled with Fmoc-D-Dap(Dde)-OH (GSP3a). After cleavage of the Dde-protecting group (GSP4b), the resulting N^{β}-amine was coupled to *t*BuO-L-Glu(O*t*Bu)-urea-L-Glu-O*t*Bu (**IX**) according to GSP3a. The Fmoc-protected ligand was subsequently cleaved from the resin under removal of acid-labile *t*Bu-protecting groups (GSP5a), followed by purification *via* prep. RP-HPLC (column V, 40→70% C in A, 20 min, $\lambda = 220$ nm, $t_R = 11.7$ min, $K' = 5.3$). The obtained peptide was finally Fmoc-deprotected (GSP2) and again purified *via* prep. RP-HPLC. siPSMA-**16β** was afforded as a colorless solid.

siPSMA-**16β**: Prep. RP-HPLC (column IX, 35→45% C in A, 20 min, $\lambda = 220$ nm): $t_R = 11.6$ min, $K' = 5.6$; yield: 3.48 mg (2.30 µmol, 21%); anal. RP-HPLC (column II, 10→70% B in A, 15 min, $\lambda = 220$ nm): $t_R = 11.4$ min, $K' = 7.2$, purity: 97%; MS (ESI, positive): *m/z* calc. m.i. mass ($C_{58}H_{89}FN_{12}O_{25}Si$): 1400.6, *m/z* found: 701.7 $[M+2H]^{2+}$, 1402.0 $[M+H]^{+}$.

siPSMA-**19** to -**21a**

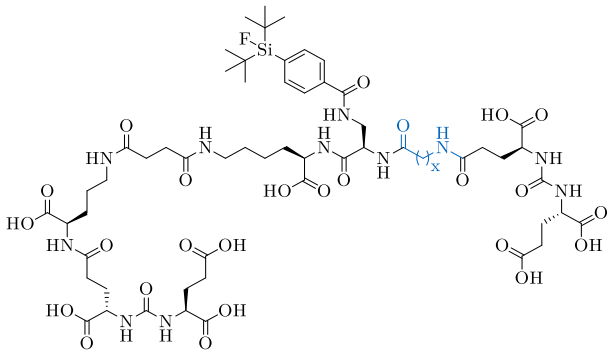

siPSMA-**19** to **-21a**

siPSMA-**19**	siPSMA-**20**	siPSMA-**21a**
x = 1: Gly	x = 2: β-Ala	x = 5: Ahx
Chemical Formula: $C_{57}H_{86}FN_{11}O_{25}Si$	Chemical Formula: $C_{58}H_{88}FN_{11}O_{25}Si$	Chemical Formula: $C_{61}H_{94}FN_{11}O_{25}Si$
Molecular Weight: 1372.45 g/mol	Molecular Weight: 1386.48 g/mol	Molecular Weight: 1428.56 g/mol

Resin-bound ligand precursor **XVIII** was coupled with the respective Fmoc-protected amino acid (Fmoc-Gly-OH, Fmoc-β-Ala-OH, or Fmoc-Ahx-OH) according to GSP3a. After cleavage of the Fmoc-protecting group (GSP2), the resulting free amine was coupled to *t*BuO-L-Glu(O*t*Bu)-urea-L-Glu-O*t*Bu (**IX**) according to GSP3a. The ligands were finally cleaved from the resin under removal of acid-labile *t*Bu-protecting groups (GSP5a), followed by purification *via* prep. RP-HPLC. siPSMA-**19** to -**21a** were obtained as colorless solids.

siPSMA-**19**: Prep. RP-HPLC (column IX, 38→45% C in A, 20 min, λ = 220 nm): t_R = 10.5 min, *K'* = 5.0; yield: 7.46 mg (5.44 µmol, 50%); anal. RP-HPLC (column IV, 10→70% B in A, 15 min, λ = 220 nm): t_R = 11.1 min, *K'* = 4.1, purity: 98%; MS (ESI, positive): *m/z* calc. m.i. mass ($C_{57}H_{86}FN_{11}O_{25}Si$): 1371.6, *m/z* found: 687.3 $[M+2H]^{2+}$, 1373.6 $[M+H]^{+}$.

siPSMA-**20**: Prep. RP-HPLC (column VIII, 40→50% C in A, 20 min, λ = 220 nm): t_R = 17.0 min, *K'* = 2.5; yield: 3.89 mg (2.81 µmol, 25%); anal. RP-HPLC (column IV, 10→70% B in A, 15 min, λ = 220 nm): t_R = 10.9 min, *K'* = 4.0, purity: 97%; MS (ESI, positive): *m/z* calc. m.i. mass ($C_{58}H_{88}FN_{11}O_{25}Si$): 1385.6, *m/z* found: 694.0 $[M+2H]^{2+}$, 1386.8 $[M+H]^{+}$.

siPSMA-**21a**: Prep. RP-HPLC (column VIII, 45→55% C in A, 20 min, λ = 220 nm): t_R = 13.0 min, *K'* = 1.7; yield: 5.00 mg (3.50 µmol, 29%); anal. RP-HPLC (column IV, 10→70% B in A, 15 min, λ = 220 nm): t_R = 11.1 min, *K'* = 4.1, purity: 96%; MS (ESI, positive): *m/z* calc. m.i. mass ($C_{61}H_{94}FN_{11}O_{25}Si$): 1427.6, *m/z* found: 714.4 $[M+2H]^{2+}$, 1427.4 $[M+H]^{+}$.

siPSMA-**21b**

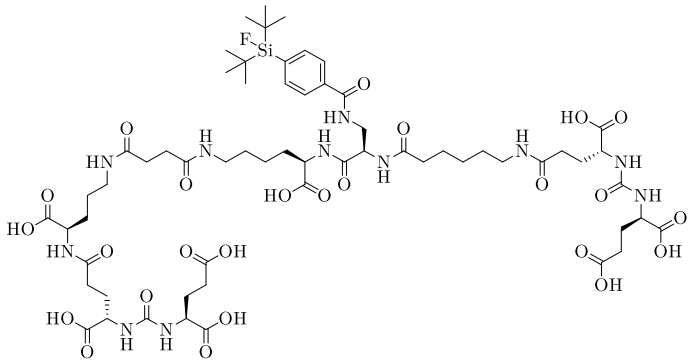

siPSMA-**21b**
Chemical Formula: $C_{61}H_{94}FN_{11}O_{25}Si$
Molecular Weight: 1428.56 g/mol

Resin-bound ligand precursor **XVIII** was coupled with Fmoc-Ahx-OH (GSP3a) and subsequently Fmoc-deprotected (GSP2). Thereafter, the resulting free amine was coupled to *t*BuO-D-Glu(O*t*Bu)-urea-D-Glu-O*t*Bu (**XIII**) according to GSP3a. The ligand was finally cleaved from the resin under removal of acid-labile *t*Bu-protecting groups (GSP5a), followed by purification *via* prep. RP-HPLC. siPSMA-**21b** was isolated as a colorless solid.

siPSMA-**21b**: Prep. RP-HPLC (column IX, 45→55% C in A, 20 min, λ = 220 nm): t_R = 5.4 min, *K'* = 2.1; yield: 1.24 mg (868 nmol, 7%); anal. RP-HPLC (column IV, 10→70% B in A, 15 min, λ = 220 nm): t_R = 11.0 min, *K'* = 4.0, purity: >99%; MS (ESI, positive): *m/z* calc. m.i. mass ($C_{61}H_{94}FN_{11}O_{25}Si$): 1427.6, *m/z* found: 714.5 $[M+2H]^{2+}$, 1427.6 $[M+H]^{+}$.

siPSMA-**22**

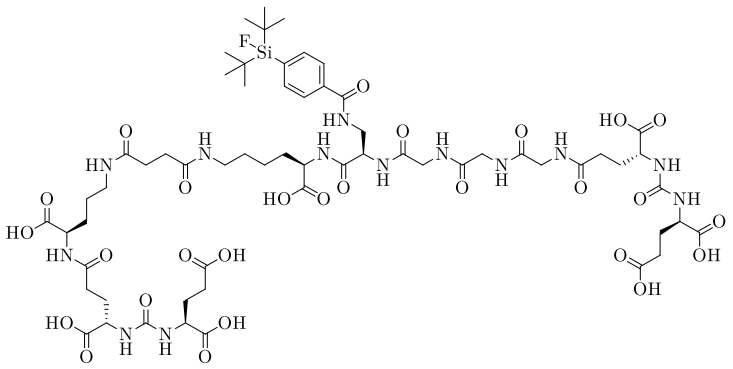

siPSMA-**22**
Chemical Formula: $C_{61}H_{92}FN_{13}O_{27}Si$
Molecular Weight: 1486.55 g/mol

Resin-bound ligand precursor **XVIII** was coupled with Fmoc-Gly-OH and subsequently Fmoc-deprotected (GSP2). This procedure was repeated two more times. Thereafter, the resulting free amine was coupled to *t*BuO-L-Glu(O*t*Bu)-urea-L-Glu-O*t*Bu (**IX**) according to GSP3a. The ligand was finally cleaved from the resin under removal of acid-labile *t*Bu-protecting groups (GSP5a), followed by purification *via* prep. RP-HPLC. siPSMA-**22** was afforded as a colorless solid.

siPSMA-**22**: Prep. RP-HPLC (column IX, 38→45% C in A, 20 min, λ = 220 nm): t_R = 9.8 min, *K'* = 4.6; yield: 2.12 mg (1.43 µmol, 12%); anal. RP-HPLC (column IV, 10→70% B in A, 15 min, λ = 220 nm): t_R = 10.5 min, *K'* = 3.8, purity: 96%; MS (ESI, positive): *m/z* calc. m.i. mass ($C_{61}H_{92}FN_{13}O_{27}Si$): 1485.6, *m/z* found: 743.9 $[M+2H]^{2+}$, 1486.4 $[M+H]^{+}$.

siPSMA-**23**

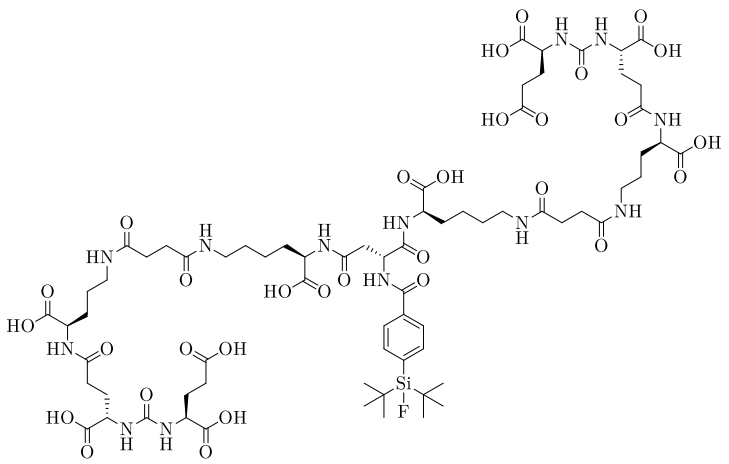

siPSMA-**23**

Chemical Formula: $C_{71}H_{108}FN_{13}O_{31}Si$

Molecular Weight: 1686.79 g/mol

Resin-bound ligand precursor **XVII** was coupled with SiFA-BzA-D-Asp-OH (**XV**) according to GSP3a. The pseudo-dimerized ligand was subsequently cleaved from the resin under removal of acid-labile *t*Bu-protecting groups (GSP5a), followed by purification *via* prep. RP-HPLC. siPSMA-**23** was obtained as a colorless solid.

siPSMA-**23**: Prep. RP-HPLC (column IX, 38→45% C in A, 20 min, λ = 220 nm): t_R = 7.6 min, K' = 3.3; yield: 3.42 mg (4.47 µmol, 14%); anal. RP-HPLC (column II, 10→70% B in A, 15 min, λ = 220 nm): t_R = 11.1 min, K' = 7.0, purity: 97%; MS (ESI, positive): *m/z* calc. m.i. mass ($C_{71}H_{108}FN_{13}O_{31}Si$): 1685.7, *m/z* found: 844.4 $[M+2H]^{2+}$, 1687.5 $[M+H]^{+}$.

siPSMA-**24**

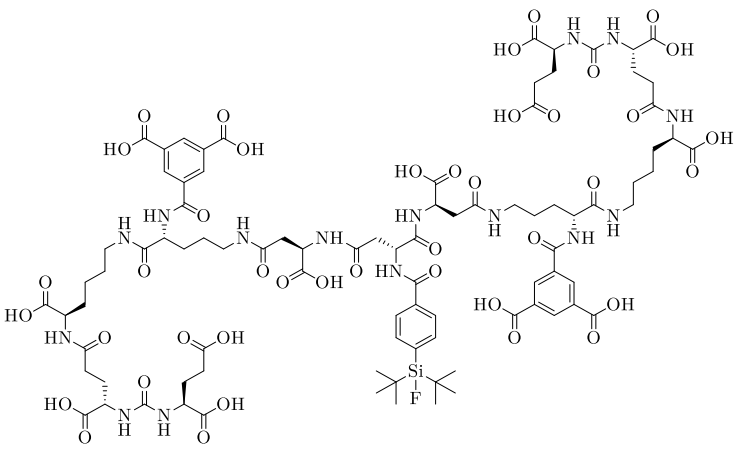

siPSMA-**24**
Chemical Formula: $C_{89}H_{118}FN_{15}O_{41}Si$
Molecular Weight: 2101.07 g/mol

Resin-bound ligand precursor **XIX** was coupled with 3,5-bis(*tert*-butoxycarbonyl)benzoic acid (**XIV**) according to GSP3a. The Dde-protecting group was subsequently cleaved (GSP4a) and the resulting N^{δ}-amine was coupled to Fmoc-D-Asp-O*t*Bu (GSP3a). After Fmoc-deprotection (GSP2), the resin-bound peptide was coupled with SiFA-BzA-D-Asp-OH (**XV**) according to GSP3a. The pseudo-dimerized ligand was finally cleaved from the resin under removal of acid-labile *t*Bu-protecting groups (GSP5a), followed by purification *via* prep. RP-HPLC. siPSMA-**24** was isolated as a colorless solid.

siPSMA-**24**: Prep. RP-HPLC (column IX, 40→50% C in A, 20 min, λ = 220 nm): t_R = 7.5 min, *K'* = 3.3; yield: 10.5 mg (4.99 µmol, 25%); anal. RP-HPLC (column IV, 10→70% B in A, 15 min, λ = 220 nm): t_R = 10.3 min, *K'* = 3.7, purity: 99%; MS (ESI, positive): *m/z* calc. m.i. mass ($C_{89}H_{118}FN_{15}O_{41}Si$): 2099.7, *m/z* found: 1050.7 $[M+2H]^{2+}$.

2.2.4 Synthesis of ^{nat}Lu-rhFolate Ligands

H-D-Dap(DOTA(O*t*Bu)$_3$)-D-Dap(SiFA-BzA)-2-CT resin (**XX**)

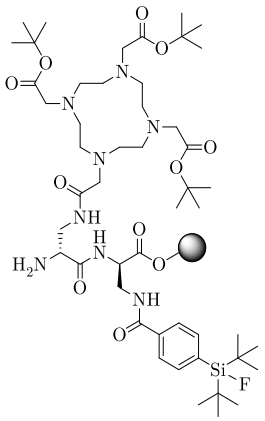

XX

Chemical Formula: $C_{49}H_{85}FN_8O_{11}Si$
Molecular Weight: 1009.35 g/mol

2-CTC resin was loaded with Fmoc-D-Dap(Dde)-OH according to GSP1. The amino acid was subsequently Dde-deprotected (GSP4b) and the resulting N^{β}-amine was coupled to SiFA-BzA (**V**) following GSP3c. Upon cleavage of the Fmoc-protecting group (GSP2), the N^{α}-amine was coupled to Fmoc-D-Dap(Dde)-OH (GSP3a). Thereafter, the Dde-protecting group was cleaved (GSP4b) and the N^{β}-amine was coupled to DOTA(O*t*Bu)$_3$ following GSP3e. The resin-bound peptide was finally Fmoc-deprotected (GSP2), affording the FR ligand precursor **XX**.

Coupling reaction control: method B; anal. RP-HPLC (column III, 10→90% B in A, 15 min, λ = 220 nm): t_R = 10.8 min, K' = 4.7; MS (ESI, positive): *m/z* calc. m.i. mass ($C_{49}H_{85}FN_8O_{11}Si$): 1008.6, *m/z* found: 1009.0 $[M+H]^+$, 1031.0 $[M+Na]^+$.

H-D-Dap(DOTA(O*t*Bu)$_3$)-D-Dap(SiFA-Bn-*N*,*N*-dimethyl-Gly)-2-CT resin (**XXI**)

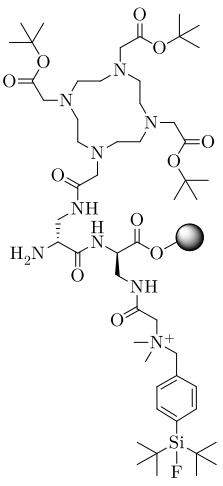

XXI

Chemical Formula: $C_{53}H_{95}FN_9O_{11}Si^+$
Molecular Weight: 1081.48 g/mol

2-CTC resin was loaded with Fmoc-D-Dap(Dde)-OH according to GSP1. The amino acid was subsequently Dde-deprotected (GSP4b) and the N^{β}-amine was coupled to *N*,*N*-dimethyl-Gly-OH (GSP3a). Thereafter, SiFA-BnBr (**IV**) was coupled to the dimethylated amine following GSP3d. The Fmoc-protecting group was then cleaved (GSP2) and the resulting N^{α}-amine was coupled to Fmoc-D-Dap(Dde)-OH (GSP3a). Upon cleavage of the Dde-protecting group (GSP4b), the N^{β}-amine was coupled to DOTA(O*t*Bu)$_3$ following GSP3e. The resin-bound peptide was finally Fmoc-deprotected (GSP2), giving the FR ligand precursor **XXI**.

Coupling reaction control: method B; anal. RP-HPLC (column III, 10→90% B in A, 15 min, λ = 220 nm): t_R = 10.0 min, K' = 4.3; MS (ESI, positive): *m/z* calc. m.i. mass ($C_{53}H_{95}FN_9O_{11}Si^+$): 1080.7, *m/z* found: 1080.1 $[M]^+$.

^{nat}Lu-rhFolate-**01** and -**02**

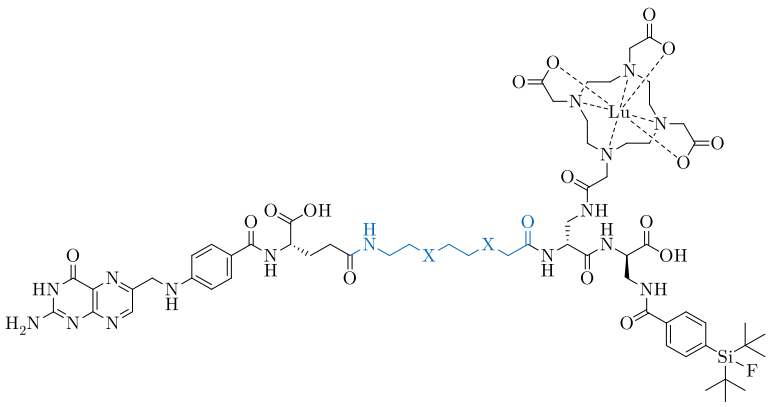

^{nat}Lu-rhFolate-**01** and **-02**

^{nat}Lu-rhFolate-**01**	^{nat}Lu-rhFolate-**02**
X = CH_2: 8-Aoc	X = O: AEEAc
Chemical Formula: $C_{64}H_{90}FLuN_{16}O_{17}Si$	Chemical Formula: $C_{62}H_{86}FLuN_{16}O_{19}Si$
Molecular Weight: 1577.57 g/mol	Molecular Weight: 1581.51 g/mol

The resin-bound ligand precursor **XX** was coupled with the respective Fmoc-protected amino acid (Fmoc-8-Aoc-OH or Fmoc-AEEAc-OH) following GSP3a. After cleavage of the Fmoc-protecting group (GSP2), the resulting free amine was coupled to Fmoc-L-Glu-O*t*Bu (GSP3a). The Fmoc-protecting group was cleaved again (GSP2) and the N^{α}-amine was subsequently coupled to 1-(2-*N*-Teoc-pteroyl)imidazole (**XII**) following GSP3f. The ligands were cleaved from the resin under removal of acid-labile protecting groups (GSP5b) and purified *via* prep. RP-HPLC. Uncomplexed rhFolate-**01** and -**02** were obtained as orange solids.

rhFolate-**01**: Prep. RP-HPLC (column X, 40→45% C in A, 30 min, λ = 220 nm): t_R = 17.9 min, *K'* = 3.6; yield: 4.84 mg (2.96 µmol, 11%); anal. RP-HPLC (column III, 10→70% B in A, 15 min, λ = 220 nm): t_R = 11.0 min, *K'* = 4.8, purity: 80%; MS (ESI, positive): *m/z* calc. m.i. mass ($C_{64}H_{93}FN_{16}O_{17}Si$): 1404.7, *m/z* found: 703.0 $[M+2H]^{2+}$, 1404.8 $[M+H]^{+}$.

rhFolate-**02**: Prep. RP-HPLC (column X, 40→45% C in A, 30 min, λ = 220 nm): t_R = 15.0 min, *K'* = 2.9; yield: 5.61 mg (3.43 µmol, 16%); anal. RP-HPLC (column III, 10→70% B in A, 15 min, λ = 220 nm): t_R = 10.6 min, *K'* = 4.6,

purity: 91%; MS (ESI, positive): *m/z* calc. m.i. mass ($C_{62}H_{89}FN_{16}O_{19}Si$): 1408.6, *m/z* found: 704.9 $[M+2H]^{2+}$, 1409.1 $[M+H]^{+}$.

The respective complexes ^{nat}Lu-rhFolate-**01** and -**02** were prepared according to GSP6, purified *via* prep. RP-HPLC, and finally isolated as pale-yellow solids.

^{nat}Lu-rhFolate-**01**: Prep. RP-HPLC (column X, 40→45% C in A, 30 min, λ = 220 nm): t_R = 18.0 min, *K'* = 3.6; yield: 2.24 mg (1.24 µmol, 83%); anal. RP-HPLC (column III, 10→70% B in A, 15 min, λ = 220 nm): t_R = 11.2 min, *K'* = 4.9, purity: 94%; MS (ESI, positive): *m/z* calc. m.i. mass ($C_{64}H_{90}FLuN_{16}O_{17}Si$): 1576.6, *m/z* found: 789.2 $[M+2H]^{2+}$, 1577.1 $[M+H]^{+}$.

^{nat}Lu-rhFolate-**02**: Prep. RP-HPLC (column X, 40→45% C in A, 30 min, λ = 220 nm): t_R = 13.5 min, *K'* = 2.5; yield: 2.04 mg (1.13 µmol, 61%); anal. RP-HPLC (column III, 10→70% B in A, 15 min, λ = 220 nm): t_R = 10.7 min, *K'* = 4.7, purity: 98%; MS (ESI, positive): *m/z* calc. m.i. mass ($C_{62}H_{86}FLuN_{16}O_{19}Si$): 1580.5, *m/z* found: 528.2 $[M+3H]^{3+}$, 791.6 $[M+2H]^{2+}$, 1582.5 $[M+H]^{+}$.

^{nat}Lu-rhFolate-**03** and -**04**

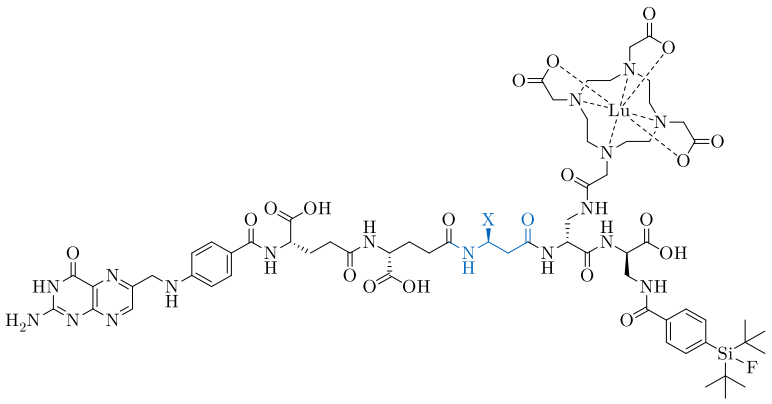

^{nat}Lu-rhFolate-**03** and -**04**

^{nat}Lu-rhFolate-**03**
X = H: β-Ala
Chemical Formula: $C_{64}H_{87}FLuN_{17}O_{20}Si$
Molecular Weight: 1636.55 g/mol

^{nat}Lu-rhFolate-**04**
X = COOH: D-Asp
Chemical Formula: $C_{65}H_{87}FLuN_{17}O_{22}Si$
Molecular Weight: 1680.56 g/mol

The resin-bound ligand precursor **XX** was coupled with the respective Fmoc-protected amino acid (Fmoc-β-Ala-OH or Fmoc-D-Asp-O*t*Bu) following GSP3a, and the peptide was subsequently Fmoc-deprotected (GSP2). The resulting free amine was coupled to Fmoc-D-Glu-O*t*Bu (GSP3a) and the peptide was again Fmoc-deprotected (GSP2). Thereafter, the N^{α}-amine was coupled to Fmoc-L-Glu-O*t*Bu following GSP3a. Upon cleavage of the Fmoc-protecting group (GSP2), the resin-bound peptide was coupled to 1-(2-*N*-Teoc-pteroyl)imidazole (**XII**) following GSP3f. The ligands were cleaved from the resin under removal of acid-labile protecting groups (GSP5b) and purified *via* prep. RP-HPLC. Uncomplexed rhFolate-**03** and -**04** were afforded as orange solids.

rhFolate-**03**: Prep. RP-HPLC (column X, 40→45% C in A, 30 min, λ = 220 nm): t_R = 12.0 min, *K'* = 2.1; yield: 8.18 mg (4.83 µmol, 14%); anal. RP-HPLC (column III, 10→70% B in A, 15 min, λ = 220 nm): t_R = 10.2 min, *K'* = 4.4, purity: 89%; MS (ESI, positive): *m/z* calc. m.i. mass ($C_{64}H_{90}FN_{17}O_{20}Si$): 1463.6, *m/z* found: 732.0 $[M+2H]^{2+}$, 1462.8 $[M+H]^{+}$.

rhFolate-**04**: Prep. RP-HPLC (column X, 40→45% C in A, 30 min, λ = 220 nm): t_R = 11.8 min, *K'* = 2.0; yield: 6.10 mg (3.51 µmol, 16%); anal. RP-HPLC (column III, 10→70% B in A, 15 min, λ = 220 nm): t_R = 10.1 min, *K'* = 4.4, purity: 94%; MS (ESI, positive): *m/z* calc. m.i. mass ($C_{65}H_{90}FN_{17}O_{22}Si$): 1507.6, *m/z* found: 754.4 $[M+2H]^{2+}$, 1508.5 $[M+H]^{+}$.

The respective complexes ^{nat}Lu-rhFolate-**03** and -**04** were synthesized following GSP6, purified *via* prep. RP-HPLC, and finally obtained as pale-yellow solids.

^{nat}Lu-rhFolate-**03**: Prep. RP-HPLC (column X, 40→45% C in A, 30 min, λ = 220 nm): t_R = 11.6 min, *K'* = 2.0; yield: 1.79 mg (960 nmol, 68%); anal. RP-HPLC (column III, 10→70% B in A, 15 min, λ = 220 nm): t_R = 10.7 min, *K'* = 4.7, purity: >99%; MS (ESI, positive): *m/z* calc. m.i. mass ($C_{64}H_{87}FLuN_{17}O_{20}Si$): 1635.6, *m/z* found: 818.7 $[M+2H]^{2+}$, 1637.2 $[M+H]^{+}$.

^{nat}Lu-rhFolate-**04**: Prep. RP-HPLC (column X, 40→45% C in A, 30 min, λ = 220 nm): t_R = 11.6 min, *K'* = 2.0; yield: 1.46 mg (765 nmol, 44%); anal. RP-HPLC

(column III, 10→70% B in A, 15 min, λ = 220 nm): t_R = 10.1 min, *K'* = 4.4, purity: 96%; MS (ESI, positive): *m/z* calc. m.i. mass ($C_{65}H_{87}FLuN_{17}O_{22}Si$): 1679.5, *m/z* found: 561.0 $[M+3H]^{3+}$, 841.1 $[M+2H]^{2+}$, 1681.4 $[M+H]^{+}$.

^{nat}Lu-rhFolate-**05**

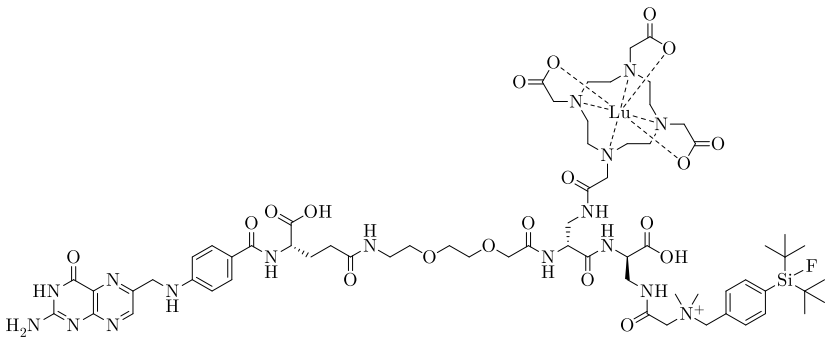

^{nat}Lu-rhFolate-**05**
Chemical Formula: $C_{66}H_{96}FLuN_{17}O_{19}Si^{+}$
Molecular Weight: 1653.64 g/mol

The resin-bound ligand precursor **XXI** was coupled with Fmoc-AEEAc-OH following GSP3a. After cleavage of the Fmoc-protecting group (GSP2), the resulting free amine was coupled to Fmoc-L-Glu-O*t*Bu (GSP3a). The Fmoc-protecting group was cleaved again (GSP2) and the N^{α}-amine was subsequently coupled to 1-(2-*N*-Teoc-pteroyl)imidazole (**XII**) following GSP3f. The ligand was cleaved from the resin under removal of acid-labile protecting groups (GSP5b) and purified *via* prep. RP-HPLC. Uncomplexed rhFolate-**05** was isolated as an orange solid.

rhFolate-**05**: Prep. RP-HPLC (column X, 40→45% C in A, 30 min, λ = 220 nm): t_R = 12.2 min, *K'* = 2.1; yield: 2.98 mg (1.63 µmol, 4%); anal. RP-HPLC (column IV, 10→70% B in A, 15 min, λ = 220 nm): t_R = 11.1 min, *K'* = 4.1, purity: 84%; MS (ESI, positive): *m/z* calc. m.i. mass ($C_{66}H_{99}FN_{17}O_{19}Si^{+}$): 1480.7, *m/z* found: 740.8 $[M+2H]^{2+}$, 1480.8 $[M+H]^{+}$.

The respective complex ^{nat}Lu-rhFolate-**05** was synthesized according to GSP6, purified *via* prep. RP-HPLC, and finally afforded as a pale-yellow solid.

^{nat}Lu-rhFolate-**05**: Prep. RP-HPLC (column X, 40→45% C in A, 30 min, λ = 220 nm): t_R = 12.2 min, *K'* = 2.1; yield: 2.71 mg (1.36 µmol, 83%); anal. RP-HPLC

(column III, 10→70% B in A, 15 min, λ = 220 nm): t_R = 10.8 min, *K'* = 4.7, purity: >99%; MS (ESI, positive): *m/z* calc. m.i. mass ($C_{66}H_{96}FLuN_{17}O_{19}Si^+$): 1652.6, *m/z* found: 826.3 $[M+H]^{2+}$, 1652.2 $[M]^+$.

2.2.5 Synthesis of Reference Precursors and Cold Reference Ligands

*t*BuO-L-Glu(O*t*Bu)-urea-L-Lys(4-(tri-*n*-butylstannyl)benzoic acid)-O*t*Bu (**XXII**)

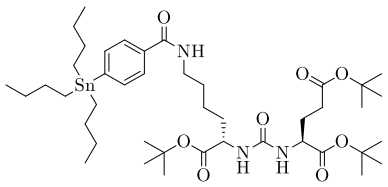

XXII

Chemical Formula: $C_{43}H_{75}N_3O_8Sn$
Molecular Weight: 880.80 g/mol

The PSMA reference precursor **XXII** was synthesized in accordance with a published procedure[228]. Briefly, *t*BuO-L-Glu(O*t*Bu)-urea-L-Lys-O*t*Bu (**XI**, 86.4 mg, 177 µmol, 1.2 eq.) and *N*-succinimidyl 4-(tri-*n*-butylstannyl)benzoate (75.0 mg, 148 µmol, 1.0 eq.) were dissolved in DCM (1.5 mL), and TEA (92.6 µL, 664 µmol, 4.5 eq.) was added. The reaction mixture was stirred overnight at rt and subsequently washed with water (50 mL). Finally, the separated organic phase was concentrated *in vacuo*, yielding the reference precursor **XXII** (119 mg) as a pale-yellow oil. The crude product was used for the ^{125}I-labeling reaction without further purification.

Anal. RP-HPLC: (column III, 95% B in A, 15 min, λ = 220 nm): t_R = 10.9 min, *K'* = 4.8; MS (ESI, positive): *m/z* calc. m.i. mass ($C_{43}H_{75}N_3O_8Sn$): 881.5, *m/z* found: 880.9 $[M+H]^+$, 1761.0 $[2M+H]^+$, 1782.9 $[2M+Na]^+$.

Pteroyl-L-Glu(L-Tyr-OH)-OH (**XXIII**)

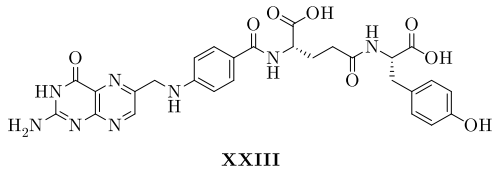

XXIII

Chemical Formula: $C_{28}H_{28}N_8O_8$
Molecular Weight: 604.58 g/mol

The previously published FR reference precursor **XXIII** was prepared *via* Fmoc-based SPPS[229]. In short, 2-CTC resin was loaded with Fmoc-L-Tyr(*t*Bu)-OH according to GSP1. The

amino acid was subsequently Fmoc-deprotected (GSP2) and the N^{α}-amine was coupled to Fmoc-L-Glu-O*t*Bu (GSP3a). Thereafter, the Fmoc-protecting group was cleaved (GSP2) and the resulting N^{α}-amine was coupled to pteroic acid in analogy to GSP3f. Upon cleavage from the resin under removal of acid-labile *t*Bu-protecting groups (GSP5a), the reference precursor **XXIII** was purified *via* prep. RP-HPLC and isolated as a dark orange solid (15.6 mg, 18.7 µmol, 15%).

Prep. RP-HPLC (column V, 15→25% C in A, 20 min, λ = 220 nm): t_R = 13.7 min, *K'* = 6.4; anal. RP-HPLC (column III, 10→40% B in A, 15 min, λ = 220 nm): t_R = 6.4 min, *K'* = 2.4, purity: 84%; MS (ESI, positive): *m/z* calc. m.i. mass ($C_{28}H_{28}N_8O_8$): 604.2, *m/z* found: 604.4 $[M+H]^+$.

Pteroyl-L-Glu(3-iodo-L-Tyr-OH)-OH (**XXIV**)

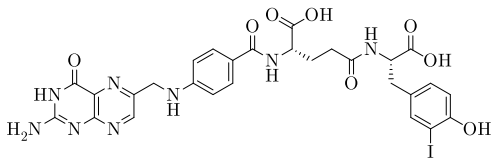

XXIV

Chemical Formula: $C_{28}H_{27}IN_8O_8$
Molecular Weight: 730.48 g/mol

The previously published cold FR reference ligand pteroyl-L-Glu(3-iodo-L-Tyr-OH)-OH (**XXIV**) was synthesized following a literature procedure[229-230]. A solution (10 mM, 25.0 µL, 250 nmol, 1.0 eq.) of pteroyl-L-Glu(L-Tyr-OH)-OH (**XXIII**) in a mixture (4:3:3, *v/v/v*) of DMSO, MeCN, and water was combined with a solution (10 mM, 8.75 µL, 87.5 nmol, 0.35 eq.) of *N*-iodosuccinimide in MeCN. The mixture was subsequently incubated for 5 min at rt. For qualitative isolation of **XXIV**, the whole solution was subjected to purification *via* anal. RP-HPLC.

Anal. RP-HPLC (column III, 10→40% B in A, 20 min, λ = 220 nm): t_R = 13.0 min, *K'* = 5.9; MS (ESI, positive): *m/z* calc. m.i. mass ($C_{28}H_{27}IN_8O_8$): 730.5, *m/z* found: 730.8 $[M+H]^+$, 1460.5 $[2M+H]^+$.

2.3 Radiolabeling of Compounds and Ligands

2.3.1 Radiolabeling Equipment

Manual Radiolabeling on Laboratory Scale

Aq. [^{18}F]fluoride (approximately (approx.) 0.6–2.0 GBq/mL) was supplied by the *University Hospital rechts der Isar* (Munich, Germany) and produced at the on-site PETtrace™ 880 cyclotron (*GE Healthcare GmbH*, Solingen, Germany). Moreover, Na[^{125}I]I as a basic solution (3.1 GBq/mL, 74 TBq/mmol, 40 mM aq. NaOH) was obtained from *Hartmann Analytic GmbH* (Braunschweig, Germany).

A CRC®-55tR dose calibrator from *Capintec Inc.* (Florham Park, NJ, United States) was used for activity measurements.

[^{18}F]Fluoride trapping for on-cartridge drying was performed on Sep-Pak® Accell Plus QMA Carbonate Plus Light cartridges (46 mg sorbent weight, 40 µm particle size, 230 µeq/g ion exchange capacity) delivered by *Waters GmbH* (Eschborn, Germany). Purification of radiolabeled compounds and ligands through SPE was conducted on Oasis® HLB Plus Light cartridges (30 mg sorbent weight, 30 µm particle size), or Sep-Pak® C18 Plus Short cartridges (360 mg sorbent weight, 55–105 µm particle size) purchased from *Waters GmbH*.

NH_4HCOO (quality grade "≥99.995%, trace metals basis"), NH_4OAc (quality grade "≥98%, for molecular biology"), NMe_4OAc (quality grade ">98.0%"), NH_4I (quality grade "≥99%"), NBu_4I (quality grade "≥99.0%"), NBu_4OTf (quality grade "99%"), KOH (quality grade "99.99%, semiconductor grade"), oxalic acid (quality grade "99.999%, trace metals basis"), and Kryptofix® 222 (quality grade "for synthesis") were provided by *Sigma-Aldrich Chemie GmbH*, *TCI Deutschland GmbH*, *Merck KGaA*, and *Thermo Fisher GmbH* (Kandel, Germany). Anhyd. MeCN (quality grade "≥99.9%, for DNA synthesis"), anhyd. DMSO (quality grade "≥99.9%"), pure water (quality grade "Tracepur®"), abs. EtOH (quality grade "EMPARTA®"), MeCN (quality grade "≥99.8%, for HPLC"), and MeOH (quality grade "≥98.5%, technical") were supplied by *VWR International GmbH*, *Merck KGaA*, and *Sigma-Aldrich Chemie GmbH*. Water was obtained from a Barnstead™ MicroPure™ purification system (*Fisher Scientific*

GmbH). Further reagents (quality grade "for synthesis"), additives and buffers, including phosphate-buffered saline (PBS) and Hanks' Balanced Salt Solution (HBSS), were purchased from either *Sigma-Aldrich Chemie GmbH*, *VWR International GmbH*, *Alfa Aesar GmbH & Co. KG*, or *Merck KGaA*.

The $[K^+\subset 2.2.2]OH^-$ elution cocktail kits were dried by lyophilization using the Christ Martin™ freeze dryer Alpha 1-4 LSC (*Martin Christ Gefriertrocknungsanlagen GmbH*).

A FC1200 compact recirculating cooler (*JULABO GmbH*, Seelbach, Germany) with a coolant mixture (1:1, *v/v*) composed of ethylene glycol and water was applied for temperature setting during radiofluorination of model compound **VI**.

The S20-SevenEasy™ pH meter from *Mettler Toledo GmbH* (Gießen, Germany) was employed to adjust the pH of solutions.

Anal. characterization and prep. purification of radiolabeled compounds and ligands was performed on the aforementioned (*Section 2.2.1*) column II (Multospher®100 RP 18-5µ, 125 × 4.6 mm dimension, 5 µm particle size, 1 mL/min flow rate), column III (MultoKrom® 100-5 C18, 125 × 4.6 mm dimension, 5 µm particle size, 1 mL/min flow rate), and column IV (MultoKrom® 100-5 C18, 150 × 4.6 mm dimension, 5 µm particle size, 1 mL/min flow rate) in an HPLC system (*Shimadzu Deutschland GmbH*) consisting of gradient pumps (two LC-20AD), an autosampler (SIL-20AHT), a system controller (CBM-20A), a column oven (CTO-10ASVP), an UV-visible detector (SPD-20A), and an LB 500 HERM radioflow monitor with NaI detector (*Berthold Technologies GmbH & Co.KG*, Bad Wildbad, Germany). Radiolabeled compounds and ligands were eluted by applying different gradients of the previously introduced (*Section 2.1.1*) solvent A and solvent B at a constant flow. LabSolutions 5.92 software (*Shimadzu Deutschland GmbH*) was employed for analysis of radiochromatograms.

For radio-TLC analysis of ^{18}F-labeled ligands, samples were chromatographed on silica gel 60 F_{254} or silica gel 60 RP-18 F_{254}s plates (*Merck KGaA*) and subsequently analyzed using a Scan-RAM™ radio-TLC detector equipped with the software Laura 4.2.4.50 SP6 (*LabLogic Systems Inc.*, Brandon, FL, United States).

Automated Radiofluorination for First-in-Human Applications

Automated radiosynthesis of [^{18}F]siPSMA-**14** was performed on a GRP 2V module with a double-cassette setup (*Scintomics GmbH,* Fürstenfeldbruck, Germany) at the *University Hospital Ulm* (Ulm, Germany) using in-house (PETtrace™ 860 cyclotron, *GE Healthcare GmbH*) produced aq. [^{18}F]fluoride (approx. 6.9–16.2 GBq/mL). The stopcock manifolds were equipped with a Sep-Pak® Accell Plus QMA Carbonate Plus Light cartridge (46 mg sorbent weight, 40 µm particle size, 230 µeq/g ion exchange capacity) and an Oasis® HLB Plus Short cartridge (225 mg sorbent weight, 60 µm particle size), both supplied by *Waters GmbH*. Sterile Millex-GS syringe filters (0.22 µm pore size, 33 mm diameter) as well as sterile Cathivex-GV filters (0.22 µm pore size, 25 mm diameter) were obtained from *Merck KGaA*.

KOH (quality grade "99.99%, semiconductor grade"), Kryptofix® 222 (quality grade "for synthesis"), oxalic acid (quality grade "99.999%, trace metals basis"), $NaH_2PO_4 \cdot 2H_2O$ (quality grade "Emprove® Essential"), and NaOH (quality grade "Emprove® Essential") were provided by *Sigma-Aldrich Chemie GmbH* and *Merck KGaA*. Anhyd. MeCN (quality grade "LiChrosolv®"), anhyd. DMSO (quality grade "≥99.9%"), pure water (quality grade "Tracepur®"), ultrapure EtOH (quality grade "Emprove® Expert"), and ultrapure water (quality grade "Ampuwa") were purchased from *Sigma-Aldrich Chemie GmbH*, *Merck KGaA*, and *Fresenius Kabi Deutschland GmbH* (Bad Homburg, Germany).

The $[K^+\subset 2.2.2]OH^-$ elution cocktail kits were dried by lyophilization using the Christ Martin™ freeze dryer Alpha 1-4 LSC (*Martin Christ Gefriertrocknungsanlagen GmbH*).

2.3.2 Recovery Experiments for Development of the *SiFA-tailored Method*

Recovery of dried [^{18}F]Fluoride by various salts

Aq. [^{18}F]fluoride was trapped (male-to-female Luer direction) onto a Sep-Pak® Accell Plus QMA Carbonate Plus Light cartridge, which had previously been conditioned with pure water (10 mL). After drying with air (2 × 20 mL, female-to-male Luer direction), the cartridge was slowly rinsed with anhyd. MeCN (10 mL, female-to-male Luer direction) and subsequently dried with air (2 × 20 mL, female-to-male Luer direction) again. Dried [^{18}F]fluoride was eluted

(female-to-male Luer direction) from the cartridge using prepared elution cocktails, including NBu_4OTf (248 mg, 634 µmol) in anhyd. MeCN (500 µL), NBu_4I (235 mg, 635 µmol) in anhyd. MeCN (500 µL), NH_4I (92.5 mg, 638 µmol) in anhyd. DMSO (500 µL), NMe_4OAc (84.3 mg, 633 µmol) in anhyd. DMSO (500 µL), NH_4OAc (49.2 mg, 639 µmol) in anhyd. DMSO (500 µL), NH_4HCOO (40.6 ± 0.1 mg, 645 ± 1 µmol) in anhyd. DMSO (500 µL), and NH_4HCOO (40.0 ± 0.2 mg, 634 ± 3 µmol) in anhyd. DMSO (1000 µL). Upon elution, the cartridge was flushed with air (5 mL, female-to-male Luer direction) and the residual activity as well as the activity of the eluate were measured using the dose calibrator to calculate the [^{18}F]fluoride recovery.

Recovery of dried [^{18}F]Fluoride by various concentrations of NH_4HCOO

Aq. [^{18}F]fluoride was trapped (male-to-female Luer direction) onto a Sep-Pak® Accell Plus QMA Carbonate Plus Light cartridge, which had previously been conditioned with pure water (10 mL). After drying with air (2 × 20 mL, female-to-male Luer direction), the cartridge was slowly rinsed with anhyd. DMSO (8 mL, female-to-male Luer direction) and subsequently dried with air (2 × 20 mL, female-to-male Luer direction) again. Dried [^{18}F]fluoride was eluted (female-to-male Luer direction) from the cartridge using prepared elution cocktails with various amounts of NH_4HCOO in anhyd. DMSO (500 µL), including 0 mg, 5.00 mg (79.3 µmol), 10.0 mg (159 µmol), 25.0 mg (396 µmol), and 40.0 mg (634 µmol). Upon elution, the cartridge was flushed with air (5 mL, female-to-male Luer direction) and the residual activity as well as the activity of the eluate were measured using the dose calibrator to calculate the [^{18}F]fluoride recovery.

Recovery of dried [^{18}F]Fluoride by elution cocktails with various aq. percentages

Aq. [^{18}F]fluoride was trapped (male-to-female Luer direction) onto a Sep-Pak® Accell Plus QMA Carbonate Plus Light cartridge, which had previously been conditioned with pure water (10 mL). After drying with air (2 × 20 mL, female-to-male Luer direction), the cartridge was slowly rinsed with anhyd. DMSO (8 mL, female-to-male Luer direction) and subsequently dried with air (2 × 20 mL, female-to-male Luer direction) again. Dried [^{18}F]fluoride was eluted (female-to-male Luer direction) from the cartridge using prepared elution cocktails of

NH_4HCOO (40.0 mg, 634 µmol) in various mixtures (500 µL) of anhyd. DMSO with increasing water percentages, including 0%, 1%, 2%, 4%, 5%, and 10%. Upon elution, the cartridge was flushed with air (5 mL, female-to-male Luer direction) and the residual activity as well as the activity of the eluate were measured using the dose calibrator to calculate the [^{18}F]fluoride recovery. Subsequent radiofluorination of ^{nat}Ga-rhPSMA-7.3 was accomplished by combining the corresponding eluates with a solution (1 mM, 150 µL, 150 nmol) of the ligand in anhyd. DMSO and incubating the mixture for 5 min at rt. Purification of the resulting [^{18}F]^{nat}Ga-rhPSMA-7.3 was performed according to a slightly modified protocol[76]. The reaction mixture was diluted with PBS (pH 3 with 1 M aq. HCl, 10 mL) and passed (female-to-male Luer direction) through an Oasis® HLB Plus Light cartridge, which had previously been conditioned with abs. EtOH (10 mL) and pure water (10 mL). Finally, the cartridge was rinsed with PBS (10 mL, female-to-male Luer direction), dried with air (20 mL, female-to-male Luer direction), and [^{18}F]^{nat}Ga-rhPSMA-7.3 was eluted with a mixture (1:1, *v/v*, 300 µL, female-to-male Luer direction) of abs. EtOH and pure water. Radiochemical purity (RCP) of the ^{18}F-labeled ligand was determined by radio-RP-HPLC and/or radio-TLC. For the latter, an aliquot (approx. 0.5 MBq) was mixed with an equal volume of solvent (MeCN/water/2 M aq. NaOAc/TFA, 6:4:1:1, *v/v/v/v*) and chromatographed on a silica gel 60 RP-18 F_{254}s plate.

2.3.3 General Labeling Procedures

GLP1 ^{18}F-Labeling of Silicon-based Fluoride Acceptors *via* Isotopic Exchange Reaction

a) Radiofluorination of model compound VI with Munich-dried [^{18}F]fluoride for kinetic measurements

^{18}F-Labeling of model compound **VI** for kinetic studies was performed according to a published protocol with minor changes[76]. Prior to radiofluorination, a $[K^+\subset 2.2.2]OH^-$ kit had been prepared by dissolving Kryptofix® 222 (42.9 mg, 114 µmol, 1.1 eq.) and KOH (5.61 mg, 100 µmol, 1.0 eq.) in pure water (1 mL), and freeze-drying the mixture. Aq. [^{18}F]fluoride (approx. 75 MBq) was loaded (male-to-female Luer direction) onto a Sep-Pak® Accell Plus QMA Carbonate Plus Light cartridge, which had previously been conditioned with pure water (10 mL). After drying with air (2 × 20 mL, female-to-male Luer direction), the cartridge was

slowly rinsed with anhyd. MeCN (10 mL, female-to-male Luer direction) and subsequently dried with air (2 × 20 mL, female-to-male Luer direction) again. The cartridge was finally purged (female-to-male Luer direction) with a solution of prepared $[K^+\subset 2.2.2]OH^-$ in anhyd. MeCN (500 µL), followed by air (5 mL, female-to-male Luer direction) in order to elute the dried [^{18}F]fluoride. A solution (1 mM, 150 µL, 150 nmol) of the model compound **VI** in anhyd. DMSO was combined with a solution (1 M, 30 µL, 30 µmol) of oxalic acid in anhyd. MeCN, and diluted with further anhyd. MeCN (120 µL). The mixture as well as the [^{18}F]fluoride eluate were separately equilibrated for 15 min at the respective reaction temperature (–10°C, –5°C, 0°C, 5°C, or 10°C). Initiation of the labeling reaction was performed by adding the prepared solution of model compound **VI** to the [^{18}F]fluoride eluate. The reaction mixture was kept at the respective temperature while aliquots (3–5 µL, approx. 0.3 MBq) were taken at various time points up to 40 min, quenched with solvent (MeCN/water/2 M aq. NaOAc/TFA, 9:1:1:1, *v/v/v/v*, 9 µL), chromatographed on a silica gel 60 F_{254} plate, and analyzed *via* radio-TLC to determine the percentage of residual [^{18}F]fluoride. Subsequent evaluation of kinetic measurements was accomplished using the OriginPro 2018b software (*OriginLab Corp.*, Northampton, MA, United States).

b) Radiofluorination of ligands with Munich-dried [^{18}F]fluoride

^{18}F-Labeling of ligands with *Munich*-dried [^{18}F]fluoride was performed following several reported procedures with slight modifications[76, 82]. Prior to radiofluorination, a $[K^+\subset 2.2.2]OH^-$ kit had been prepared by dissolving Kryptofix® 222 (51.3 mg, 136 µmol, 1.1 eq.) and KOH (7.01 mg, 125 µmol, 1.0 eq.) in pure water (1 mL), and freeze-drying the mixture. Aq. [^{18}F]fluoride (approx. 22–1˙650 MBq) was trapped (male-to-female Luer direction) onto a Sep-Pak® Accell Plus QMA Carbonate Plus Light cartridge, which had previously been conditioned with pure water (10 mL). After drying with air (2 × 20 mL, female-to-male Luer direction), the cartridge was slowly rinsed with anhyd. MeCN (10 mL, female-to-male Luer direction) and subsequently dried with air (2 × 20 mL, female-to-male Luer direction) again. The prepared $[K^+\subset 2.2.2]OH^-$ kit was dissolved in anhyd. MeCN (750 µL) and two-thirds of this cocktail (500 µL, female-to-male Luer direction), followed by air (5 mL, female-to-male Luer direction) were used to elute dried [^{18}F]fluoride from the cartridge. Afterwards, the eluate was partially neutralized with a

solution (1 M, 30 µL, 30 µmol) of oxalic acid in anhyd. MeCN. The mixture was incubated with a solution (1 mM) of the ligand in anhyd. DMSO according to the specified conditions (*Table 1*).

Table 1. Labeling conditions for the radiofluorination of ligands with *Munich*-dried [^{18}F]fluoride.

entry	**n(ligand)** [nmol]	**reaction time** [min]	**temperature**
I	30	5	rt
II	30	10	rt
III	30	10	95°C
IV	150	5	rt

Thereafter, the reaction mixture was diluted with PBS (pH 3 with 1 M aq. HCl, 10 mL) and passed (female-to-male Luer direction) through an Oasis® HLB Plus Light cartridge, which had previously been conditioned with abs. EtOH (10 mL) and pure water (10 mL). Finally, the cartridge was rinsed with PBS (10 mL, female-to-male Luer direction), dried with air (20 mL, female-to-male Luer direction), and the radiofluorinated ligand was eluted with a mixture (1:1, *v/v*, 300 µL, female-to-male Luer direction) of abs. EtOH and pure water. RCP of ^{18}F-labeled ligands was determined by radio-RP-HPLC and/or radio-TLC. For the latter, an aliquot (approx. 0.5 MBq) was mixed with an equal volume of solvent (MeCN/water/ 2 M aq. NaOAc/TFA, 6:4:1:1, *v/v/v/v*) and chromatographed on a silica gel 60 RP-18 F_{254}s plate.

c) Radiofluorination of ligands with dried [^{18}F]fluoride prepared by the SiFA-tailored Method

^{18}F-Labeling of ligands with [^{18}F]fluoride prepared by the *SiFA-tailored Method* was carried out according to a self-developed protocol. Aq. [^{18}F]fluoride (approx. 23–815 MBq) was trapped (male-to-female Luer direction) onto a Sep-Pak® Accell Plus QMA Carbonate Plus Light cartridge, which had previously been conditioned with pure water (10 mL). After drying with air (2 × 20 mL, female-to-male Luer direction), the cartridge was slowly rinsed with anhyd. DMSO (8 mL, female-to-male Luer direction) and subsequently dried with air (2 × 20 mL, female-to-male Luer direction) again. Dried [^{18}F]fluoride was eluted from the cartridge with a solution of NH_4HCOO (40.0 mg, 634 µmol) in anhyd. DMSO (500 µL, female-to-male Luer

direction), followed by air (5 mL, female-to-male Luer direction). The eluate was incubated with a solution (1 mM) of the ligand in anhyd. DMSO according to the specified conditions (*Table 2*).

Table 2. Labeling conditions for the radiofluorination of ligands with [^{18}F]fluoride prepared by the *SiFA-tailored Method*.

entry	**n(ligand)** [nmol]	**reaction time** [min]	**temperature**
I	0.5	5	70°C
II	0.5	8	65°C
III	20	10	95°C
IV	30	5	rt
V	30	10	rt
VI	30	10	95°C
VII	150	5	rt

Thereafter, the ^{18}F-labeled product was purified following a slightly modified protocol[76]. The reaction mixture was diluted with PBS (pH 3 with 1 M aq. HCl, 10 mL) and passed (female-to-male Luer direction) through an Oasis® HLB Plus Light cartridge, which had previously been conditioned with abs. EtOH (10 mL) and pure water (10 mL). Finally, the cartridge was rinsed with PBS (10 mL, female-to-male Luer direction), dried with air (20 mL, female-to-male Luer direction), and the radiofluorinated ligand was eluted with a mixture (1:1, *v/v*, 300 µL, female-to-male Luer direction) of abs. EtOH and pure water. RCP of ^{18}F-labeled ligands was determined by radio-RP-HPLC and/or radio-TLC. For the latter, an aliquot (approx. 0.5 MBq) was mixed with an equal volume of solvent (MeCN/water/2 M aq. NaOAc/TFA, 6:4:1:1, *v/v/v/v*) and chromatographed on a silica gel 60 RP-18 F_{254}s plate.

d) Automated radiofluorination of siPSMA-14 with Munich-dried [^{18}F]fluoride

The automated production of [^{18}F]siPSMA-**14** (*Figure 26*) for first-in-human applications was conducted in analogy to a literature protocol[82]. The GRP 2V module was equipped with two stopcock manifolds comprising a total of ten three-way valves (V1–V10). Transfer of fluids was accomplished through an integrated vacuum pump or a motor syringe.

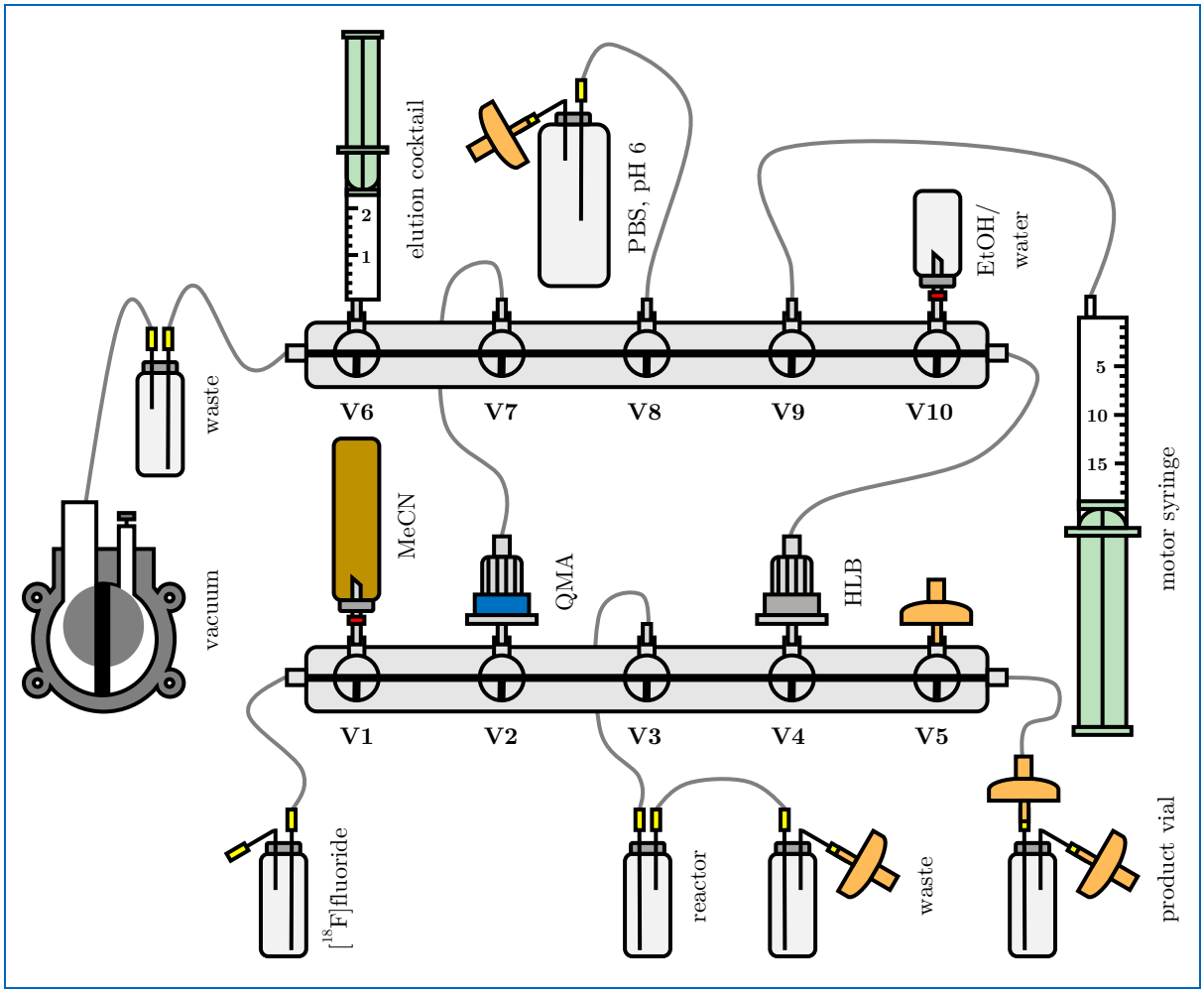

Figure 26. General scheme for the automated radiosynthesis of [^{18}F]siPSMA-**14** on a GRP 2V module with a double-cassette setup[82].

Prior to ^{18}F-labeling, a [K^+⊂2.2.2]OH^- kit had been prepared by dissolving Kryptofix® 222 (51.3 mg, 136 µmol, 1.1 eq.) and KOH (7.01 mg, 125 µmol, 1.0 eq.) in pure water (1 mL), and freeze-drying the mixture. In a first step, aq. [^{18}F]fluoride (approx. 583–11˙940 MBq) was transferred by means of vacuum through V1–V2–QMA–V7–V6–*waste*. Thereby, the activity was trapped onto a Sep-Pak® Accell Plus QMA Carbonate Plus Light cartridge, while the aq. solution was collected in the waste container. Anhyd. MeCN (8 mL) was subsequently transferred *via* vacuum through V1–V2–QMA–V7–V6–*waste* in order to dry the [^{18}F]fluoride on the cartridge. After the drying process, the vacuum pump was turned off and standard pressure was restored through a Millex-GS syringe filter connected to V5. Then, an elution cocktail of prepared [K^+⊂2.2.2]OH^- in anhyd. MeCN (750 µL) connected to V6 was pressurized with air (approx. 2 mL) from the motor syringe. After establishing a connection between the

elution cocktail and V6–V7–QMA–V2–V3–*reactor*, the $[K^+ \subset 2.2.2]OH^-$ solution was passively transferred into the capillary linking V7–QMA. The cocktail was passed with air from the motor syringe through QMA–V2–V3, eluting the dried [^{18}F]fluoride into the pre-filled reactor containing a solution (1 M, 30 µL, 30 µmol) of oxalic acid in anhyd. MeCN, as well as a solution (1 mM, 150 µL, 150 nmol) of siPSMA-**14** in anhyd. DMSO. ^{18}F-Labeling of the mixture was carried out for 5 min at rt, followed by dilution with PBS (pH 6, composed of $NaH_2PO_4 \cdot 2H_2O$ and NaOH dissolved in ultrapure water, 11.5 mL), which was transferred *via* the motor syringe through V8–V9–V10–HLB–V4–V3. Afterwards, the diluted mixture was passed by means of vacuum through V3–V4–HLB–V10–V9–V8–V7–V6–*waste*. [^{18}F]siPSMA-**14** was thereby retained onto an Oasis® HLB Plus Short cartridge, which was subsequently rinsed with PBS (pH 6, composed of $NaH_2PO_4 \cdot 2H_2O$ and NaOH dissolved in ultrapure water, 16 mL) that was transferred by the motor syringe through V8–V9–V10–HLB–V4–V3–*reactor*. A mixture (1:1, *v/v*, 3 mL) of ultrapure EtOH and ultrapure water, passed *via* the motor syringe through V10–HLB–V4–V5–*product vial*, was used to elute purified [^{18}F]siPSMA-**14** from the cartridge through a Cathivex-GV filter into the sterile vial. The radiofluorinated PSMA ligand was finally diluted with PBS (pH 6, composed of $NaH_2PO_4 \cdot 2H_2O$ and NaOH dissolved in ultrapure water, 16 mL), which was transferred by the motor syringe through V8–V9–V10–HLB–V4–V5–*product vial*.

GLP2 ^{125}I-Labeling of Reference Precursors

a) Synthesis of the radioiodinated reference ligand for evaluation of siPSMA ligands

HO-L-Glu-urea-L-Lys(4-[^{125}I]iodobenzoic acid)-OH (**XXV**)

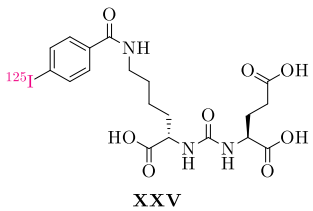

XXV

Chemical Formula: $C_{19}H_{24}{}^{125}IN_3O_8$
Molecular Weight: 547.32 g/mol

The radioiodinated PSMA reference ligand HO-L-Glu-urea-L-Lys(4-[^{125}I]iodobenzoic acid)-OH (**XXV**) was generated according to a previously published protocol[228, 231]. Initial preparation of peracetic acid was achieved by mixing aq. H_2O_2 (30%, *w/w*, 130 µL) with acetic acid (50 µL),

followed by incubation of the mixture for 2 h at rt. Afterwards, the reference precursor **XXII** (approx. 100 µg) was dissolved in a solution of peracetic acid (20 µL), acetic acid (10 µL), MeCN (20 µL), and basic Na[^{125}I]I (5–8 µL, 14–45 MBq). The reaction mixture was incubated for 15 min at rt and subsequently loaded (female-to-male Luer direction) onto a Sep-Pak® C18 Plus Short cartridge, which had previously been conditioned with MeOH (10 mL) and pure water (10 mL). After rinsing the cartridge with water (10 mL, female-to-male Luer direction) and air (2 × 20 mL, female-to-male Luer direction), the radioiodinated product was eluted (female-to-male Luer direction) with a mixture (1:1, *v/v*, 1.5 mL) of abs. EtOH/MeCN, and evaporated to dryness under a stream of nitrogen. The residue was redissolved in TFA (400 µL) and incubated for 30 min at rt. Finally, the solvent was evaporated to dryness and the crude product was redissolved in a mixture (1:5, *v/v*, 400 µL) of MeCN in water. After purification by prep. radio-RP-HPLC, **XXV** was afforded as a solution in MeCN/water (3.7–12 MBq, 20–41% RCY). The reference ligand solution was stored at 8°C and used for a maximum of three weeks. After activity determination of a defined volume, a solution (2 nM) of HO-L-Glu-urea-L-Lys(4-[^{125}I]iodobenzoic acid)-OH (**XXV**) in HBSS (add. 1% bovine serum albumin (BSA), *w/v*) was prepared for PSMA-binding and internalization studies (*Section 2.5.2* and *2.5.3*).

Prep. radio-RP-HPLC (column II, 20→40% B in A, 20 min, λ = 220 nm): t_R = 12.1 min, *K'* = 7.7.

b) Synthesis of the radioiodinated reference ligand for evaluation of ^{nat}Lu-rhFolate ligands

Pteroyl-L-Glu(3-[^{125}I]iodo-L-Tyr-OH)-OH (**XXVI**)

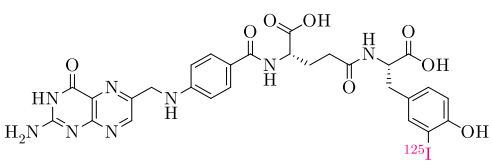

XXVI

Chemical Formula: $C_{28}H_{27}{}^{125}IN_8O_8$
Molecular Weight: 728.48 g/mol

Preparation of the radioiodinated FR reference ligand pteroyl-L-Glu(3-[^{125}I]iodo-L-Tyr-OH)-OH (**XXVI**) was accomplished using the *Iodo-Gen® Method* in analogy to a described protocol[232]. In brief, a solution of the reference precursor **XXIII** (approx. 200 µg) in DMSO (20 µL) was added to a buffer (pH 7.5, 250 µL) composed of 0.4 M aq. NaCl and 25 mM aq. tris(hydroxy-

methyl)aminomethane (TRIS) hydrochloride. The solution was subsequently transferred into a test tube coated with 1,3,4,6-tetrachloro-3α,6α-diphenylglycoluril (150 µg), and treated with basic Na[^{125}I]I (3–5 µL, 9.5–17 MBq). Upon incubation for 15 min at rt, the reaction mixture was separated from the insoluble residue and purified *via* prep. radio-RP-HPLC, giving **XXVI** as a solution in MeCN/water (1.7–2.3 MBq, 14–18% RCY). The identity of the radioiodinated reference ligand was confirmed through co-injection with the cold counterpart **XXIV**. The reference ligand solution was subsequently diluted with 0.1 M aq. sodium ascorbate (NaAsc, 40 µL), stored at 8°C, and used for a maximum of two weeks. After activity determination of a defined volume, a solution (1 nM) of pteroyl-L-Glu(3-[^{125}I]iodo-L-Tyr-OH)-OH (**XXVI**) in HBSS (add. 1% BSA, *w/v*) was prepared for FR-binding studies (*Section 2.5.2*).

Prep. radio-RP-HPLC (column II, 10→40% B in A, 20 min, λ = 220 nm): t_R = 12.7 min, K' = 8.1.

2.3.4 ^{18}F-Labeled siPSMA and ^{nat}Lu-rhFolate Ligands

[^{18}F]siPSMA Ligands

Radiofluorination of siPSMA ligands for respective characterization as well as *in vitro* and *in vivo* experiments was accomplished following GLP1b-I and GLP1c-I/II. Radiosynthesis of [^{18}F]siPSMA-**14** for first-in-human applications was performed *via* automated production (GLP1d).

[^{18}F]siPSMA-**0a**: Anal. radio-RP-HPLC (column II, 10→70% B in A, 15 min, λ = 220 nm): t_R = 13.6 min, K' = 8.8, purity: 99%.

[^{18}F]siPSMA-**0b**: Anal. radio-RP-HPLC (column IV, 10→70% B in A, 15 min, λ = 220 nm): t_R = 11.6 min, K' = 4.3, purity: >99%.

[^{18}F]siPSMA-**01**: Anal. radio-RP-HPLC (column II, 10→70% B in A, 15 min, λ = 220 nm): t_R = 11.3 min, K' = 7.1, purity: 97%.

[^{18}F]siPSMA-**02**: Anal. radio-RP-HPLC (column II, 10→70% B in A, 15 min, λ = 220 nm): t_R = 11.3 min, K' = 7.1, purity: 98%.

[^{18}F]siPSMA-**03**: Anal. radio-RP-HPLC (column IV, 10→70% B in A, 15 min, λ = 220 nm): t_R = 10.2 min, *K'* = 3.6, purity: >99%.

[^{18}F]siPSMA-**04**: Anal. radio-RP-HPLC (column II, 10→70% B in A, 15 min, λ = 220 nm): t_R = 11.1 min, *K'* = 7.0, purity: >99%.

[^{18}F]siPSMA-**05**: Anal. radio-RP-HPLC (column IV, 10→70% B in A, 15 min, λ = 220 nm): t_R = 11.4 min, *K'* = 4.2, purity: >99%.

[^{18}F]siPSMA-**06α**: Anal. radio-RP-HPLC (column II, 10→70% B in A, 15 min, λ = 220 nm): t_R = 11.2 min, *K'* = 7.1, purity: 95%.

[^{18}F]siPSMA-**06β**: Anal. radio-RP-HPLC (column IV, 10→70% B in A, 15 min, λ = 220 nm): t_R = 10.0 min, *K'* = 3.6, purity: >99%.

[^{18}F]siPSMA-**07**: Anal. radio-RP-HPLC (column IV, 10→70% B in A, 15 min, λ = 220 nm): t_R = 9.7 min, *K'* = 3.4, purity: 98%.

[^{18}F]siPSMA-**08**: Anal. radio-RP-HPLC (column II, 10→70% B in A, 15 min, λ = 220 nm): t_R = 10.7 min, *K'* = 6.7, purity: 96%.

[^{18}F]siPSMA-**09**: Anal. radio-RP-HPLC (column IV, 10→70% B in A, 15 min, λ = 220 nm): t_R = 10.3 min, *K'* = 3.7, purity: 97%.

[^{18}F]siPSMA-**10**: Anal. radio-RP-HPLC (column II, 10→70% B in A, 15 min, λ = 220 nm): t_R = 10.9 min, *K'* = 6.9, purity: >99%.

[^{18}F]siPSMA-**11**: Anal. radio-RP-HPLC (column II, 10→70% B in A, 15 min, λ = 220 nm): t_R = 11.3 min, *K'* = 7.1, purity: 94%.

[^{18}F]siPSMA-**12D**: Anal. radio-RP-HPLC (column II, 10→70% B in A, 15 min, λ = 220 nm): t_R = 11.4 min, *K'* = 7.2, purity: 97%.

[^{18}F]siPSMA-**12L**: Anal. radio-RP-HPLC (column II, 10→70% B in A, 15 min, λ = 220 nm): t_R = 11.5 min, *K'* = 7.3, purity: >99%.

[^{18}F]siPSMA-**13**: Anal. radio-RP-HPLC (column II, 10→70% B in A, 15 min, λ = 220 nm): t_R = 11.5 min, *K'* = 7.3, purity: 99%.

[^{18}F]siPSMA-**14**: Anal. radio-RP-HPLC (column II, 10→70% B in A, 15 min, λ = 220 nm): t_R = 11.1 min, *K'* = 7.0, purity: >99%.

[^{18}F]siPSMA-**15**: Anal. radio-RP-HPLC (column IV, 10→70% B in A, 15 min, λ = 220 nm): t_R = 12.6 min, *K'* = 4.7, purity: 99%.

[^{18}F]siPSMA-**16α**: Anal. radio-RP-HPLC (column IV, 10→70% B in A, 15 min, λ = 220 nm): t_R = 10.1 min, *K'* = 3.6, purity: 97%.

[^{18}F]siPSMA-**16β**: Anal. radio-RP-HPLC (column IV, 10→70% B in A, 15 min, λ = 220 nm): t_R = 10.5 min, *K'* = 3.8, purity: 97%.

[^{18}F]siPSMA-**17**: Anal. radio-RP-HPLC (column II, 10→70% B in A, 15 min, λ = 220 nm): t_R = 11.1 min, *K'* = 7.0, purity: 99%.

[^{18}F]siPSMA-**18D**: Anal. radio-RP-HPLC (column II, 10→70% B in A, 15 min, λ = 220 nm): t_R = 11.0 min, *K'* = 6.9, purity: >99%.

[^{18}F]siPSMA-**18L**: Anal. radio-RP-HPLC (column IV, 10→70% B in A, 15 min, λ = 220 nm): t_R = 10.2 min, *K'* = 3.6, purity: 97%.

[^{18}F]siPSMA-**19**: Anal. radio-RP-HPLC (column IV, 10→70% B in A, 15 min, λ = 220 nm): t_R = 11.4 min, *K'* = 4.2, purity: 98%.

[^{18}F]siPSMA-**20**: Anal. radio-RP-HPLC (column IV, 10→70% B in A, 15 min, λ = 220 nm): t_R = 10.9 min, *K'* = 4.0, purity: 96%.

[^{18}F]siPSMA-**21a**: Anal. radio-RP-HPLC (column IV, 10→70% B in A, 15 min, λ = 220 nm): t_R = 11.1 min, *K'* = 4.1, purity: 97%.

[^{18}F]siPSMA-**21b**: Anal. radio-RP-HPLC (column II, 10→70% B in A, 15 min, λ = 220 nm): t_R = 11.7 min, *K'* = 7.4, purity: 99%.

[^{18}F]siPSMA-**22**: Anal. radio-RP-HPLC (column IV, 10→70% B in A, 15 min, λ = 220 nm): t_R = 10.5 min, *K'* = 3.8, purity: 93%.

[^{18}F]siPSMA-**23**: Anal. radio-RP-HPLC (column II, 10→70% B in A, 15 min, λ = 220 nm): t_R = 11.2 min, *K'* = 7.1, purity: 97%.

[^{18}F]siPSMA-**24**: Anal. radio-RP-HPLC (column IV, 10→70% B in A, 15 min, λ = 220 nm): t_R = 10.4 min, *K'* = 3.7, purity: 95%.

[^{18}F]^{nat}Lu-rhFolate Ligands

Radiofluorination of ^{nat}Lu-rhFolate ligands for respective characterization as well as *in vitro* and *in vivo* experiments was conducted according to GLP1c-III/VI.

[^{18}F]^{nat}Lu-rhFolate-**01**: Anal. radio-RP-HPLC (column IV, 10→70% B in A, 15 min, λ = 220 nm): t_R = 12.6 min, *K'* = 4.7, purity: 92%.

[^{18}F]^{nat}Lu-rhFolate-**02**: Anal. radio-RP-HPLC (column III, 10→70% B in A, 15 min, λ = 220 nm): t_R = 10.7 min, *K'* = 4.7, purity: 91%.

[^{18}F]^{nat}Lu-rhFolate-**03**: Anal. radio-RP-HPLC (column IV, 10→70% B in A, 15 min, λ = 220 nm): t_R = 11.6 min, *K'* = 4.3, purity: >99%.

[^{18}F]^{nat}Lu-rhFolate-**04**: Anal. radio-RP-HPLC (column III, 10→70% B in A, 15 min, λ = 220 nm): t_R = 10.2 min, *K'* = 4.4, purity: 94%.

[^{18}F]^{nat}Lu-rhFolate-**05**: Anal. radio-RP-HPLC (column III, 10→70% B in A, 15 min, λ = 220 nm): t_R = 10.6 min, *K'* = 4.6, purity: 95%.

2.4 Characterization of Ligands

2.4.1 Human Serum Albumin Binding

In accordance with a published protocol, binding of siPSMA and ^{nat}Lu-rhFolate ligands to human serum albumin (HSA) was measured on the aforementioned (*Section 2.1.1*) HPLC system (*Shimadzu Deutschland GmbH*) equipped with a Chiralpak® HSA column (50 × 3 mm dimension, 5 µm particle size, 0.5 mL/min flow rate, *Chiral Technologies Europe SAS*, Illkirch-Graffenstaden, France)[233]. The mobile phase, composed of solvent D (50 mM aq. NH_4OAc solution, pH 7) and solvent E (2-propanol), was freshly prepared for each experiment and used only once. The nine reference substances benzyl alcohol, aniline, phenol, benzoic acid, carbamazepine, 4-nitrophenol, estradiol, probenecid, and glibenclamide (*Table 3*), as well as the analyzed ligands (0.5 mg/mL), were dissolved in a mixture (1:1, *v/v*) of solvent D/ solvent E and eluted from the HSA column (0–3 min: 100% D, 3–20 min: 20% E in D, λ = 254 nm). The column was kept at rt during the experiment and each run was stopped after detection of the signal in order to reduce the acquisition time.

Table 3. Reference substances used for the calibration curve with t_R determined on the Chiralpak® HSA column, calculated log(t_R), respective literature (lit.) HSA binding, and calculated log(K_{HSA})[233].

reference	t_R [min]	**log(t_R)**	**lit. HSA binding** [%]	**log(K_{HSA})**
benzyl alcohol	2.167	0.33586	13.15	–0.82482
aniline	2.467	0.39217	14.06	–0.79123
phenol	2.913	0.46434	20.69	–0.58901
benzoic acid	3.796	0.57933	34.27	–0.28941
carbamazepine	3.858	0.58636	75.00	0.46009
4-nitrophenol	4.914	0.69144	77.65	0.52185
estradiol	7.114	0.85211	94.81	1.18516
probenecid	8.430	0.92583	95.00	1.19957
glibenclamide	29.646	1.47197	99.00	1.69461

The nine reference substances covering an HSA-binding range from 13% to 99% were sequentially injected, and the log(K_{HSA}) values were plotted against the determined log(t_R) values using the OriginPro 2018b software (*OriginLab Corp.*) to generate a sigmoidal calibration curve (*Figure 27*)[233].

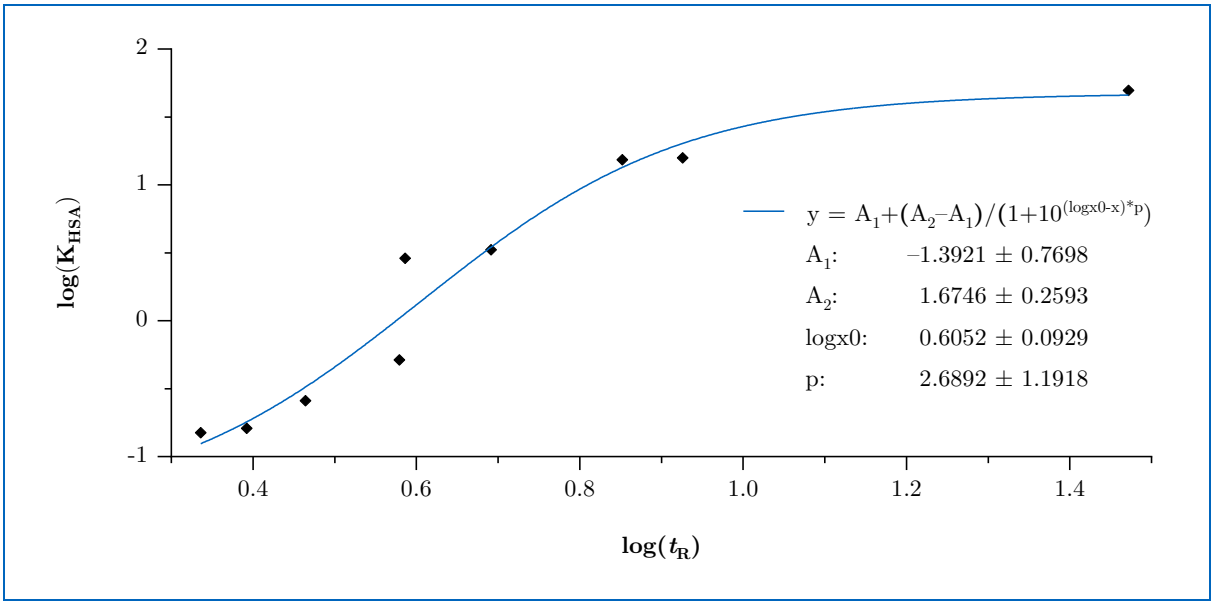

Figure 27. Exemplary sigmoidal calibration curve for HSA-binding determination displaying log(K_{HSA}) of literature reference substances *vs.* respective log(t_R) measured on the Chiralpak® HSA column[233].

2.4.2 Logarithmic *n*-Octanol-PBS Partition Coefficient

Determination of the logarithmic *n*-octanol-PBS partition coefficient at pH 7.4 (log$D_{7.4}$) was conducted according to a literature protocol with minor changes[76]. *n*-Octanol (quality grade "≥99%") and PBS used for this purpose were supplied by *Honeywell Deutschland Holding GmbH* (Offenbach am Main, Germany) and *Sigma-Aldrich Chemie GmbH*, respectively. An aliquot (approx. 0.5 MBq, ≤20 µL) of [^{18}F]siPSMA (GLP1b-I) or [^{18}F]^{nat}Lu-rhFolate ligand (GLP1c-VI) was added into a test tube containing *n*-octanol (500 µL) and PBS (pH 7.4, 500 µL). After vigorously shaking (Fisherbrand™ Wizard™ infrared vortex mixer, *Fisher Scientific GmbH*) the two-phase mixture for 3 min at rt, the test tube was ultracentrifuged (9˙000 rpm, 5 min) with a Heraeus™ Pico™ 17 microcentrifuge (*Fisher Scientific GmbH*) to achieve quantitative phase separation. Finally, 150 µL of each layer were pipetted off and measured for activity using a 2480 WIZARD^2® automatic gamma counter (*PerkinElmer Inc.*, Waltham, MA, United States). After repeating the experiment for at least five times, the *n*-octanol-PBS partition coefficient at pH 7.4, expressed in logarithmic form, was calculated according to the following equation (*Formula 2*).

$$\log D_{7.4} = \log \frac{\text{cpm}(n\text{-octanol})}{\text{cpm(PBS, pH 7.4)}}$$

$D_{7.4}$ = n-octanol-PBS partition coefficient at pH 7.4

cpm = counts per minute [1/min]

Formula 2. Calculation of the $\log D_{7.4}$ value.

2.5 *In vitro* Experiments

2.5.1 Cell Culture

Culture media supplements, including fetal calf serum (FCS) and L-glutamine, were obtained from *Merck KGaA*. Buffered solutions like PBS and HBSS were purchased from *VWR International GmbH* and *Merck KGaA*. BSA as an assay medium supplement and 2-(phosphonomethyl)pentanedioic acid (2-PMPA) as a blockade in internalization studies (*Section 2.5.3*) were delivered by *Sigma-Aldrich Chemie GmbH*.

PSMA-expressing LNCaP cells (human prostate carcinoma cell line) were purchased from the *Leibniz-Institute German Collection of Microorganisms and Cell Cultures* (Braunschweig, Germany) and grown as monolayers in Dulbecco's Modified Eagle Medium/Nutrient Mixture F-12 (DMEM/F-12, *Fisher Scientific GmbH*), supplemented with 10% (*v/v*) FCS[234].

FR-expressing KB cells (human cervix carcinoma cell line) were again supplied by the *Leibniz-Institute German Collection of Microorganisms and Cell Cultures* and grown as monolayers in folate-free RPMI medium without folic acid, vitamin B12, and phenol red (FFRPMI, *Cell Culture Technologies LLC*, Gravesano, Switzerland), supplemented with 300 mg/L (200 mM) L-glutamine and 10% (*v/v*) FCS[235].

Cells were continuously cultured in 75 cm^2 flasks (*Greiner Bio-One International GmbH*, Kremsmünster, Austria) and housed in a Heracell™ 150i incubator (*Fisher Scientific GmbH*), providing a humidified atmosphere with 5% CO_2 and a constant temperature of 37°C. To ensure optimum growth, cells were subcultured when a confluency of about 80% was reached. Therefore, the adherent cell layer was washed with PBS (10 mL, 37°C) and detached by a solution (0.05%/0.02%, *w/v*, 5 mL, 37°C) of trypsine/EDTA in PBS (*Merck KGaA*). Trypsinization of LNCaP or KB cells was conducted for 5 min at rt, followed by the addition of corresponding growth medium (5 mL, 37°C). After ultracentrifugation (1˙300 rpm, 3 min) of the suspension using a Heraeus™ Megafuge™ 16R (*Fisher Scientific GmbH*), the cell pellet was resuspended in the respective culture medium (20 mL, 37°C). Cell concentration (*Formula 3*) was determined under an AE2000 inverted microscope (*Motic Deutschland GmbH*, Wetzlar, Germany) by counting the cell number in a *Neubauer chamber* (*Paul Marienfeld*

GmbH & Co. KG, Lauda-Königshofen, Germany) loaded with a mixture (1:1, *v/v*, 100 µL) of the cell suspension and a solution (0.4%, *w/v*, *Sigma-Aldrich Chemie GmbH*) of trypan blue in aq. NaCl (0.81%, *w/v*) and aq. K_2HPO_4 (0.06%, *w/v*).

$$c_{cell} = Z \cdot 5{\cdot}000$$

c_{cell} = cell concentration [cells/mL]
Z = cell number in counting chamber

Formula 3. Calculation of the cell concentration in the *Neubauer chamber*.

2.5.2 Binding Affinity

IC$_{50}$ Determination of siPSMA Ligands

The binding assay for determination of PSMA affinity, expressed as half maximal inhibitory concentration (*IC*$_{50}$), was performed according to a slightly modified literature protocol[76]. LNCaP cells were harvested 24 ± 2 h prior to the experiment and seeded in 24-well plates (*Greiner Bio-One International GmbH*) at a concentration of 1.5×10^5 cells in 1 mL/well. After removal of the culture medium, LNCaP cells were washed with HBSS (add. 1% BSA, *w/v*, 500 µL, 4°C) and subsequently left 15 min on ice for equilibration in HBSS (add. 1% BSA, *w/v*, 200 µL, 4°C). Afterwards, the siPSMA ligand solution in HBSS at the appropriate concentration (10^{-4}–10^{-10} M, 25 µL), as well as a solution (2 nM, 25 µL) of the radioiodinated reference compound **XXV** (GLP2a) in HBSS (add. 1% BSA, *w/v*) were added, giving 10^{-5}–10^{-11} M solutions of the siPSMA inhibitor in the well supernatants. For the control series, HBSS (add. 1% BSA, *w/v*, 25 µL) was used instead of the siPSMA ligand solution. Each concentration and the control were prepared in triplicate. Upon 1 h incubation on ice, the assay medium was removed and cells were washed with HBSS (200 µL, 4°C). The wash fraction was combined with the supernatant, giving the unbound fraction of competitor **XXV**. Subsequently, LNCaP cells were treated with 1 M aq. NaOH (200 µL) for at least 10 min and the resulting cell lysate was removed. The wells were treated again with 1 M aq. NaOH (200 µL) and the wash fraction was combined with the previous lysate, affording the PSMA-bound fraction of radioligand **XXV**. Finally, both the supernatant and the lysate were measured for activity in the

2480 WIZARD²® automatic gamma counter (*PerkinElmer Inc.*). The experiment was repeated for at least three times and the IC_{50} value was calculated using the GraphPad PRISM 8.0.2 software (*Graphpad Software Inc.*, La Jolla, CA, United States).

IC_{50} Determination of ^{nat}Lu-rhFolate Ligands

The binding assay for determination of FR affinity, expressed as IC_{50}, was carried out according to a self-developed protocol. KB cells were harvested 24 ± 2 h prior to the experiment and seeded in poly-L-lysine-coated 24-well plates (*Greiner Bio-One International GmbH*) at a concentration of 4.0×10^5 cells in 1 mL/well. After removal of the culture medium, KB cells were washed with PBS (500 µL, 4°C) and subsequently left 15 min on ice for equilibration in FFRPMI (200 µL, 4°C). Afterwards, the ^{nat}Lu-rhFolate ligand solution in HBSS (add. 1% BSA, *w/v*) at the appropriate concentration (10^{-4}–10^{-10} M, 25 µL), as well as a solution (1 nM, 25 µL) of the radioiodinated reference compound **XXVI** (GLP2b) in HBSS (add. 1% BSA, *w/v*) were added, giving 10^{-5}–10^{-11} M solutions of the ^{nat}Lu-rhFolate ligand in the well supernatants. For the control series, HBSS (add. 1% BSA, *w/v*, 25 µL) was used instead of the ^{nat}Lu-rhFolate ligand solution. Each concentration and the control were prepared in triplicate. Upon 4 h incubation on ice, the assay medium was removed and cells were washed with HBSS (200 µL, 4°C). The wash fraction was combined with the supernatant, affording the unbound fraction of competitor **XXVI**. Subsequently, KB cells were treated with 1 M aq. NaOH (200 µL) for at least 10 min and the resulting cell lysate was removed. The wells were treated again with 1 M aq. NaOH (200 µL) and the wash fraction was combined with the previous lysate, giving the FR-bound fraction of the radioiodinated reference **XXVI**. Finally, both the supernatant and the lysate were measured for activity in the 2480 WIZARD²® automatic gamma counter (*PerkinElmer Inc.*). The experiment was repeated for at least three times and the IC_{50} value was calculated using the GraphPad PRISM 8.0.2 software (*Graphpad Software Inc.*).

2.5.3 Internalization

Internalization studies of [^{18}F]siPSMA ligands were conducted following a modified protocol described in the literature[76]. LNCaP cells were harvested 24 ± 2 h prior to the experiment and seeded in poly-L-lysine-coated 24-well plates (*Greiner Bio-One International GmbH*) at a

concentration of 1.25×10^5 cells in 1 mL/well. After removal of the culture medium, cells were washed with DMEM-F12 (add. 5% BSA, *w/v*, 500 µL) and left to equilibrate in DMEM-F12 (add. 5% BSA, *w/v*, 175 µL) for 15 min at 37°C. Afterwards, a combined solution (5 nM, 25 µL) of the [^{18}F]siPSMA ligand (GLP1c-I/II) in PBS and the reference compound **XXV** (GLP2a, 2 nM, 25 µL) in HBSS (add. 1% BSA, *w/v*) was added. Each well was subsequently treated with either DMEM-F12 (add. 5% BSA, *w/v*, 25 µL) or a solution (100 µM, 25 µL) of 2-PMPA in PBS for blockade, and LNCaP cells were incubated for 1 h at 37°C. The control as well as the blockade experiments were performed in triplicate. The 24-well plate was subsequently placed on ice for 3 min and the assay medium was removed. Each well was rinsed with PBS (250 µL, 4°C) and the fractions were combined with the previous assay media, giving the unbound fraction of the [^{18}F]siPSMA ligand. To obtain the surface-bound fraction, LNCaP cells were incubated with a solution (10 µM, 250 µL, 4°C) of 2-PMPA in PBS for 5 min and rinsed again with PBS (250 µL, 4°C). The internalized fraction was afforded by incubating the cells with 1 M aq. NaOH (250 µL) for at least 10 min and subsequently rinsing the wells again with 1 M aq. NaOH (250 µL). Finally, the supernatant, the surface-bound fraction, and the lysate were measured for activity in the 2480 WIZARD^2® automatic gamma counter (*PerkinElmer Inc.*). Determined data were corrected for unspecific internalization and normalized to the specific internalization observed for the reference compound **XXV**.

2.6 *In vivo* Experiments

Unless otherwise stated, the same culture media, buffers, reagents, and solvents were used as previously described (*Section 2.1.1*, *2.3.1*, and *2.5.1*). All animal experiments were conducted in accordance with general animal welfare regulations in Germany (approval ROB-55.2-2532.Vet_02-18-109) and institutional guidelines for the care and use of animals.

2.6.1 Preparation of Tumor Mice

To establish tumor xenografts for the *in vivo* evaluation of [^{18}F]siPSMA ligands, LNCaP cells (approx. 1×10^7) were resuspended in a mixture (1:1, *v/v*, 200 µL) of Cultrex® BME Type 3 (*Trevigen Inc.*, Gaithersburg, MD, United States) and DMEM-F12. Thereafter, the cell suspension was inoculated subcutaneously in the right shoulder of 6- to 8-week-old CB17-SCID male mice purchased from *Charles River Laboratories Germany GmbH* (Sulzfeld, Germany). Animals were used for experiments when the tumor volume reached 4–10 mm in diameter (approx. 3–4 weeks after inoculation).

In vivo experiments for the evaluation of [^{18}F]^{nat}Lu-rhFolate ligands were conducted on 6- to 7-week-old CD1-Foxn1^{nu} female nude mice obtained from *Charles River Laboratories Germany GmbH*. Throughout the whole study, starting seven days prior to tumor inoculation, animals were kept on a folic acid deficient (<0.5 mg/kg) purified rodent diet (*ssniff Spezialdiäten GmbH*, Soest, Germany). To establish tumor xenografts, KB cells (approx. 5×10^6) were resuspended in FFRPMI (150 µL) and inoculated subcutaneously in the right shoulder. Animals were used for experiments when the tumor volume reached 3–6 mm in diameter (approx. 8–10 days after inoculation).

2.6.2 Biodistribution Studies

For biodistribution studies, isoflurane-anesthetized tumor-bearing mice (n = 3–5) were injected *via* the tail vein with a solution (150 µL) of the diluted [^{18}F]siPSMA (approx. 0.6–4.3 MBq, 0.2 nmol, GLP1b-I) or [^{18}F]^{nat}Lu-rhFolate ligand (approx. 1.3–4.4 MBq, 0.2 nmol, GLP1c-III) in PBS. Mice were subsequently sacrificed at 1 h p.i. In the competition study with [^{18}F]^{nat}Lu-rhFolate-**02** (n = 3), a solution of folic acid (100 µg, 227 nmol) in PBS (150 µL) was adminis-

tered 5 min prior to radiotracer injection. Selected organs, tissues, and body fluids (blood, heart, lung, liver, spleen, pancreas, stomach without contents, intestine with contents, kidney, adrenal gland, muscle, bone, tumor, salivary gland, and tail) were removed by dissection, weighted, and measured for activity using the 2480 WIZARD^{2}® gamma counter (*PerkinElmer Inc.*).

2.6.3 Small Animal µPET/CT Imaging

For µPET/CT imaging studies of [^{18}F]^{nat}Lu-rhFolate ligands, tumor-bearing mice were anesthetized with isoflurane and injected *via* the tail vein with a solution (150 µL) of the diluted [^{18}F]^{nat}Lu-rhFolate ligand (approx. 1.5–4.1 MBq, 0.2 nmol, GLP1c-III) in PBS. In the competition study with [^{18}F]^{nat}Lu-rhFolate-**02**, a solution of folic acid (100 µg, 227 nmol) in PBS (150 µL) was administered 5 min prior to radiotracer injection. Small animal µPET/CT imaging was conducted on a VECTor^{4}CT scanner (*MILabs B.V.*, Utrecht, the Netherlands) equipped with a HE-GP-RM collimator. Static images were recorded at 1 h p.i. with an acquisition time of 15 min. Recorded data were subsequently processed applying a pixel-based Similarity-Regulated Ordered Subsets Expectation Maximization (SROSEM) algorithm and reconstructed using the software PMOD 4.0 (*PMOD Technologies LLC*, Zürich, Switzerland).

2.6.4 Metabolite Analysis

To identify the *in vivo* metabolites of [^{18}F]^{nat}Lu-rhFolate-**03**, an isoflurane-anesthetized 15-week-old CB17-SCID female mouse (*Charles River Laboratories Germany GmbH*) was injected *via* the tail vein with a solution (150 µL) of the diluted ^{18}F-labeled FR ligand (approx. 19 MBq, 2.4 nmol, GLP1c-III) in PBS. The mouse was subsequently sacrificed at 40 min p.i. Selected body fluids (urine, blood) and tissues (liver, kidney) were removed by dissection and processed according to a slightly modified literature protocol[168]. Ultracentrifugation of samples was performed on the Heraeus™ Pico™ 17 microcentrifuge (*Fisher Scientific GmbH*), while homogenization of tissue was accomplished using an MM 400 ball mill (*Retsch GmbH*, Haan, Germany).

Collected urine was ultracentrifuged (13'000 times gravity (× g), 5 min), which provided the injectable supernatant for metabolite analysis.

The recovered blood sample was diluted with water to 1 mL and subsequently ultracentrifuged (13˙000 × g, 5 min) twice. Thereafter, the resulting supernatant was loaded onto a Strata-X® cartridge (33 µm polymeric RP, 500 mg sorbent weight, *Phenomenex Ltd. Deutschland*, Aschaffenburg, Germany), which had previously been conditioned with MeOH (5 mL) and water (5 mL). The cartridge was subsequently washed with water (5 mL), followed by elution with a mixture (60:40:1, *v/v/v*, 5 mL) of MeCN, water, and TFA. During this process, the eluate was fractionally (500 µL) collected. Fractions with the highest amount of radioactivity were combined and diluted with an equal volume of water, which resulted in the injectable sample for metabolite analysis.

Solid tissue samples of collected liver and kidney were respectively transferred into a test tube containing three grinding balls (3 mm diameter) and an extraction buffer composed of 20 mM aq. folic acid (100 µL), 1 M aq. 4-(2-hydroxyethyl)-1-piperazineethanesulfonic acid (pH 7.4, 850 µL), and 1 M aq. NaCl (100 µL). The tissues were subsequently homogenized (30 Hz, 10 min) and the resulting mixtures were subjected to ultracentrifugation (13˙000 × g, 5 min). After separation of the supernatants, the entire procedure was repeated with the organ residues. Finally, the combined supernatant fractions were purified by SPE as described for the blood sample. Fractions with the highest amount of radioactivity were combined and diluted with an equal volume of water, resulting in the injectable sample for metabolite analysis.

Processed samples were analyzed *via* radio-RP-HPLC on the aforementioned (*Section 2.2.1*) column II (Multospher® 100 RP 18-5µ, 125 × 4.6 mm dimension, 5 µm particle size, 1 mL/min flow rate) in an HPLC system (*Shimadzu Deutschland GmbH*) consisting of gradient pumps (two LC-20AD), a system controller (CBM-20A), a column oven (CTO-10ASVP), an UV-visible detector (SPD-20A), and a Flowstar^2 LB 514 radiodetector (*Berthold Technologies GmbH & Co.KG*). Samples were eluted by applying the previously introduced (*Section 2.1.1*) solvent A and solvent B at a constant flow. LabSolutions 5.92 software (*Shimadzu Deutschland GmbH*) was employed for analysis of radiochromatograms.

Anal. radio-RP-HPLC (column II, 10→70% B in A, 15 min, $\lambda = 220$ nm): $t_R = 11.3$ min, $K' = 7.1$.

2.7 Human Application

First applications of [^{18}F]siPSMA-**14** in humans were conducted at the *University Hospital Ulm* in compliance with the respective institutional review board and the German Medicinal Products Act (AMG §13 para. 2b). PET/CT images were recorded on a Biograph mCT (40)S (*Siemens Healthineers AG*, Erlangen, Germany) in 3D modality with an acquisition time of 3 min per bed position using time-of-flight technique.

Mean standardized uptake values (SUV_{mean}) for [^{18}F]siPSMA-**14** were determined under consideration of 47 prostate cancer patients (69 ± 7 years, Gleason score 6–9, median prostate-specific antigen (PSA) of 3.20 ng/mL, PSA range of 0.09–1000 ng/mL)[236]. After intravenous application of [^{18}F]siPSMA-**14** (344 ± 12 MBq, GLP1d) without additional administration of furosemide for forced diuresis, PET/CT scans were recorded at T1 (60 min p.i., head to mid-thigh, $n = 7$), T2 (90 min p.i., head to mid-thigh, $n = 40$), and T3 (120 min p.i., lower thorax to upper thigh, $n = 7$)[236]. SUV_{mean} were measured for normal tissues (blood pool, liver, spleen, duodenum, kidney cortex, and bladder) and malignant masses (prostatic, lymphatic, and bone lesions) by respectively drawing a fixed-size region of interest around the area with increased radiotracer accumulation[236].

The primary staging and restaging performance of [^{18}F]siPSMA-**14** was evaluated under consideration of a mixed patient population[237]. Among a total of 134 patients with prostate cancer (70 ± 8 years, Gleason score 6–9, median PSA of 2.36 ng/mL, PSA range of 0.08–1898 ng/mL), 54 patients underwent primary staging and 80 patients were subjected to restaging[237]. Application of [^{18}F]siPSMA-**14** (374 ± 8 MBq, GLP1d) was performed intravenously without administration of furosemide for forced diuresis[237]. PET/CT images were acquired at 90 min p.i. and further evaluated by two nuclear medicine physicians and radiologists[237]. The investigated lesions, including the local tumor as well as lymph node, bone, and visceral metastases, were graded using a five-scale system ranging from C1 (definitely benign) to C5 (definitely malignant)[237]. Interobserver agreement was finally assessed using Cohen's kappa[237].

PSA-stratified detection rates for [^{18}F]siPSMA-**14** were determined in a retrospective analysis involving a subgroup of 87 patients (median PSA of 1.06 ng/mL, PSA range of 0.02–1500 ng/mL) who underwent restaging[238]. After intravenous application of [^{18}F]siPSMA-**14** (346 ± 9 MBq, GLP1d) without further administration of furosemide for forced diuresis, PET/CT scans were recorded at 90 min p.i.[238]. The determined detection rates for lesions, including local tumor as well as lymph node and bone metastases, were stratified by PSA subgroups (0 to <0.5 ng/mL, 0.5 to <2.0 ng/mL, or ≥2.0 ng/mL)[238].

3 Results and Discussion

3.1 Radiofluorination of Silicon-based Fluoride Acceptor-bearing compounds by Isotopic Exchange Reaction

Up to the early 2000s, isotopic exchange was considered an unsuitable approach for the preparation of radiofluorinated tracers, primarily because of the inherently poor A_ms resulting from the inability to separate the significant amounts of chemically identical precursor. Unexpectedly, *Schirrmacher* and colleagues were able to break this dogma by demonstrating highly efficient ^{18}F-for-^{19}F isotopic exchange on Silicon-based Fluoride Acceptors even with minimal precursor quantities, thereby opening a new chapter in ^{18}F-labeling chemistry[54].

3.1.1 Synthetic Preparation of Building Blocks and the Model Compound

The synthesis of Silicon-based Fluoride Acceptor-bearing building blocks utilized in this doctoral thesis was carried out following several published protocols (*Scheme 1*)[65, 77, 220].

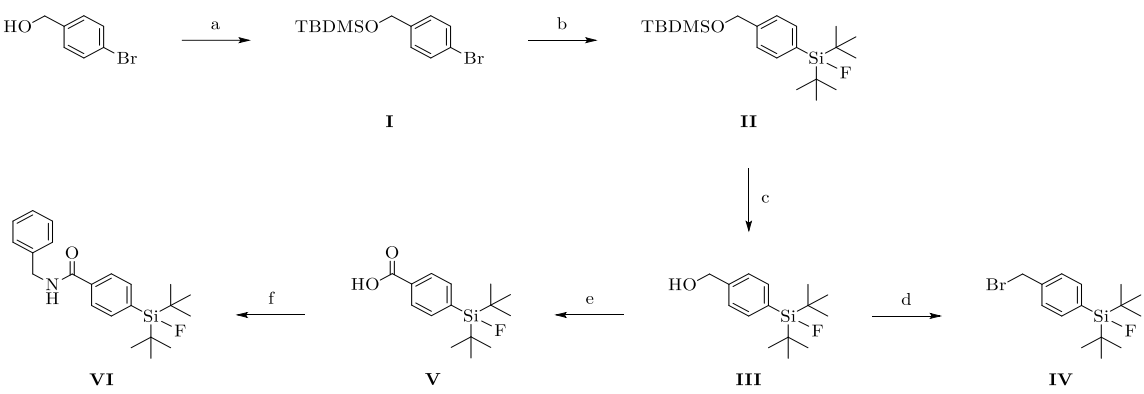

Scheme 1. Synthesis of Silicon-based Fluoride Acceptor-bearing building blocks **II** to **V** and model compound **VI**: a) imidazole, TBDMSCl, (DMF); b) *t*BuLi, di-*tert*-butyldifluorosilane, (THF); c) aq. HCl, (MeOH); d) triphenylphosphine, tetrabromomethane, (DCM); e) aq. $KMnO_4$, *t*BuOH, aq. NaH_2PO_4, $KMnO_4$, (DCM); f) HOBt, TBTU, DIPEA, benzylamine, (DMF).

SiFA-BnBr (**IV**) was prepared in moderate total yield (47%) by *Appel reaction* on alcohol **III**. A minor modification was made for the synthesis of SiFA-BzA (**V**). In order to avoid the stepwise oxidation route, alcohol **III** was directly converted to the respective acid **V** with an

acceptable overall yield of 36%. Its conversion with benzylamine afforded the Silicon-based Fluoride Acceptor-bearing model compound **VI**.

3.1.2 Radiofluorination using [^{18}F]Fluoride prepared by the *Munich Method*

First attempts to radiolabel Silicon-based Fluoride Acceptor-bearing compounds were conducted using azeotropically dried [^{18}F]fluoride[80]. In this context, it was soon recognized that partial neutralization of the required base during activity preparation represented a prerequisite for efficient radiofluorination[80]. Unfortunately, the exact amount of acid needed for neutralization was difficult to determine due to variable base adsorption on the drying vessel wall[80]. As a consequence, RCYs for the radiofluorination of Silicon-based Fluoride Acceptor-bearing compounds were only reproducible to a limited extent[80]. It was later on realized that [^{18}F]fluoride preparation according to the so-called *Munich Method* constituted the preferable technique for this purpose[80]. Originally developed by *Wessmann et al.*, the *Munich Method* consists of trapping aq. [^{18}F]fluoride on an anion exchange resin, followed by on-cartridge drying of the activity using an anhyd. solvent, and recovery of dried [^{18}F]fluoride with an elution cocktail composed of [K$^+$⊂2.2.2]OH$^-$ in MeCN[239]. Application of this approach to obtain [^{18}F]fluoride intended for radiolabeling of Silicon-based Fluoride Acceptors allowed to reach two goals at once. On the one hand, preparation of dried [^{18}F]fluoride by SPE evaded the laborious and time-consuming azeotropic distillation procedure[239]. On the other hand, partial neutralization of the eluate was easier to achieve due to the absence of adsorption effects[80]. *Wängler et al.* were the first to exactly quantify the influence of eluate neutralization on the subsequent radiofluorination of a Silicon-based Fluoride Acceptor-bearing SSTR ligand[80]. The group adjusted the hydroxide-containing [^{18}F]fluoride eluate by addition of oxalic acid and determined the highest radiochemical conversion (RCC) using [K$^+$⊂2.2.2]OH$^-$ and the acid in a molar ratio of 4[80]. A similar observation was made by *Wurzer et al.* investigating the isotopic exchange reaction on the Silicon-based Fluoride Acceptor-bearing ligand ^{nat}Ga-rhPSMA-7 with the identical [^{18}F]fluoride preparation strategy[240]. Thereby, substantial ^{18}F-incorporation was only reported when the molar ratio between [K$^+$⊂2.2.2]OH$^-$ and oxalic acid corresponded to 2.8–5.6[240]. Their elaborated radiofluorination protocol included [^{18}F]fluoride preparation by the *Munich Method*, neutralization of the eluate with oxalic acid, optimized reaction conditions for

the isotopic exchange reaction, and final radiotracer workup by means of SPE (*Figure 28*)[76, 82]. Owing to its simplicity, this protocol was initially applied for ^{18}F-labeling of Silicon-based Fluoride Acceptor-bearing ligands developed in the present work.

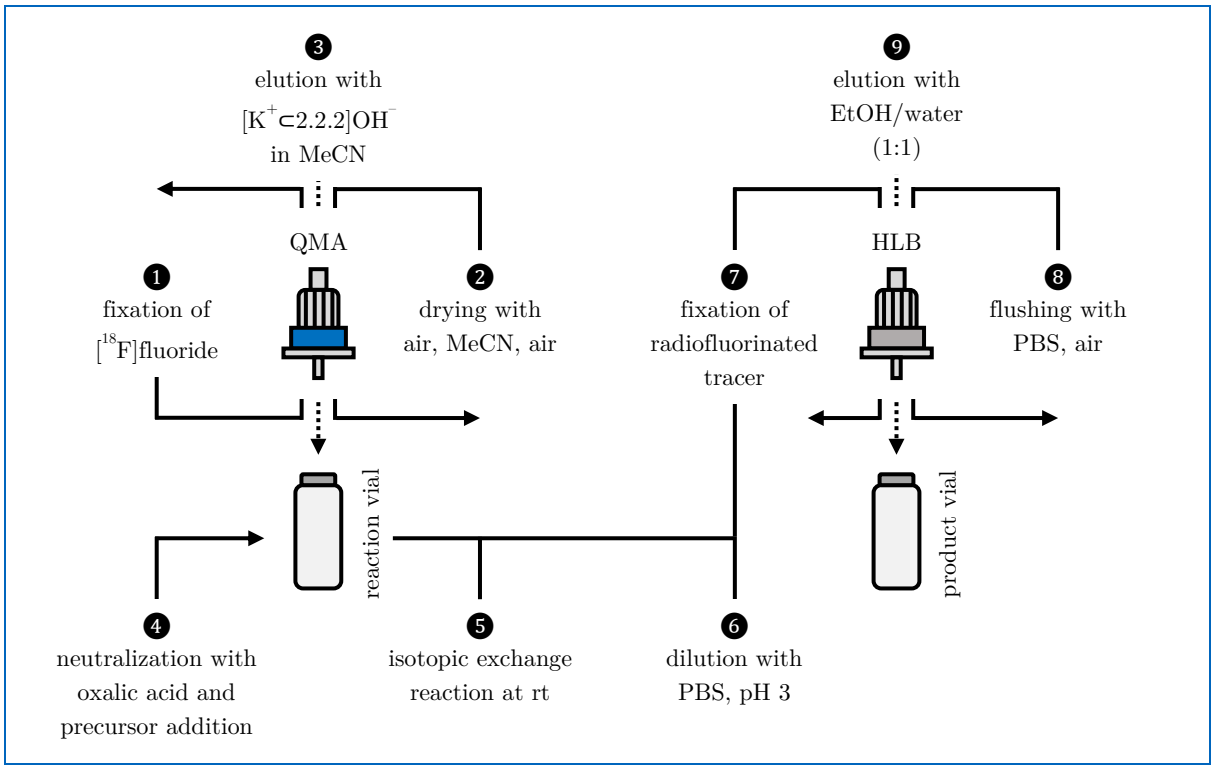

Figure 28. General scheme describing [^{18}F]fluoride preparation according to the *Munich Method* (steps 1–3), its subsequent application for radiofluorination of a Silicon-based Fluoride Acceptor-bearing compound (steps 4–5), and final radiotracer purification *via* SPE (steps 6–9)[76, 82].

In detail, the optimized radiofluorination procedure established by *Wurzer et al.* starts with the loading of aq. [^{18}F]fluoride onto a strong anion exchange (Sep-Pak® Accell Plus QMA Carbonate Plus Light) cartridge and subsequent on-cartridge drying of the activity with air (40 mL), MeCN (10 mL), and air (40 mL) again[82]. Recovery of dried [^{18}F]fluoride is realized by inverse purging of the cartridge with an elution cocktail containing a solution of KOH (83 µmol) and Kryptofix® 222 (91 µmol) in MeCN (500 µL)[82]. Afterwards, the eluate is partially neutralized by addition of oxalic acid (1 M in MeCN, 30 µL, 30 µmol) and diluted with the Silicon-based Fluoride Acceptor-bearing compound (1 mM in DMSO, 30–150 µL, 30–150 nmol)[82]. Labeling occurs for 5 min at rt, followed by dilution of the reaction mixture with an acidic PBS buffer (pH 3, 10 mL)[82]. Tracer purification is conducted *via* simple SPE, since unincorporated [^{18}F]fluoride represents the only impurity that needs to be separated[76].

Therefore, the ^{18}F-labeled compound is retained onto a purification (Oasis® HLB Plus Light) cartridge, which is subsequently flushed with PBS (10 mL) and air (20 mL)[82]. Elution of the radiotracer is finally accomplished with a mixture (1:1, *v/v*, 300 µL) of EtOH and water[82].

3.1.3 Determination of Rate Constants and *Arrhenius Parameters*

Previously reported density-functional theory calculations by *Schirrmacher et al.* showed that the efficiency of ^{18}F-incorporation in Silicon-based Fluoride Acceptors relies on the relatively low activation energy barrier for the ^{18}F-for-^{19}F isotopic exchange reaction[54]. The mechanism of [^{18}F]fluoride insertion was suggested to follow the scheme of S_N2, involving the formation of a thermodynamically stable penta-coordinated silicon intermediate during the transition state[54]. In this context, *Kostikov et al.* were the first to experimentally measure the *Arrhenius parameters* (activation energy and pre-exponential factor) of the isotopic exchange on a Silicon-based Fluoride Acceptor, namely *N*-(4-(di-*tert*-butylfluorosilyl)benzyl)-2-hydroxy-*N*,*N*-dimethylethylammonium bromide (SiFAN$^+$Br$^-$)[77]. For radiofluorination of this model compound and related kinetic measurements, the research group applied scrupulously dried [^{18}F]fluoride aliquots afforded by laborious azeotropic co-evaporation with a solution of $[K^+\subset 2.2.2]_2C_2O_4^{2-}$ in MeCN[77]. By contrast, the later established use of *Munich*-dried [^{18}F]fluoride adjusted through the addition of oxalic acid provided a considerably simpler alternative[80]. Yet, this method for [^{18}F]fluoride preparation implies a completely different labeling environment for radiofluorination. Noteworthy, although the neutralization reaction generates a certain amount of water in the eluate, the isotopic exchange was found to proceed with high efficiency[80, 240]. It was consequently intriguing to determine the *Arrhenius parameters* using partially neutralized *Munich*-dried [^{18}F]fluoride, since the specific reaction environment appeared to play a significant role. For this purpose, a relatively simple Silicon-based Fluoride Acceptor model compound **VI** without any further functional groups was prepared and its isotopic exchange with [^{18}F]fluoride was investigated at temperatures between 263 K and 283 K. Therefore, the model compound **VI** was combined with oxalic acid and diluted with *Munich*-dried [^{18}F]fluoride (61 ± 22 MBq, molar ratio between $[K^+\subset 2.2.2]OH^-$ and oxalic acid of 3.3), giving a 1.88×10^{-4} M solution. This mixture was kept at the respective temperature and aliquots were analyzed by radio-TLC at different time points to monitor reaction kinetics (*Figure 29*).

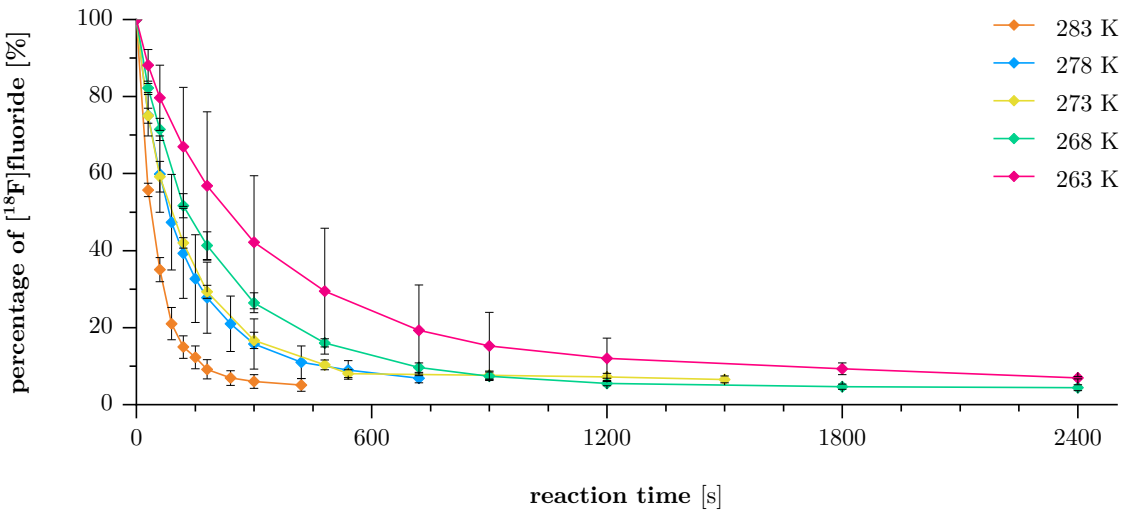

Figure 29. Kinetic curves for the ^{18}F-for-^{19}F isotopic exchange reaction on model compound **VI** (1.88×10^{-4} M, 61 ± 22 MBq [^{18}F]fluoride starting activity) illustrating the [^{18}F]fluoride consumption at 263 K (red line), 268 K (green line), 273 K (yellow line), 278 K (blue line), and 283 K (orange line) over time.

As the isotopic exchange reaction is assumed to follow pseudo-first order kinetics, the temperature-dependent rate constants were determined according to the following equations (*Formula 4*)[77].

$$[^{18}\text{F}]\text{fluoride} + [^{19}\text{F}]\mathbf{VI} \rightleftharpoons [^{19}\text{F}]\text{fluoride} + [^{18}\text{F}]\mathbf{VI}$$

$$-\frac{dc}{dt}([^{18}\text{F}]\text{fluoride}) = k \cdot c([^{18}\text{F}]\text{fluoride}) \cdot c([^{19}\text{F}]\mathbf{VI})$$

(i) under the assumption that $c_0([^{19}\text{F}]\mathbf{VI}) \neq c_0([^{18}\text{F}]\text{fluoride})$:

$$\frac{1}{c_0([^{19}\text{F}]\mathbf{VI}) - c_0([^{18}\text{F}]\text{fluoride})} \cdot \ln\frac{c([^{19}\text{F}]\mathbf{VI}) \cdot c_0([^{18}\text{F}]\text{fluoride})}{c([^{18}\text{F}]\text{fluoride}) \cdot c_0([^{19}\text{F}]\mathbf{VI})} = k \cdot t$$

(ii) under the assumption that $c_0([^{19}\text{F}]\mathbf{VI}) \gg c_0([^{18}\text{F}]\text{fluoride})$ and $c_0([^{19}\text{F}]\mathbf{VI}) \approx c([^{19}\text{F}]\mathbf{VI})$:

$$\frac{1}{c_0([^{19}\text{F}]\mathbf{VI}) - c_0([^{18}\text{F}]\text{fluoride})} \cdot \ln\frac{c([^{19}\text{F}]\mathbf{VI}) \cdot c_0([^{18}\text{F}]\text{fluoride})}{c([^{18}\text{F}]\text{fluoride}) \cdot c_0([^{19}\text{F}]\mathbf{VI})} \approx \frac{1}{c_0([^{19}\text{F}]\mathbf{VI})} \cdot \ln\frac{c_0([^{18}\text{F}]\text{fluoride})}{c([^{18}\text{F}]\text{fluoride})} = k \cdot t$$

$$\ln\frac{c_0([^{18}\text{F}]\text{fluoride})}{c([^{18}\text{F}]\text{fluoride})} = k \cdot t \cdot c_0([^{19}\text{F}]\mathbf{VI})$$

c = concentration at time t [M] — k = rate constant [1/Ms]

c_0 = initial concentration [M] — t = time [s]

Formula 4. Calculation of temperature-dependent rate constants assuming pseudo-first order kinetics for the ^{18}F-for-^{19}F isotopic exchange reaction on Silicon-based Fluoride Acceptors[77, 241].

Thus, when plotting the natural logarithm of reciprocal residual [^{18}F]fluoride percentage against the reaction time for the respective temperature, the initial slope of the curve reflects the product between the temperature-dependent rate constant and the initial concentration of model compound **VI** (*Figure 30*).

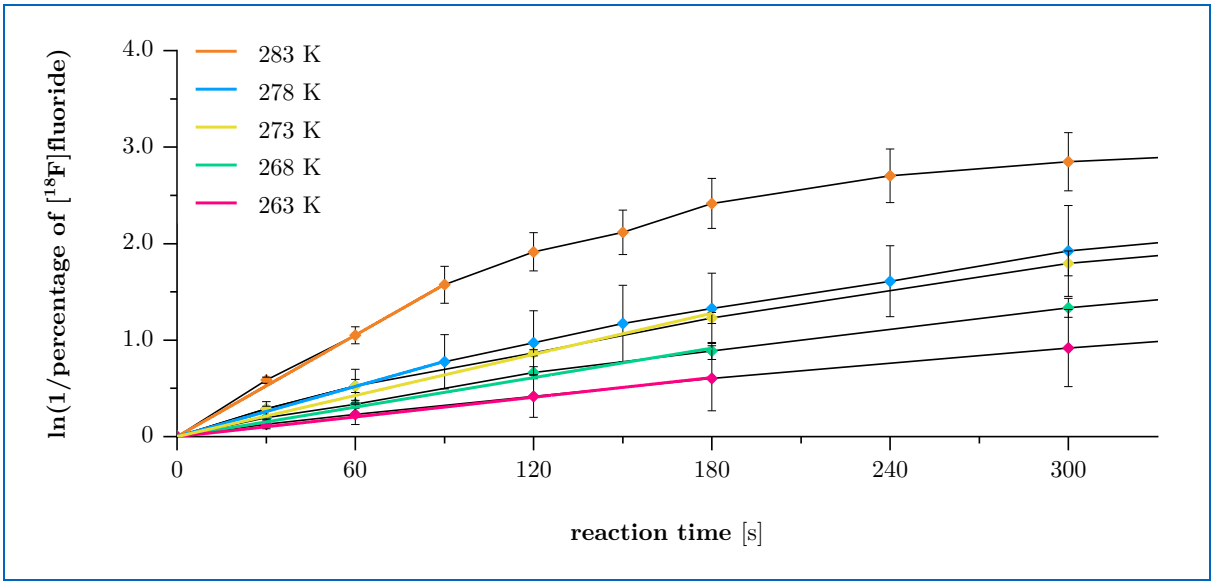

Figure 30. Determination of temperature-dependent rate constants for the ^{18}F-for-^{19}F isotopic exchange reaction on model compound **VI** (1.88×10^{-4} M, 61 ± 22 MBq [^{18}F]fluoride starting activity) by plotting the natural logarithm of reciprocal residual [^{18}F]fluoride percentage against the reaction time for respective temperatures. Bold lines through the origin depict the best fit for initial data measured at 263 K (red line), 268 K (green line), 273 K (yellow line), 278 K (blue line), and 283 K (orange line).

Taking into account the initial concentration of model compound **VI**, the temperature-dependent rate constants for the assumed pseudo-first order kinetics of the ^{18}F-for-^{19}F isotopic exchange reaction were calculated as follows (*Table 4*).

Table 4. Determined rate constants (k) for the ^{18}F-for-^{19}F isotopic exchange reaction on model compound **VI** (1.88×10^{-4} M, 61 ± 22 MBq [^{18}F]fluoride starting activity) as a function of temperature (T).

T [K]	**1/T** [1/K]	**k** [1/Ms]	**ln(k)**
263	0.00380	18.1273	2.89742
268	0.00373	27.1626	3.30184
273	0.00366	37.8825	3.63449
278	0.00359	46.1945	3.83286
283	0.00353	93.4347	4.53726

The obtained rate constants were subsequently used to determine the questioned parameters with the aid of the *Arrhenius equation* (*Formula 5*).

$$\ln(k) = -\frac{E_a}{R} \cdot \frac{1}{T} + \ln(A)$$

k = rate constant [1/Ms] — E_a = activation energy [J/mol]
R = molar gas constant [J/Kmol] — A = pre-exponential factor [1/Ms]
T = temperature [K]

Formula 5. *Arrhenius equation* for calculation of activation energy and pre-exponential factor[241].

After setting up an *Arrhenius plot* displaying the natural logarithm of the rate constants against the reciprocal absolute temperatures (*Figure 31*), the resulting linear regression line was used to calculate both the activation energy (*via* the slope) and the pre-exponential factor (*via* the y-intercept).

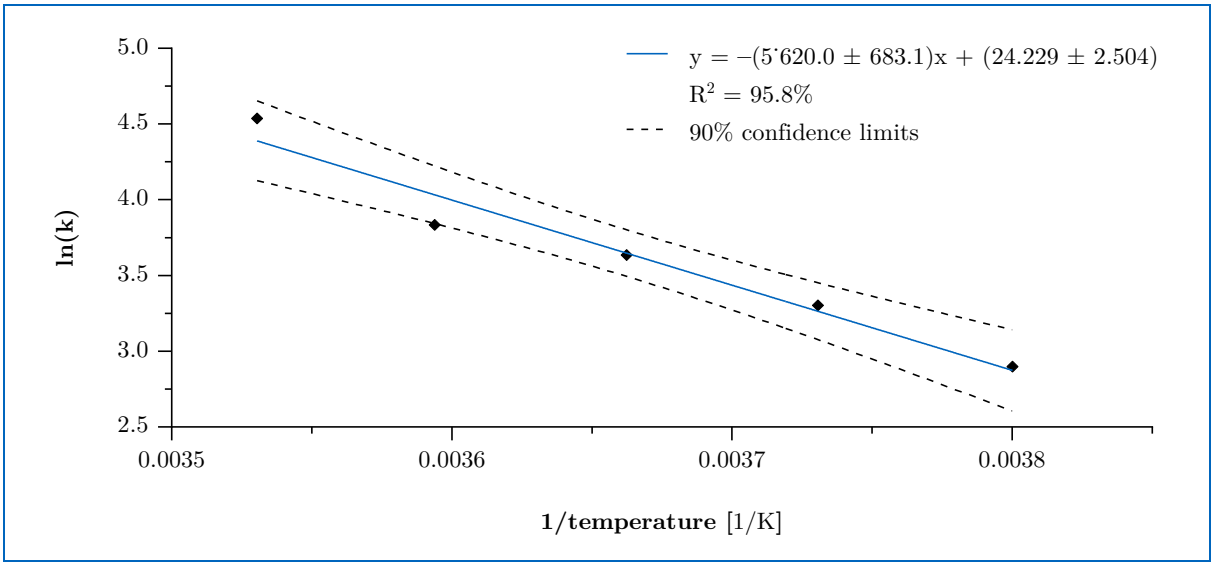

Figure 31. *Arrhenius plot* for the ^{18}F-for-^{19}F isotopic exchange reaction on model compound **VI** (1.88×10^{-4} M, 61 ± 22 MBq [^{18}F]fluoride starting activity) showing the best fit calculated by linear regression (blue line) and the 90% confidence limits (dashed black lines).

The activation energy for the isotopic exchange reaction on model compound **VI** was determined to be 46.7 ± 5.7 kJ/mol, while calculation of the pre-exponential factor resulted in a value of 3.33×10^{10} 1/Ms. Notably, the measured activation energy stood out when compared

to the energy barriers of conventional radiofluorination reactions in which carbon-[^{18}F]fluorine bonds are formed (*Table 5*).

Table 5. Activation energies (E_a) for the radiofluorination of selected substrates[77, 242-243].

substrate	reaction mechanism	bond formation	E_a [kJ/mol]
1,2-bis(*p*-toluenesulfonyloxy)ethane	S_N2	carbon-[^{18}F]fluorine	71.5
diaryliodonium chlorides	S_NAr	carbon-[^{18}F]fluorine	75–117
polyfluorinated benzenes	S_NAr (isotopic exchange)	carbon-[^{18}F]fluorine	79–117
SiFAN$^+$Br$^-$	S_N2 (isotopic exchange)	silicon-[^{18}F]fluorine	65.6
model compound **VI**	S_N2 (isotopic exchange)	silicon-[^{18}F]fluorine	46.7 ± 5.7

In fact, activation energies for ^{18}F-labeling based on carbon-[^{18}F]fluorine bond formation were found to be significantly higher, as exemplified by radiofluorination *via* S_N2 reaction of 1,2-bis(*p*-toluenesulfonyloxy)ethane (71.5 kJ/mol) and *via* S_NAr of various diaryliodonium chlorides (75–117 kJ/mol) reported in the literature[77, 242]. An analogous observation was made for the ^{18}F-for-^{19}F isotopic exchange reaction on organofluorine compounds, such as polyfluorinated benzenes (79–117 kJ/mol)[243]. Most interesting in the context of isotopic exchange was a direct comparison with the *Arrhenius parameters* obtained by *Kostikov et al.* in the aforementioned study. Thereby, an activation energy of 65.6 kJ/mol was determined for the radiofluorination of the Silicon-based Fluoride Acceptor-bearing compound SiFAN$^+$Br$^-$ using meticulously dried [^{18}F]fluoride[77]. This value is roughly 1.4-fold higher than the energy barrier calculated in the present work, although both investigated compounds share the same di-*tert*-butylphenylfluorosilane labeling functionality. A potential explanation for this discrepancy could indeed be attributed to the different labeling environments. While *Kostikov et al.* performed the isotopic exchange reaction under anhyd. conditions, the *Munich*-dried [^{18}F]fluoride employed here was subjected to partial neutralization, resulting in small amounts of water within the labeling mixture[77]. As previously speculated by *Wurzer et al.*, the presence of water traces might promote [^{19}F]fluoride abstraction during the isotopic exchange reaction, which would lead to a lowered activation energy barrier as a consequence of this catalytic effect[82]. Accordingly, the use of partially neutralized *Munich*-dried [^{18}F]fluoride provides ideal conditions for remarkably fast and efficient radiofluorination of Silicon-based Fluoride Acceptors *via* isotopic exchange reaction[80, 240].

3.1.4 Radiofluorination using [^{18}F]Fluoride prepared by the *SiFA-tailored Method*

Although utilization of *Munich*-dried [^{18}F]fluoride emerged as method of choice for the radiofluorination of Silicon-based Fluoride Acceptors, a series of limitations persist. Most notably, the exact addition of oxalic acid for partial neutralization of the strongly basic eluate remains a critical step affecting radiolabeling efficiency[80, 240]. Furthermore, since the adjusted eluate still exhibits an alkaline character, radiofluorination of particularly base-labile precursors appears to be out of reach. Another aspect concerns the application of *Munich*-dried [^{18}F]fluoride in clinical routine. Due to its toxicity, the concentration of Kryptofix® 222 has to be determined in the final radiotracer formulation before administration[244]. It was therefore captivating to develop an alternative [^{18}F]fluoride preparation procedure that would overcome the mentioned constraints. As the on-cartridge drying method demonstrated to be superior to classical azeotropic distillation in terms of ease and efficiency, this approach was integrated in the novel preparation technique. Thus, aq. [^{18}F]fluoride was first trapped onto a strong anion exchange (Sep-Pak® Accell Plus QMA Carbonate Plus Light) cartridge and subsequently dried with air (40 mL), MeCN (10 mL), and air (40 mL) again before inverse elution. The main challenge consisted in finding an alternative elution cocktail composition that could efficiently release the dried activity from the anion exchange resin. This step was deemed crucial, because it particularly affects the technically achievable RCY for the subsequent radiofluorination reaction and hence the success of the entire method. In this context, the elution cocktail used by the *Munich Method* (83 µmol KOH and 91 µmol Kryptofix® 222 in 500 µL MeCN) represents an ideal composition, as it allows for an almost quantitative [^{18}F]fluoride recovery ($98.3 \pm 0.6\%$, $n = 9$)[82]. Small volumes (500–1000 µL) of MeCN and DMSO were considered for the elution of dried [^{18}F]fluoride. The choice of the eluting salt was highly restricted by the solubility in the mentioned dipolar aprotic media. With the aim to avoid the need of toxic Kryptofix® 222 for metal ion complexation, ammonium and tetraalkylammonium were selected as salt cations. As for the corresponding counterions, special attention was paid to their basicity, which had to be substantially lower when compared to hydroxide. Such a condition was supposed to be the key to circumvent the basicity-related constraints of the *Munich* eluate.

Accordingly, several species, including triflate, iodide, acetate, and formate, were investigated with respect to their ability to displace [^{18}F]fluoride from the QMA resin (*Table 6*).

Table 6. Recovery of dried [^{18}F]fluoride from the QMA cartridge using various elution cocktails composed of ammonium or tetraalkylammonium salts dissolved in dipolar aprotic media.

entry	**salt**	**n(salt)** [µmol]	**solvent**	**V(solvent)** [µL]	**recovery** [%]	***n***
1	NBu_4OTf	634	MeCN	500	0.4	1
2	NBu_4I	635	MeCN	500	2.3	1
3	NH_4I	638	DMSO	500	46.7	1
4	NMe_4OAc	633	DMSO	500	9.2	1
5	NH_4OAc	639	DMSO	500	77.4	1
6	NH_4HCOO	645 ± 1	DMSO	500	87.4 ± 4.0	2
7	NH_4HCOO	634 ± 3	DMSO	1000	89.7 ± 2.1	3

A high molar amount of salt, which was roughly equal in all entries, was used in order to facilitate the release of dried [^{18}F]fluoride. However, both investigated solutions with tetrabutylammonium salts in MeCN (*entries 1* and *2*) revealed to be unsuitable as eluents. For the latter salt, the use of its ammonium counterpart in combination with DMSO as solvent (*entry 3*) significantly increased the elution efficiency to about 47%. A similar effect was observed for the evaluated acetate salts. While a solution of NMe_4OAc in DMSO (*entry 4*) only marginally displaced the activity from the QMA resin, the elution cocktail composed of NH_4OAc in DMSO (*entry 5*) achieved a recovery of more than 77%. Replacing the acetate with formate proved to be even more advantageous. Hence, elution efficiencies increased to almost 90% when using NH_4HCOO in DMSO (*entries 6* and *7*). In this context, doubling the DMSO volume to 1000 µL (*entry 7*) resulted in slightly improved [^{18}F]fluoride recovery. As the increase through higher eluent volume was not worth to slow down the concentration-dependent isotopic exchange rate in a subsequent radiofluorination reaction, the solvent amount was limited to 500 µL.

The correlation between the molar amount of applied NH_4HCOO in DMSO and its respective [^{18}F]fluoride elution capacity was elucidated in a further optimization study (*Table 7*). In this experiment series, drying of the QMA-trapped activity was performed with DMSO (8 mL) in order to avoid the need of different solvents during [^{18}F]fluoride preparation. Since dissolving

634 µmol of NH_4HCOO in 500 µL DMSO afforded an almost sat. solution, only lower or equal molar amounts were investigated.

Table 7. Recovery of dried [^{18}F]fluoride from the QMA cartridge using elution cocktails with various amounts of NH_4HCOO dissolved in DMSO.

entry	**salt**	**n(salt)** [µmol]	**solvent**	**V(solvent)** [µL]	**recovery** [%]	***n***
1	NH_4HCOO	0	DMSO	500	0.1 ± 0.0	3
2	NH_4HCOO	79	DMSO	500	65.2 ± 1.1	3
3	NH_4HCOO	159	DMSO	500	74.2 ± 0.7	3
4	NH_4HCOO	396	DMSO	500	83.6 ± 0.6	3
5	NH_4HCOO	634	DMSO	500	88.4 ± 2.2	75

As expected, the elution efficiency augmented with increasing amount of salt and reached a maximum of more than 88% when 634 µmol of NH_4HCOO were applied (*entry 5*). The [^{18}F]fluoride recovery was consistent with the previously determined value using a comparable elution cocktail composition (*Table 6*, *entry 6*). Consequently, the choice of dipolar aprotic solvent (10 mL MeCN or 8 mL DMSO) for prior [^{18}F]fluoride drying on the QMA cartridge had no impact on the elution step. Interestingly, when compared to the moles of salt used by the *Munich* elution cocktail (83 µmol KOH), a more than 7-fold higher amount of NH_4HCOO was required to achieve good elution efficiency (*entry 5*).

With the aim of further increasing the [^{18}F]fluoride recovery, the impact of defined water amounts in the elution cocktail was studied. The beneficial effect of this strategy had previously been demonstrated by different groups. For instance, *Brichard et Aigbirhio* applied elution cocktails with 78 µmol of NEt_4HCO_3 dissolved in 1 mL of an aprotic solvent (MeCN, DMSO, or DMF) with up to 5% of water[245]. Thereby, both authors observed a gradual increase in [^{18}F]fluoride recovery correlating with the water concentration[245]. The same effect was also reported by *Inkster et al.*, who found consistently higher elution efficiencies when using various tetraethylammonium salts in solutions of MeCN or DMSO with increasing water content[246]. However, when developing the novel [^{18}F]fluoride preparation method, it had to be taken into account that the increased recovery by water addition occurs at the expense of the eluate reactivity. In order to estimate the advantage of a defined water content in the elution cocktail, it was crucial to test the labeling efficiency with such an eluate. Accordingly, the Silicon-based

Fluoride Acceptor-bearing ligand ^{nat}Ga-rhPSMA-7.3 was used as a model compound in this context (*Table 8*).

Table 8. Recovery of dried [^{18}F]fluoride from the QMA cartridge using elution cocktails composed of NH_4HCOO (634 µmol) dissolved in 500 µL of DMSO with variable water content, and RCYs for the subsequent radiofluorination of ^{nat}Ga-rhPSMA-7.3 with corresponding eluates. Radiolabeling was performed by combining the recovered eluate with ^{nat}Ga-rhPSMA-7.3 (150 nmol) and incubating the mixture for 5 min at rt. Subsequent radiotracer purification occurred *via* SPE.

entry	**water content (*v/v*)** [%]	**recovery** [%]	***n***	**RCY** [%]	***n***
1	0	88.4 ± 2.2	75	78.4 ± 0.4	2
2	1	92.7 ± 0.6	3	77.3 ± 1.5	3
3	2	94.2 ± 0.9	3	80.3 ± 1.2	3
4	4	94.8 ± 1.7	5	73.4 ± 3.9	4
5	5	95.3 ± 0.8	5	78.1 ± 6.0	5
6	10	95.6 ± 0.9	4	69.9 ± 7.7	4

In line with the aforementioned literature observations, the [^{18}F]fluoride elution efficiency was found to further increase by the addition of water to the elution cocktail. While an eluent with 1% of water content demonstrated [^{18}F]fluoride recovery of almost 93% (*entry 2*), the anhyd. composition (*entry 1*) released about 88% of trapped activity. The most efficient [^{18}F]fluoride displacement (about 96%) was observed when using the elution cocktail with 10% of its volume corresponding to water (*entry 6*). With the aim to assess the eluate reactivity, subsequent ^{18}F-labeling of ^{nat}Ga-rhPSMA-7.3 (150 nmol) was conducted for 5 min at rt. Interestingly, RCYs for the radiofluorination reaction were in a similar range when using eluates with water content up to 2% (*entries 1, 2,* and *3*). Higher [^{18}F]fluoride recoveries were consequently relativized by the lower eluate reactivity due to the respective amount of water. Radiofluorination reactions involving eluates with even higher water content tended to give lower RCYs (*entries 4* and *6*) and were generally less reproducible (*entries 5* and *6*). Since the addition of water to the elution cocktail did not provide a significant advantage, the eluent was kept in its anhyd. composition (*entry 1*).

In order to assess the performance of the newly developed [^{18}F]fluoride preparation technique, a direct comparison was made with the *Munich Method*. For this purpose, radiofluorination of

the Silicon-based Fluoride Acceptor-bearing ligand ^{nat}Ga-rhPSMA-7.3 was included as a benchmark, and both activity recoveries and RCYs for the final radiotracer were compared (*Table 9*).

Table 9. Recovery of dried [^{18}F]fluoride from the QMA cartridge using the *Munich Method* (GLP1b-IV) or the novel preparation technique (GLP1c-VII), and RCYs for the subsequent radiofluorination of ^{nat}Ga-rhPSMA-7.3 with corresponding eluates. Radiolabeling was performed by combining the recovered eluate with ^{nat}Ga-rhPSMA-7.3 (150 nmol) and incubating the mixture for 5 min at rt. Subsequent radiotracer purification was accomplished *via* SPE.

entry	**elution cocktail composition**	**recovery** [%]	***n***	**RCY** [%]	***n***
1*	KOH (83 µmol) and Kryptofix® 222 (91 µmol) in MeCN (500 µL)	98.3 ± 0.6	9	74.9 ± 0.5	2
2**	NH_4HCOO (634 µmol) in DMSO (500 µL)	88.4 ± 2.2	75	78.4 ± 0.4	2

* [^{18}F]Fluoride preparation according to the *Munich Method*. The eluate was subjected to partial neutralization prior to radiofluorination.

** [^{18}F]Fluoride preparation according to the novel technique.

With regard to the activity recovery from the QMA cartridge, the *Munich* elution cocktail demonstrated near-quantitative displacement of dried [^{18}F]fluoride (*entry 1*), exceeding the elution efficiency of the newly developed method (*entry 2*) by about 10%. However, subsequent radiofluorination of ^{nat}Ga-rhPSMA-7.3 with the respective eluates (including partial neutralization for the *Munich* eluate) led to an unexpected outcome. Despite the considerably lower [^{18}F]fluoride recovery observed for the novel technique, RCYs for the ^{18}F-labeled ligand were found to be slightly higher in comparison to the radiofluorination results obtained with *Munich*-dried activity. This intriguing finding suggests that the isotopic exchange reaction proceeds with higher efficiency when using [^{18}F]fluoride eluate afforded by the herein developed method, even compensating for the minor activity recovery. In view of this favorable result related to the radiolabeling of Silicon-based Fluoride Acceptors, the novel [^{18}F]fluoride preparation procedure was denominated as *SiFA-tailored Method* (*Figure 32*).

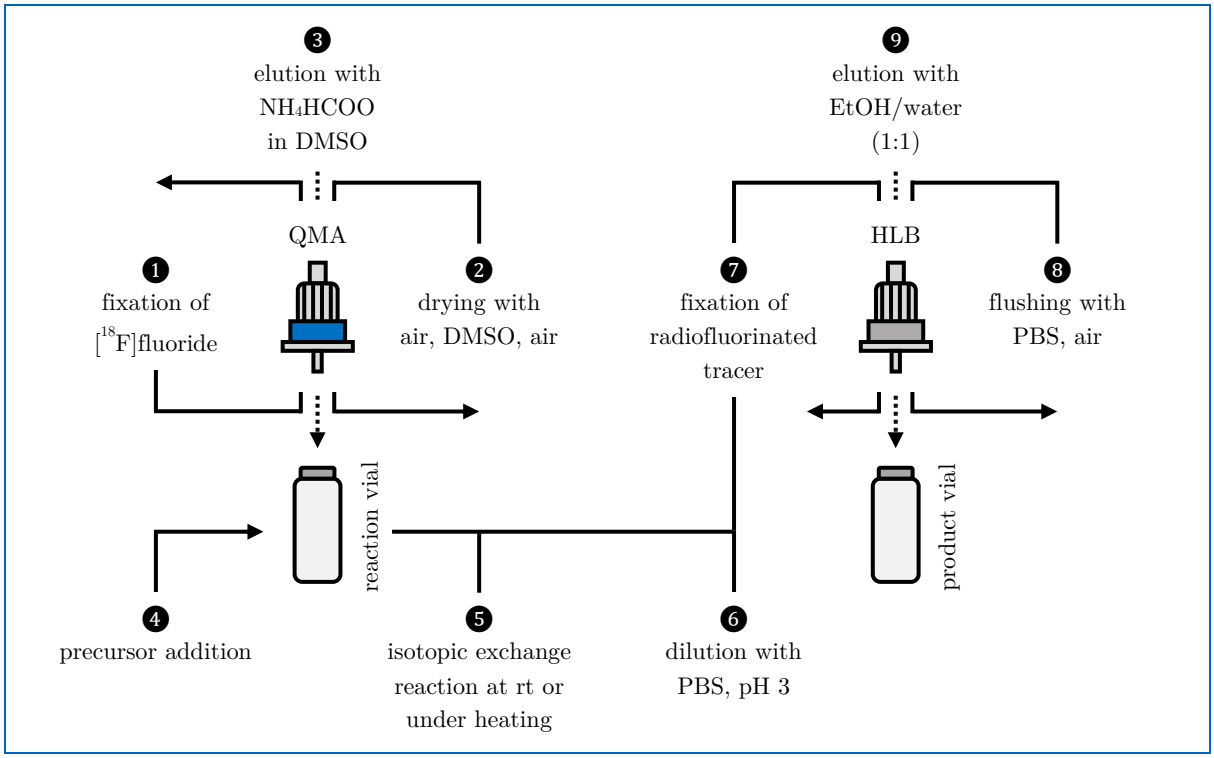

Figure 32. General scheme describing [^{18}F]fluoride preparation according to the *SiFA-tailored Method* (steps 1–3), its subsequent application for radiofluorination of a Silicon-based Fluoride Acceptor-bearing compound (steps 4–5), and final radiotracer purification *via* SPE (steps 6–9).

Recapitulating, the preparation of dried [^{18}F]fluoride according to the *SiFA-tailored Method* consists of three operational steps. Aq. [^{18}F]fluoride is initially retained onto a strong anion exchange (Sep-Pak® Accell Plus QMA Carbonate Plus Light) cartridge and subsequently flushed with air (40 mL), DMSO (8 mL), and air (40 mL) again to remove the bulk of water. The dried activity is then inversely recovered with a solution of NH_4HCOO (634 µmol) in DMSO (500 µL). This elution cocktail proved to be particularly advantageous when compared to the composition employed by the *Munich Method*. While the ammonium cation obviates the need for toxic Kryptofix® 222 as phase transfer catalyst, the formate anion successfully circumvents the basicity limitations imposed by the hydroxide. Thus, partial neutralization of dried [^{18}F]fluoride recovered by the *SiFA-tailored Method* is not required, and the eluate is immediately applicable for the radiofluorination of Silicon-based Fluoride Acceptor-bearing compounds. As demonstrated previously, ^{18}F-labeling using the *SiFA-tailored* eluate proceeds with high efficiency. In combination with subsequent SPE-based purification, final radiotracers can hence be obtained with excellent RCYs in a relatively short overall synthesis time.

To explore the application range of the novel [^{18}F]fluoride preparation technique, both the partially neutralized *Munich* eluate and the *SiFA-tailored* eluate were investigated with respect to the radiofluorination of a base-sensitive fibroblast activation protein (FAP) inhibitor comprising a Silicon-based Fluoride Acceptor. Thereby, labeling conditions (30 nmol precursor, 5 min at rt) as well as tracer workup (*via* SPE) were identical for both approaches. Radio-RP-HPLC traces of the purified ^{18}F-labeled FAP inhibitor were finally compared to each other (*Figure 33*).

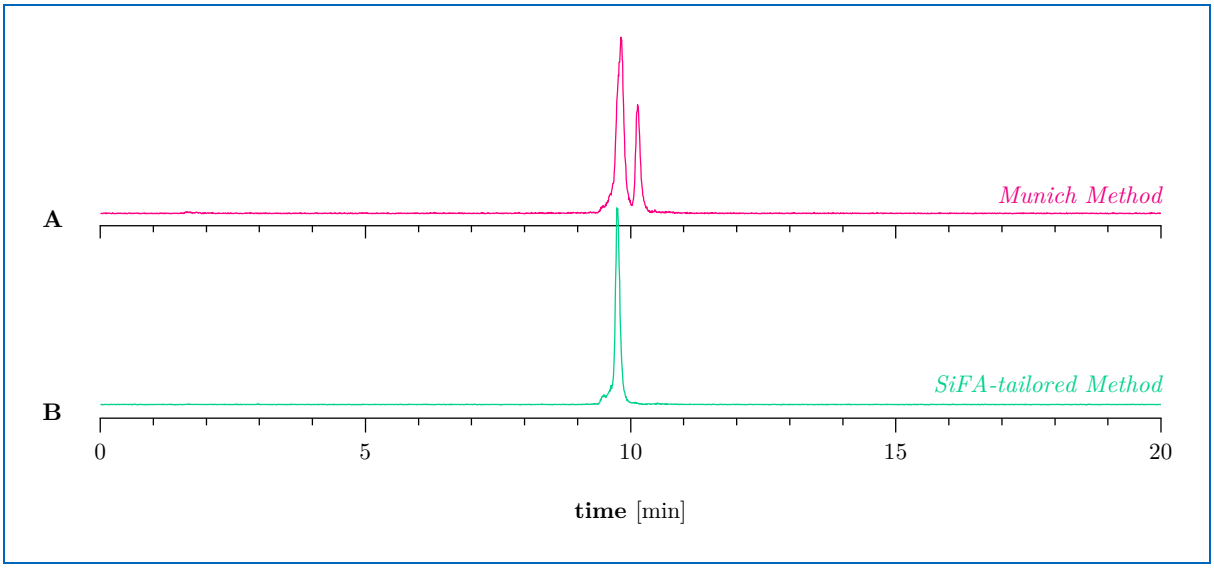

Figure 33. Radio-RP-HPLC chromatograms (column II, 0–15 min: 10→90% B in A, 15–20 min: 95% B in A, t_R = 9.8 min) of a purified ^{18}F-labeled base-sensitive Silicon-based Fluoride Acceptor-bearing FAP inhibitor synthesized with [^{18}F]fluoride prepared by the **A**) *Munich Method* including partial neutralization (GLP1b-I) or the **B**) *SiFA-tailored Method* (GLP1c-IV). Radiolabeling was performed by combining the respective eluates with the ligand (30 nmol) and incubating the mixture for 5 min at rt. Subsequent radiotracer purification occurred *via* SPE.

As for ^{18}F-labeling of the base-sensitive FAP inhibitor with partially neutralized *Munich* eluate, radio-RP-HPLC analysis (*Figure 33A*) revealed not only the desired product (t_R = 9.8 min) but also the substantial presence (28%) of a radiofluorinated impurity (t_R = 10.1 min) in the final formulation. In contrast, radiofluorination of the same compound with [^{18}F]fluoride prepared by the *SiFA-tailored Method* resulted only in the formation of pure ^{18}F-labeled FAP inhibitor (*Figure 33B*). This outcome illustrates the incompatibility of the labeling environment provided by the *Munich* eluate with regard to the radiofluorination of base-sensitive structures. By virtue of its mild elution cocktail composition, the *SiFA-tailored* eluate

successfully overcomes this limitation. As such, the newly developed [^{18}F]fluoride preparation technique holds the potential to further expand the application range of ^{18}F-labeling in combination with Silicon-based Fluoride Acceptors.

Another key advantage of the *SiFA-tailored* eluate consists in the fact that upon incubation with the precursor compound, the labeling mixture can be heated up in order to increase the reaction rate and consequently the RCC. More details in this context are presented in the chapters focusing on the radiofluorination of novel PSMA inhibitors (*Section 3.2.3*) and FR-targeting ligands (*Section 3.3.2*).

3.2 Development of novel ^{18}F-labeled PSMA Ligands

PSMA certainly constitutes one of the best studied target structures in nuclear medicine. This has led to the development of numerous specific radiopharmaceutical agents, of which [^{68}Ga]Ga-PSMA-11 (Locametz® and Illuccix®), [^{18}F]DCFPyL (Pylarify®), and [^{177}Lu]Lu-PSMA-617 (Pluvicto™) have recently been approved by health authorities after convincingly demonstrating their *in vivo* efficacy[151, 247-248]. Given the increasing clinical demand for ^{18}F-labeled ligands, novel PSMA inhibitors based on alternative radiofluorination strategies have emerged during the past few years[76, 153, 249]. Noteworthy in this regard would be the promising [^{18}F]^{nat}Ga-rhPSMA-7.3, which has set new standards among radiofluorinated PSMA ligands owing to its exceptionally fast, simple, and highly efficient labeling by means of Silicon-based Fluoride Acceptors[82]. In order to counterbalance the pronounced lipophilicity of the labeling functionality, a hydrophilic chelate was incorporated into the structure of [^{18}F]^{nat}Ga-rhPSMA-7.3. During development of the latter compound, similar ^{18}F-labeled inhibitors, termed siPSMA ligands, were conceived as part of the present doctoral thesis. A unique feature of the novel imaging agents designed in this work was the structural introduction of a PKM comprising linked amino acids. Such a modifier was hypothesized to allow for compensation and fine-tuning of the siPSMA ligand lipophilicity, with the overall goal of providing optimized radiotracers with a favorable pharmacokinetic profile *in vivo*.

3.2.1 Design, Preparation, Characterization, and *in vitro* Evaluation of siPSMA Ligands

Minimalistic siPSMA Ligands

For the first generation of siPSMA ligands, the development focused on rather simple inhibitors. Their structure comprises an L-Glu-urea-L-Glu binding motif that is attached to the Silicon-based Fluoride Acceptor moiety *via* a linker unit. The length of the linker was chosen with the intention of enabling interactions between the Silicon-based Fluoride Acceptor and specific lipophilic regions of the PSMA-binding pocket. The first inhibitor, siPSMA-**0a**, attempted to accommodate the Silicon-based Fluoride Acceptor moiety within the S1 accessory hydrophobic pocket by utilizing a short D-Orn linker[126]. In parallel, siPSMA-**0b** was designed

with an extended spacer structure that would allow the Silicon-based Fluoride Acceptor functionality to address the arene-binding site located near the enzyme pocket entrance[127]. The linker used in this context, consisting of a D-Orn(Suc(H-D-Lys-OH)) sequence, was adopted from previously developed PSMA inhibitors[76, 136]. In addition, a positively charged quaternary alkylammonium group was placed next to the Silicon-based Fluoride Acceptor to reduce the overall tracer lipophilicity. This kind of approach had earlier been applied during the development of radiofluorinated Tyr^3-octreotate ligands by *Niedermoser et al.*[73]. The respective labeling precursors of [^{18}F]siPSMA-**0a** and -**0b** were both synthesized *via* SPPS (*Scheme 2*), purified by prep. RP-HPLC, and obtained in acceptable yields (12–39%) with highest chemical purities (>99%).

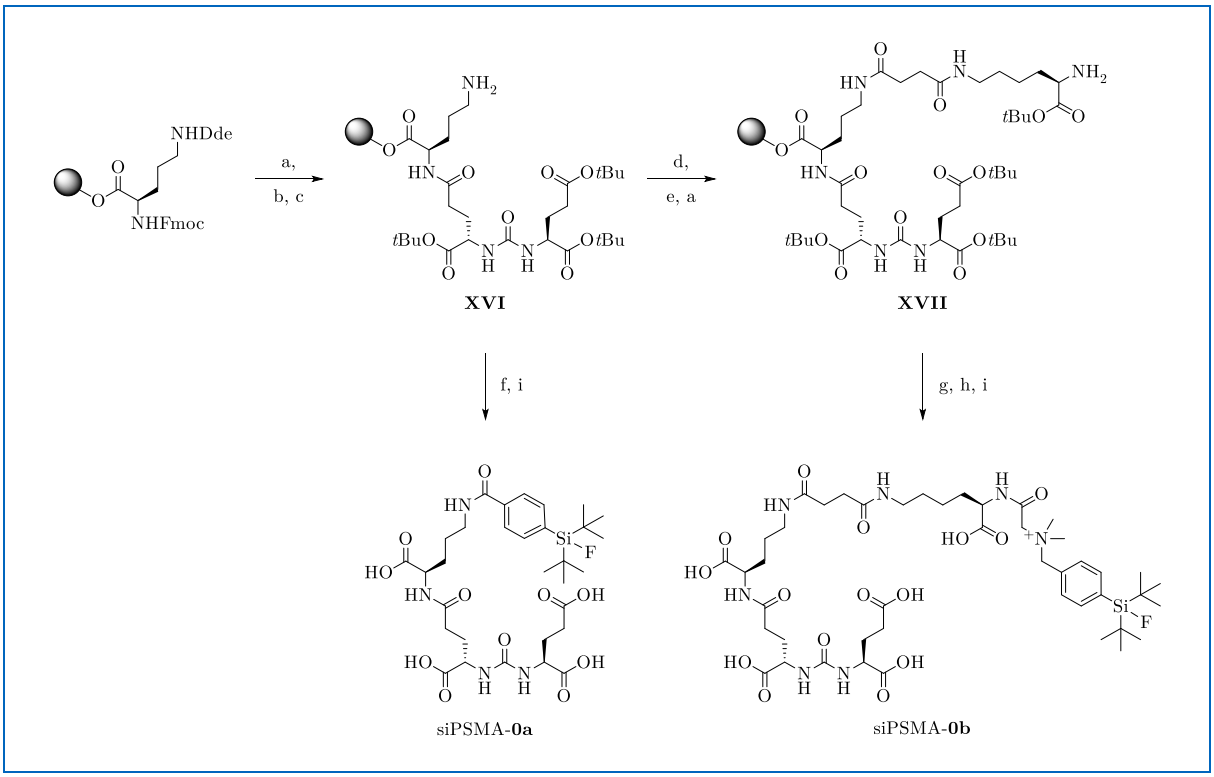

Scheme 2. Synthesis of siPSMA-**0a** and -**0b**: a) Pip, (DMF); b) *t*BuO-L-Glu(O*t*Bu)-urea-L-Glu-O*t*Bu (**IX**), HOAt, TBTU, 2,4,6-collidine, (DMF); c) hydrazine monohydrate, (DMF); d) succinic anhydride, DIPEA, (DMF); e) Fmoc-D-Lys-O*t*Bu, HOAt, TBTU, 2,4,6-collidine, (DMF); f) SiFA-BzA (**V**), HOAt, TBTU, 2,4,6-collidine, (DMF); g) *N,N*-dimethyl-Gly-OH, HOAt, TBTU, 2,4,6-collidine, (DMF); h) SiFA-BnBr (**IV**), 2,4,6-collidine, (DCM); i) TFA, TIPS, water.

Characterization and *in vitro* analysis of [$^{18/19}$F]siPSMA-**0a** and -**0b** included determination of lipophilicity (log$D_{7.4}$), assessment of PSMA-binding affinity (IC_{50}) and internalization, as well

as evaluation of HSA binding. The results, together with previously published data of clinically established radiofluorinated PSMA inhibitors evaluated under the same conditions, are summarized below (*Table 10*)[168, 250].

Table 10. Characterization and *in vitro* evaluation of [$^{18/19}$F]siPSMA-**0a** and **-0b** in comparison with [$^{18/19}$F]DCFPyL, [$^{18/19}$F]PSMA-1007, and [$^{18/19}$F]^{nat}Ga-rhPSMA-7.3 (data derived from the literature)[168, 250]. Investigated parameters include lipophilicity represented by log$D_{7.4}$ (data expressed as mean ± standard deviation (SD), $n = 5$), IC_{50} (data expressed as mean nM ± SD with **XXV** as reference, $n = 3$), internalized activity after 1 h (data corrected for unspecific binding and expressed as mean internalized activity of reference **XXV** in % ± SD, $n = 3$), and HSA binding (data expressed as % compared to standard reference compounds).

PSMA ligand	**lipophilicity** (log$D_{7.4}$)	***IC*$_{50}$** [nM]	**internalized activity** [% of **XXV**]	**HSA binding** [%]
[$^{18/19}$F]siPSMA-**0a**	–2.99 ± 0.02	60.0 ± 6.5	14 ± 1	≥98.9
[$^{18/19}$F]siPSMA-**0b**	–2.81 ± 0.08	16.7 ± 0.9	51 ± 6	91.1
[$^{18/19}$F]DCFPyL	–3.4 ± 0.03	12.3 ± 1.2	118 ± 4	14.3
[$^{18/19}$F]PSMA-1007	–1.6 ± 0.02	4.2 ± 0.5	118 ± 5	97.8
[$^{18/19}$F]^{nat}Ga-rhPSMA-7.3	–3.3 ± 0.2	4.4 ± 1.1	161 ± 9	97

[^{18}F]siPSMA-**0a** and **-0b** were found to exhibit similar log$D_{7.4}$ values despite their considerable structural differences. Interestingly, the additional carboxylate functionality in the linker sequence and the quaternary alkylammonium in close proximity to the Silicon-based Fluoride Acceptor moiety failed to increase the hydrophilicity of [^{18}F]siPSMA-**0b**. In comparison with both [^{18}F]siPSMA ligands, the references [^{18}F]DCFPyL and [^{18}F]^{nat}Ga-rhPSMA-7.3 revealed to be substantially more hydrophilic[168, 250]. [^{18}F]PSMA-1007, on the contrary, appeared to possess a pronounced lipophilic character (log$D_{7.4}$ = –1.6 ± 0.02)[250].

With respect to the determined IC_{50} values, siPSMA-**0a** displayed a 5- to 14-fold lower PSMA-binding affinity when compared to the references[168, 250]. This finding suggested that an accommodation of the Silicon-based Fluoride Acceptor moiety within the S1 accessory hydrophobic pocket might not be tolerated by the enzyme. In contrast, the IC_{50} value of siPSMA-**0b** revealed to be in a low double-digit nanomolar range, demonstrating that addressing the arene-binding site with the Silicon-based Fluoride Acceptor unit represented the strategy of choice to enhance

the inhibitor's affinity. Direct comparison with ^{nat}Ga-rhPSMA-7.3 (IC_{50} = 4.4 ± 1.1 nM), which shares the same binding motif and linker structure as siPSMA-**0b**, evidenced that further potentiation of the affinity properties could be accomplished by introducing suitable residues after the Silicon-based Fluoride Acceptor moiety[168].

Consistent with the minor binding affinity, [^{18}F]siPSMA-**0a** also demonstrated a significantly lower internalization rate (14 ± 1% of **XXV**) when compared to [^{18}F]DCFPyL, [^{18}F]PSMA-1007, or [^{18}F]^{nat}Ga-rhPSMA-7.3[168, 250]. In the case of [^{18}F]siPSMA-**0b**, the internalized activity after 1 h revealed to be higher (51 ± 6% of **XXV**), but still about one-half to one-third the rate determined for the radiofluorinated PSMA reference ligands[168, 250].

In analogy to ^{nat}Ga-rhPSMA-7.3, siPSMA-**0a** showed strong binding to HSA (≥98.9%), which could be ascribed to the Silicon-based Fluoride Acceptor moiety[168]. High HSA binding (91.1%) was also observed for siPSMA-**0b**, although not as pronounced as for the aforementioned inhibitors[168]. In retrospect, siPSMA-**0b** exhibited the lowest HSA binding among all the developed siPSMA ligands. The slightly diminished interaction with the plasma protein could be attributed to the quaternary alkylammonium in proximity to the Silicon-based Fluoride Acceptor. Indeed, as reported in the literature, the presence of a positive charge close to an albumin binder reduces its binding capacity, presumably due to electrostatic repulsion in the HSA-binding pocket[251-252].

A graphical comparison of the parameters described above for [$^{18/19}$F]siPSMA-**0a** and -**0b**, [$^{18/19}$F]DCFPyL, [$^{18/19}$F]PSMA-1007, as well as [$^{18/19}$F]^{nat}Ga-rhPSMA-7.3 is provided below (*Figure 34*).

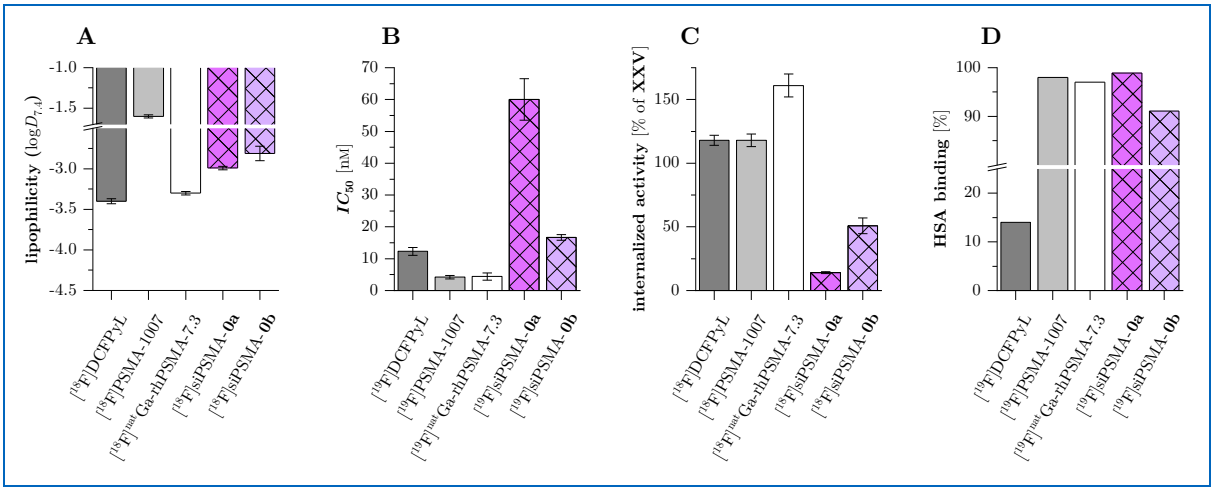

Figure 34. Graphical comparison of previously introduced data for [$^{18/19}$F]siPSMA-**0a** and -**0b**, [$^{18/19}$F]DCFPyL, [$^{18/19}$F]PSMA-1007, as well as [$^{18/19}$F]^{nat}Ga-rhPSMA-7.3 (data derived from the literature), including **A**) lipophilicity represented by log$D_{7.4}$ (data expressed as mean ± SD, $n = 5$), **B**) IC_{50} (data expressed as mean nM ± SD with **XXV** as reference, $n = 3$), **C**) internalized activity after 1 h (data corrected for unspecific binding and expressed as mean internalized activity of reference **XXV** in % ± SD, $n = 3$), and **D**) HSA binding (data expressed as % compared to standard reference compounds)[168, 250].

After evaluation of the *in vitro* data, it became clear that accommodation of the Silicon-based Fluoride Acceptor within the arene-binding site constituted a convenient approach to improve the inhibitor's binding affinity as well as the internalization rate. In addition, the overall lipophilicity required further adjustment as log$D_{7.4}$ values for both [^{18}F]siPSMA-**0a** and -**0b** were considered to be outside the predicted range for favorable pharmacokinetic behavior.

siPSMA Ligands with Peptide-based PKM

The next generation of siPSMA inhibitors aimed to solve the pronounced lipophilicity observed for [^{18}F]siPSMA-**0a** and -**0b**. Based on the previously described scaffold L-Glu-urea-L-Glu(D-Orn(Suc(H-D-Lys-OH))), further introduction of D-Dap as trifunctional unit allowed to insert a peptidic PKM close to the Silicon-based Fluoride Acceptor moiety. In this context, the modifier structure was defined as a sequence of three linearly linked amino acids in D-configuration to prevent potential metabolic degradation *in vivo*. Within siPSMA-**01** to -**09**, D-Glu was established as the second and third amino acid of the PKM to substantially increase the hydrophilic character through the additionally provided amine and carboxylate functionalities. The first position, in contrast, was occupied by an amino acid carrying either a negatively charged (D-Asp, D-Glu), a polar uncharged (D-Thr, D-Cit), a non-polar aromatic (D-Phe), a

positively charged (D-Dap, β-linked D-Dap, D-Orn, D-Lys), or a non-polar aliphatic (Gly) side chain functionality. Permutation of this first amino acid served to fine-tune the degree of ligand lipophilicity with the overall goal of obtaining inhibitors within a preferred log$D_{7.4}$ range. For evaluation of the hydrophilicity enhancement induced by the modifier, siPSMA-**10** bearing a PKM with exclusively polar uncharged amino acids (D-Cit-D-Cit-D-Cit) was designed as a reference. The labeling precursors of [^{18}F]siPSMA-**01** to -**10** with peptide-based PKM were synthesized by SPPS (*Scheme 3*), purified *via* prep. RP-HPLC, and finally obtained in reasonable yields (17–46%) with high chemical purities (≥95%).

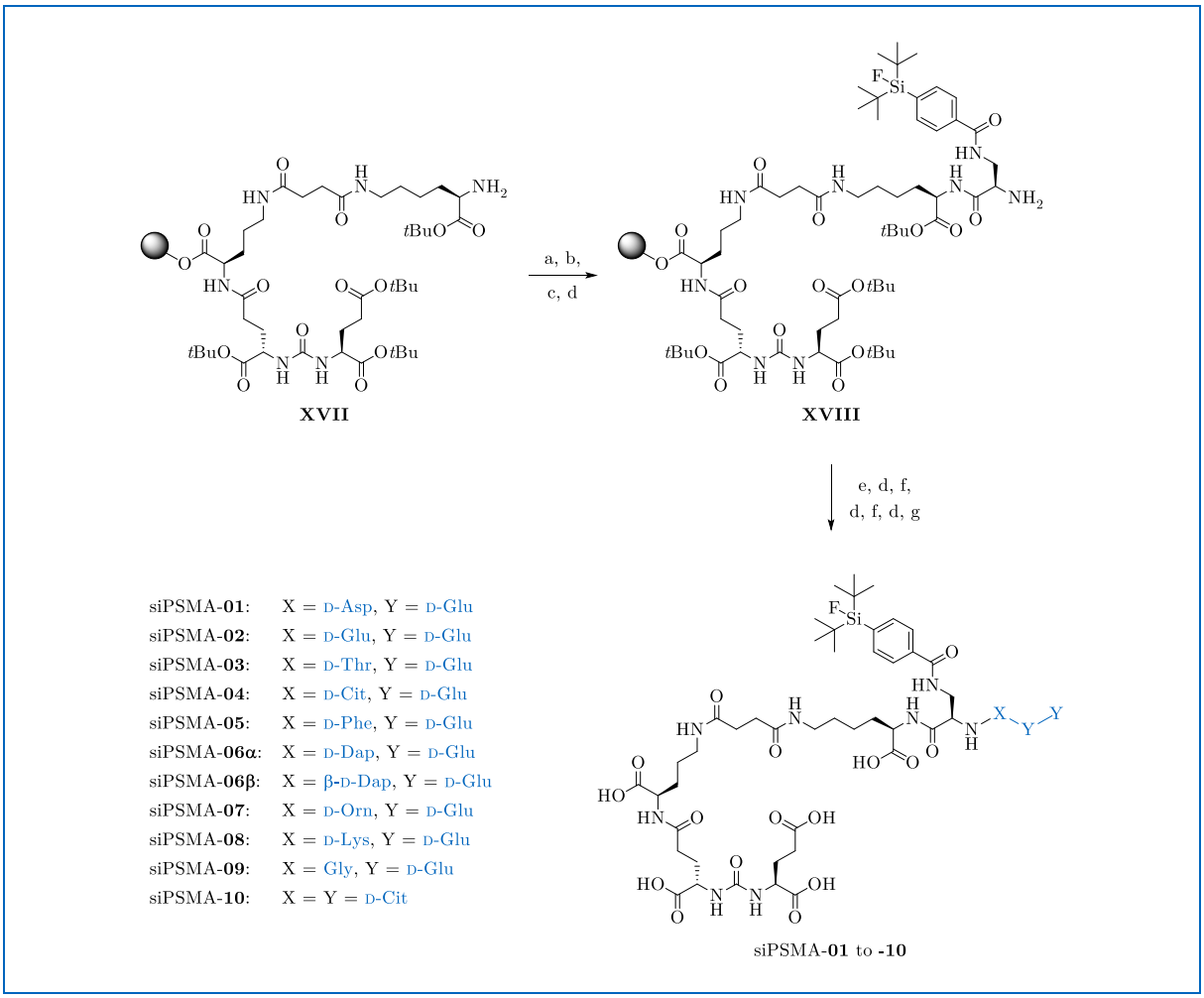

Scheme 3. Synthesis of siPSMA-**01** to -**10**: a) Fmoc-D-Dap(Dde)-OH, HOAt, TBTU, 2,4,6-collidine, (DMF); b) imidazole, hydroxylamine hydrochloride, (DCM/NMP); c) SiFA-BzA (**V**), HOAt, TBTU, 2,4,6-collidine, (DMF); d) Pip, (DMF); e) Fmoc-D-Asp(O*t*Bu)-OH or Fmoc-D-Glu(O*t*Bu)-OH or Fmoc-D-Thr(*t*Bu)-OH or Fmoc-D-Cit-OH or Fmoc-D-Phe-OH or Fmoc-D-Dap(Boc)-OH or Boc-D-Dap(Fmoc)-OH or Fmoc-D-Orn(Boc)-OH or Fmoc-D-Lys(Boc)-OH or Fmoc-Gly-OH, HOAt, TBTU, 2,4,6-collidine, (DMF); f) Fmoc-D-Glu(O*t*Bu)-OH or Fmoc-D-Cit-OH, HOAt, TBTU, 2,4,6-collidine, (DMF); g) TFA, TIPS, water.

Characterization and *in vitro* analysis of [$^{18/19}$F]siPSMA-**01** to -**10** included determination of lipophilicity (log$D_{7.4}$), PSMA-binding affinity (IC_{50}) and internalization, as well as evaluation of HSA binding. The results, together with published data of clinically established ^{18}F-labeled PSMA ligands evaluated under identical conditions, are summarized below (*Table 11*)[168, 250].

Table 11. Characterization and *in vitro* evaluation of [$^{18/19}$F]siPSMA-**01** to -**10** in comparison with [$^{18/19}$F]DCFPyL, [$^{18/19}$F]PSMA-1007, and [$^{18/19}$F]^{nat}Ga-rhPSMA-7.3 (data derived from the literature)[168, 250]. Investigated parameters include lipophilicity represented by log$D_{7.4}$ (data expressed as mean ± SD, $n = 5$), IC_{50} (data expressed as mean nM ± SD with **XXV** as reference, $n = 3$), internalized activity after 1 h (data corrected for unspecific binding and expressed as mean internalized activity of reference **XXV** in % ± SD, $n = 3$), and HSA binding (data expressed as % compared to standard reference compounds).

PSMA ligand	**PKM** (X = D-Glu-D-Glu)	**lipophilicity** (log$D_{7.4}$)	IC_{50} [nM]	**internalized activity** [% of **XXV**]	**HSA binding** [%]
[$^{18/19}$F]siPSMA-**01**	D-Asp-X	–3.80 ± 0.06	9.3 ± 1.7	136 ± 7	98.8
[$^{18/19}$F]siPSMA-**02**	D-Glu-X	–3.85 ± 0.04	8.8 ± 1.0	136 ± 6	98.9
[$^{18/19}$F]siPSMA-**03**	D-Thr-X	–3.66 ± 0.03	10.7 ± 2.1	107 ± 4	97.8
[$^{18/19}$F]siPSMA-**04**	D-Cit-X	–3.31 ± 0.02	11.7 ± 1.5	88 ± 2	98.6
[$^{18/19}$F]siPSMA-**05**	D-Phe-X	–2.30 ± 0.03	20.6 ± 1.8	50 ± 3	98.9
[$^{18/19}$F]siPSMA-**06α**	D-Dap-X	–3.42 ± 0.05	9.1 ± 0.8	143 ± 6	97.2
[$^{18/19}$F]siPSMA-**06β**	β-D-Dap-X	–3.33 ± 0.11	12.2 ± 1.9	125 ± 3	97.9
[$^{18/19}$F]siPSMA-**07**	D-Orn-X	–3.40 ± 0.17	8.5 ± 1.2	112 ± 4	97.5
[$^{18/19}$F]siPSMA-**08**	D-Lys-X	–3.43 ± 0.02	6.9 ± 1.0	94 ± 6	96.9
[$^{18/19}$F]siPSMA-**09**	Gly-X	–3.56 ± 0.04	11.9 ± 2.0	121 ± 4	98.4
[$^{18/19}$F]siPSMA-**10**	D-Cit-D-Cit-D-Cit	–3.17 ± 0.02	16.2 ± 2.0	90 ± 6	95.7
[$^{18/19}$F]DCFPyL	-	–3.4 ± 0.03	12.3 ± 1.2	118 ± 4	14.3
[$^{18/19}$F]PSMA-1007	-	–1.6 ± 0.02	4.2 ± 0.5	118 ± 5	97.8
[$^{18/19}$F]^{nat}Ga-rhPSMA-7.3	DOTA-GA(^{nat}Ga)	–3.3 ± 0.2	4.4 ± 1.1	161 ± 9	97

The second generation of inhibitors, including [^{18}F]siPSMA-**01** to -**10**, revealed to possess a broad log$D_{7.4}$ spectrum with determined values ranging from –3.85 to –2.30, based on the individual hydrophilicity contribution of the PKM. Not surprisingly, [^{18}F]siPSMA-**01** and -**02**, containing three negatively charged side chain functionalities within the modifier (PKM net charge of –2), emerged as the most hydrophilic ligands among this series. In comparison, the inhibitors with a polar uncharged or non-polar aliphatic amino acid at the permuted position

– [^{18}F]siPSMA-**03**, **-04**, and **-09** (all with a PKM net charge of –1) – displayed somewhat higher log$D_{7.4}$ values. [^{18}F]siPSMA-**05**, featuring a D-Phe close to the Silicon-based Fluoride Acceptor, turned out to be the most lipophilic among the designed siPSMA ligands. For inhibitors with a cationic amino acid within the PKM, [^{18}F]siPSMA-**06α** to **-08**, log$D_{7.4}$ values proved to be similar to each other. These ligands were found to exhibit a slightly higher lipophilic character than [^{18}F]siPSMA-**01** and **-02** due to charge balance (PKM net charge of 0 *vs.* –2). As for the hydrophilicity contribution of each amino acid within the PKM, the first position seemed to have a greater influence. This became evident when comparing [^{18}F]siPSMA-**02**, **-04**, and **-10**. Although the PKM of [^{18}F]siPSMA-**04** (D-Cit-D-Glu-D-Glu) contains two negatively charged side chain functionalities in contrast to [^{18}F]siPSMA-**10** (D-Cit-D-Cit-D-Cit), respective lipophilicity values appeared to differ only slightly (log$D_{7.4}$ = –3.31 ± 0.02 *vs.* –3.17 ± 0.02). However, further substitution of D-Cit by D-Glu, giving the modifier sequence of [^{18}F]siPSMA-**02** (D-Glu-D-Glu-D-Glu), resulted in substantially decreased overall lipophilicity (log$D_{7.4}$ = –3.85 ± 0.04). A possible explanation for this effect might be the vicinity of the PKM's first amino acid to the Silicon-based Fluoride Acceptor.

In terms of PSMA-binding affinity, all second-generation ligands apart from siPSMA-**05** (IC_{50} = 20.6 ± 1.8 nM) and siPSMA-**10** (IC_{50} = 16.2 ± 2.0 nM) displayed very low IC_{50} values ranging from 6.9 nM to 12.2 nM. The first exception evidenced decreased binding characteristics caused by the introduction of the non-polar aromatic amino acid D-Phe in proximity to the Silicon-based Fluoride Acceptor moiety. As a consequence, accommodation of both structures within the arene-binding site of PSMA turned out to be disfavored. Furthermore, the use of negatively charged amino acids (D-Glu-D-Glu) for the last two positions of the PKM had a beneficial impact on the binding affinity, as demonstrated by direct comparison between siPSMA-**04** (IC_{50} = 11.7 ± 1.5 nM) and siPSMA-**10**. In summary, the affinity properties of most second-generation siPSMA ligands were similar or even better than those of DCFPyL, but still inferior when compared with the characteristics of PSMA-1007 or ^{nat}Ga-rhPSMA-7.3.

With respect to the internalized activity after 1 h, [^{18}F]siPSMA-**01** to **-10** showed varying values between 50–143% of the rate determined for the reference compound **XXV**. A clear tendency in relation to the permuted amino acids within the PKM was not observed. Highest

internalization rates among the second-generation ligands were found for [^{18}F]siPSMA-**01** (136 ± 7% of **XXV**), -**02** (136 ± 6% of **XXV**), and -**06α** (143 ± 6% of **XXV**), exceeding the reported values for both references [^{18}F]DCFPyL and [^{18}F]PSMA-1007.

As already noticed for the minimalistic ligand siPSMA-**0a**, the presence of the Silicon-based Fluoride Acceptor moiety implies remarkably strong binding to HSA, which was also evident in this second series of inhibitors. Hence, siPSMA-**01** to -**10** showed elevated HSA-binding values (95.7–98.9%) similar to those of PSMA-1007 (97.8%) and ^{nat}Ga-rhPSMA-7.3 (97%).

A graphical comparison of the parameters described above for [$^{18/19}$F]siPSMA-**01** to -**10**, [$^{18/19}$F]DCFPyL, [$^{18/19}$F]PSMA-1007, and [$^{18/19}$F]^{nat}Ga-rhPSMA-7.3 is shown below (*Figure 35*).

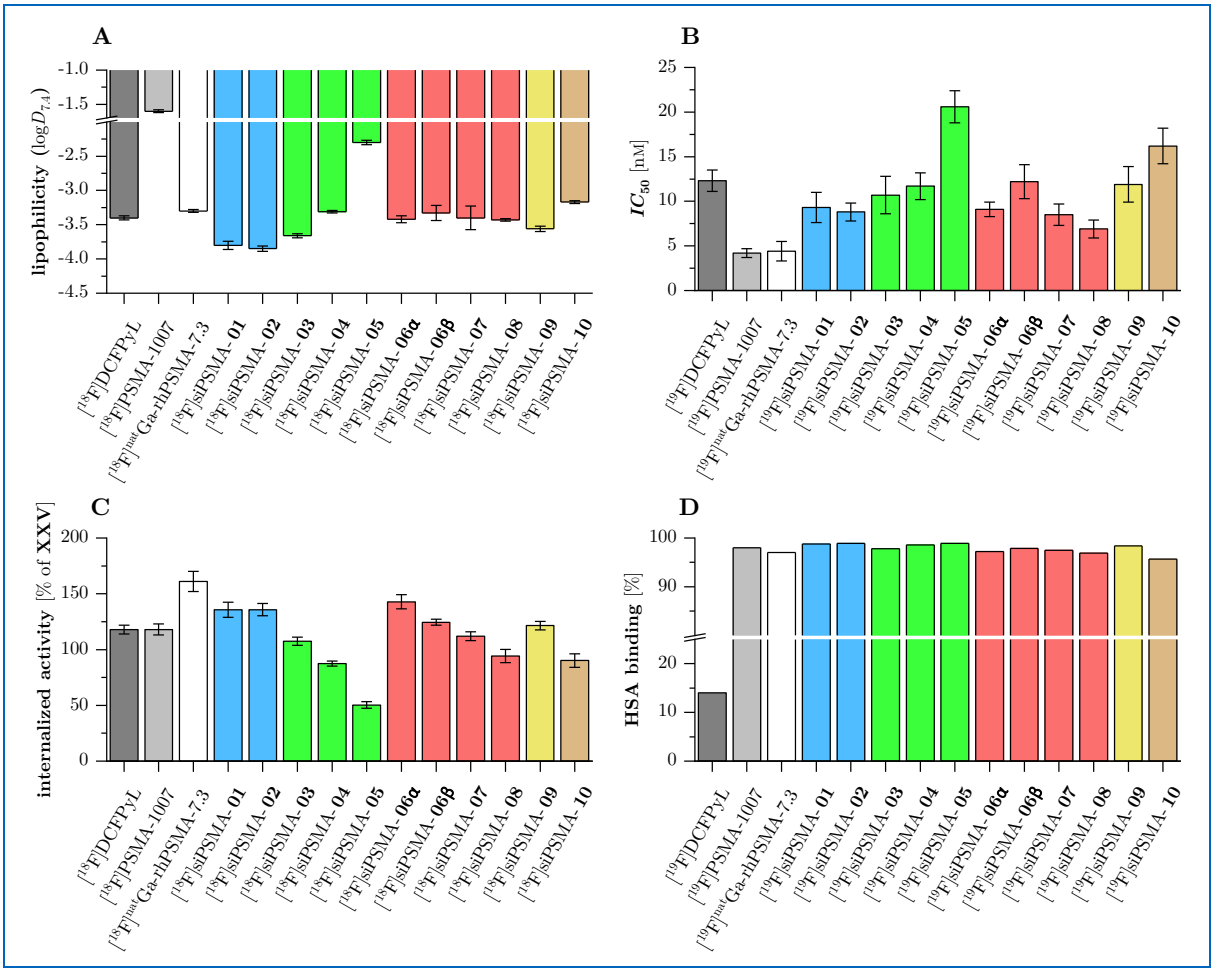

Figure 35. Graphical comparison of previously introduced data for [$^{18/19}$F]siPSMA-**01** to -**10**, [$^{18/19}$F]DCFPyL, [$^{18/19}$F]PSMA-1007, and [$^{18/19}$F]^{nat}Ga-rhPSMA-7.3 (data derived from the literature), including **A**) lipophilicity represented by log$D_{7.4}$ (data expressed as mean ± SD, $n = 5$), **B**) IC_{50} (data expressed as mean nM ± SD with **XXV** as reference, $n = 3$), **C**) internalized activity after 1 h (data corrected for unspecific binding and expressed as mean internalized activity of reference **XXV** in % ± SD, $n = 3$), and **D**) HSA binding (data expressed as % compared to standard reference compounds)[168, 250].

To conclude, the second-generation siPSMA ligands significantly outperformed the previous ones with respect to the investigated characteristics. The hereby chosen inhibitor design, based on a formerly established scaffold in combination with a novel peptide-based PKM, resulted in several promising ligands showing competitive *in vitro* properties when compared to clinically established references[76]. Moreover, most modifier sequences allowed to overcome the inherent lipophilicity contribution of the Silicon-based Fluoride Acceptor moiety, leading to PSMA inhibitors with reasonable $\log D_{7.4}$ values.

siPSMA Ligands with Urea-based PKM

Driven by the ambition to further improve both PSMA-binding affinity and internalization rate, a third generation of siPSMA ligands with a structurally altered PKM was developed. The first position within the modifier sequence was again permuted with either a negatively charged (D-Asp, D-Glu, L-Glu), a polar uncharged (D-Thr, D-Cit), a non-polar aromatic (D-Phe), a positively charged (D-Dap, β-linked D-Dap, D-Orn, D-Lys, L-Lys), or a non-polar aliphatic (Gly, β-Ala, Ahx) amino acid. With the aim to increase the hydrophilicity contribution of the PKM by avoiding the charge-balancing *N*-terminus, it was envisaged to link the second and third amino acid – both corresponding to D-Glu within most of the second-generation siPSMA inhibitors – *via* a urea bridge. Since L-Glu-urea-L-Glu applied for the synthesis of the PSMA-binding motif was already available as an equivalent, *in vivo* stable building block, this entity was integrated into the PKM, giving rise to the next generation of ligands [^{18}F]siPSMA-**11** to -**21a**. The respective labeling precursors were synthesized *via* SPPS (*Scheme 4*), purified by prep. RP-HPLC, and finally obtained in acceptable yields (15–59%) with high chemical purities (≥95%).

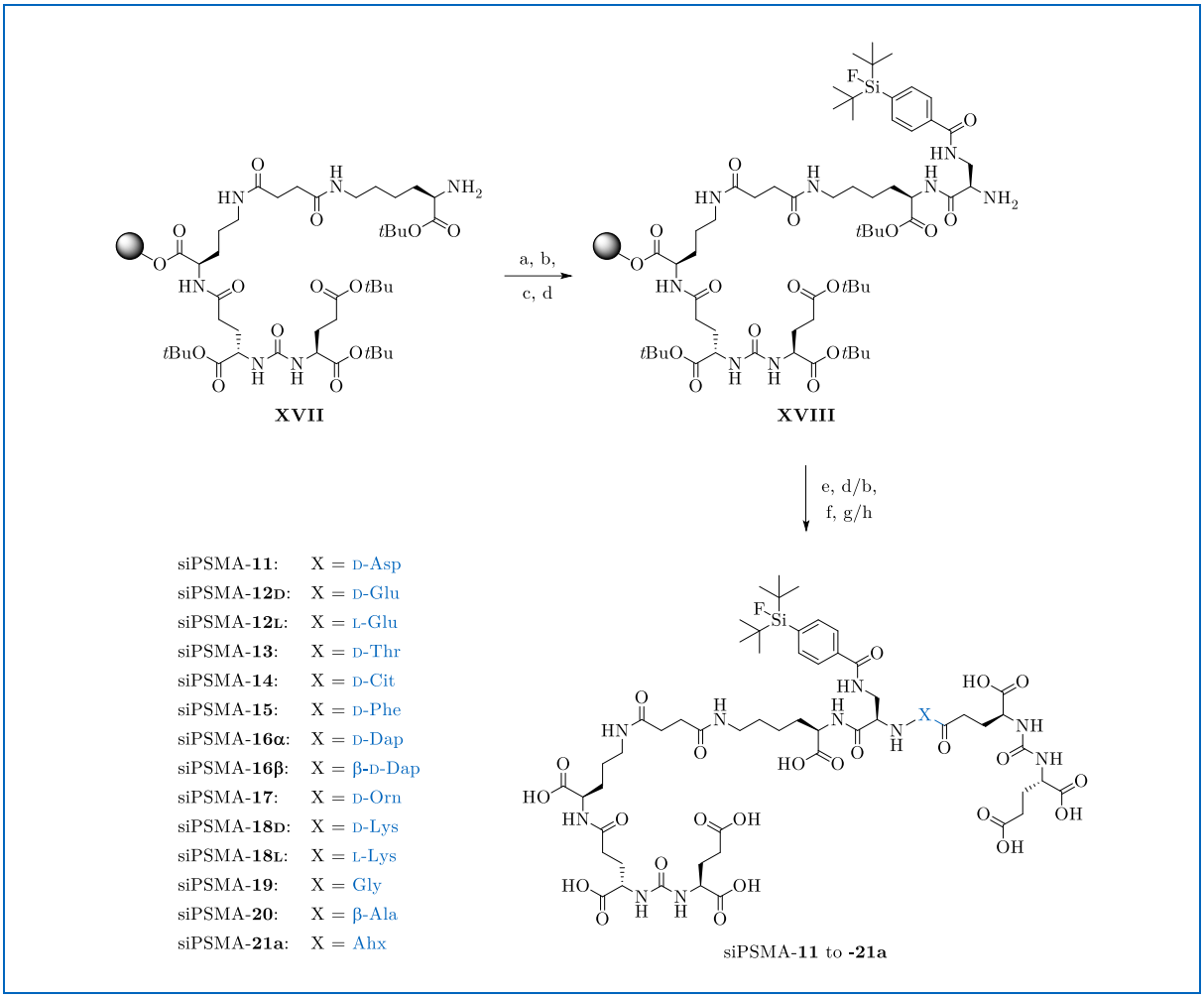

Scheme 4. Synthesis of siPSMA-**11** to -**21a**: a) Fmoc-D-Dap(Dde)-OH, HOAt, TBTU, 2,4,6-collidine, (DMF); b) imidazole, hydroxylamine hydrochloride, (DCM/NMP); c) SiFA-BzA (**V**), HOAt, TBTU, 2,4,6-collidine, (DMF); d) Pip, (DMF); e) Fmoc-D-Asp(O*t*Bu)-OH or Fmoc-D-Glu(O*t*Bu)-OH or Fmoc-L-Glu(O*t*Bu)-OH or Fmoc-D-Thr(*t*Bu)-OH or Fmoc-D-Cit-OH or Fmoc-D-Phe-OH or Fmoc-D-Dap(Boc)-OH or Fmoc-D-Dap(Dde)-OH or Fmoc-D-Orn(Boc)-OH or Fmoc-D-Lys(Boc)-OH or Fmoc-L-Lys(Boc)-OH or Fmoc-Gly-OH or Fmoc-β-Ala-OH or Fmoc-Ahx-OH, HOAt, TBTU, 2,4,6-collidine, (DMF); f) *t*BuO-L-Glu(O*t*Bu)-urea-L-Glu-O*t*Bu (**IX**), HOAt, TBTU, 2,4,6-collidine, (DMF); g) TFA, TIPS, water; h) TFA, TIPS, water; and Pip, (DMF).

Characterization and *in vitro* analysis of [$^{18/19}$F]siPSMA-**11** to -**21a** included determination of lipophilicity ($\log D_{7.4}$), assessment of PSMA-binding affinity (IC_{50}) and internalization, as well as evaluation of HSA binding. The results, together with previously published data of clinically established radiofluorinated PSMA inhibitors evaluated under the same conditions, are summarized below (*Table 12*)[168, 250].

Table 12. Characterization and *in vitro* evaluation of [$^{18/19}$F]siPSMA-**11** to -**21a** in comparison with [$^{18/19}$F]DCFPyL, [$^{18/19}$F]PSMA-1007, and [$^{18/19}$F]^{nat}Ga-rhPSMA-7.3 (data derived from the literature)[168, 250]. Investigated parameters include lipophilicity represented by log$D_{7.4}$ (data expressed as mean ± SD, $n = 5$), IC_{50} (data expressed as mean nM ± SD with **XXV** as reference, $n = 3$), internalized activity after 1 h (data corrected for unspecific binding and expressed as mean internalized activity of reference **XXV** in % ± SD, $n = 3$), and HSA binding (data expressed as % compared to standard reference compounds).

PSMA ligand	**PKM** (X = γ-L-Glu-urea-L-Glu)	**lipophilicity** (log$D_{7.4}$)	IC_{50} [nM]	**internalized activity** [% of **XXV**]	**HSA binding** [%]
[$^{18/19}$F]siPSMA-**11**	D-Asp-X	–4.02 ± 0.04	7.8 ± 0.8	163 ± 7	≥99.0
[$^{18/19}$F]siPSMA-**12D**	D-Glu-X	–4.04 ± 0.08	11.8 ± 2.2	126 ± 4	≥99.0
[$^{18/19}$F]siPSMA-**12L**	L-Glu-X	–3.72 ± 0.02	17.0 ± 0.9	175 ± 6	≥98.9
[$^{18/19}$F]siPSMA-**13**	D-Thr-X	–3.86 ± 0.07	9.2 ± 1.2	121 ± 1	≥98.9
[$^{18/19}$F]siPSMA-**14**	D-Cit-X	–3.28 ± 0.03	13.0 ± 1.2	96 ± 10	≥98.9
[$^{18/19}$F]siPSMA-**15**	D-Phe-X	–2.99 ± 0.02	29.4 ± 0.6	62 ± 1	≥98.9
[$^{18/19}$F]siPSMA-**16α**	D-Dap-X	–3.96 ± 0.07	9.2 ± 1.4	126 ± 1	≥99.0
[$^{18/19}$F]siPSMA-**16β**	β-D-Dap-X	–3.65 ± 0.09	10.2 ± 1.2	232 ± 14	98.8
[$^{18/19}$F]siPSMA-**17**	D-Orn-X	–3.65 ± 0.09	8.3 ± 1.5	123 ± 2	98.8
[$^{18/19}$F]siPSMA-**18D**	D-Lys-X	–3.71 ± 0.03	8.7 ± 0.7	105 ± 4	98.8
[$^{18/19}$F]siPSMA-**18L**	L-Lys-X	–3.71 ± 0.16	8.7 ± 0.6	143 ± 7	98.7
[$^{18/19}$F]siPSMA-**19**	Gly-X	–3.96 ± 0.04	8.8 ± 1.7	161 ± 3	98.9
[$^{18/19}$F]siPSMA-**20**	β-Ala-X	–3.70 ± 0.02	5.6 ± 1.3	201 ± 3	≥98.9
[$^{18/19}$F]siPSMA-**21a**	Ahx-X	–3.27 ± 0.02	5.9 ± 1.0	157 ± 13	≥99.0
[$^{18/19}$F]DCFPyL	-	–3.4 ± 0.03	12.3 ± 1.2	118 ± 4	14.3
[$^{18/19}$F]PSMA-1007	-	–1.6 ± 0.02	4.2 ± 0.5	118 ± 5	97.8
[$^{18/19}$F]^{nat}Ga-rhPSMA-7.3	DOTA-GA(^{nat}Ga)	–3.3 ± 0.2	4.4 ± 1.1	161 ± 9	97

With regard to the lipophilicity, log$D_{7.4}$ values between –4.04 and –2.99 were observed for the third generation of inhibitors comprising [^{18}F]siPSMA-**11** to -**21a**. The generally increased hydrophilic character compared to the previous ligand series was ascribed to the altered PKM. Indeed, the net charge contribution of the L-Glu-urea-L-Glu building block is considerably greater than that of the D-Glu-D-Glu sequence (PKM net charge contribution of –3 *vs.* –1). Similar to the second-generation ligands, inhibitors with a negatively charged amino acid at the permuted first position of the modifier (PKM net charge of –4) exhibited highest overall hydrophilicity, while [^{18}F]siPSMA-**15** bearing a D-Phe showed the most pronounced lipophilic character. Log$D_{7.4}$ values of [^{18}F]siPSMA ligands containing a neutral (PKM net charge of –3)

or positively charged amino acid (PKM net charge of –2) within the modifier sequence were found to be between these two extrema.

As for the binding affinity, a majority of the third-generation siPSMA inhibitors exhibited low IC_{50} values within the single-digit nanomolar range. Most notably, the affinity values determined for siPSMA-**20** (IC_{50} = 5.6 ± 1.3 nM) and -**21a** (IC_{50} = 5.9 ± 1.0 nM) set new standards among the newly developed ligands and were roughly comparable to the references PSMA-1007 (IC_{50} = 4.2 ± 0.5 nM) and ^{nat}Ga-rhPSMA-7.3 (IC_{50} = 4.4 ± 1.1 nM). As such, a non-polar aliphatic amino acid at the first position of the PKM appeared to be particularly advantageous. In contrast, the lowest PSMA-binding affinity (IC_{50} = 29.4 ± 0.6 nM) was once again observed for the inhibitor comprising a D-Phe within the PKM sequence, namely siPSMA-**15**.

In analogy to the previous inhibitor series, [^{18}F]siPSMA-**11** to -**21a** did not show a clear correlation between the structural composition of the PKM and the internalized activity after 1 h. The respective values were found to oscillate between 62–232% of the rate determined for the radioiodinated reference compound **XXV**. The highest internalization rates were observed for [^{18}F]siPSMA-**12L** (175 ± 6% of **XXV**), -**20** (201 ± 3% of **XXV**), and -**16β** (232 ± 14% of **XXV**), which were comparable or superior to the reported value for [^{18}F]^{nat}Ga-rhPSMA-7.3 (161 ± 9% of **XXV**).

Not surprisingly, siPSMA-**11** to -**21a** showed marked HSA binding as a result of the PKM composition featuring an overall negative net charge in combination with the lipophilic Silicon-based Fluoride Acceptor. Hence, highest values (≥98.7%) were determined for the third generation of siPSMA ligands in this regard.

A graphical comparison of the parameters described above for [$^{18/19}$F]siPSMA-**11** to -**21a**, [$^{18/19}$F]DCFPyL, [$^{18/19}$F]PSMA-1007, and [$^{18/19}$F]^{nat}Ga-rhPSMA-7.3 is shown below (*Figure 36*).

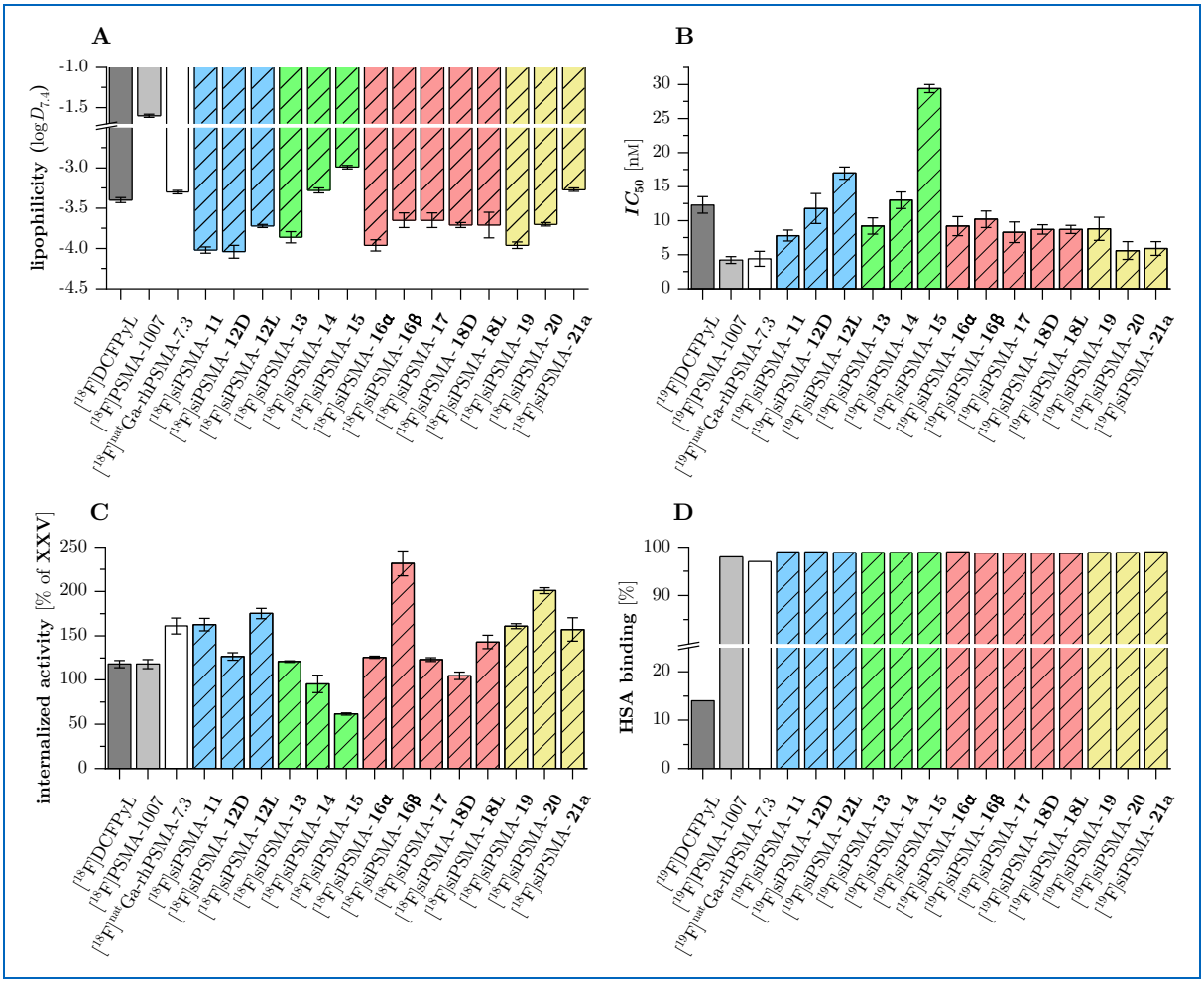

Figure 36. Graphical comparison of previously introduced data for [$^{18/19}$F]siPSMA-**11** to -**21a**, [$^{18/19}$F]DCFPyL, [$^{18/19}$F]PSMA-1007, and [$^{18/19}$F]^{nat}Ga-rhPSMA-7.3 (data derived from the literature), including **A**) lipophilicity represented by log$D_{7.4}$ (data expressed as mean ± SD, $n = 5$), **B**) IC_{50} (data expressed as mean nM ± SD with **XXV** as reference, $n = 3$), **C**) internalized activity after 1 h (data corrected for unspecific binding and expressed as mean internalized activity of reference **XXV** in % ± SD, $n = 3$), and **D**) HSA binding (data expressed as % compared to standard reference compounds)[168, 250].

In summary, the development of novel PSMA inhibitors with urea-based PKM resulted in several candidates with further improved properties. The structurally altered modifier, consisting of a permuted amino acid linked to an L-Glu-urea-L-Glu entity, conferred generally increased hydrophilicity to the third-generation siPSMA ligands. Moreover, new benchmarks were set in terms of PSMA-binding affinity and internalization rate, which was found to be particularly true for the inhibitors bearing a non-polar aliphatic amino acid at the PKM's first position.

Optimized siPSMA Ligands with Urea-based PKM

Since siPSMA-**21a** demonstrated favorable lipophilicity ($\log D_{7.4} = -3.27 \pm 0.02$), elevated binding affinity ($IC_{50} = 5.9 \pm 1.0$ nM), and high internalization rate after 1 h (157 ± 13% of **XXV**), this inhibitor became the lead compound for further optimization. Aiming to clarify whether the improved *in vitro* properties resulted from enhanced PSMA binding through the L-Glu-urea-L-Glu sequence within the PKM, siPSMA-**21b** was designed as a ligand variant bearing a D-configured modifier. In addition, it was also investigated if a structurally more rigid moiety in place of Ahx would further improve the ligand characteristics. For this purpose, siPSMA-**22** was conceived with a PKM comprising a linear Gly-Gly-Gly sequence prior to the L-Glu-urea-L-Glu building block. The labeling precursors of [^{18}F]siPSMA-**21b** and -**22** were synthesized by SPPS (*Scheme 5*), purified *via* prep. RP-HPLC, and finally obtained in low yields (7–12%) but with high chemical purities (≥96%).

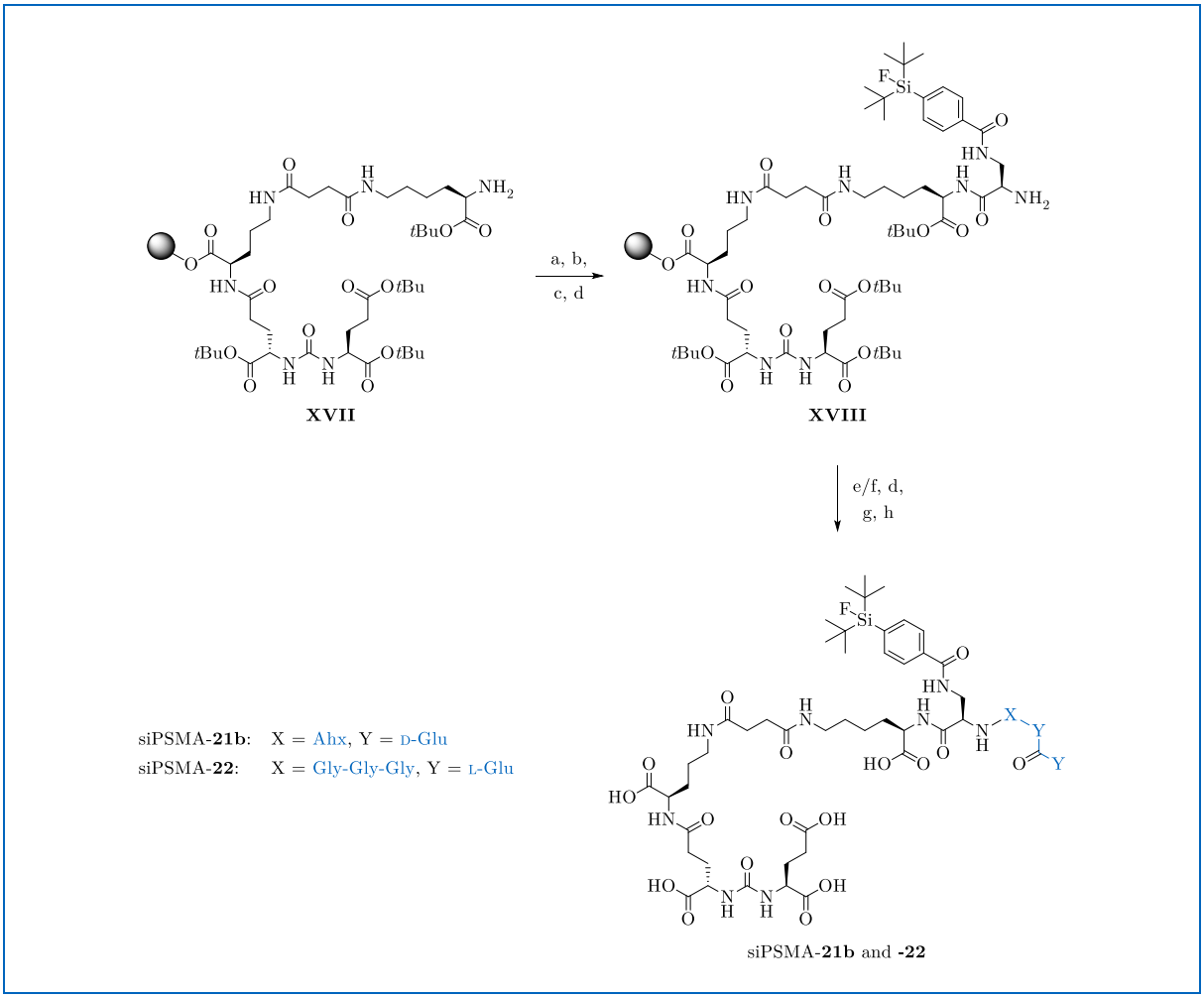

Scheme 5. Synthesis of siPSMA-**21b** and -**22**: a) Fmoc-D-Dap(Dde)-OH, HOAt, TBTU, 2,4,6-collidine, (DMF); b) imidazole, hydroxylamine hydrochloride, (DCM/NMP); c) SiFA-BzA (**V**), HOAt, TBTU, 2,4,6-collidine, (DMF); d) Pip, (DMF); e) Fmoc-Ahx-OH, HOAt, TBTU, 2,4,6-collidine, (DMF); f) Fmoc-Gly-OH, HOAt, TBTU, 2,4,6-collidine, (DMF); and Pip, (DMF); and Fmoc-Gly-OH, HOAt, TBTU, 2,4,6-collidine, (DMF); and Pip, (DMF); and Fmoc-Gly-OH, HOAt, TBTU, 2,4,6-collidine, (DMF); g) *t*BuO-D-Glu(O*t*Bu)-urea-D-Glu-O*t*Bu (**XIII**) or *t*BuO-L-Glu(O*t*Bu)-urea-L-Glu-O*t*Bu (**IX**), HOAt, TBTU, 2,4,6-collidine, (DMF); h) TFA, TIPS, water.

Characterization and *in vitro* analysis of [$^{18/19}$F]siPSMA-**21b** and -**22** included determination of lipophilicity (log$D_{7.4}$), assessment of PSMA-binding affinity (IC_{50}) and internalization, as well as evaluation of HSA binding. The results are summarized below (*Table 13*), along with those of the lead compound [$^{18/19}$F]siPSMA-**21a** and previously published data of clinically established radiofluorinated PSMA inhibitors evaluated under the same conditions[168, 250].

Table 13. Characterization and *in vitro* evaluation of [$^{18/19}$F]siPSMA-**21a** to -**22** in comparison with [$^{18/19}$F]DCFPyL, [$^{18/19}$F]PSMA-1007, and [$^{18/19}$F]^{nat}Ga-rhPSMA-7.3 (data derived from the literature)[168, 250]. Investigated parameters include lipophilicity represented by log$D_{7.4}$ (data expressed as mean ± SD, $n = 5$), IC_{50} (data expressed as mean nM ± SD with **XXV** as reference, $n = 3$), internalized activity after 1 h (data corrected for unspecific binding and expressed as mean internalized activity of reference **XXV** in % ± SD, $n = 3$), and HSA binding (data expressed as % compared to standard reference compounds).

PSMA ligand	**PKM** (X = γ-L-Glu-urea-L-Glu, Y = γ-D-Glu-urea-D-Glu)	**lipophilicity** (log$D_{7.4}$)	IC_{50} [nM]	**internalized activity** [% of **XXV**]	**HSA binding** [%]
[$^{18/19}$F]siPSMA-**21a**	Ahx-X	–3.27 ± 0.02	5.9 ± 1.0	157 ± 13	≥99.0
[$^{18/19}$F]siPSMA-**21b**	Ahx-Y	–3.24 ± 0.03	9.9 ± 0.8	120 ± 6	≥98.9
[$^{18/19}$F]siPSMA-**22**	Gly-Gly-Gly-X	–3.50 ± 0.04	9.0 ± 2.2	190 ± 17	≥98.9
[$^{18/19}$F]DCFPyL	-	–3.4 ± 0.03	12.3 ± 1.2	118 ± 4	14.3
[$^{18/19}$F]PSMA-1007	-	–1.6 ± 0.02	4.2 ± 0.5	118 ± 5	97.8
[$^{18/19}$F]^{nat}Ga-rhPSMA-7.3	DOTA-GA(^{nat}Ga)	–3.3 ± 0.2	4.4 ± 1.1	161 ± 9	97

Not surprisingly, [^{18}F]siPSMA-**21a** and -**21b** displayed fairly identical log$D_{7.4}$ values, while [^{18}F]siPSMA-**22** exhibited a slightly more hydrophilic character owing to the additional amide functionalities within the Gly-Gly-Gly sequence.

Notable results were observed with respect to the *in vitro* properties. siPSMA-**21b**, differing from siPSMA-**21a** solely in the configuration of the Glu-urea-Glu building block within the modifier, demonstrated a considerably lower PSMA-binding affinity (IC_{50} = 9.9 ± 0.8 nM *vs.* 5.9 ± 1.0 nM) as well as a decreased internalization rate (120 ± 6% of **XXV** *vs.* 157 ± 13% of **XXV**). Given the inability of D-Glu-urea-D-Glu to act as a pharmacophore, these findings indicate that the L-configured binding motif within the PKM might also contribute to PSMA recognition[253-254].

Substitution of Ahx in siPSMA-**21a** by a linear Gly-Gly-Gly sequence, exhibiting increased rigidity due to the partial double-bond character of its amide groups, proved to be beneficial for the internalization rate (190 ± 17% of **XXV** *vs.* 157 ± 13% of **XXV**) but disadvantageous in terms of binding affinity (IC_{50} = 9.0 ± 2.2 nM *vs.* 5.9 ± 1.0 nM).

No differences were found with regard to the HSA-binding properties, which appeared to be equally high (≥98.9%) for siPSMA-**21a**, -**21b**, and -**22**.

A graphical comparison of the parameters described above for [$^{18/19}$F]siPSMA-**21a** to -**22**, [$^{18/19}$F]DCFPyL, [$^{18/19}$F]PSMA-1007, and [$^{18/19}$F]^{nat}Ga-rhPSMA-7.3 is shown below (*Figure 37*).

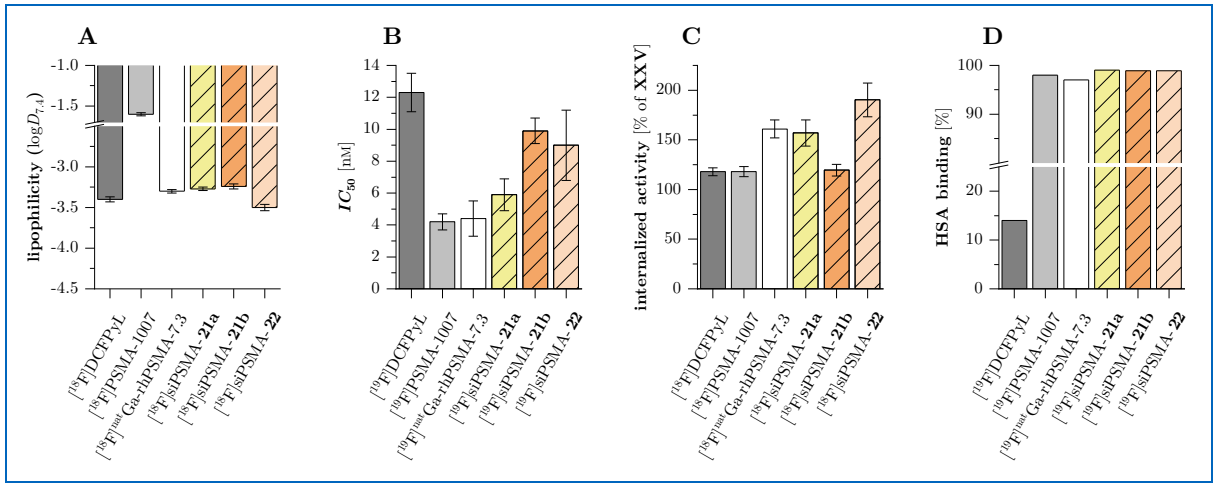

Figure 37. Graphical comparison of previously introduced data for [$^{18/19}$F]siPSMA-**21a** to -**22**, [$^{18/19}$F]DCFPyL, [$^{18/19}$F]PSMA-1007, and [$^{18/19}$F]^{nat}Ga-rhPSMA-7.3 (data derived from the literature), including **A**) lipophilicity represented by log$D_{7.4}$ (data expressed as mean ± SD, $n = 5$), **B**) IC_{50} (data expressed as mean nM ± SD with **XXV** as reference, $n = 3$), **C**) internalized activity after 1 h (data corrected for unspecific binding and expressed as mean internalized activity of reference **XXV** in % ± SD, $n = 3$), and **D**) HSA binding (data expressed as % compared to standard reference compounds)[168, 250].

Briefly, none of the optimized siPSMA ligands with urea-based PKM displayed superior characteristics when compared to the lead compound siPSMA-**21a**. However, evidence was found that further ligand improvement could be accomplished by leveraging the PSMA-binding properties of the L-Glu-urea-L-Glu moiety within the PKM.

siPSMA Ligands with Pseudo-dimeric Structure

The last generation of siPSMA inhibitors was designed with a pseudo-dimeric structure in order to exploit the second L-Glu-urea-L-Glu motif not only as PKM but also for efficient targeting of PSMA[255]. In this context, the trifunctional unit carrying the Silicon-based Fluoride Acceptor moiety was changed from D-Dap to D-Asp, thus permitting the coupling of the pharmacophore-linker sequences to both carboxylate functionalities. For siPSMA-**23**, dimerization was conducted with the L-Glu-urea-L-Glu(D-Orn(Suc(H-D-Lys-OH))) scaffold adopted in

preceding siPSMA inhibitors. In a further ligand, siPSMA-**24**, the linker structure was modified to include trimesic acid, as previous investigations reported increased internalization when incorporating an electron-deficient aromatic system at this specific position[136]. The corresponding labeling precursors of [^{18}F]siPSMA-**23** and -**24** were synthesized *via* SPPS involving direct dimerization on the resin (*Scheme 6*). After purification by prep. RP-HPLC, both compounds were obtained in acceptable yields (14–25%) and with high chemical purities (≥97%).

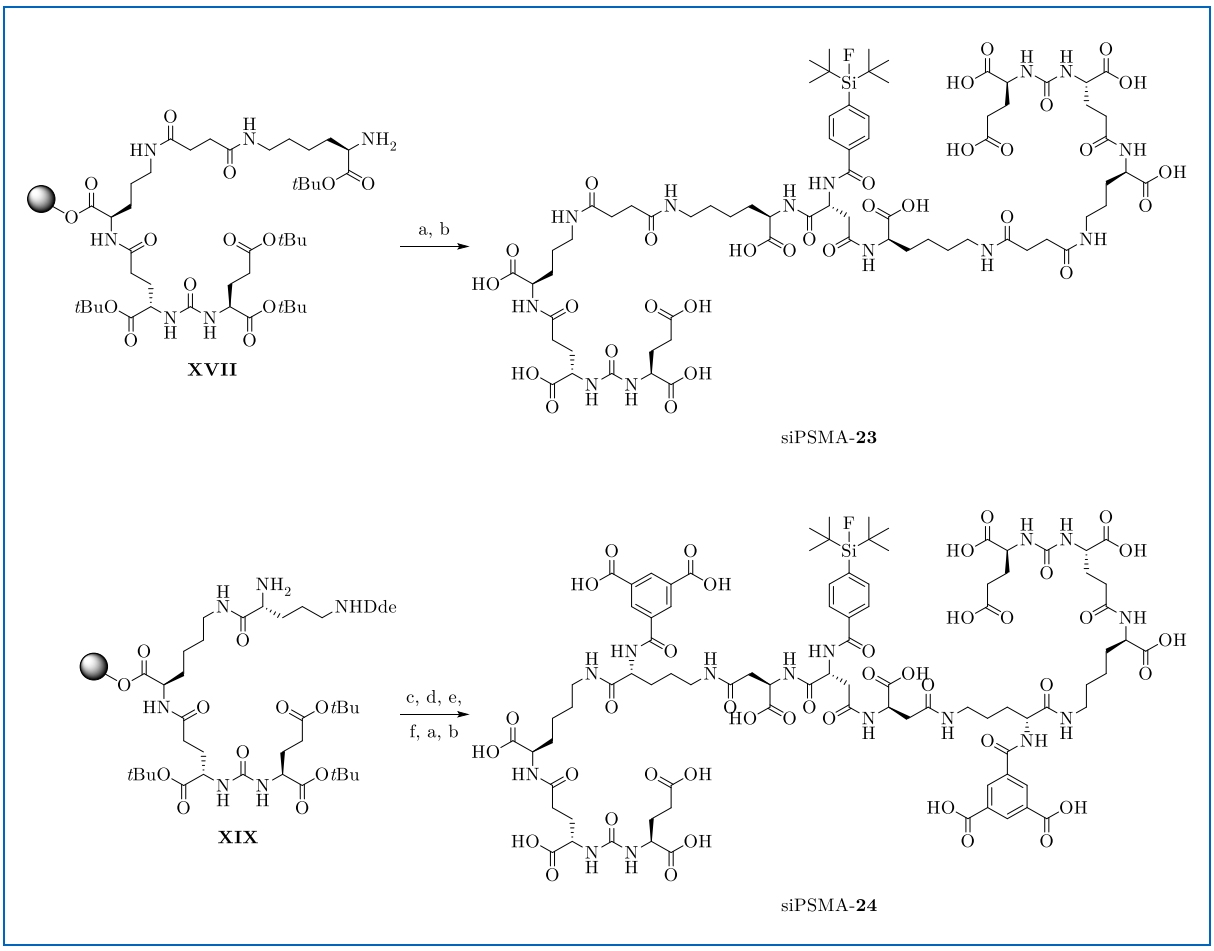

Scheme 6. Synthesis of siPSMA-**23** and -**24**: a) SiFA-BzA-D-Asp-OH (**XV**), HOAt, TBTU, 2,4,6-collidine, (DMF); b) TFA, TIPS, water; c) 3,5-bis(*tert*-butoxycarbonyl)benzoic acid (**XIV**), HOAt, TBTU, 2,4,6-collidine, (DMF); d) hydrazine monohydrate, (DMF); e) Fmoc-D-Asp-O*t*Bu, HOAt, TBTU, 2,4,6-collidine, (DMF); f) Pip, (DMF).

Characterization and *in vitro* analysis of [$^{18/19}$F]siPSMA-**23** and -**24** included determination of lipophilicity ($\log D_{7.4}$), assessment of PSMA-binding affinity (IC_{50}) and internalization, as well as evaluation of HSA binding. The results, together with previously published data of clinically

established radiofluorinated PSMA inhibitors evaluated under the same conditions, are summarized below (*Table 14*)[168, 250].

Table 14. Characterization and *in vitro* evaluation of [$^{18/19}$F]siPSMA-**23** and -**24** in comparison with [$^{18/19}$F]DCFPyL, [$^{18/19}$F]PSMA-1007, and [$^{18/19}$F]^{nat}Ga-rhPSMA-7.3 (data derived from the literature)[168, 250]. Investigated parameters include lipophilicity represented by log$D_{7.4}$ (data expressed as mean ± SD, $n = 5$), IC_{50} (data expressed as mean nM ± SD with **XXV** as reference, $n = 3$), internalized activity after 1 h (data corrected for unspecific binding and expressed as mean internalized activity of reference **XXV** in % ± SD, $n = 3$), and HSA binding (data expressed as % compared to standard reference compounds).

PSMA ligand	**lipophilicity** (log$D_{7.4}$)	***IC*$_{50}$** [nM]	**internalized activity** [% of **XXV**]	**HSA binding** [%]
[$^{18/19}$F]siPSMA-**23**	–3.77 ± 0.04	7.4 ± 1.9	270 ± 16	≥98.9
[$^{18/19}$F]siPSMA-**24**	–3.45 ± 0.01	5.5 ± 0.6	312 ± 7	≥98.9
[$^{18/19}$F]DCFPyL	–3.4 ± 0.03	12.3 ± 1.2	118 ± 4	14.3
[$^{18/19}$F]PSMA-1007	–1.6 ± 0.02	4.2 ± 0.5	118 ± 5	97.8
[$^{18/19}$F]^{nat}Ga-rhPSMA-7.3	–3.3 ± 0.2	4.4 ± 1.1	161 ± 9	97

In terms of lipophilicity, the measured log$D_{7.4}$ for [^{18}F]siPSMA-**24** was quite comparable to the reported values for the reference ligands [^{18}F]DCFPyL and [^{18}F]^{nat}Ga-rhPSMA-7.3. By contrast, [^{18}F]siPSMA-**23** exhibited a more hydrophilic character due to the lack of aromatic systems within the linker structures.

With respect to the binding affinity, low IC_{50} values in the single-digit nanomolar range were observed for both pseudo-dimeric siPSMA ligands. However, the determined affinities showed no substantial improvement when compared to the performance of monomeric PSMA inhibitors, suggesting that the second binding motif within siPSMA-**23** and -**24** contributes only to a minor extent to PSMA recognition.

On the contrary, a significant effect was identified with regard to the internalized activity. Indeed, among all newly developed ligands, [^{18}F]siPSMA-**23** and -**24** displayed the highest internalization rate after 1 h (270 ± 16% of **XXV** and 312 ± 7% of **XXV**), significantly outperforming the clinically established references.

In analogy to the previous generations of ligands, siPSMA-**23** and -**24** evidenced pronounced binding to HSA (≥98.9%).

A graphical comparison of the parameters described above for [$^{18/19}$F]siPSMA-**23** and -**24**, [$^{18/19}$F]DCFPyL, [$^{18/19}$F]PSMA-1007, and [$^{18/19}$F]^{nat}Ga-rhPSMA-7.3 is shown below (*Figure 38*).

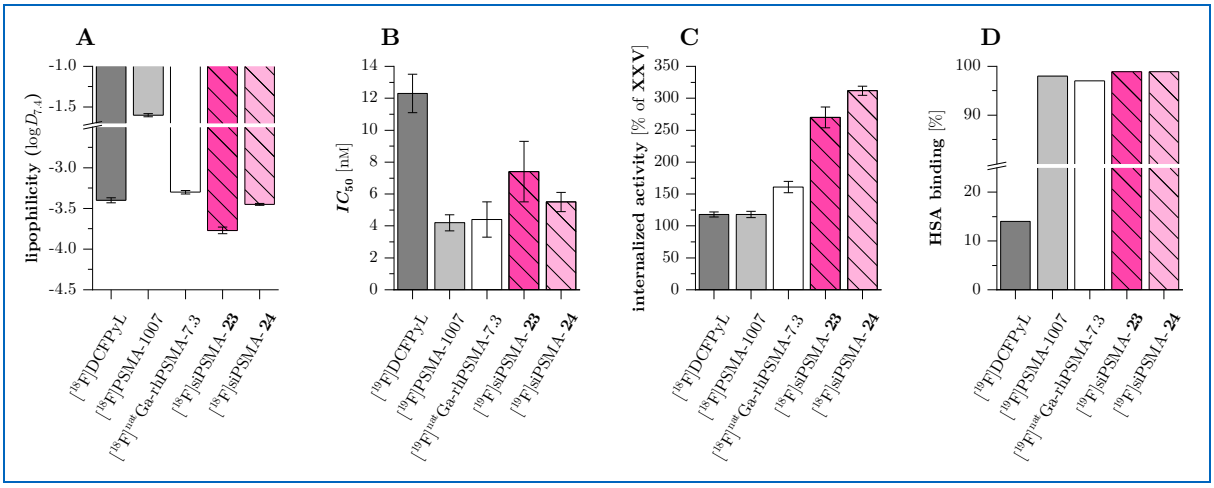

Figure 38. Graphical comparison of previously introduced data for [$^{18/19}$F]siPSMA-**23** and -**24**, [$^{18/19}$F]DCFPyL, [$^{18/19}$F]PSMA-1007, as well as [$^{18/19}$F]^{nat}Ga-rhPSMA-7.3 (data derived from the literature), including **A**) lipophilicity represented by log$D_{7.4}$ (data expressed as mean ± SD, $n = 5$), **B**) IC_{50} (data expressed as mean nM ± SD with **XXV** as reference, $n = 3$), **C**) internalized activity after 1 h (data corrected for unspecific binding and expressed as mean internalized activity of reference **XXV** in % ± SD, $n = 3$), and **D**) HSA binding (data expressed as % compared to standard reference compounds)[168, 250].

To sum up, the pseudo-dimeric siPSMA ligands were designed with the purpose of exploiting the second L-Glu-urea-L-Glu binding motif not only as a vehicle to compensate for the high lipophilicity of the Silicon-based Fluoride Acceptor moiety, but also to further improve the ligand properties. In this context, siPSMA-**24** stood out as a particularly promising inhibitor, showing reasonable lipophilicity (log$D_{7.4}$ = –3.45 ± 0.01), potent PSMA-binding affinity (IC_{50} = 5.5 ± 0.6 nM), and an exceptionally high internalization rate (312 ± 7% of **XXV**).

3.2.2 *In vivo* Evaluation of siPSMA Ligands

Selection of siPSMA Ligands for *in vivo* Evaluation

The most promising candidates for subsequent *in vivo* evaluation in LNCaP tumor-bearing mice were selected by analyzing the determined properties (log$D_{7.4}$, IC_{50}, and internalization rate after 1 h) in a bubble chart (*Figure 39*). Thereby, the plot was restricted to ligands

exhibiting high PSMA-binding affinity (IC_{50} ≤14 nM). Since all of these further considered inhibitors revealed pronounced binding to HSA (>95%), this parameter was not included as a selection criterion.

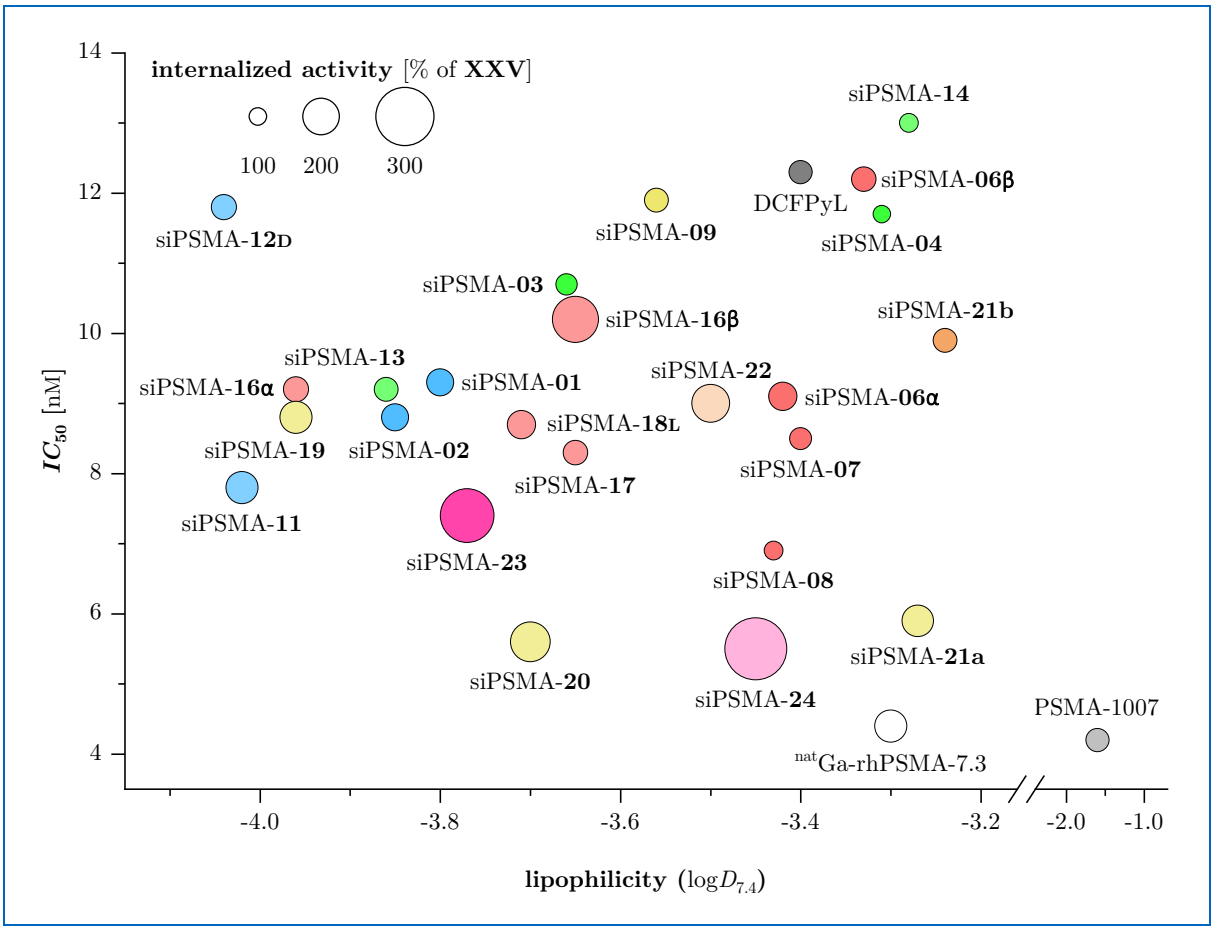

Figure 39. Summary of the previously determined properties ($\log D_{7.4}$, IC_{50}, and internalized activity after 1 h) for high-affinity siPSMA ligands in direct comparison with the references DCFPyL, PSMA-1007, and ^{nat}Ga-rhPSMA-7.3 (data derived from the literature)[168, 250].

The presence of a PKM constitutes a distinctive feature of the newly developed siPSMA-**01** to -**24**. Depending on its structural composition, the tracer's lipophilicity ($\log D_{7.4}$ values ranging from –4.04 to –2.30) could be precisely adjusted. This strategy was exploited with the purpose of developing PSMA ligands that exhibit intentionally delayed excretion kinetics. Such a characteristic was deemed to be the key for clear visualization of locoregional prostatic tumor lesions without interferences caused by premature activity accumulation in the urinary system. Since [^{18}F]^{nat}Ga-rhPSMA-7.3 was reported to display the desired *in vivo* behavior in human application, its lipophilicity ($\log D_{7.4} = -3.3 \pm 0.2$) served as a reference during the selection

process of promising siPSMA ligands[137]. Taking this into account and by virtue of their high binding affinity, [^{18}F]siPSMA-**08**, -**21a**, and -**24** emerged as ideal candidates for subsequent evaluation in mice. The group of selected inhibitors was further extended to include [^{18}F]siPSMA-**14**, given the almost identical lipophilicity shared with [^{18}F]^{nat}Ga-rhPSMA-7.3. Moreover, [^{18}F]siPSMA-**11** and -**23** were also considered in order to cover the entire log$D_{7.4}$ spectrum and to evaluate possible effects on biodistribution.

Biodistribution Studies with selected siPSMA Ligands

The first round of biodistribution studies included the selected inhibitors with peptide-based and urea-based PKM. Thereby, [^{18}F]siPSMA-**08**, -**11**, -**14**, and -**21a** were evaluated in LNCaP tumor-bearing CB17-SCID mice at 1 h p.i. and subsequently compared to each other (*Table 15*).

Table 15. Biodistribution of [^{18}F]siPSMA-**08** ($n = 4$), -**11** ($n = 4$), -**14** ($n = 4$), and -**21a** ($n = 4$) at 1 h p.i. in LNCaP tumor-bearing CB17-SCID mice. Results are presented as mean %ID/g ± SD.

organ	[^{18}F]siPSMA-**08** [%ID/g]	[^{18}F]siPSMA-**11** [%ID/g]	[^{18}F]siPSMA-**14** [%ID/g]	[^{18}F]siPSMA-**21a** [%ID/g]
blood	0.96 ± 0.60	0.97 ± 0.18	0.94 ± 0.30	1.33 ± 0.08
heart	0.55 ± 0.33	1.10 ± 0.08	0.94 ± 0.28	0.76 ± 0.17
lung	1.24 ± 0.55	1.83 ± 0.28	1.78 ± 0.45	1.57 ± 0.20
liver	0.51 ± 0.21	0.92 ± 0.09	0.91 ± 0.24	1.04 ± 0.06
spleen	10.98 ± 6.14	25.94 ± 12.04	31.70 ± 16.91	11.49 ± 2.42
pancreas	0.29 ± 0.06	0.77 ± 0.22	0.56 ± 0.09	0.40 ± 0.08
stomach	0.60 ± 0.38	0.55 ± 0.23	0.40 ± 0.13	0.44 ± 0.07
intestine	0.47 ± 0.12	0.57 ± 0.12	0.54 ± 0.15	0.53 ± 0.09
kidney	119.52 ± 24.29	214.23 ± 19.05	164.12 ± 70.02	160.88 ± 22.44
adrenal gland	2.40 ± 0.71	5.38 ± 3.23	5.72 ± 2.63	3.79 ± 0.85
muscle	0.23 ± 0.12	0.40 ± 0.25	0.42 ± 0.15	0.19 ± 0.03
bone	2.07 ± 0.60	1.15 ± 0.33	1.77 ± 0.46	0.74 ± 0.21
tumor	7.03 ± 1.83	15.03 ± 3.32	14.30 ± 5.11	8.93 ± 1.76
salivary gland	1.25 ± 0.47	1.63 ± 0.35	2.04 ± 0.70	1.50 ± 0.16

The investigated inhibitors [^{18}F]siPSMA-**08**, -**11**, -**14**, and -**21a** exhibited rather similar *in vivo* distribution with negligible activity accumulation in non-target tissue and major uptake in PSMA-expressing organs such as spleen, kidney, adrenal gland, salivary gland, and LNCaP

tumor[111, 115-117]. Despite differences in lipophilicity, with log$D_{7.4}$ values covering a range between –4.02 to –3.27, all four ligands were rapidly cleared from the blood pool and excreted almost exclusively *via* the renal pathway. Interestingly, radiotracer uptake in PSMA-specific tissue followed a rather consistent distribution pattern. In this regard, [^{18}F]siPSMA-**11** and -**14** demonstrated highest activity accumulation in organs with physiological PSMA expression along with the most pronounced LNCaP tumor uptake (15.03 ± 3.32 %ID/g and 14.30 ± 5.11 %ID/g). On the contrary, accumulation of both [^{18}F]siPSMA-**08** and -**21a** revealed to be lower in PSMA-expressing tissues, especially in spleen (10.98 ± 6.14 %ID/g and 11.49 ± 2.42 %ID/g) and LNCaP tumor (7.03 ± 1.83 %ID/g and 8.93 ± 1.76 %ID/g). Taken together, these results were particularly unexpected for [^{18}F]siPSMA-**14**, as the other three ligands had shown stronger binding affinities by a factor of 1.7 to 2.2 and comparable to considerably higher internalization rates. The discrepancy between the determined *in vitro* properties and the observed *in vivo* behavior indicates that additional unknown tracer-specific characteristics exert a major influence on the biodistribution performance. Since [^{18}F]siPSMA-**14** and -**21a** displayed the highest LNCaP tumor uptake among the investigated ligands with favorable predefined lipophilicity (log$D_{7.4}$ = –3.3 ± 0.2), both inhibitors were further considered as promising candidates.

A graphical comparison of the biodistribution results for [^{18}F]siPSMA-**08**, -**11**, -**14**, and -**21a** is provided below (*Figure 40*).

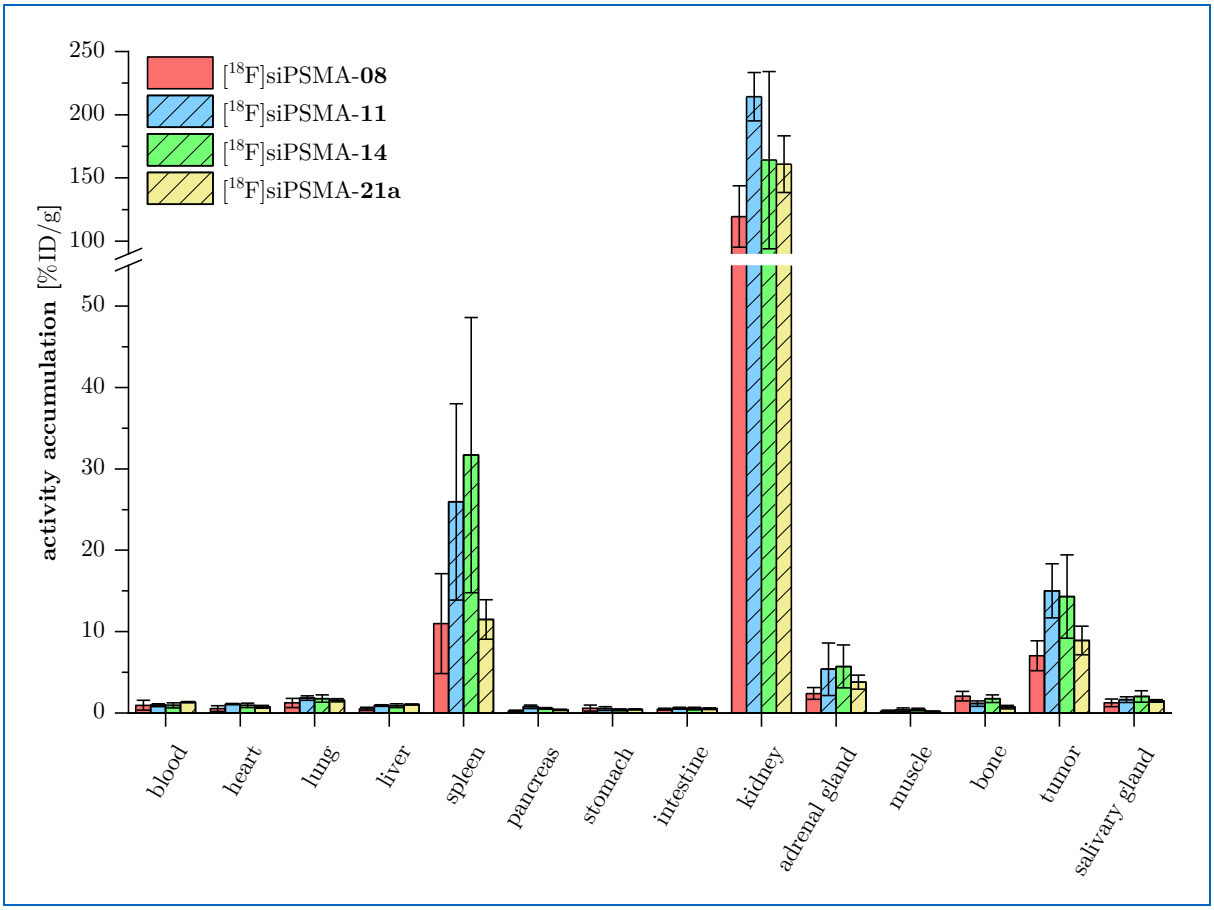

Figure 40. Graphical presentation of the biodistribution data for [^{18}F]siPSMA-**08** ($n = 4$), **-11** ($n = 4$), **-14** ($n = 4$), and **-21a** ($n = 4$) at 1 h p.i. in LNCaP tumor-bearing CB17-SCID mice. Results are presented as mean %ID/g ± SD.

The second round of biodistribution studies included the novel pseudo-dimeric inhibitors [^{18}F]siPSMA-**23** and **-24**, which had previously stood out for their exceptionally high internalization rates. The *in vivo* distribution of both ligands was again assessed in LNCaP tumor-bearing CB17-SCID mice at 1 h p.i. and subsequently compared with the earlier determined data for [^{18}F]siPSMA-**14** and **-21a** (*Table 16*).

Table 16. Biodistribution of [^{18}F]siPSMA-**14** ($n = 4$), -**21a** ($n = 4$), -**23** ($n = 4$), and -**24** ($n = 5$) at 1 h p.i. in LNCaP tumor-bearing CB17-SCID mice. Results are presented as mean %ID/g ± SD.

organ	[^{18}F]siPSMA-**14** [%ID/g]	[^{18}F]siPSMA-**21a** [%ID/g]	[^{18}F]siPSMA-**23** [%ID/g]	[^{18}F]siPSMA-**24** [%ID/g]
blood	0.94 ± 0.30	1.33 ± 0.08	0.41 ± 0.05	1.09 ± 0.76
heart	0.94 ± 0.28	0.76 ± 0.17	0.51 ± 0.14	0.75 ± 0.42
lung	1.78 ± 0.45	1.57 ± 0.20	1.16 ± 0.21	1.32 ± 0.72
liver	0.91 ± 0.24	1.04 ± 0.06	0.35 ± 0.04	0.90 ± 0.30
spleen	31.70 ± 16.91	11.49 ± 2.42	19.92 ± 6.45	5.23 ± 3.99
pancreas	0.56 ± 0.09	0.40 ± 0.08	0.42 ± 0.14	0.37 ± 0.22
stomach	0.40 ± 0.13	0.44 ± 0.07	0.23 ± 0.07	0.43 ± 0.24
intestine	0.54 ± 0.15	0.53 ± 0.09	0.26 ± 0.01	0.60 ± 0.28
kidney	164.12 ± 70.02	160.88 ± 22.44	184.44 ± 33.05	201.51 ± 14.72
adrenal gland	5.72 ± 2.63	3.79 ± 0.85	2.23 ± 0.73	1.63 ± 0.67
muscle	0.42 ± 0.15	0.19 ± 0.03	0.43 ± 0.50	0.20 ± 0.10
bone	1.77 ± 0.46	0.74 ± 0.21	0.49 ± 0.33	1.87 ± 0.88
tumor	14.30 ± 5.11	8.93 ± 1.76	8.82 ± 2.33	6.23 ± 2.01
salivary gland	2.04 ± 0.70	1.50 ± 0.16	1.35 ± 0.32	0.76 ± 0.49

The biodistribution profiles of both pseudo-dimeric ligands, [^{18}F]siPSMA-**23** and -**24**, revealed rapid washout from non-target tissue and high activity accumulation in the kidney (184.44 ± 33.05 %ID/g and 201.51 ± 14.72 %ID/g). When directly compared with the radiotracer uptake of [^{18}F]siPSMA-**14** in further PSMA-expressing organs such as spleen, adrenal gland, and salivary gland, both pseudo-dimeric inhibitors evidenced consistently lower accumulation[115-117]. Most surprisingly, uptake of [^{18}F]siPSMA-**23** and -**24** in the LNCaP tumor was significantly lower (8.82 ± 2.33 %ID/g and 6.23 ± 2.01 %ID/g), although both ligands had previously demonstrated excellent internalization rates (270 ± 16% of **XXV** and 312 ± 7% of **XXV**). This observation indicates that, at least for diagnostic PSMA inhibitors, the internalized activity exerts a minor influence on tumor accumulation during the investigated time period. Since [^{18}F]siPSMA-**14** once again stood out as the most favorable ligand after this second round of biodistribution studies, it was selected as the lead compound among the newly developed siPSMA inhibitors.

A graphical comparison of the biodistribution results for [^{18}F]siPSMA-**14**, -**21a**, -**23**, and -**24** is provided below (*Figure 41*).

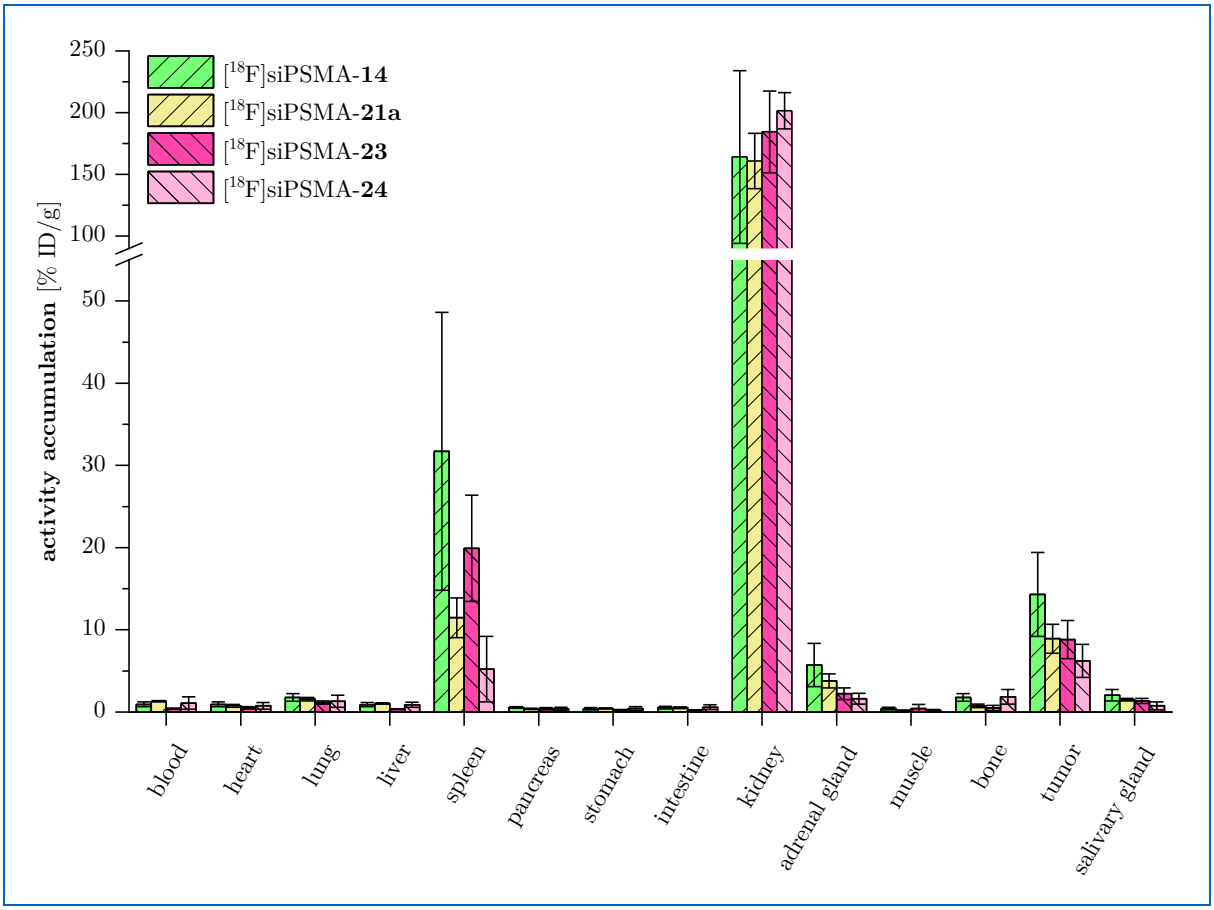

Figure 41. Graphical presentation of the biodistribution data for [^{18}F]siPSMA-**14** ($n = 4$), -**21a** ($n = 4$), -**23** ($n = 4$), and -**24** ($n = 5$) at 1 h p.i. in LNCaP tumor-bearing CB17-SCID mice. Results are presented as mean %ID/g ± SD.

In a final head-to-head comparison, the acquired biodistribution data for the most promising inhibitor [^{18}F]siPSMA-**14** were confronted with the published results for the clinically established ligands [^{18}F]DCFPyL, [^{18}F]PSMA-1007, and [^{18}F]^{nat}Ga-rhPSMA-7.3, which were evaluated under the same conditions (*Table 17*)[168, 250].

Table 17. Biodistribution of [^{18}F]siPSMA-**14** (n = 4) in comparison with the references (n = 4, data derived from the literature) [^{18}F]DCFPyL, [^{18}F]PSMA-1007, and [^{18}F]^{nat}Ga-rhPSMA-7.3 at 1 h p.i. in LNCaP tumor-bearing CB17-SCID mice[168, 250]. Results are presented as mean %ID/g ± SD.

organ	[^{18}F]DCFPyL [%ID/g]	[^{18}F]PSMA-1007 [%ID/g]	[^{18}F]^{nat}Ga-rhPSMA-7.3 [%ID/g]	[^{18}F]siPSMA-**14** [%ID/g]
blood	0.34 ± 0.3	0.48 ± 0.29	0.96 ± 0.24	0.94 ± 0.30
heart	0.25 ± 0.09	1.4 ± 0.5	0.87 ± 0.17	0.94 ± 0.28
lung	0.46 ± 0.05	1.8 ± 1	2.2 ± 0.35	1.78 ± 0.45
liver	1.7 ± 0.2	1.2 ± 0.5	0.69 ± 0.13	0.91 ± 0.24
spleen	9.6 ± 4.4	16.68 ± 5.09	16.6 ± 2.6	31.70 ± 16.91
pancreas	0.2 ± 0.1	1.4 ± 0.7	0.63 ± 0.44	0.56 ± 0.09
stomach	0.2 ± 0.03	0.96 ± 0.86	0.44 ± 0.23	0.40 ± 0.13
intestine	0.14 ± 0.02	1.1 ± 0.3	0.35 ± 0.07	0.54 ± 0.15
kidney	152.4 ± 15.3	123.3 ± 52.1	292 ± 45.1	164.12 ± 70.02
adrenal gland	5 ± 4	7.5 ± 3.4	2.2 ± 0.83	5.72 ± 2.63
muscle	0.11 ± 0.02	0.64 ± 0.41	0.33 ± 0.15	0.42 ± 0.15
bone	0.12 ± 0.02	0.89 ± 0.67	0.38 ± 0.32	1.77 ± 0.46
tumor	7.3 ± 1.5	7.4 ± 0.7	18.3 ± 7.2	14.30 ± 5.11

Overall, [^{18}F]siPSMA-**14** and the three radiofluorinated reference ligands showed a comparable *in vivo* distribution pattern with pronounced activity accumulation in PSMA-specific tissue and low background uptake. Some differences were observed with regard to the radiotracers' pharmacokinetics. As a consequence of their marked binding to HSA (≥97%), [^{18}F]siPSMA-**14** and [^{18}F]^{nat}Ga-rhPSMA-7.3 revealed prolonged retention in the blood pool (0.94 ± 0.30 %ID/g and 0.96 ± 0.24 %ID/g)[168]. With respect to the excretion pathway, [^{18}F]^{nat}Ga-rhPSMA-7.3, [^{18}F]siPSMA-**14**, and [^{18}F]DCFPyL displayed rapid renal clearance. In contrast, [^{18}F]PSMA-1007 was found to undergo hepatobiliary elimination to a certain extent, as evidenced by increased accumulation in the pancreas, stomach, and intestine. This behavior can be ascribed to the lipophilicity of [^{18}F]PSMA-1007 ($\log D_{7.4}$ = –1.6 ± 0.02), which is substantially more pronounced when compared to [^{18}F]^{nat}Ga-rhPSMA-7.3 ($\log D_{7.4}$ = –3.3 ± 0.2), [^{18}F]siPSMA-**14** ($\log D_{7.4}$ = –3.28 ± 0.03), and [^{18}F]DCFPyL ($\log D_{7.4}$ = –3.4 ± 0.03)[168, 250]. Further differences among the ^{18}F-labeled PSMA inhibitors were found with regard to the retention in PSMA-expressing tissue. Most notably, both radiotracers relying on Silicon-based Fluoride Acceptors – [^{18}F]siPSMA-**14** and [^{18}F]^{nat}Ga-rhPSMA-7.3 – showed the highest absolute retention in the LNCaP tumor (14.30 ± 5.11 %ID/g and 18.3 ± 7.2 %ID/g), well exceeding the performance

of [^{18}F]DCFPyL (7.3 ± 1.5 %ID/g) and [^{18}F]PSMA-1007 (7.4 ± 0.7 %ID/g)[168, 250]. In agreement with this finding, [^{18}F]siPSMA-**14** and [^{18}F]^{nat}Ga-rhPSMA-7.3 also revealed the highest kidney uptake (164.12 ± 70.02 %ID/g and 292 ± 45.1 %ID/g)[168].

A graphical comparison of the biodistribution results for [^{18}F]siPSMA-**14** with the respective literature data for the reference compounds [^{18}F]DCFPyL, [^{18}F]PSMA-1007, and [^{18}F]^{nat}Ga-rhPSMA-7.3 is provided below (*Figure 42*).

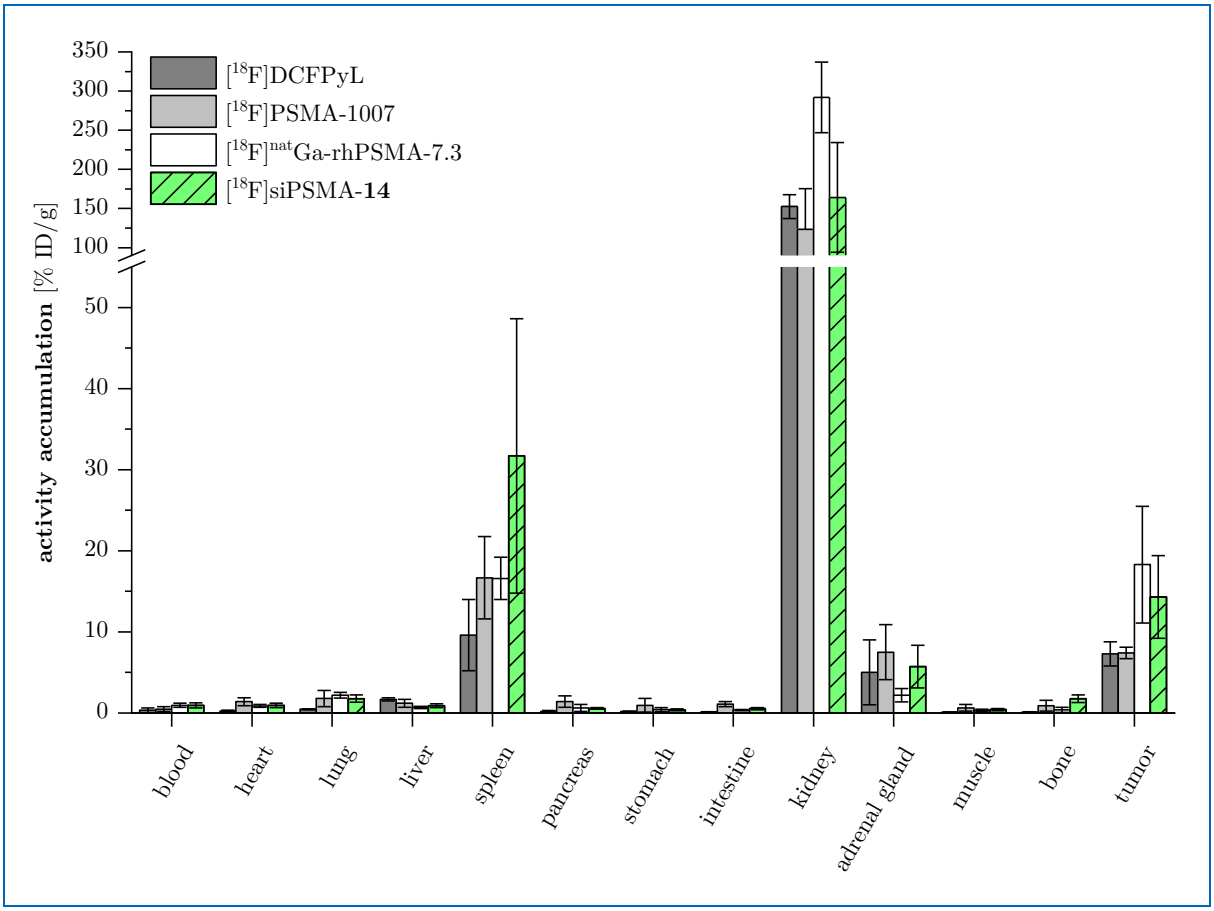

Figure 42. Graphical presentation of the biodistribution data for [^{18}F]siPSMA-**14** (n = 4) in comparison with the references (n = 4, data derived from the literature) [^{18}F]DCFPyL, [^{18}F]PSMA-1007, and [^{18}F]^{nat}Ga-rhPSMA-7.3 at 1 h p.i. in LNCaP tumor-bearing CB17-SCID mice[168, 250]. Results are presented as mean %ID/g ± SD.

In light of the favorable preclinical results obtained with [^{18}F]siPSMA-**14**, especially with respect to the biodistribution performance relative to established reference ligands, the novel radiotracer was considered for first-in-human applications.

3.2.3 Radiofluorination of siPSMA Ligands

Manual Radiofluorination on Laboratory Scale of siPSMA Ligands

Manual ^{18}F-labeling of newly developed siPSMA inhibitors on laboratory scale was performed using both [^{18}F]fluoride prepared by the *Munich* and the *SiFA-tailored Method* (*Table 18*).

Table 18. RCYs for the manual radiofluorination of siPSMA ligands with [^{18}F]fluoride prepared by either the *Munich* (GLP1b-I) or the *SiFA-tailored Method* (GLP1c-I/II). Radiolabeling was performed according to the specified conditions, followed by radiotracer purification *via* SPE.

PSMA ligand	*Munich Method*		*SiFA-tailored Method*	
	RCY[a] [%]	***n***	**RCY** [%]	***n***
[^{18}F]siPSMA-**0a**	15	1	9[c]	1
[^{18}F]siPSMA-**0b**	59	1	14[c]	1
[^{18}F]siPSMA-**01**	34	1	9[b]	1
[^{18}F]siPSMA-**02**	61	1	10[b]	1
[^{18}F]siPSMA-**03**	36	1	9[b]	1
[^{18}F]siPSMA-**04**	44	1	11[b]	1
[^{18}F]siPSMA-**05**	40 ± 4	2	9[b]	1
[^{18}F]siPSMA-**06α**	43	1	12[b]	1
[^{18}F]siPSMA-**06β**	29	1	11[b]	1
[^{18}F]siPSMA-**07**	64 ± 2	2	11[b]	1
[^{18}F]siPSMA-**08**	57 ± 3	3	12[b]	1
[^{18}F]siPSMA-**09**	32	1	8[b]	1
[^{18}F]siPSMA-**10**	39	1	9[c]	1
[^{18}F]siPSMA-**11**	56	1	10 ± 1[c]	2
[^{18}F]siPSMA-**12D**	75	1	9[b]	1
[^{18}F]siPSMA-**12L**	40	1	11[c]	1
[^{18}F]siPSMA-**13**	67	1	9[b]	1
[^{18}F]siPSMA-**14**	48	1	6 ± 1[b]	3
[^{18}F]siPSMA-**15**	41	1	7[b]	1
[^{18}F]siPSMA-**16α**	42	1	5[b]	1
[^{18}F]siPSMA-**16β**	60 ± 11	5	10[c]	1
[^{18}F]siPSMA-**17**	67 ± 7	4	12[c]	1
[^{18}F]siPSMA-**18D**	72	1	14[c]	1
[^{18}F]siPSMA-**18L**	36 ± 7	2	13[c]	1

[a] Radiofluorination of the siPSMA ligand (1 mM in DMSO, 30 µL, 30 nmol) occurred for 5 min at rt.

[b] Radiofluorination of the siPSMA ligand (1 mM in DMSO, 0.5 µL, 0.5 nmol) occurred for 5 min at 70°C.

[c] Radiofluorination of the siPSMA ligand (1 mM in DMSO, 0.5 µL, 0.5 nmol) occurred for 8 min at 65°C.

Table 18 Continued. RCYs for the manual radiofluorination of siPSMA ligands with [^{18}F]fluoride prepared by either the *Munich* (GLP1b-I) or the *SiFA-tailored Method* (GLP1c-I/II). Radiolabeling was performed according to the specified conditions, followed by radiotracer purification *via* SPE.

PSMA ligand	***Munich Method***		***SiFA-tailored Method***	
	RCY[(a)] [%]	***n***	**RCY** [%]	***n***
[^{18}F]siPSMA-**19**	56	1	8[(b)]	1
[^{18}F]siPSMA-**20**	62	1	8[(c)]	1
[^{18}F]siPSMA-**21a**	55 ± 11	2	10 ± 1[(c)]	2
[^{18}F]siPSMA-**21b**	34	1	8[(c)]	1
[^{18}F]siPSMA-**22**	22	1	9 ± 0[(c)]	2
[^{18}F]siPSMA-**23**	36 ± 3	2	7[(c)]	1
[^{18}F]siPSMA-**24**	34 ± 2	2	8[(c)]	1

[(a)] Radiofluorination of the siPSMA ligand (1 mM in DMSO, 30 µL, 30 nmol) occurred for 5 min at rt.

[(b)] Radiofluorination of the siPSMA ligand (1 mM in DMSO, 0.5 µL, 0.5 nmol) occurred for 5 min at 70°C.

[(c)] Radiofluorination of the siPSMA ligand (1 mM in DMSO, 0.5 µL, 0.5 nmol) occurred for 8 min at 65°C.

Partially neutralized [^{18}F]fluoride prepared by the *Munich Method* was selected to synthesize [^{18}F]siPSMA ligands, which were subsequently employed for log$D_{7.4}$ determination and biodistribution studies. In this context, 30 nmol of the labeling precursor were radiofluorinated with 22–1˙650 MBq of *Munich*-dried [^{18}F]fluoride for 5 min at rt, followed by simple radiotracer purification *via* SPE. The resulting [^{18}F]siPSMA ligands were obtained in about 25 min total synthesis time and with generally high RCYs (50 ± 15%, n = 46), which is consistent with the previously reported labeling results for [^{18}F]^{nat}Ga-rhPSMA-5 to -10 prepared under similar conditions[76]. In addition, quality control by radio-RP-HPLC and radio-TLC confirmed specificity of the isotopic exchange reaction and efficiency of the [^{18}F]fluoride separation as sole impurity by means of SPE.

The preparation of [^{18}F]siPSMA ligands intended for internalization studies necessitated a different strategy. Given that a minimal amount (0.125 pmol) of the radiofluorinated ligand was required for each experiment, [^{18}F]siPSMA inhibitors had to be synthesized with high A_ms (≥18 GBq/µmol) in order to allow for detection of radioactivity in the gamma counter. Since only limited [^{18}F]fluoride activity was available for practical feasibility of the experiment, the

sole option to provide radiotracers with the desired A_ms consisted in a substantial reduction of the labeling precursor amount used for radiofluorination. However, due to the concentration dependency of the isotopic exchange reaction, this strategy resulted in lower [^{18}F]fluoride incorporation rates and thus reduced RCYs for the final [^{18}F]siPSMA ligands when applying the abovementioned conditions (use of partially neutralized [^{18}F]fluoride prepared by the *Munich Method* and labeling for 5 min at rt)[240]. During the concurrent development of the *SiFA-tailored Method*, it was exemplarily shown for the radiofluorination of newly developed ^{nat}Lu-rhFolate ligands that the incorporation rate could be enhanced through heating of the labeling mixture. As described in more detail below (*Section 3.3.2*), the same strategy turned out to be incompatible with *Munich*-dried [^{18}F]fluoride. Hence, radiosynthesis of [^{18}F]siPSMA ligands for internalization experiments was conducted under heating (8 min at 65°C, or 5 min at 70°C) of small precursor amounts (0.5 nmol) mixed with dried [^{18}F]fluoride obtained by the *SiFA-tailored Method*. When starting with 125–312 MBq of [^{18}F]fluoride, radiotracers with acceptable RCYs (9 ± 2%, n = 36) were generated in about 25 min after SPE-based purification. Gratifyingly, the resulting A_ms (37 ± 12 GBq/µmol, n = 36) revealed to be remarkably high, meeting the requirements for internalization studies. As such, radiofluorination of siPSMA inhibitors in combination with the *SiFA-tailored Method* emerged as an advantageous strategy for the laboratory-scale synthesis of radiotracers with high A_ms.

Automated Radiofluorination of siPSMA-14

In order to perform first-in-human applications, a large-scale production of [^{18}F]siPSMA-**14** was established at the *University Hospital Ulm* by means of a fully automated radiosynthesis protocol previously developed by *Wurzer et al.*[82]. In analogy to this procedure, 150 nmol (221 µg) of siPSMA-**14** were labeled with *Munich*-dried [^{18}F]fluoride for 5 min at rt, followed by SPE purification of the resulting radiotracer[82]. Since the implementation of the automated synthesis in February 2019, more than 120 routine productions were carried out until April 2021. Based on a data set comprising 48 exemplary radiosyntheses with an average starting activity of 25 ± 4 GBq (18–42 GBq), [^{18}F]siPSMA-**14** was obtained in RCYs of 52 ± 16% and A_ms of 87 ± 27 GBq/µmol (17–144 GBq/µmol) in a total synthesis time of about 16 min. RCPs as measured by radio-RP-HPLC and radio-TLC always met the specification (≥90% for

[^{18}F]siPSMA-**14** and ≤5% for [^{18}F]fluoride) within the investigated data set. Overall, these results were well consistent with published data on the automated synthesis of [^{18}F]^{nat}Ga-rhPSMA-7.3, further highlighting the efficiency and reliability of large-scale radiofluorination exploiting the Silicon-based Fluoride Acceptor technology[82]. The great potential for clinical routine production becomes even more evident when considering current automated synthesis procedures of PSMA inhibitors prepared by conventional radiofluorination methods. In the case of [^{18}F]DCFPyL, the recently published large-scale production protocols by *Dornan et al.* (25 ± 9% RCY within 21 min) and *Bouvet et al.* (23 ± 5% RCY within 55 min) achieved only about half the RCY obtained for [^{18}F]siPSMA-**14**[149, 256]. By contrast, although the automated production of [^{18}F]PSMA-1007 as reported by *Naka et al.* (42 ± 4% RCY within 62 min) and *Cardinale et al.* (25–80% RCY within 35–55 min) proved to be comparably efficient, the required synthesis time was considerably longer[257-258]. As such, the convenient automated production of radiofluorinated Silicon-based Fluoride Acceptor-bearing ligands holds the potential to pave the way for a widespread application of ^{18}F-labeled radiopharmaceuticals in clinical routine.

3.2.4 First-in-human Applications with siPSMA-14

Owing to the promising *in vitro* and *in vivo* behavior exhibited by siPSMA-**14** in preclinical evaluation, the inhibitor was selected as a candidate for first applications in prostate cancer patients which were conducted at the Department of Nuclear Medicine, *University Hospital Ulm*.

In a first investigation, seven prostate cancer patients were imaged with [^{18}F]siPSMA-**14** at 60 min p.i. (T1) and 120 min p.i. (T3) in order to evaluate radiotracer accumulation and pharmacokinetics over time[236]. Herein, SUV_{mean} were determined for normal tissue and different tumor lesions (*Figure 43*)[236].

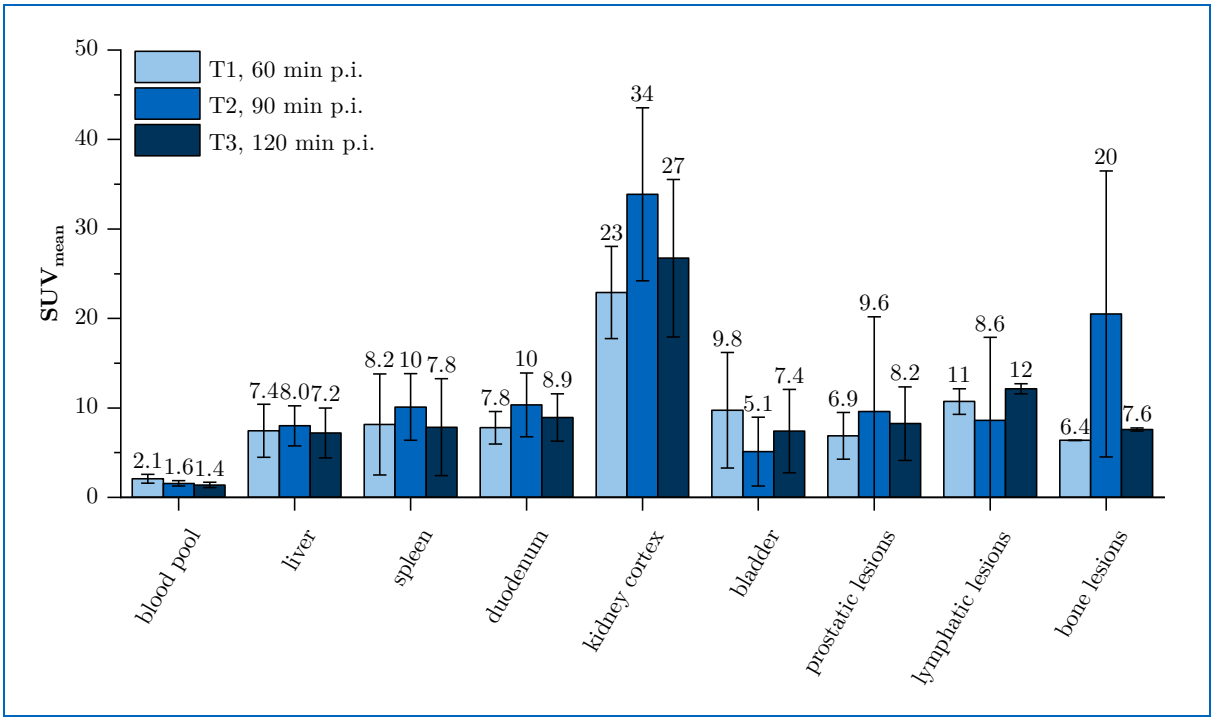

Figure 43. Measured SUV_{mean} of [^{18}F]siPSMA-**14** in normal tissue and different tumor lesions at 60 min (T1, $n = 7$), 90 min (T2, $n = 40$), and 120 min (T3, $n = 7$) p.i.[236]. Results are presented as mean ± SD.

When comparing the scan time points T1 and T3, most normal tissues (blood pool, liver, spleen, and bladder) demonstrated constant to slightly decreased radiotracer accumulation[236]. In contrast, increasing SUV_{mean} were measured for PSMA-expressing organs, including the duodenum and the kidney cortex[236]. The malignant lesions, independently from their location, displayed higher tracer uptake when PET acquisition was performed at T3[236]. Due to this circumstance and conditioned by logistical reasons, the scan time point was changed to 90 min p.i. (T2)[236]. This new imaging protocol was applied to the subsequent cohort of 40 prostate cancer patients and SUV_{mean} were also assessed for T2 (*Figure 43*)[236].

According to the obtained data set for the larger patient population scanned at T2, [^{18}F]siPSMA-**14** showed a comparable *in vivo* distribution pattern to the one observed with previously established ^{18}F-labeled PSMA ligands[236, 259]. In normal organs, the kidney cortex showed most predominant uptake ($SUV_{mean} = 33.9 \pm 9.7$), whereas radiotracer accumulation in the liver ($SUV_{mean} = 8.0 \pm 2.2$), spleen ($SUV_{mean} = 10.1 \pm 3.7$) and duodenum ($SUV_{mean} = 10.3 \pm 3.6$) was found to be moderate[236]. Malignant masses, including prostatic lesions ($SUV_{mean} = 9.6 \pm 10.6$), lymphatic lesions ($SUV_{mean} = 8.6 \pm 9.3$), and bone lesions ($SUV_{mean} =$

20.5 ± 16.0), were displayed with favorable contrast, as particularly low levels of the radiotracer accumulated in the blood pool (SUV_{mean} = 1.6 ± 0.3) and the bladder (SUV_{mean} = 5.1 ± 3.8)[236]. The slow excretion kinetics of [^{18}F]siPSMA-**14** revealed to be a decisive advantage, allowing for excellent visualization of lesions in the prostate bed despite close proximity to the bladder[238]. Noteworthy, high imaging quality was achieved without prior administration of furosemide for forced diuresis[236].

[^{18}F]siPSMA-**14** proved to be well tolerated in patients and enabled clear delineation of the local tumor down to the smallest metastases[87, 236]. These favorable imaging properties are illustrated below by an exemplary patient scan (*Figure 44*)[238].

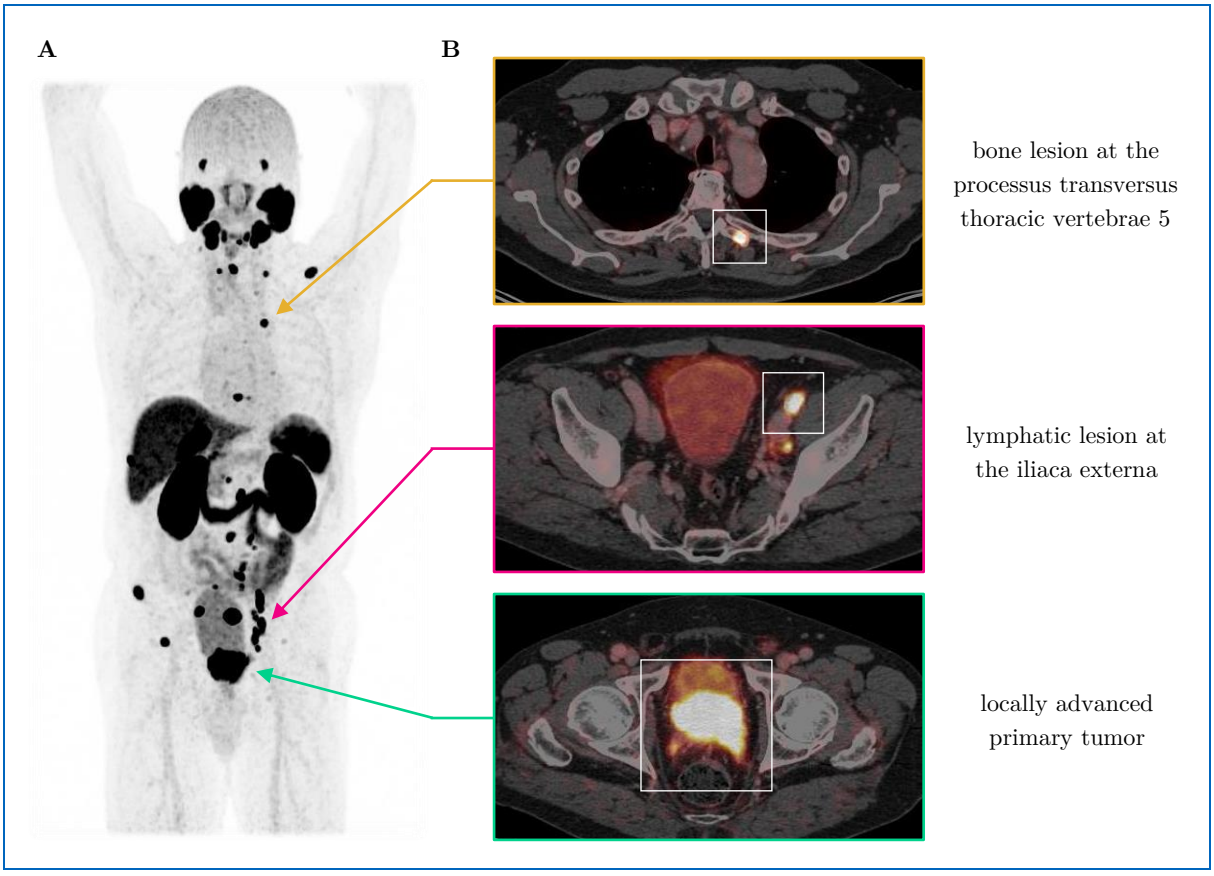

Figure 44. Exemplary biodistribution of [^{18}F]siPSMA-**14** in a 64-year-old prostate cancer patient (Gleason score 9, PSA of 100 ng/mL) with progressive disease after chemotherapy treatment (modified from the source)[238]. Images were acquired at 90 min p.i., including **A**) a whole-body maximum intensity projection PET scan and **B**) axial PET/CT fusion scans of selected lesions (white box)[238].

The lesion detection efficacy of [^{18}F]siPSMA-**14** for primary staging and restaging of prostate cancer was evaluated in a further investigation involving a total of 134 patients[237]. In the

primary staging subgroup, which included 54 patients, the detection rate was found to be 94% (51/54) for the local tumor, 43% (23/54) for lymph node lesions, and 41% (22/54) for bone metastases[237]. Among the subgroup of 80 patients referred for restaging, an overall detection efficacy of 86% (69/80) was observed[237]. In detail, the frequency of local tumor recurrence, lymph node lesions, bone metastases, and visceral lesions was 34% (27/80), 59% (47/80), 34% (27/80), and 3.8% (3/80), respectively[237]. These results were subsequently compared with the primary staging (*Figure 45A*) and restaging (*Figure 45B*) performance of the radiofluorinated reference ligands [^{18}F]DCFPyL, [^{18}F]PSMA-1007, and [^{18}F]^{nat}Ga-rhPSMA-7.3[166, 169, 237, 260].

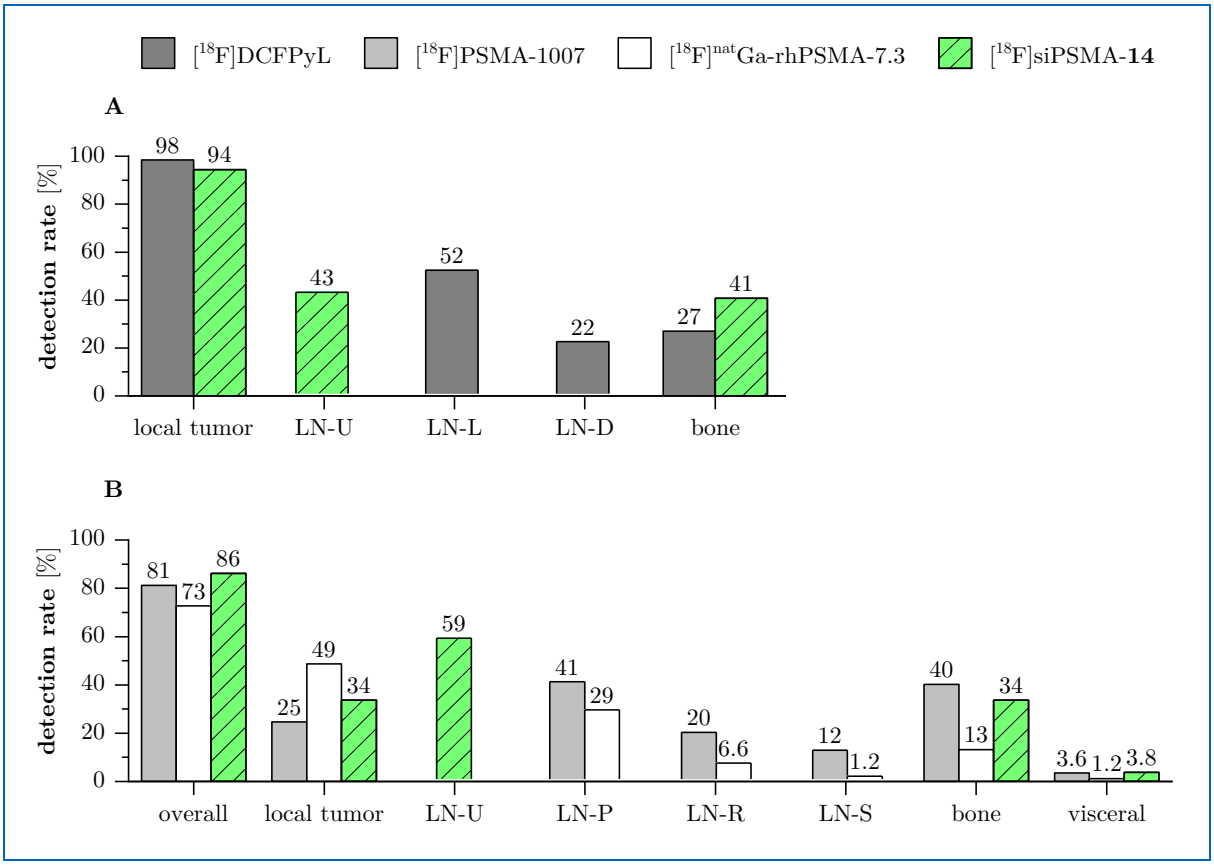

Figure 45. Detection rate of lesions for [^{18}F]DCFPyL, [^{18}F]PSMA-1007, and [^{18}F]^{nat}Ga-rhPSMA-7.3 in comparison to [^{18}F]siPSMA-**14** in **A**) primary staging or **B**) restaging of prostate cancer[166, 169, 237, 260]. Investigated lesions include the local tumor as well as lymph node, bone, and visceral metastases. Depending on the data set of the investigation, lymph node lesions are unspecified in location (LN-U) or classified as loco-regional (LN-L), distant (LN-D), pelvic (LN-P), retroperitoneal (LN-R), or supradiaphragmatic (LN-S).

When compared to the performance of [^{18}F]DCFPyL in primary staging, [^{18}F]siPSMA-**14** demonstrated a similar detection rate for the local tumor (94% *vs.* 98%) and a better efficacy in visualizing bone metastases (41% *vs.* 27%)[237, 260]. On the contrary, lymphatic lesions

appeared to be generally better detected with [^{18}F]DCFPyL[237, 260]. In this regard, it should be noted that a direct comparison was not feasible due to different counting and specification of such metastases in both investigations[237, 260].

With respect to the overall detection efficacy in patients referred for restaging, [^{18}F]siPSMA-**14** exhibited similar (86% *vs.* 81%) or even better (86% *vs.* 73%) performance when compared to [^{18}F]PSMA-1007 and [^{18}F]^{nat}Ga-rhPSMA-7.3, respectively[166, 169, 237]. Considering the detection rates for local tumor recurrence and bone metastases, [^{18}F]siPSMA-**14** turned out to represent a good compromise between both radiofluorinated references[166, 169, 237]. Once again, the detection efficacy for lymph node lesions could not be precisely compared due to different classification[166, 169, 237]. Nevertheless, [^{18}F]siPSMA-**14** demonstrated a satisfactory detection rate in this context[237].

In another investigation comprising a cohort of 87 patients who underwent restaging with [^{18}F]siPSMA-**14**, the determined lesion detection rates were stratified by PSA subgroups[238]. Overall, malignant masses were identified in 73/87 (84%) patients with detection rates of 61% (17/28), 92% (24/26), and 97% (32/33) for the respective subgroups with PSA levels ranging from 0 to <0.5 ng/mL, 0.5 to <2.0 ng/mL, and ≥2.0 ng/mL[238]. These results were found to be in line with the corresponding data published for [^{18}F]DCFPyL, [^{18}F]PSMA-1007, and [^{18}F]^{nat}Ga-rhPSMA-7.3 (*Figure 46*)[166, 169, 238, 261].

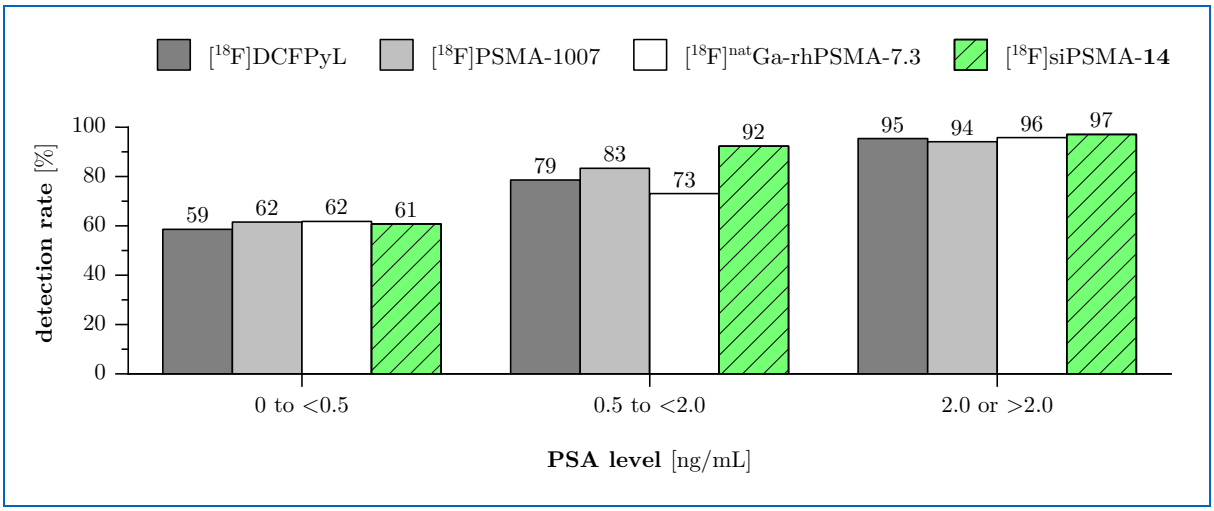

Figure 46. Detection rate of malignant lesions stratified by PSA subgroups in prostate cancer patients referred for restaging with [^{18}F]DCFPyL, [^{18}F]PSMA-1007, [^{18}F]^{nat}Ga-rhPSMA-7.3, or [^{18}F]siPSMA-**14**[166, 169, 238, 261].

Summarizing the experience gained from first-in-human applications, PET imaging with [^{18}F]siPSMA-**14** revealed to be safe and highly effective for staging and restaging of prostate cancer patients[237]. The superior performance in visualizing lesions adjacent to the bladder represents a major advantage of [^{18}F]siPSMA-**14**, that holds great promise for the early detection of locoregional recurrences and thereby resulting treatment options. This characteristic can be attributed to the particular pharmacokinetic profile of the novel radiotracer. Similar to [^{18}F]^{nat}Ga-rhPSMA-7.3, the excretion of [^{18}F]siPSMA-**14** appears to proceed *via* both hepatobiliary and renal pathways[88, 236, 259]. In contrast to [^{18}F]DCFPyL, which is rapidly cleared through the urinary system, and [^{18}F]PSMA-1007, with its predominant hepatobiliary elimination route, [^{18}F]siPSMA-**14** provides a balanced alternative allowing for clear detection of locoregional and distant lesions in patients[87, 145, 165]. Exemplary PET images showing the typical *in vivo* behavior of the four radiofluorinated PSMA ligands are summarized below (*Figure 47*)[88, 236, 262]. Importantly, each scan independently illustrates the relative tracer biodistribution, as images were not windowed to the same absolute intensity[88, 236, 262].

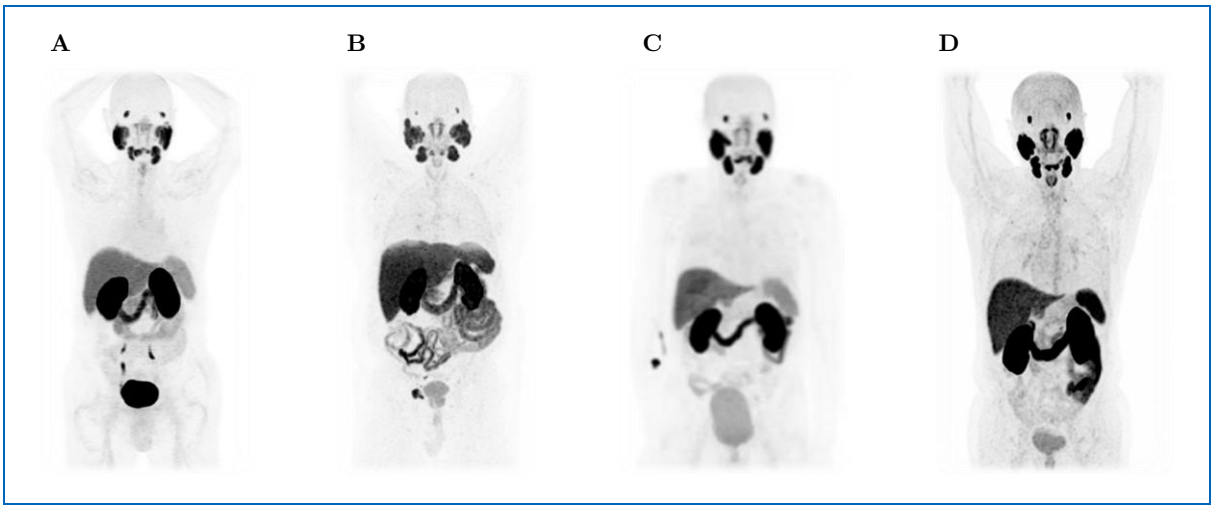

Figure 47. Exemplary whole-body maximum intensity projection PET images with **A**) [^{18}F]DCFPyL, **B**) [^{18}F]PSMA-1007, **C**) [^{18}F]^{nat}Ga-rhPSMA-7.3, and **D**) [^{18}F]siPSMA-**14** (modified from sources)[88, 236, 262].

The promising results observed throughout first-in-human applications of [^{18}F]siPSMA-**14** once again highlighted the tremendous potential of radiopharmaceuticals exploiting the Silicon-based Fluoride Acceptor technology. In this context, the herein adopted strategy of introducing a PKM to overcome the lipophilicity issue and to adjust the ligand's pharmacokinetic profile proved to be key for the development of a highly competitive PSMA-targeting radiotracer.

3.3 Development of novel ^{18}F-labeled FR Ligands

In recent years, a broad variety of radiofluorinated ligands for FR-targeted imaging have been reported[205]. Although some of these tracers demonstrated encouraging preclinical results, only [^{18}F]AzaFol has entered first-in-human studies so far[219]. The challenging radiofluorination of FR ligands represents one of the major obstacles on the way to a clinically applicable radiotracer[205]. To overcome this limitation, the present doctoral thesis focused on the development of novel FR-targeting ligands in combination with the highly efficient Silicon-based Fluoride Acceptor labeling technology. Since the FR is also being investigated as a target for ^{177}Lu- or $^{149/161}$Tb-based radionuclide therapy, the herein reported ligands were conceived as theragnostic agents by adopting the *radiohybrid* concept previously introduced by *Wurzer et al.*[76, 263-270]. These newly designed ^{nat}Lu-rhFolate ligands feature, on the one hand, a chelate that substantially contributes to compensate for the Silicon-based Fluoride Acceptor-associated lipophilicity. On the other hand, an integrated PKM, primarily responsible for fine-tuning the radiotracer's pharmacokinetics, links the FR-binding motif to the *radiohybrid* moiety.

3.3.1 Design and Preparation of ^{nat}Lu-rhFolate Ligands

A popular strategy for designing high-affinity FR ligands consists of elongating the γ-carboxylate in folic acid with the desired cargo[207-212, 214-215]. This so-called *pendant approach* exploits the fact that conjugates at the aforementioned position are located outside the FR-binding pocket, thus exerting negligible influence on the affinity properties[206]. Regarding the preparation of such ligands, various synthesis strategies have been described[271]. A common and simple method is based on the pre-activation of folic acid, followed by coupling with an amine-bearing component[271]. Unfortunately, since folic acid comprises two carboxylate functionalities, this approach results in the formation of an α-regioisomer besides the usually desired γ-conjugate[271]. Separation of both isomers is known to be laborious and frequently leads to FR-targeting ligands with reduced purity[271]. In order to circumvent this inconvenience, many research groups typically rely on the use of specifically protected folic acid derivatives[210-211, 215-216]. However, these compounds are often difficult to synthesize or only available from specialized vendors[210-211, 215-217]. With the aim of establishing a simple and efficient synthesis strategy for novel

Silicon-based Fluoride Acceptor-bearing FR ligands, a stepwise preparation route *via* SPPS was envisaged for the respective labeling precursors (*Scheme 7*).

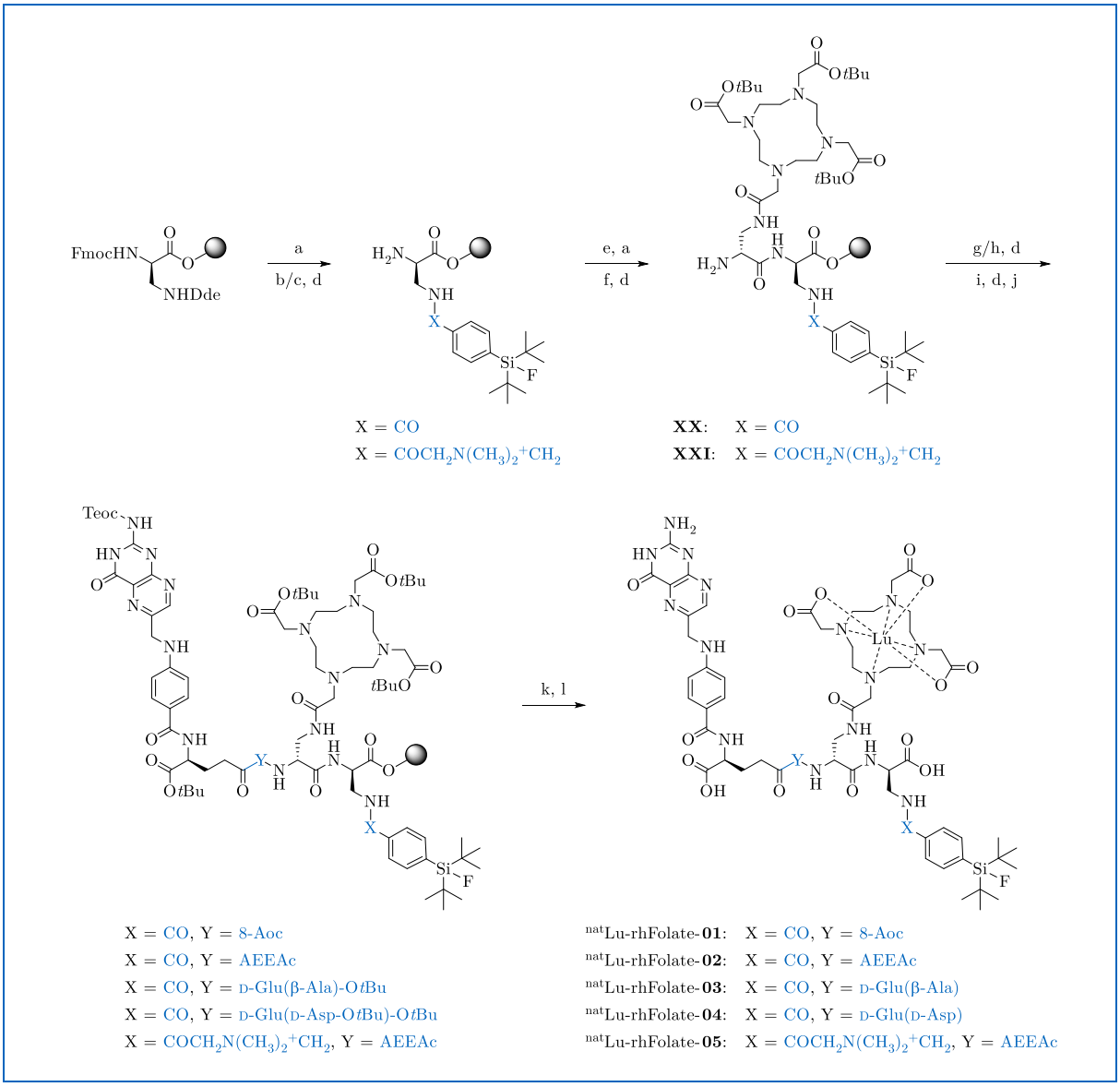

Scheme 7. Synthesis of ^{nat}Lu-rhFolate-**01** to -**05**: a) imidazole, hydroxylamine hydrochloride, (DCM/NMP); b) SiFA-BzA (**V**), HOAt, TBTU, 2,4,6-collidine, (DMF); c) *N,N*-dimethyl-Gly-OH, HOAt, TBTU, 2,4,6-collidine, (DMF); and SiFA-BnBr (**IV**), 2,4,6-collidine, (DCM); d) Pip, (DMF); e) Fmoc-D-Dap(Dde)-OH, HOAt, TBTU, 2,4,6-collidine, (DMF); f) DOTA(O*t*Bu)$_3$, HOAt, TBTU, 2,4,6-collidine, (DMF); g) Fmoc-8-Aoc-OH or Fmoc-AEEAc-OH, HOAt, TBTU, 2,4,6-collidine, (DMF); h) Fmoc-β-Ala-OH or Fmoc-D-Asp-O*t*Bu, HOAt, TBTU, 2,4,6-collidine, (DMF); and Pip, (DMF); and Fmoc-D-Glu-O*t*Bu, HOAt, TBTU, 2,4,6-collidine, (DMF); i) Fmoc-L-Glu-O*t*Bu, HOAt, TBTU, 2,4,6-collidine, (DMF); j) 1-(2-*N*-Teoc-pteroyl)imidazole (**XII**), HOAt, PyBOP, DIPEA, (DMSO); k) TFA, TIPS, water; l) LuCl$_3$, (DMSO/water).

Within the novel FR ligands ^{nat}Lu-rhFolate-**01** to -**05**, folic acid as a binding motif was linked through a PKM to the *radiohybrid* unit. The latter consists of the Silicon-based Fluoride Acceptor in combination with a ^{nat}Lu-complexed DOTA chelate. Preparation of the labeling precursors began with the syntheses of the *radiohybrid* moieties, which were obtained by attaching both the Silicon-based Fluoride Acceptor and the chelator DOTA to a peptidic D-Dap-D-Dap backbone (**XX** and **XXI**). The resulting building blocks were further extended with various PKMs differing in structure but sharing the same length. In order to synthesize FR-targeting ligands with a certain variety in terms of overall lipophilicity, the PKM was selected among compounds of aliphatic and peptidic nature, including 8-Aoc, AEEAc, D-Glu(β-Ala), and D-Glu(D-Asp). Subsequent introduction of folic acid as the binding motif was accomplished through a stepwise approach using derivatives of its components L-Glu and pteroic acid. For the latter, previously published 1-(2-*N*-Teoc-pteroyl)imidazole (**XII**) revealed to be a highly suitable building block due to its facile synthetic accessibility and favorable solubility in organic media[222]. Furthermore, simultaneous cleavage of the Teoc-protecting group could be achieved during global deprotection of the ligand precursors under acidic conditions[226]. Although the coupling reaction with 1-(2-*N*-Teoc-pteroyl)imidazole (**XII**) on the resin was not quantitative, purified uncomplexed FR ligand precursors were synthesized with satisfactory yields (4–16%). After ^{nat}Lu-complexation of the chelator moiety and repeated prep. RP-HPLC purification, ^{nat}Lu-rhFolate-**01** to -**05** were obtained with high chemical purities (≥94%) and acceptable final yields of 3–10%. Small amounts of impurities corresponded to the respective uncomplexed ligand precursors as prep. RP-HPLC purification turned out to be challenging due to similar chromatographic behavior.

3.3.2 Radiofluorination of ^{nat}Lu-rhFolate Ligands

Manual radiosynthesis on laboratory scale of newly developed FR ligands was first evaluated on ^{nat}Lu-rhFolate-**01**. The labeling reaction occurred with [^{18}F]fluoride prepared by either the *Munich* or the *SiFA-tailored Method*, followed by radiotracer purification *via* facile SPE (*Table 19*).

Table 19. RCYs for the manual radiofluorination of ^{nat}Lu-rhFolate ligands with [^{18}F]fluoride prepared by either the *Munich* (GLP1b-II/III) or the *SiFA-tailored Method* (GLP1c-V/VI). Radiolabeling was performed according to the specified conditions, followed by radiotracer purification *via* SPE.

FR ligand	*Munich Method*				*SiFA-tailored Method*			
	RCY[(a)] [%]	***n***	**RCY**[(b)] [%]	***n***	**RCY**[(a)] [%]	***n***	**RCY**[(b)] [%]	***n***
[^{18}F]^{nat}Lu-rhFolate-**01**	36 ± 2	2	20 ± 2[*]	2	22 ± 3	3	54 ± 10	4
[^{18}F]^{nat}Lu-rhFolate-**02**	-	-	-	-	-	-	66	1
[^{18}F]^{nat}Lu-rhFolate-**03**	-	-	-	-	-	-	57	1
[^{18}F]^{nat}Lu-rhFolate-**04**	-	-	-	-	-	-	62	1
[^{18}F]^{nat}Lu-rhFolate-**05**	-	-	-	-	-	-	53	1

[(a)] Radiofluorination of the ^{nat}Lu-rhFolate ligand (1 mM in DMSO, 30 µL, 30 nmol) occurred for 10 min at rt.

[(b)] Radiofluorination of the ^{nat}Lu-rhFolate ligand (1 mM in DMSO, 30 µL, 30 nmol) occurred for 10 min at 95°C.

[*] Purified radioligand included non-separable impurity by SPE.

Accordingly, when performing the isotopic exchange reaction with 30 nmol of labeling precursor for 10 min at rt, RCYs for the resulting [^{18}F]^{nat}Lu-rhFolate-**01** were somewhat higher employing *Munich*-dried [^{18}F]fluoride (36 ± 2%) instead of the eluate prepared by the *SiFA-tailored Method* (22 ± 3%). Since both approaches provided only moderate RCYs, radiofluorination reactions with ^{nat}Lu-rhFolate-**01** were also investigated at 95°C under otherwise unchanged conditions. In that case, ^{18}F-labeling with the *Munich* eluate resulted in decreased RCYs (20 ± 2%), whereas isotopic exchange under heating with dried [^{18}F]fluoride obtained by the *SiFA-tailored Method* turned out to be highly efficient (54 ± 10%). As a consequence, ^{nat}Lu-rhFolate-**02** to -**05** were labeled by the latter procedure, which provided remarkably high RCYs of 53–66% for the corresponding radiofluorinated FR ligands within a total synthesis time of about 30 min. Unexpected results were observed upon analyzing the RCP of [^{18}F]^{nat}Lu-rhFolate-**01** generated by each of the investigated radiofluorination approaches (*Figure 48*).

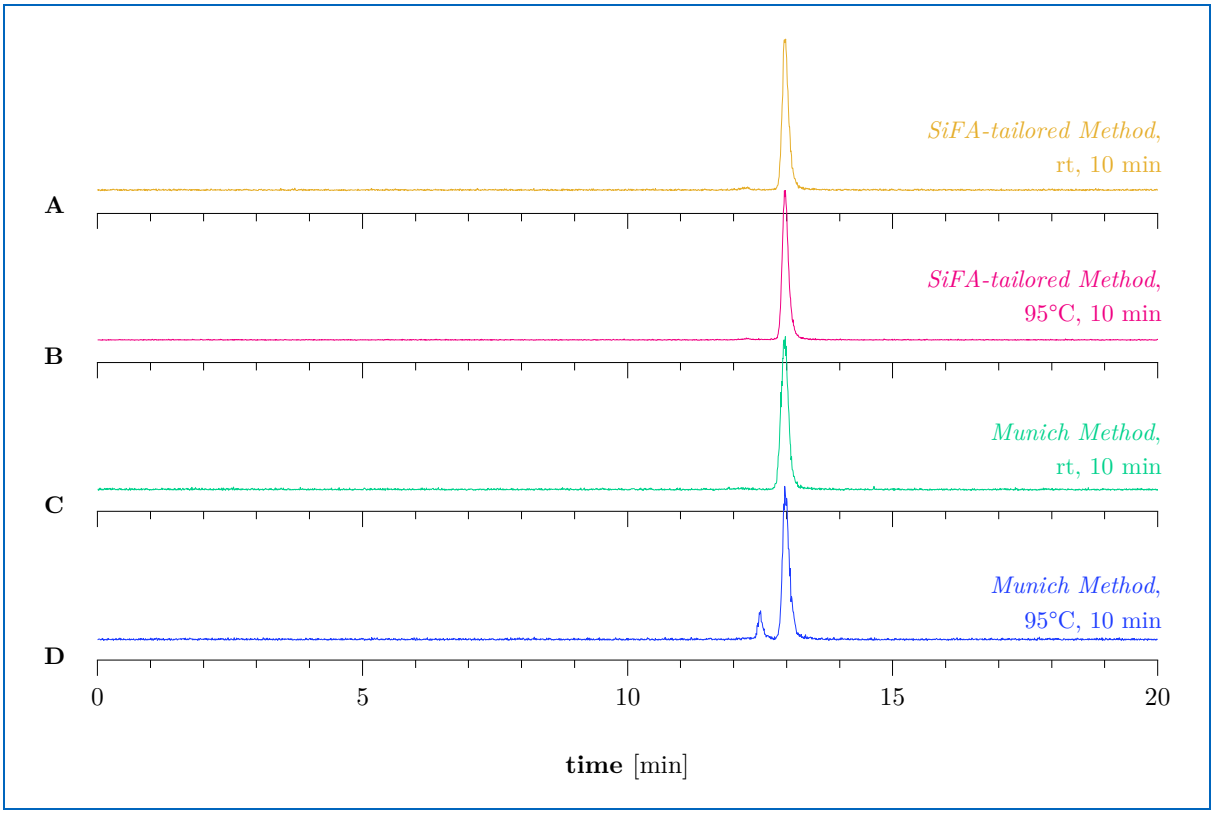

Figure 48. Radio-RP-HPLC chromatograms (column IV, 10→70% B in A for 15 min, 95% B in A for 5 min, t_R = 13.0 min) of SPE-purified [^{18}F]^{nat}Lu-rhFolate-**01** synthesized with [^{18}F]fluoride prepared by the **A**) *SiFA-tailored Method* and radiofluorination performed for 10 min at rt, **B**) *SiFA-tailored Method* and ^{18}F-labeling performed for 10 min at 95°C, **C**) *Munich Method* and radiofluorination performed for 10 min at rt, **D**) *Munich Method* and ^{18}F-labeling performed for 10 min at 95°C.

Both [^{18}F]^{nat}Lu-rhFolate-**01** preparations under the use of [^{18}F]fluoride obtained by the *SiFA-tailored Method* (labeling at rt and 95°C) provided the intact radiotracer (*Figure 48A* and *48B*) with high RCP (≥97%). Among the radiosyntheses involving *Munich*-dried eluate, [^{18}F]^{nat}Lu-rhFolate-**01** with similarly high RCP could only be produced when performing the radiofluorination reaction at rt (*Figure 48C*). In case where ^{18}F-labeling occurred at 95°C, an undesired impurity (t_R = 12.5 min) was identified in the final radiotracer formulation (*Figure 48D*). Given that such contaminant was not separable *via* SPE, respective RCPs for generated [^{18}F]^{nat}Lu-rhFolate-**01** were significantly reduced (89 ± 1%, n = 2). This finding underscores the incompatibility of the *Munich*-dried eluate with labeling reactions performed at elevated temperatures, as the increased reactivity of its composition leads to the uncontrolled formation of by-products precluding simple radiotracer workup *via* SPE. In contrast, [^{18}F]fluoride prepared by the *SiFA-tailored Method* exhibits a broader application range, allowing for

considerable improvement of RCYs through heating of the labeling mixture. Owing to this versatility, impressive radiosynthesis results (57 ± 8% RCY, $n = 8$, approx. 30 min overall synthesis time) were accomplished for the novel [^{18}F]^{nat}Lu-rhFolate ligands, well exceeding the radiofluorination performances of most FR ligands previously reported in the literature[207, 212-218]. As such, ^{18}F-labeling *via* Silicon-based Fluoride Acceptors in combination with the *SiFA-tailored Method* proved to be a simple, fast, and highly efficient alternative to conventional radiofluorination strategies.

3.3.3 Characterization and *in vitro* Evaluation of ^{nat}Lu-rhFolate Ligands

Development of an *in vitro* Binding Assay for FR-targeting Ligands

Determination of binding affinity to the respective target structure represents a key parameter in the preclinical evaluation of a radiotracer candidate. For FR-targeting ligands, the most common literature method consists in a competitive binding assay on KB cells with [^{3}H]folic acid as a reference[210-211, 213-217]. The cell line used in this context represents a HeLa subclone (human cervical carcinoma) and has become the gold standard for *in vitro* studies because of its rapid growth, ease of cultivation, and high FR expression rate[235, 272]. Due to the inaccessibility of ^{3}H-labeled compounds at the *Chair of Pharmaceutical Radiochemistry*, it was necessary to develop a novel binding assay using a ^{125}I-labeled reference. For the latter, pteroyl-L-Glu(3-iodo-L-Tyr-OH)-OH (**XXIV**), previously characterized by *Reber et al.*, was identified as a suitable structure[229]. Radiosynthesis of the corresponding ^{125}I-labeled counterpart **XXVI** was carried out by the *Iodo-Gen® Method* with pteroyl-L-Glu(L-Tyr-OH)-OH (**XXIII**) as starting compound (*Scheme 8*)[229, 232].

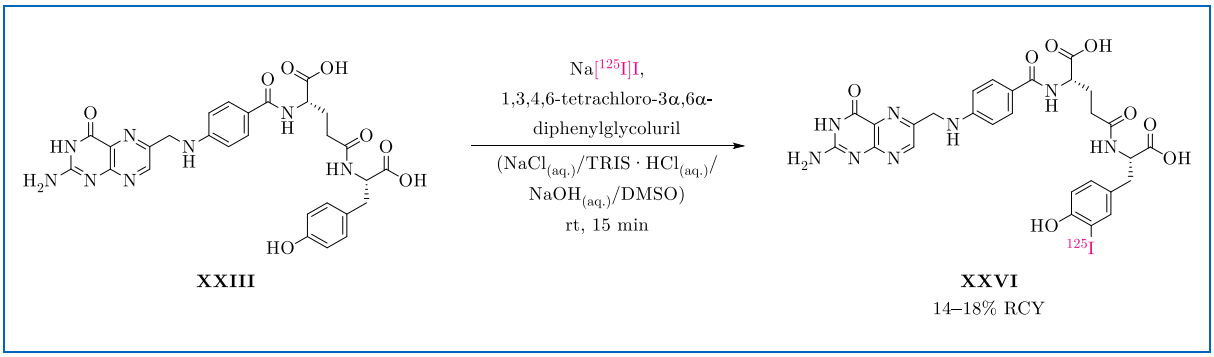

Scheme 8. Radiosynthesis of pteroyl-L-Glu(3-[^{125}I]iodo-L-Tyr-OH)-OH (**XXVI**) as reference compound.

After purification *via* radio-RP-HPLC, the radioiodinated FR reference ligand **XXVI** was afforded in acceptable RCYs of 14–18% and further diluted with an aq. NaAsc solution as radioprotective agent. Since efficient separation of the precursor **XXIII** was ensured during purification, A_ms were assumed to correspond to the maximum possible (74 TBq/mmol) of purchased Na[^{125}I]I. Repeated radio-RP-HPLC analysis of the radioiodinated reference ligand solution confirmed high stability (>98% RCP) up to 14 days after preparation (*Figure 49*). The reference ligand identity was additionally verified *via* co-injection with the cold compound **XXIV**.

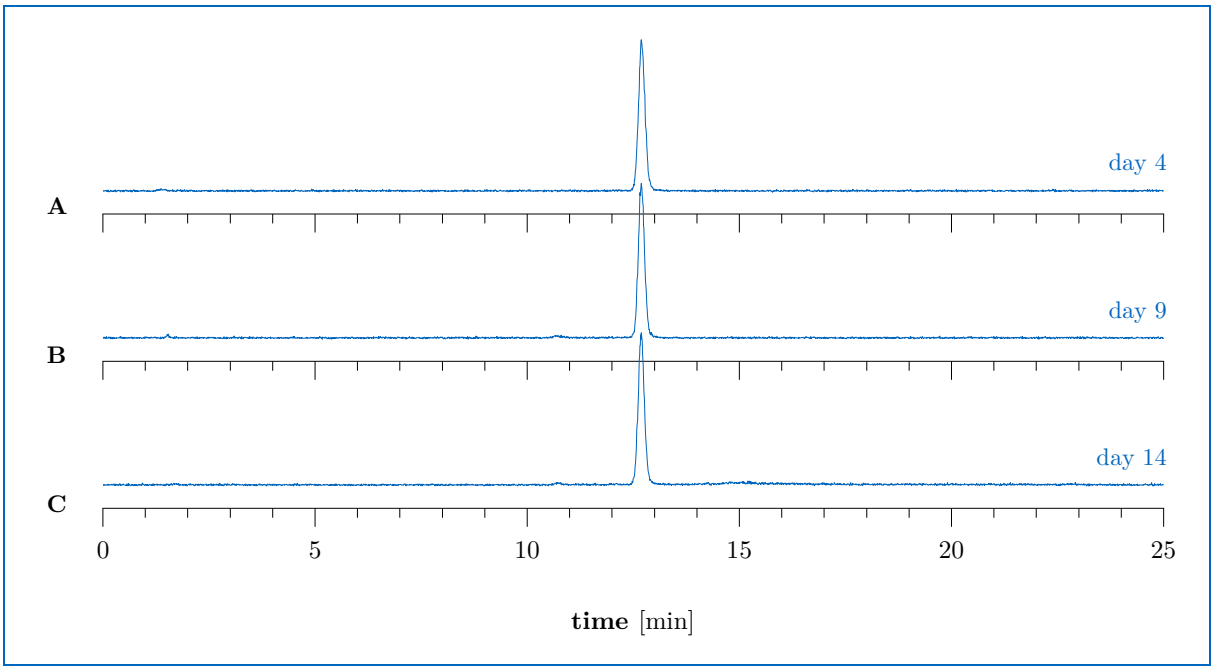

Figure 49. Radio-RP-HPLC chromatograms (column II, 10→40% B in A for 20 min, 95% B in A for 5 min, t_R = 12.7 min) showing the quality control of pteroyl-L-Glu(3-[^{125}I]iodo-L-Tyr-OH)-OH (**XXVI**) performed at **A**) day 4, **B**) day 9, and **C**) day 14 after preparation.

As a starting point for the development of the novel binding assay, some conditions were taken from the literature[273]. Since the FR is known to internalize ligands *via* receptor-mediated endocytosis upon binding, the assay was performed on ice in order to suppress this temperature-dependent process[188]. Furthermore, folate-deficient FFRPMI was used as assay buffer to preserve cell vitality during the incubation period. Preliminary binding studies were performed on KB cells, varying the number of cells (100˙000, 200˙000, 300˙000, and 400˙000), the concentration of radioligand **XXVI** (20 pM, 80 pM, 100 pM, and 120 pM), and the incubation time (2 h, 3 h, and 4 h). Adequate binding was observed when the maximum cell number (400˙000)

was incubated for 4 h with a radioligand concentration of 100 pM. These optimized conditions were finally adopted for the *in vitro* binding assay. To ensure comparability between the affinities obtained with the established assay and the results reported in the literature, determined IC_{50} values were always referred to the measured one for folic acid in the respective assay. In this context, a relative binding of >1 indicates higher affinity to the FR in comparison to folic acid, while values of <1 imply weaker binding. The IC_{50} value for folic acid in the newly developed assay was found to be 2.8 ± 0.4 nM (*Figure 50*).

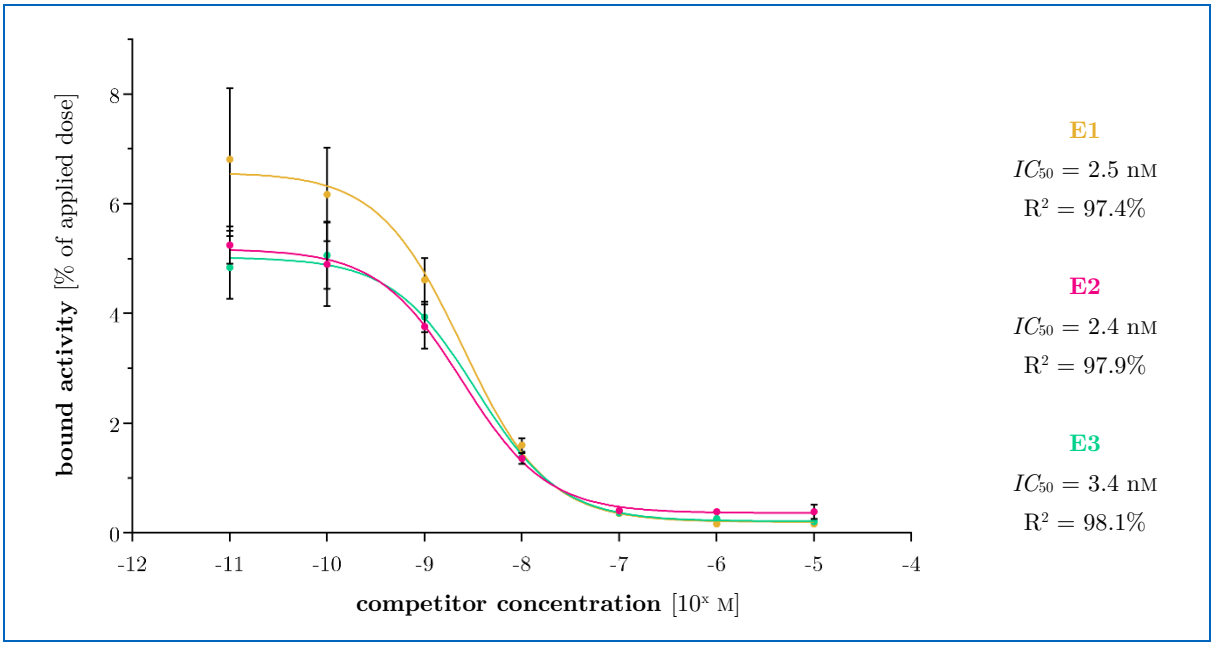

Figure 50. Competitive binding curves and IC_{50} values determined for folic acid ($n = 3$) with the established *in vitro* binding assay on KB cells using **XXVI** as radioiodinated reference compound.

Determination of log$D_{7.4}$, IC_{50}, and HSA Binding for ^{nat}Lu-rhFolate Ligands

Characterization and *in vitro* analysis of newly developed [$^{18/19}$F]^{nat}Lu-rhFolate-**01** to **-05** included determination of lipophilicity (log$D_{7.4}$), assessment of FR-binding affinity (IC_{50}), and evaluation of HSA binding. The results and respective data obtained for folic acid are summarized below along with the published parameters for the most promising FR ligand [$^{18/19}$F]AzaFol (*Table 20*)[217].

Table 20. Characterization and *in vitro* evaluation of [$^{18/19}$F]^{nat}Lu-rhFolate-**01** to -**05** in comparison with folic acid and [$^{18/19}$F]AzaFol (data derived from the literature)[217]. Investigated parameters include lipophilicity represented by log$D_{7.4}$ (data expressed as mean ± SD, $n = 5$), IC_{50} (data expressed as mean nM ± SD with **XXVI** as reference, $n = 3$), relative binding to folic acid (data expressed as ratio of the IC_{50} values measured in the respective experiments), and HSA binding (data expressed as % compared to standard reference compounds).

FR ligand	**structural differences** (X = linkage to amine, Y = PKM)	**lipophilicity** (log$D_{7.4}$)	***IC*$_{50}$** [nM]	**relative binding** (to folic acid)	**HSA binding** [%]
[$^{18/19}$F]^{nat}Lu-rhFolate-**01**	X = CO, Y = 8-Aoc	–2.11 ± 0.01	13.3 ± 2.0	0.21	92.8
[$^{18/19}$F]^{nat}Lu-rhFolate-**02**	X = CO, Y = AEEAc	–2.86 ± 0.01	20.5 ± 1.7	0.13	88.8
[$^{18/19}$F]^{nat}Lu-rhFolate-**03**	X = CO, Y = D-Glu(β-Ala)	–3.14 ± 0.02	10.2 ± 1.8	0.27	95.1
[$^{18/19}$F]^{nat}Lu-rhFolate-**04**	X = CO, Y = D-Glu(D-Asp)	–3.58 ± 0.03	13.5 ± 2.1	0.20	98.5
[$^{18/19}$F]^{nat}Lu-rhFolate-**05**	X = $COCH_2N(CH_3)_2^+CH_2$, Y = AEEAc	–2.82 ± 0.03	33.1 ± 0.7	0.08	64.7
folic acid	-	-	2.8 ± 0.4	1.00	61.7
[$^{18/19}$F]AzaFol	-	–4.2 ± 0.1	-	0.79	-

In terms of lipophilicity, the determined log$D_{7.4}$ values for novel [^{18}F]^{nat}Lu-rhFolate ligands were found to correlate with the respective structural composition of the PKM. Thereby, [^{18}F]^{nat}Lu-rhFolate-**01** comprising the aliphatic 8-Aoc linker was identified as the most lipophilic ligand (log$D_{7.4}$ = –2.11 ± 0.01). By applying AEEAc as PKM in [^{18}F]^{nat}Lu-rhFolate-**02** and -**05**, compounds with slightly higher hydrophilicity were obtained (log$D_{7.4}$ = –2.86 ± 0.01 and –2.82 ± 0.03). Interestingly, both ligands exhibited very similar log$D_{7.4}$ values, although [^{18}F]^{nat}Lu-rhFolate-**05** features an additional positive charge in close proximity to the Silicon-based Fluoride Acceptor. [^{18}F]^{nat}Lu-rhFolate-**03** and -**04** with peptidic PKMs revealed to be the most hydrophilic among the newly developed FR ligands. Depending on the number of negatively charged carboxylate functionalities included in the linker structure, log$D_{7.4}$ values of –3.14 ± 0.02 and –3.58 ± 0.03 were respectively determined. When finally compared to

[^{18}F]AzaFol ($\log D_{7.4} = -4.2 \pm 0.1$), all of the novel [^{18}F]^{nat}Lu-rhFolate ligands appeared to be moderately to substantially more lipophilic.

As for the binding affinity, IC_{50} values of ^{nat}Lu-rhFolate ligands were all found to be in the nanomolar range. In this context, ^{nat}Lu-rhFolate-**01**, -**03**, and -**04** showed similarly high affinity to the FR ($IC_{50} = 13.3 \pm 2.0$ nM, 10.2 ± 1.8 nM, and 13.5 ± 2.1 nM), whereas the AEEAc-bearing ligands ^{nat}Lu-rhFolate-**02** and -**05** displayed somewhat weaker binding affinity ($IC_{50} = 20.5 \pm 1.7$ nM and 33.1 ± 0.7 nM). The newly developed ligands, however, revealed to possess inferior binding properties when directly compared with folic acid (4- to 12-fold lower IC_{50}) or AzaFol (3- to 9-fold lower IC_{50}).

With respect to HSA binding, marked differences were observed among novel ^{nat}Lu-rhFolate ligands. The FR-targeting compounds with peptidic linker structures, ^{nat}Lu-rhFolate-**03** and -**04**, showed the highest binding to HSA with 95.1% and 98.5%, respectively. Slightly lower values were measured for ^{nat}Lu-rhFolate-**01** with aliphatic 8-Aoc (92.8%) and ^{nat}Lu-rhFolate-**02** with AEEAc (88.8%) as PKM. Compared to the latter ligand, ^{nat}Lu-rhFolate-**05** – which shares the same AEEAc linker but contains an additional positive charge adjacent to the Silicon-based Fluoride Acceptor – revealed considerably reduced HSA binding (64.7%). Interestingly, this value was similar to that of folic acid (61.7%).

A graphical comparison of the parameters described above for [$^{18/19}$F]^{nat}Lu-rhFolate ligands, folic acid, and [$^{18/19}$F]AzaFol is provided below (*Figure 51*).

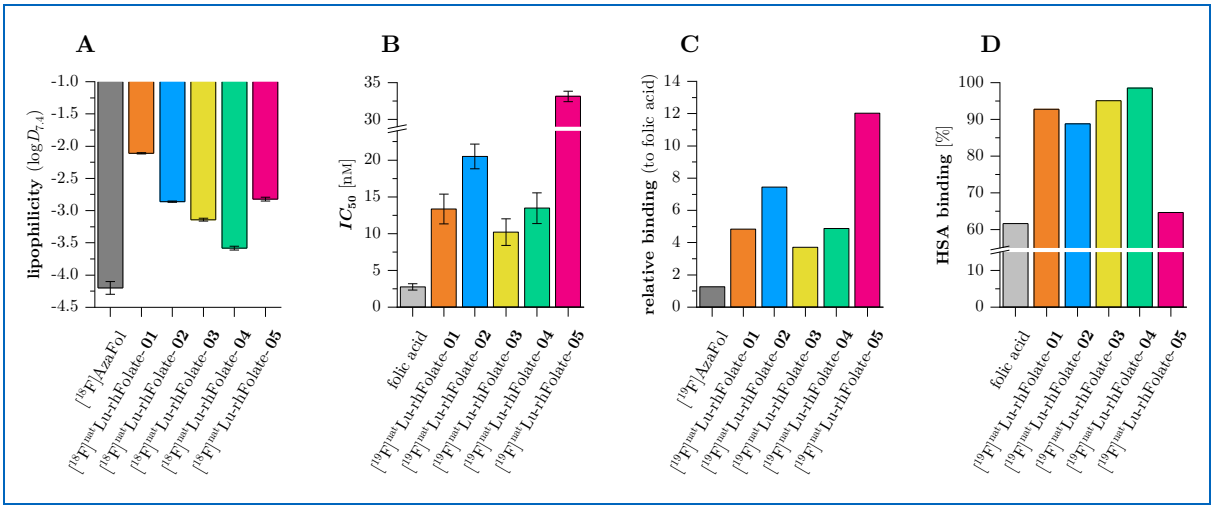

Figure 51. Graphical comparison of previously introduced data for [$^{18/19}$F]^{nat}Lu-rhFolate-**01** to -**05**, folic acid, and [$^{18/19}$F]AzaFol (data derived from the literature), including **A**) lipophilicity represented by log$D_{7.4}$ (data expressed as mean ± SD, $n = 5$), **B**) IC_{50} (data expressed as mean nM ± SD with **XXVI** as reference, $n = 3$), **C**) relative binding to folic acid (data expressed as ratio of the IC_{50} values measured in the respective experiments), and **D**) HSA binding (data expressed as % compared to standard reference compounds)[217].

Depending on the PKM's composition, log$D_{7.4}$ values of novel [^{18}F]^{nat}Lu-rhFolate ligands were found to cover a range between –3.58 and –2.11. In particular, the introduction of negatively charged carboxylate functionalities into the linker structure proved to be a useful strategy to obtain FR ligands with higher hydrophilicity. On the contrary, insertion of a positive charge close to the Silicon-based Fluoride Acceptor turned out to be ineffective in decreasing the radiotracer's lipophilicity. As previously noted by *Kettenbach et al.*, this parameter plays a key role in FR-targeting ligands and needs to be carefully adjusted to achieve ideal pharmacokinetic distribution *in vivo*[212]. In light of the previously conducted lipophilicity optimization work on siPSMA ligands, log$D_{7.4}$ values within –3.3 ± 0.2 were considered as favorable. As such, [^{18}F]^{nat}Lu-rhFolate-**01** (log$D_{7.4}$ = –2.11 ± 0.01) revealed to be excessively lipophilic, while [^{18}F]^{nat}Lu-rhFolate-**03** (log$D_{7.4}$ = –3.14 ± 0.02) emerged as an ideal candidate.

The *pendant approach* pursued to generate ^{18}F-labeled FR ligands comprising Silicon-based Fluoride Acceptors demonstrated to be highly suitable, as all developed ^{nat}Lu-rhFolate ligands evidenced strong binding affinity (IC_{50} = 10.2–33.1 nM). Although the relative binding to folic acid was considerably weaker (0.08–0.27) when compared to minimally altered structures like AzaFol (0.79), ^{nat}Lu-rhFolate-**01** to -**05** showed affinity performances similar to those observed

for other ligands based on the *pendant approach*. In this respect, the newly developed compounds were comparable or even better than the aforementioned click-folate (0.06), NOTA(AlF)-PEG_{12}-folate (0.14), DBCO-folate (0.17), NOTA(AlF)-folate (0.24), OEG-folate (0.29), and Ala-folate (0.30)[210-212, 214-215].

As noted by *Wurzer et al.*, the *radiohybrid* unit consisting of the Silicon-based Fluoride Acceptor in combination with a chelate displays strong binding to HSA[76, 168]. This observation is well reflected in ^{nat}Lu-rhFolate-**01** to -**04**, all of which evidenced pronounced HSA binding (88.8–98.5%). Within these ligands, there is a tendency for additional carboxylate groups within the PKM to contribute to enhanced HSA binding. Accordingly, ^{nat}Lu-rhFolate-**04** (two carboxylate groups) showed the strongest binding to HSA, followed by ^{nat}Lu-rhFolate-**03** (one carboxylate group) and ^{nat}Lu-rhFolate-**01** and -**02** without additional negatively charged functionalities in the linker unit. This result is in agreement with the described binding capacity of HSA, which holds a particular preference for anionic lipophilic building blocks[252, 274]. Interestingly, ^{nat}Lu-rhFolate-**05** stood out from the other FR ligands and revealed significantly lower HSA binding. A direct comparison with ^{nat}Lu-rhFolate-**02**, featuring the same AEEAc linker, indicated that this effect could be attributed to the additional positive charge in close proximity to the Silicon-based Fluoride Acceptor. This structural difference resulted to be sufficient to almost compensate for the HSA-binding contribution of the *radiohybrid* moiety, since ^{nat}Lu-rhFolate-**05** and folic acid were found to exhibit comparable values. The same effect in an attenuated form was also described previously for siPSMA-**0b** (*Section 3.2.1*).

3.3.4 *In vivo* Evaluation of ^{nat}Lu-rhFolate Ligands

Biodistribution Studies with ^{nat}Lu-rhFolate Ligands

Apart from [^{18}F]^{nat}Lu-rhFolate-**01**, which was deemed as excessively lipophilic, all other newly developed FR ligands were considered for subsequent evaluation in animal experiments. The *in vivo* behavior of novel [^{18}F]^{nat}Lu-rhFolate-**02** to -**05** was first investigated in biodistribution studies with KB tumor-bearing CD1-Foxn1^{nu} nude mice at 1 h p.i. (*Table 21*).

Table 21. Biodistribution of [^{18}F]^{nat}Lu-rhFolate-**02** (n = 3), -**03** (n = 3), -**04** (n = 4), and -**05** (n = 3) in comparison with [^{18}F]AzaFol (n = 4, data derived from the literature) at 1 h p.i. in KB tumor-bearing CD1-Foxn1^{nu} nude mice[217]. The competition study for [^{18}F]^{nat}Lu-rhFolate-**02** (n = 3) was conducted under prior injection of folic acid (100 µg). Results are presented as mean %ID/g ± SD.

organ	[^{18}F]AzaFol [%ID/g]	[^{18}F]^{nat}Lu-rhFolate-**02** [%ID/g]	[^{18}F]^{nat}Lu-rhFolate-**02** competition [%ID/g]	[^{18}F]^{nat}Lu-rhFolate-**03** [%ID/g]	[^{18}F]^{nat}Lu-rhFolate-**04** [%ID/g]	[^{18}F]^{nat}Lu-rhFolate-**05** [%ID/g]
blood	0.55 ± 0.07	1.82 ± 0.05	6.05 ± 0.94	0.56 ± 0.07	0.33 ± 0.06	0.20 ± 0.05
heart	1.89 ± 0.28	2.34 ± 0.22	1.84 ± 0.18	2.57 ± 0.32	1.55 ± 0.07	1.44 ± 0.11
lung	1.52 ± 0.21	1.36 ± 0.35	2.50 ± 0.35	1.34 ± 0.22	0.82 ± 0.12	0.85 ± 0.13
liver	10.59 ± 0.89	1.84 ± 0.30	1.60 ± 0.21	1.79 ± 0.38	1.16 ± 0.20	0.89 ± 0.15
spleen	1.85 ± 0.14	0.44 ± 0.03	0.83 ± 0.15	0.33 ± 0.09	0.19 ± 0.02	0.14 ± 0.01
pancreas	-	1.85 ± 0.42	1.02 ± 0.12	1.95 ± 0.47	1.37 ± 0.08	1.44 ± 0.26
stomach	2.83 ± 0.86	1.67 ± 0.14	1.15 ± 0.09	2.14 ± 0.17	1.18 ± 0.21	1.28 ± 0.07
intestine	1.90 ± 0.21	1.54 ± 0.07	1.99 ± 0.17	1.13 ± 0.15	0.67 ± 0.07	0.79 ± 0.10
kidney	53.60 ± 3.23	60.29 ± 6.87	6.42 ± 1.27	72.75 ± 10.16	37.61 ± 4.23	50.14 ± 4.80
adrenal g.	-	1.59 ± 0.60	1.27 ± 0.54	1.10 ± 0.31	0.81 ± 0.16	0.81 ± 0.34
muscle	1.24 ± 0.18	0.98 ± 0.20	0.56 ± 0.07	1.05 ± 0.32	0.70 ± 0.07	0.60 ± 0.04
bone	1.57 ± 0.25	1.36 ± 0.15	1.15 ± 0.14	1.37 ± 0.11	0.69 ± 0.11	1.11 ± 0.06
tumor	11.86 ± 1.73	8.00 ± 2.85	2.68 ± 0.81	6.85 ± 0.98	2.96 ± 0.65	2.84 ± 0.82
salivary g.	14.95 ± 6.09	4.74 ± 0.23	1.07 ± 0.27	4.42 ± 0.93	3.60 ± 0.92	2.00 ± 0.37

Particular differences were found with respect to the *in vivo* distribution profile of newly developed FR-targeting ligands. While [^{18}F]^{nat}Lu-rhFolate-**02** displayed rather slow clearance from the blood pool after 1 h (1.82 ± 0.05 %ID/g), considerably lower activity retention was observed for [^{18}F]^{nat}Lu-rhFolate-**03** (0.56 ± 0.07 %ID/g), -**04** (0.33 ± 0.06 %ID/g), and -**05** (0.20 ± 0.05 %ID/g). Uptake of investigated [^{18}F]^{nat}Lu-rhFolate ligands in various non-target tissues such as heart, lung, liver, spleen, adrenal gland, muscle, bone, as well as organs of the digestive system, turned out to be quite similar and did not exceed 2.57 %ID/g. Notably, accumulation of [^{18}F]AzaFol in any of these tissues resulted to be in a comparable range, except for liver (10.59 ± 0.89 %ID/g) and spleen (1.85 ± 0.14 %ID/g), which appeared to be substantially higher. As for the retention of the novel radiotracers in FR-positive tissue, distinct patterns were identified. While [^{18}F]^{nat}Lu-rhFolate-**04** and -**05** showed only minor KB tumor uptake (2.96 ± 0.65 %ID/g and 2.84 ± 0.82 %ID/g), appreciably higher accumulation was found for [^{18}F]^{nat}Lu-rhFolate-**02** (8.00 ± 2.85 %ID/g) and -**03** (6.85 ± 0.98 %ID/g). The same

trend for these two groups of radiotracers held true for the activity retention in the kidney and salivary gland. In direct comparison with the investigated [^{18}F]^{nat}Lu-rhFolate ligands, the literature lead compound [^{18}F]AzaFol evidenced superior tumor uptake (11.86 ± 1.73 %ID/g), comparable renal accumulation, and significantly (3- to 7-fold) higher retention in the salivary gland.

Binding specificity of the newly developed ligands was exemplarily demonstrated for [^{18}F]^{nat}Lu-rhFolate-**02** by performing a competition study under prior administration of folic acid. As expected, the resulting biodistribution profile revealed high blood pool activity and considerably reduced accumulation in FR-specific organs. In detail, when compared with the biodistribution of [^{18}F]^{nat}Lu-rhFolate-**02**, radiotracer uptake in the competition study was substantially lower in the kidney (6.42 ± 1.27 %ID/g *vs.* 60.29 ± 6.87 %ID/g) and salivary gland (1.07 ± 0.27 %ID/g *vs.* 4.74 ± 0.23 %ID/g). Moreover, the KB tumor showed a marked decrease in radiotracer retention (2.68 ± 0.81 %ID/g *vs.* 8.00 ± 2.85 %ID/g) to levels similar to those observed in non-target organs such as heart, lung, and intestine.

A graphical comparison of the biodistribution results for [^{18}F]^{nat}Lu-rhFolate-**02** to -**05** and [^{18}F]AzaFol is provided below (*Figure 52*).

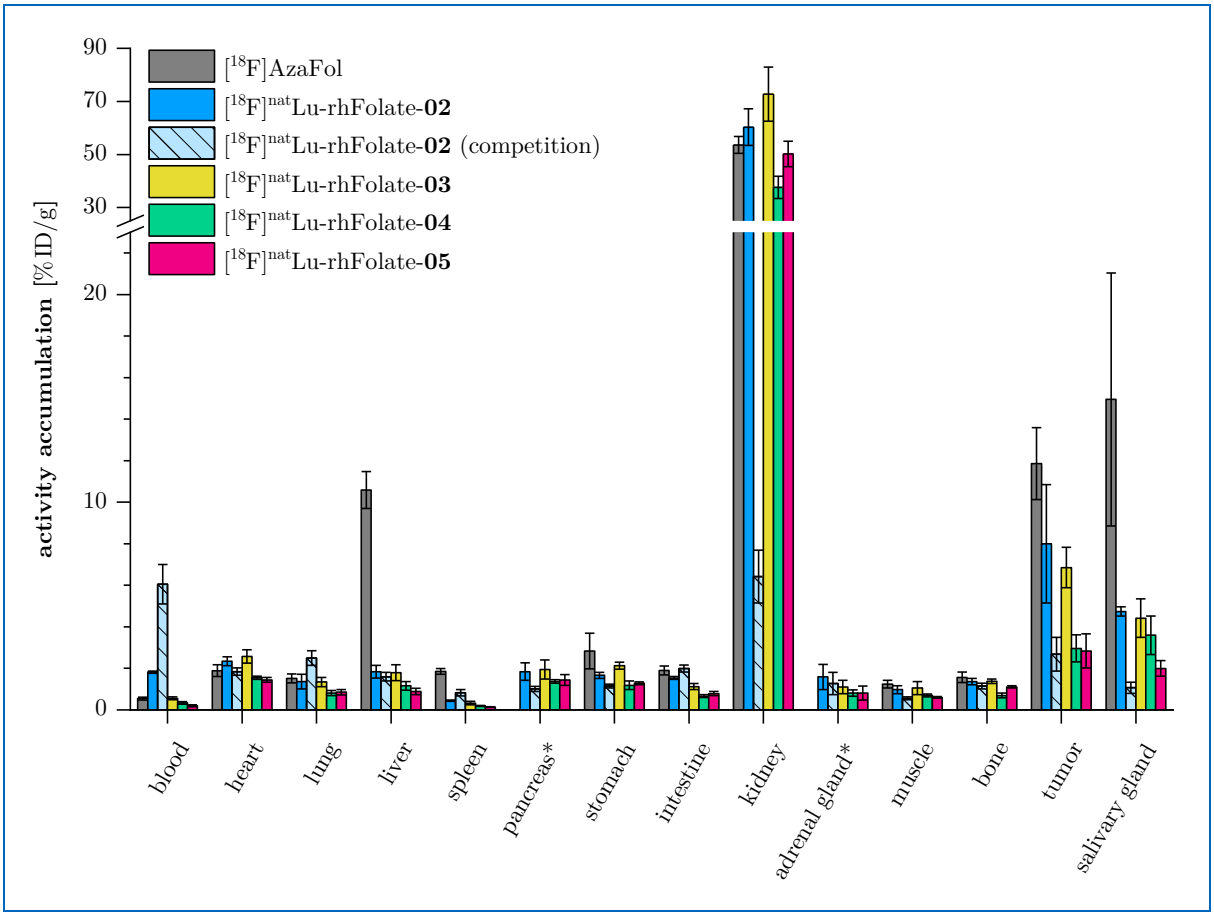

Figure 52. Graphical presentation of the biodistribution data for [^{18}F]^{nat}Lu-rhFolate-**02** (n = 3), -**03** (n = 3), -**04** (n = 4), and -**05** (n = 3) in comparison with [^{18}F]AzaFol (n = 4, *organs not determined, data derived from the literature) at 1 h p.i. in KB tumor-bearing CD1-Foxn1^{nu} nude mice[217]. The competition study for [^{18}F]^{nat}Lu-rhFolate-**02** (n = 3) was conducted under prior injection of folic acid (100 µg). Results are presented as mean %ID/g ± SD.

As a result of the biodistribution studies, the structural composition of the PKM within novel [^{18}F]^{nat}Lu-rhFolate ligands revealed to exert a considerable impact on the radiotracer's *in vivo* performance. Both ligands with aliphatic PKM, [^{18}F]^{nat}Lu-rhFolate-**02** (X = CO, Y = AEEAc) and [^{18}F]^{nat}Lu-rhFolate-**05** (X = $COCH_2N(CH_3)_2{}^+CH_2$, Y = AEEAc), showed contrasting distribution profiles. While the former compound exhibited high tumor uptake (8.00 ± 2.85 %ID/g) but slow elimination kinetics, [^{18}F]^{nat}Lu-rhFolate-**05** displayed faster clearance from the blood pool (0.20 ± 0.05 %ID/g) yet also reduced accumulation in target tissue. Since [^{18}F]^{nat}Lu-rhFolate-**02** and -**05** demonstrated nearly identical lipophilicity ($\log D_{7.4}$ = –2.86 ± 0.01 and –2.82 ± 0.03) as well as binding affinities in the same order of magnitude, the discrepancy in pharmacokinetics was attributed to the pronounced difference in HSA

binding (88.8% *vs.* 64.7%). The ligands with peptidic PKM, [^{18}F]^{nat}Lu-rhFolate-**03** (X = CO, Y = D-Glu(β-Ala)) and -**04** (X = CO, Y = D-Glu(D-Asp)), revealed a distribution profile between both aforementioned compounds. Notably, the peptidic nature of respective PKMs further enhanced HSA binding (95.1% and 98.5%) but favored excretion from the blood (0.56 ± 0.07 %ID/g and 0.33 ± 0.06 %ID/g) as a result of the corresponding increase in ligand hydrophilicity (log$D_{7.4}$ = –3.14 ± 0.02 and –3.58 ± 0.03). However, the accelerated radiotracer clearance came at the expense of tumor retention, which was slightly diminished for [^{18}F]^{nat}Lu-rhFolate-**03** (6.85 ± 0.98 %ID/g) and significantly reduced for [^{18}F]^{nat}Lu-rhFolate-**04** (2.96 ± 0.65 %ID/g). In direct comparison with [^{18}F]AzaFol, the investigated [^{18}F]^{nat}Lu-rhFolate ligands showed lower tumor accumulation, but in return stood out for low unspecific uptake. Hence, activity levels in non-target organs were comparable or even lower than for [^{18}F]AzaFol, as evidenced by the considerably decreased retention in spleen (4- to 13-fold) and liver (6- to 12-fold). The latter result is particularly interesting since several of the previously published ^{18}F-labeled FR ligands struggled with elevated hepatic radiotracer uptake[209, 211-214, 216, 218]. As a measure for defluorination, the activity accumulation of [^{18}F]^{nat}Lu-rhFolate ligands in bone (≤1.37 %ID/g) was similar or inferior when compared to [^{18}F]AzaFol, thus again confirming the *in vivo* stability of incorporated fluorine-18 within the Silicon-based Fluoride Acceptor moiety. To further evaluate the performance of the FR ligands, tumor-to-organ ratios were calculated and summarized below (*Table 22*).

Table 22. Calculated tumor-to-organ ratios at 1 h p.i. for [^{18}F]^{nat}Lu-rhFolate-**02** to -**05** in comparison with [^{18}F]AzaFol (data derived from the literature)[217]. Results are presented as mean ± SD.

ratio	[^{18}F]AzaFol	[^{18}F]^{nat}Lu-rhFolate-**02**	[^{18}F]^{nat}Lu-rhFolate-**03**	[^{18}F]^{nat}Lu-rhFolate-**04**	[^{18}F]^{nat}Lu-rhFolate-**05**
tumor-to-blood	21.58 ± 2.33	4.40 ± 1.56	12.29 ± 0.91	9.39 ± 3.40	14.02 ± 1.67
tumor-to-liver	1.13 ± 0.18	4.31 ± 1.47	3.88 ± 0.27	2.59 ± 0.54	3.14 ± 0.56
tumor-to-kidney	0.22 ± 0.02	0.13 ± 0.04	0.09 ± 0.01	0.08 ± 0.02	0.06 ± 0.02
tumor-to-muscle	-	9.04 ± 4.28	7.13 ± 2.12	4.26 ± 0.94	4.74 ± 1.48

Marked differences were found among the investigated [^{18}F]^{nat}Lu-rhFolate ligands with regard to the tumor-to-organ ratios. In line with the lower absolute tumor uptake observed for [^{18}F]^{nat}Lu-rhFolate-**04** and -**05**, the tumor-to-liver, tumor-to-kidney, and tumor-to-muscle ratios

lagged behind the respective values for [^{18}F]^{nat}Lu-rhFolate-**02** and -**03**. The latter ligands exhibited excellent tumor-to-liver ratios (4.31 ± 1.47 and 3.88 ± 0.27), well exceeding that of [^{18}F]AzaFol by a factor of 3 to 4. This characteristic proves to be particularly advantageous since FR-positive lesions near the liver might be detected with high contrast. Unfortunately, the relatively slow elimination kinetics of [^{18}F]^{nat}Lu-rhFolate-**02** resulted in a poor tumor-to-blood ratio (4.40 ± 1.56), compromising the overall *in vivo* performance. In this light, [^{18}F]^{nat}Lu-rhFolate-**03** emerged as the best candidate among the newly developed FR ligands, exhibiting good absolute tumor accumulation along with high contrast relative to the blood pool (12.29 ± 0.91).

µPET/CT Imaging Studies with ^{nat}Lu-rhFolate Ligands

Further *in vivo* investigations of [^{18}F]^{nat}Lu-rhFolate-**02** to -**05** included µPET/CT imaging studies with KB tumor-bearing CD1-Foxn1^{nu} nude mice acquired at 1 h p.i. (*Figure 53*).

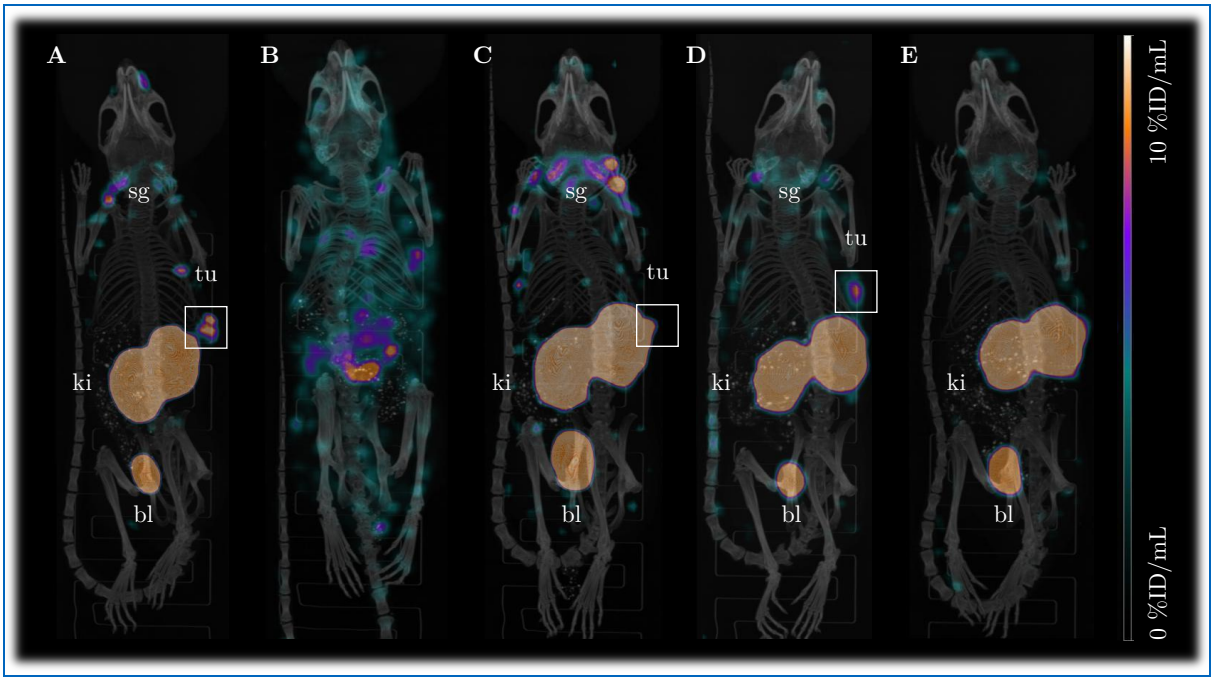

Figure 53. µPET/CT scans (maximum intensity projection) acquired at 1 h p.i. in KB tumor-bearing CD1-Foxn1^{nu} nude mice administered with **A**) [^{18}F]^{nat}Lu-rhFolate-**02**, **B**) [^{18}F]^{nat}Lu-rhFolate-**02** under prior injection of folic acid (100 µg) for competition, **C**) [^{18}F]^{nat}Lu-rhFolate-**03**, **D**) [^{18}F]^{nat}Lu-rhFolate-**04**, and **E**) [^{18}F]^{nat}Lu-rhFolate-**05**. Notable activity accumulation in salivary gland (sg), kidney (ki), bladder (bl), and KB tumor (tu, white box) is additionally indicated.

As expected from the biodistribution studies, highest activity accumulation for [^{18}F]^{nat}Lu-rhFolate-**02** (*Figure 53A*), -**03** (*Figure 53C*), and -**04** (*Figure 53D*) was detected in FR-positive tissue, including salivary gland, kidney, and KB tumor. In this context, visualization of tumor uptake for [^{18}F]^{nat}Lu-rhFolate-**03** was unfortunately compromised by the overlap with the accumulated activity in the right kidney. Based on the radiotracer level in KB tumor tissue, [^{18}F]^{nat}Lu-rhFolate-**02** and -**03** appeared to exhibit the highest uptake, which is consistent with the previously reported biodistribution results. Specificity of tumor retention was exemplarily confirmed in a competition study involving a KB tumor-bearing CD1-Foxn1^{nu} nude mouse that received an excess of folic acid before administration of [^{18}F]^{nat}Lu-rhFolate-**02**. The resulting µPET/CT image acquired at 1 h p.i. (*Figure 53B*) revealed significantly diminished accumulation in FR-positive tissues, including salivary gland, KB tumor, and kidney, whereas increased activity uptake was observed in the intestinal tract. In contrast to the favorable tissue distribution profiles of [^{18}F]^{nat}Lu-rhFolate-**02** and -**03**, no tumor retention and negligible uptake in the salivary gland were found for the mouse injected with [^{18}F]^{nat}Lu-rhFolate-**05** (*Figure 53E*). All of the FR ligands investigated *via* µPET/CT scans displayed predominant renal excretion, as evidenced by the elevated kidney and bladder accumulation as well as by the apparent lack of hepatic uptake. Indeed, this property represents a considerable advantage over numerous radiofluorinated FR ligands described in the literature, suffering from pronounced unspecific accumulation in the abdominal region due to hepatobiliary elimination[210-213, 275-276].

Metabolite Analysis of ^{nat}Lu-rhFolate-03

The most promising among the developed FR ligands, [^{18}F]^{nat}Lu-rhFolate-**03**, was subjected to additional *in vivo* metabolite analysis, in which a healthy CB17-SCID female mouse was administered with the radiotracer and sacrificed at 40 min p.i. Radioactivity was extracted from the urine, blood, liver, and kidney. Both organ and blood extracts were subsequently purified using a Strata-X® cartridge. Recoveries for sample extraction, purification, as well as for the overall preparation are summarized below (*Table 23*).

Table 23. Recovery of [^{18}F]^{nat}Lu-rhFolate-**03** from urine, blood, liver, and kidney. The percentage of recovered radioactivity (decay corrected) was calculated for both sample extraction and purification, as well as for the overall process.

sample	**recovery** [% of radioactivity]		
	extraction	**purification**	**overall**
urine	97	-	97
blood	90	93	84
liver	70	98	68
kidney	78	93	73

Recovery of radioactivity from the urine sample by ultracentrifugation turned out to be a simple and highly efficient (97%) method. A slightly decreased recovery was measured for activity extraction from the blood sample (90%), while extraction from liver and kidney by the ball mill occurred with lower but still acceptable efficiencies of 70% and 78%, respectively. Purification of extracts *via* Strata-X® cartridge demonstrated to be the method of choice, as only a marginal loss of radioactivity (2–7%) was observed. Thus, overall activity recoveries from the blood, liver, and kidney resulted to be in a good range (68–84%). Processed samples of both organs and body fluids were finally investigated for radiometabolites by radio-RP-HPLC (*Figure 54*).

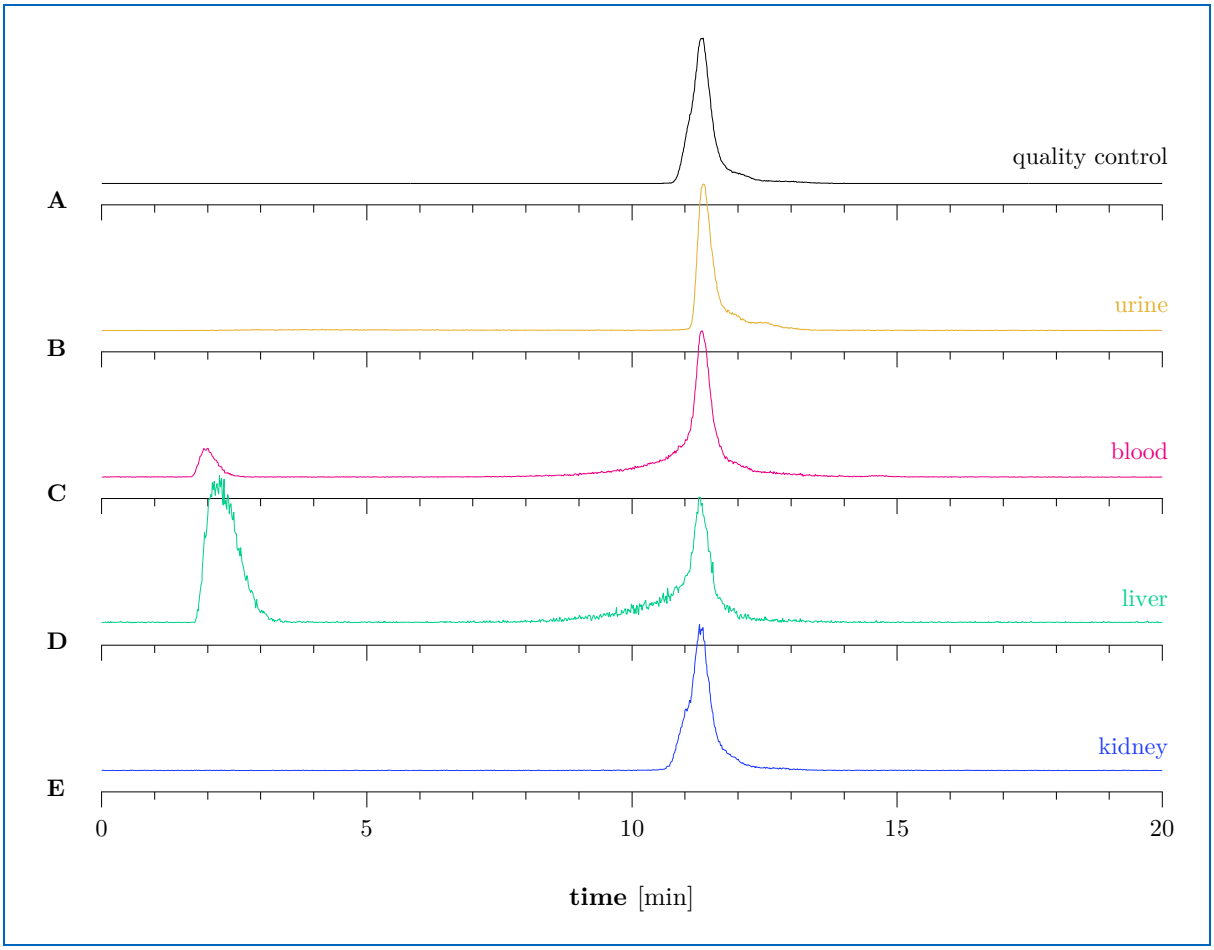

Figure 54. Metabolite analysis of [^{18}F]^{nat}Lu-rhFolate-**03** with extracts of body fluids and homogenized organs from a healthy CB17-SCID mouse sacrificed at 40 min p.i. Radio-RP-HPLC chromatograms (column II, 10→70% B in A for 15 min, 95% B in A for 5 min, t_R = 11.3 min) show the **A**) quality control of the parent radiotracer before injection and extracts from the **B**) urine, **C**) blood, **D**) liver, and **E**) kidney.

When compared to the quality control run of [^{18}F]^{nat}Lu-rhFolate-**03** (*Figure 54A*), radio-RP-HPLC chromatograms of urine (*Figure 54B*) and kidney (*Figure 54E*) extracts showed the same intact radiotracer profile. In contrast, analysis of blood (*Figure 54C*) and liver (*Figure 54D*) samples revealed the additional presence of a highly hydrophilic radiometabolite (t_R = 2.1 min), which accounted respectively for 11% and 53% of the detected radioactivity. Since degradation appeared to be most pronounced in the liver extract, it could be assumed that metabolization of [^{18}F]^{nat}Lu-rhFolate-**03** occurred during first-pass elimination, followed by release of the radiometabolite into the blood circulation. As for the identity of the radiometabolite, its structural composition remained unclear. Although the retention time would be consistent with dissociated [^{18}F]fluoride, neither the biodistribution nor the µPET/CT imaging study of [^{18}F]^{nat}Lu-rhFolate-**03** indicated enhanced bone uptake to support this assumption.

Moreover, *in vivo* stability of the Silicon-based Fluoride Acceptor moiety had previously been confirmed in an analogous metabolite analysis with the *radiohybrid* [^{18}F]^{nat}Ga-rhPSMA-7 isomers[168]. It is worth mentioning that the formation of a hydrophilic radiometabolite was also reported for ^{18}F-labeled FR ligands based on the *integrated approach*, including 2'-[^{18}F]fluoro-folic acid and [^{18}F]AzaFol[216-217]. Consequently, metabolic degradation could be related to the use of folic acid as a binding motif. Apart from these speculations, additional studies would be required to shed light on the identity of the observed radiometabolite.

Despite the outcome of the metabolite analysis, [^{18}F]^{nat}Lu-rhFolate-**03** proved to be a highly promising FR-targeting ligand. In addition to the favorable *in vitro* properties and *in vivo* tissue distribution profile, this novel FR ligand stood out for its efficient radiosynthesis, which would greatly facilitate the translation into a potential clinical application.

4 Summary and Conclusion

Over the past decades, extensive research efforts in the field of ^{18}F-radiochemistry have been undertaken to overcome the limitations hindering the widespread use of radiofluorinated PET tracers in clinical routine. In this context, the novel radiofluorination approach relying on Silicon-based Fluoride Acceptors has set new standards in terms of labeling efficiency, simplicity, and scalability. Due to its outstanding potential, this ^{18}F-labeling technique was further investigated in the present doctoral thesis and applied for the development of novel PSMA- and FR-targeting radiopharmaceuticals.

As a first objective of this work, the particular efficiency of the ^{18}F-for-^{19}F isotopic exchange reaction in Silicon-based Fluoride Acceptors was elucidated by determining the respective *Arrhenius parameters*. For this purpose, model compound **VI** was reacted with [^{18}F]fluoride prepared according to the state-of-the-art procedure, including on-cartridge drying by the *Munich Method* and partial neutralization through the addition of oxalic acid. Kinetic measurements of the [^{18}F]fluoride incorporation rate at defined temperatures were finally used to create an *Arrhenius plot*. The resulting activation energy of 46.7 ± 5.7 kJ/mol, which turned out to be significantly lower in comparison to the values for radiofluorination by conventional substitution reactions, was identified as the driver for the superior labeling efficiency.

Aiming to overcome various drawbacks related to the *Munich* approach, a novel [^{18}F]fluoride preparation technique named *SiFA-tailored Method* was developed. The procedure was based on the observation that a solution (1.27 M, 500 µL, 634 µmol) of NH_4HCOO in DMSO efficiently elutes (88 ± 2%, $n = 75$) trapped [^{18}F]fluoride from a strong anion exchanger after on-cartridge drying. The resulting eluate demonstrated to be immediately applicable for subsequent radiofluorination by isotopic exchange reaction of Silicon-based Fluoride Acceptor-bearing compounds. In detail, the mild elution cocktail composition eliminates the need for an additional neutralization step, avoids the use of toxic components such as Kryptofix® 222, and is compatible with both base-sensitive precursors and elevated reaction temperatures to enhance labeling efficiency. The newly developed [^{18}F]fluoride preparation method thus holds the

potential to further expand the application range of ^{18}F-labeling *via* Silicon-based Fluoride Acceptors.

To address the lipophilicity constraint of radiopharmaceuticals comprising Silicon-based Fluoride Acceptors, this doctoral thesis focused on the introduction of a PKM. Its structural composition was conceived of permuted amino acids, with the further goal of fine-tuning the tracer's pharmacokinetic profile to achieve favorable imaging contrast.

The outlined strategy was first exemplified with the development of novel radiofluorinated PSMA inhibitors, termed siPSMA ligands. Respective labeling precursors were generated *via* SPPS in high purity (≥95%) and overall yields of 7–59%. Manual preparation of the ^{18}F-labeled compounds on laboratory scale was accomplished within 25 min and included radiofluorination under different conditions as well as SPE-based radiotracer purification. High RCYs (50 ± 15%, $n = 46$) were achieved when precursors (30 nmol) were labeled for 5 min at rt with partially neutralized *Munich*-dried [^{18}F]fluoride. In case where elevated A_ms were desired (37 ± 12 GBq/µmol, $n = 36$), radiofluorination was conducted under heating (65–70°C) of low precursor amounts (0.5 nmol) for 5–8 min using [^{18}F]fluoride prepared by the *SiFA-tailored Method*. Structural variation of the modifier composition – including peptide-based PKMs (siPSMA-**01** to -**10**), urea-based PKMs (siPSMA-**11** to -**21a**), optimized urea-based PKMs (siPSMA-**21b** and -**22**), and PKMs as part of a pseudo-dimeric structure (siPSMA-**23** and -**24**) – led to a plethora of new inhibitors covering a log$D_{7.4}$ range between –4.04 and –2.30. Among these, siPSMA ligands with defined lipophilicity (log$D_{7.4}$ = –3.3 ± 0.2) were particularly preferred since the associated pharmacokinetic profile was expected to favor visualization of locoregional prostatic tumor lesions without interferences caused by premature radiotracer excretion. With regard to further evaluated ligand properties, siPSMA-**01** to -**24** evidenced pronounced HSA binding (≥95.7%) as well as PSMA-binding affinities in the nanomolar range (5.5–29.4 nM). Appreciable internalization rates after 1 h (up to 312% of **XXV**) were found for certain candidates, which significantly outperformed the respective values (up to 161% of **XXV**) of established reference ligands. Due to their advantageous characteristics, [^{18}F]siPSMA-**08**, -**11**, -**14** , -**21a**, -**23**, and -**24** were subsequently investigated in biodistribution

studies at 1 h p.i. Thereby, [^{18}F]siPSMA-**14** stood out for its favorable *in vivo* distribution pattern, including remarkably high uptake in LNCaP tumor tissue (14.30 ± 5.11 %ID/g) and low background accumulation. In light of these results, which exceeded the biodistribution performance of the references [^{18}F]DCFPyL and [^{18}F]PSMA-1007, [^{18}F]siPSMA-**14** was considered for first-in-human applications. For this purpose, large-scale production of the novel candidate was set up in analogy to the established automated synthesis protocol for [^{18}F]^{nat}Ga-rhPSMA-7/7.3. Based on 48 exemplary radiosyntheses starting with 25 ± 4 GBq of [^{18}F]fluoride and 150 nmol of precursor, [^{18}F]siPSMA-**14** was afforded with excellent RCYs (52 ± 16%) and good A_ms (87 ± 27 GBq/µmol) within only 16 min. In first patient applications, the new ligand demonstrated to be safe and highly effective for staging and restaging of prostate cancer. Most notably, [^{18}F]siPSMA-**14** provided excellent visualization of lesions in the prostate bed even without prior administration of furosemide. This favorable characteristic was ascribed to the optimized pharmacokinetic profile of the novel inhibitor, proving that the chosen strategy of introducing a PKM represents an excellent tool for tracer modulation.

As a second example, novel Silicon-based Fluoride Acceptor-bearing FR ligands were designed according to the *radiohybrid* concept and feature – in addition to the chelate for lipophilicity compensation – a PKM of aliphatic or peptidic nature to fine-tune the radiotracer's pharmacokinetic profile. The generally challenging precursor synthesis was approached by stepwise SPPS with the key building block 1-(2-*N*-Teoc-pteroyl)imidazole (**XII**), affording ^{nat}Lu-rhFolate-**01** to -**05** in high purity (≥94%) and acceptable yields (3–10%). Manual laboratory-scale radiofluorination of these compounds (30 nmol) was preferably conducted under heating (10 min, 95°C) using [^{18}F]fluoride prepared by the *SiFA-tailored Method*. Upon final radiotracer purification *via* SPE, [^{18}F]^{nat}Lu-rhFolate-**01** to -**05** were obtained with excellent RCYs (57 ± 8%, $n = 8$) in about 30 min, which significantly outperformed the radiofluorination results of various FR ligands reported in the literature. Permutation of the PKM within the newly developed compounds had a major impact on the tracer characteristics and *in vitro* properties. Depending on its specific composition, log$D_{7.4}$ values of [^{18}F]^{nat}Lu-rhFolate-**01** to -**05** were found to vary between –3.58 and –2.11. Given the previously accumulated experience in lipophilicity adjustment of siPSMA ligands, [^{18}F]^{nat}Lu-rhFolate-**03** (log$D_{7.4}$ = –3.14 ± 0.02) was predicted

to exhibit the most favorable pharmacokinetic profile among the novel ligands. Moreover, the integrated modifier was shown to either preserve or attenuate the pronounced HSA-binding property of the *radiohybrid* building block. Determination of FR-binding affinity was carried out by a newly established assay using KB cells and pteroyl-L-Glu(3-[^{125}I]iodo-L-Tyr-OH)-OH (**XXVI**) as radioiodinated reference. The obtained IC_{50} values for ^{nat}Lu-rhFolate-**01** to **-05** were all in the nanomolar range (10.2–33.1 nM) and consistent with the affinities of published radiotracers that had also been generated by the *pendant approach*. Subsequent investigation of the novel ligands in biodistribution and µPET/CT imaging studies at 1 h p.i. confirmed [^{18}F]^{nat}Lu-rhFolate-**03** as the lead candidate. Indeed, the FR ligand demonstrated a convenient *in vivo* profile characterized by high contrast relative to the blood pool, predominant renal excretion, and good KB tumor accumulation (6.85 ± 0.98 %ID/g). Furthermore, considerably lower unspecific uptake was observed in liver and spleen when compared to the reference ligand [^{18}F]AzaFol. Despite the identified metabolic instability in blood and liver samples, [^{18}F]^{nat}Lu-rhFolate-**03** proved to be a promising candidate worthy of further consideration due to its favorable preclinical properties and advantageous radiosynthesis.

To conclude, the Silicon-based Fluoride Acceptor technology has the potential to represent a game-changer in ^{18}F-radiochemistry. The strategies discussed in the present work to overcome the lipophilicity issue, to adjust the pharmacokinetic profile, and to optimize the radiofluorination of respective radiotracers will certainly contribute to the further diffusion of this labeling method (*Figure 55*).

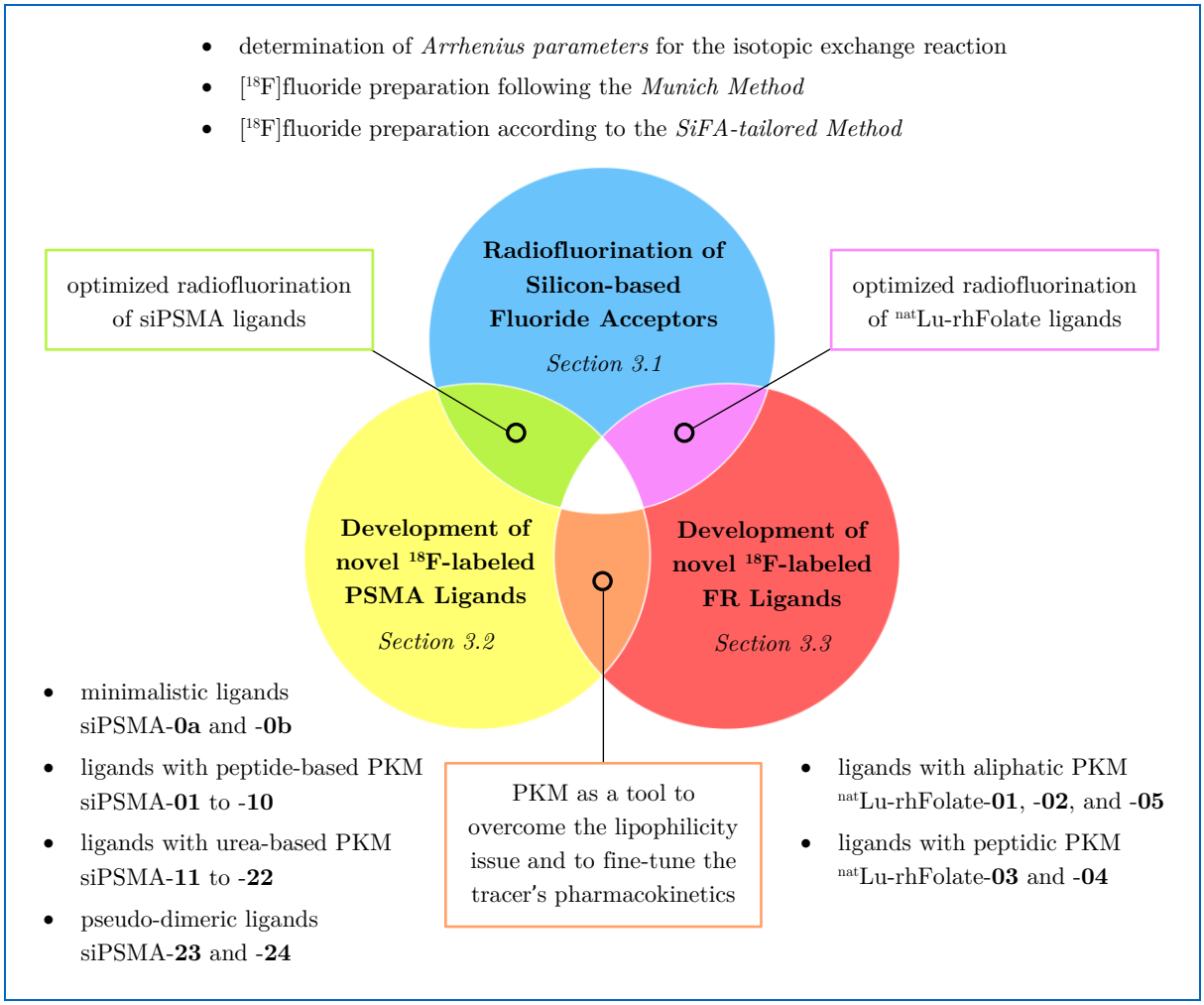

Figure 55. Research topics and investigations covered in the present doctoral thesis for the development of novel ^{18}F-labeled radiopharmaceuticals comprising Silicon-based Fluoride Acceptors.

5 References

[1] Bejot R., Gouverneur V., 18F-Radionuclide Chemistry. In *Fluorine in Pharmaceutical and Medicinal Chemistry: From Biophysical Aspects to Clinial Applications*, Gouverneur V., Müller K., Vol. 6, 1 ed., Imperial College Press, London, **2012**, 335-382.

[2] Edem P. E., Steen E. J. L., Kjær A., Herth M. M., Fluorine-18 Radiolabeling Strategies - Advantages and Disadvantages of Currently Applied Labeling Methods. In *Late-Stage Fluorination of Bioactive Molecules and Biologically-Relevant Substrates*, Postigo A., 1 ed., Elsevier Science & Technology, Amsterdam, **2018**, 30-88.

[3] Schirrmacher R., Wängler C., Schirrmacher E., Pharmaceutical Radiochemistry (I) - Fluorine-18 Radiochemistry: Theory and Practice. In *Munich Molecular Imaging Handbook Series*, Wester H.-J., Vol. 1, Scintomics Print Media & Publishing, Fürstenfeldbruck, **2010**, 5-73.

[4] Mason N. S., Mathis C. A., Radiohalogens for PET Imaging. In *Positron emission tomography*, Bailey D. L., Maisey M. N., Townsend D. W., Valk P. E., Vol. 2, Springer London Ltd, London, **2005**, 203-219.

[5] Roeda D., Dollé F., Recent Developments in the Chemistry of [18F]Fluoride for PET. In *The chemistry of molecular imaging*, Long N., Wong W.-T., 1 ed., John Wiley & Sons Inc., Hoboken, New Jersey, **2014**, 55-77.

[6] Satpati D., Recent breakthrough in 68Ga-radiopharmaceuticals cold kits for convenient PET radiopharmacy. *Bioconjug Chem* **2021**, *32* (3), 430-447.

[7] Luurtsema G., Boersma H. H., Schepers M., De Vries A. M. T., Maas B., Zijlma R., De Vries E. F. J., Elsinga P. H., Improved GMP-compliant multi-dose production and quality control of 6-[18F]fluoro-L-DOPA. *EJNMMI Radiopharm Chem* **2017**, *1* (1), 1-10.

[8] Vaulina D., Nasirzadeh M., Gomzina N., Automated radiosynthesis and purification of [18F]flumazenil with solid phase extraction. *Appl Radiat Isot* **2018**, *135*, 110-114.

[9] Cottrell T. L., *The strengths of chemical bonds*. 2 ed., Butterworths Scientific, London, **1958**, 4.41-4.50.

[10] Entzian W., Aronow S., Soloway A. H., Sweet W. H., A preliminary evaluation of F18-labeled tetrafluoroborate as a scanning agent for intracranial tumors. *J Nucl Med* **1964**, *5* (7), 542-550.

[11] Ting R., Adam M. J., Ruth T. J., Perrin D. M., Arylfluoroborates and alkylfluorosilicates as potential PET imaging agents: high-yielding aqueous biomolecular 18F-labeling. *J Am Chem Soc* **2005**, *127* (38), 13094-13095.

[12] Ting R., Harwig C. W., Lo J., Li Y., Adam M. J., Ruth T. J., Perrin D. M., Substituent effects on aryltrifluoroborate solvolysis in water: implications for Suzuki−Miyaura coupling and the design of stable 18F-labeled aryltrifluoroborates for use in PET imaging. *J Org Chem* **2008**, *73* (12), 4662-4670.

[13] auf dem Keller U., Bellac C. L., Li Y., Lou Y., Lange P. F., Ting R., Harwig C., Kappelhoff R., Dedhar S., Adam M. J., Novel matrix metalloproteinase inhibitor [18F]marimastat-aryltrifluoroborate as a probe for in vivo positron emission tomography imaging in cancer. *Cancer Res* **2010**, *70* (19), 7562-7569.

[14] Li Y., Liu Z., Harwig C. W., Pourghiasian M., Lau J., Lin K.-S., Schaffer P., Benard F., Perrin D. M., 18F-click labeling of a bombesin antagonist with an alkyne-18F-ArBF3-: in vivo PET imaging of tumors expressing the GRP-receptor. *Am J Nucl Med Mol Imaging* **2013**, *3* (1), 57.

[15] Li Y., Guo J., Tang S., Lang L., Chen X., Perrin D. M., One-step and one-pot-two-step radiosynthesis of cyclo-RGD-18F-aryltrifluoroborate conjugates for functional imaging. *Am J Nucl Med Mol Imaging* **2013**, *3* (1), 44.

[16] Li Y., Liu Z., Lozada J., Wong M. Q., Lin K.-S., Yapp D., Perrin D. M., Single step 18F-labeling of dimeric cycloRGD for functional PET imaging of tumors in mice. *Nucl Med Biol* **2013**, *40* (8), 959-966.

[17] Li Z., Chansaenpak K., Liu S., Wade C. R., Conti P. S., Gabbaï F. P., Harvesting 18F-fluoride ions in water via direct 18F–19F isotopic exchange: radiofluorination of zwitterionic aryltrifluoroborates and in vivo stability studies. *MedChemComm* **2012**, *3* (10), 1305-1308.

[18] Liu Z., Li Y., Lozada J., Wong M. Q., Greene J., Lin K.-S., Yapp D., Perrin D. M., Kit-like 18F-labeling of RGD-19F-arytrifluroborate in high yield and at extraordinarily high specific activity with preliminary in vivo tumor imaging. *Nucl Med Biol* **2013**, *40* (6), 841-849.

[19] Liu Z., Hundal-Jabal N., Wong M., Yapp D., Lin K.-S., Benard F., Perrin D., A new 18F-heteroaryltrifluoroborate radio-prosthetic with greatly enhanced stability that is labelled by 18F–19F-isotope exchange in good yield at high specific activity. *MedChemComm* **2014**, *5* (2), 171-179.

[20] Liu Z., Pourghiasian M., Radtke M. A., Lau J., Pan J., Dias G. M., Yapp D., Lin K. S., Bénard F., Perrin D. M., An organotrifluoroborate for broadly applicable one-step 18F-labeling. *Angew Chem* **2014**, *126* (44), 12070-12074.

[21] Liu Z., Pourghiasian M., Bénard F., Pan J., Lin K.-S., Perrin D. M., Preclinical evaluation of a high-affinity 18F-trifluoroborate octreotate derivative for somatostatin receptor imaging. *J Nucl Med* **2014**, *55* (9), 1499-1505.

[22] Liu Z., Lin K.-S., Bénard F., Pourghiasian M., Kiesewetter D. O., Perrin D. M., Chen X., One-step 18F labeling of biomolecules using organotrifluoroborates. *Nat Protoc* **2015**, *10* (9), 1423-1432.

[23] Kuo H.-T., Pan J., Zhang C., Rousseau J., Lau J., Benard F., Lin K.-S., A novel AmBF3-succinimide prosthetic group for facile 18F-labeling of biomolecules. *J Nucl Med* **2016**, *57* (Suppl 2), 1092.

[24] Lau J., Pan J., Rousseau E., Uribe C. F., Seelam S. R., Sutherland B. W., Perrin D. M., Lin K.-S., Bénard F., Pharmacokinetics, radiation dosimetry, acute toxicity and automated synthesis of [18F]AmBF3-TATE. *EJNMMI Res* **2020**, *10* (1), 1-10.

[25] Chausse G., Benard F., Harsini S., Pan J., Saprunoff H., Uribe C., Allan H., Perrin D., Lin K.-S., Wilson D., First-in-Human Clinical trial of [18F]AMBF3-TATE for PET imaging of neuroendocrine tumors. *J Nucl Med* **2022**, *63* (Suppl 2), 2270.

[26] McBride W. J., Sharkey R. M., Karacay H., D'Souza C. A., Rossi E. A., Laverman P., Chang C.-H., Boerman O. C., Goldenberg D. M., A novel method of 18F radiolabeling for PET. *J Nucl Med* **2009**, *50* (6), 991-998.

[27] Laverman P., McBride W. J., Sharkey R. M., Eek A., Joosten L., Oyen W. J. G., Goldenberg D. M., Boerman O. C., A novel facile method of labeling octreotide with 18F-fluorine. *J Nucl Med* **2010**, *51* (3), 454-461.

[28] Laverman P., D'Souza C. A., Eek A., McBride W. J., Sharkey R. M., Oyen W. J. G., Goldenberg D. M., Boerman O. C., Optimized labeling of NOTA-conjugated octreotide with F-18. *Tumour Biol* **2012**, *33* (2), 427-434.

[29] McBride W. J., D'Souza C. A., Sharkey R. M., Karacay H., Rossi E. A., Chang C.-H., Goldenberg D. M., Improved 18F labeling of peptides with a fluoride-aluminum-chelate complex. *Bioconjug Chem* **2010**, *21* (7), 1331-1340.

[30] Shetty D., Choi S. Y., Jeong J. M., Lee J. Y., Hoigebazar L., Lee Y.-S., Lee D. S., Chung J.-K., Lee M. C., Chung Y. K., Stable aluminium fluoride chelates with triazacyclononane derivatives proved by X-ray crystallography and 18F-labeling study. *Chem Commun* **2011**, *47* (34), 9732-9734.

[31] D'Souza C. A., McBride W. J., Sharkey R. M., Todaro L. J., Goldenberg D. M., High-yielding aqueous 18F-labeling of peptides via Al18F chelation. *Bioconjug Chem* **2011**, *22* (9), 1793-1803.

[32] McBride W. J., D'Souza C. A., Karacay H., Sharkey R. M., Goldenberg D. M., New lyophilized kit for rapid radiofluorination of peptides. *Bioconjug Chem* **2012**, *23* (3), 538-547.

[33] Tshibangu T., Cawthorne C., Serdons K., Pauwels E., Gsell W., Bormans G., Deroose C. M., Cleeren F., Automated GMP compliant production of [18F]AlF-NOTA-octreotide. *EJNMMI Radiopharm Chem* **2020**, *5* (1), 1-23.

[34] Cleeren F., Lecina J., Billaud E. M. F., Ahamed M., Verbruggen A., Bormans G. M., New chelators for low temperature Al18F-labeling of biomolecules. *Bioconjug Chem* **2016**, *27* (3), 790-798.

[35] Cleeren F., Lecina J., Ahamed M., Raes G., Devoogdt N., Caveliers V., McQuade P., Rubins D. J., Li W., Verbruggen A., Al18F-labeling of heat-sensitive biomolecules for positron emission tomography imaging. *Theranostics* **2017**, *7* (11), 2924.

[36] Russelli L., Martinelli J., De Rose F., Reder S., Herz M., Schwaiger M., Weber W., Tei L., D'Alessandria C., Room Temperature Al18F Labeling of 2-Aminomethylpiperidine-Based Chelators for PET Imaging. *ChemMedChem* **2020**, *15* (3), 284-292.

[37] Hausner S. H., Bauer N., Sutcliffe J. L., In vitro and in vivo evaluation of the effects of aluminum [18F]fluoride radiolabeling on an integrin αvβ6-specific peptide. *Nucl Med Biol* **2014**, *41* (1), 43-50.

[38] Liang S., Ma Y., Guo J., Guo R., Wang H., 18F-radiolabeled analogs of peptide RGD-A7R for simultaneous PET imaging of both αvβ3 and VEGF in tumors. *J Radioanal Nucl Chem* **2015**, *303* (3), 1891-1896.

[39] Poschenrieder A., Osl T., Schottelius M., Hoffmann F., Wirtz M., Schwaiger M., Wester H.-J., First 18F-labeled pentixafor-based imaging agent for PET imaging of CXCR4 expression in vivo. *Tomography* **2016**, *2* (2), 85-93.

[40] Boschi S., Lee J. T., Beykan S., Slavik R., Wei L., Spick C., Eberlein U., Buck A. K., Lodi F., Cicoria G., Synthesis and preclinical evaluation of an Al18F radiofluorinated Glu-urea-Lys(Ahx)-HBED-CC PSMA ligand. *Eur J Nucl Med Mol Imaging* **2016**, *43* (12), 2122-2130.

[41] Wan W., Guo N., Pan D., Yu C., Weng Y., Luo S., Ding H., Xu Y., Wang L., Lang L., First experience of 18F-alfatide in lung cancer patients using a new lyophilized kit for rapid radiofluorination. *J Nucl Med* **2013**, *54* (5), 691-698.

[42] Liu T., Liu C., Xu X., Liu F., Guo X., Li N., Wang X., Yang J., Yang X., Zhu H., Preclinical evaluation and pilot clinical study of Al18F-PSMA-BCH for prostate cancer PET imaging. *J Nucl Med* **2019**, *60* (9), 1284-1292.

[43] Giesel F. L., Adeberg S., Syed M., Lindner T., Jiménez-Franco L. D., Mavriopoulou E., Staudinger F., Tonndorf-Martini E., Regnery S., Rieken S., FAPI-74 PET/CT using either 18F-AlF or cold-kit 68Ga labeling: biodistribution, radiation dosimetry, and tumor delineation in lung cancer patients. *J Nucl Med* **2021**, *62* (2), 201-207.

[44] Pauwels E., Cleeren F., Tshibangu T., Koole M., Serdons K., Dekervel J., Van Cutsem E., Verslype C., Van Laere K., Bormans G., [18F]AlF-NOTA-octreotide PET imaging: biodistribution, dosimetry and first comparison with [68Ga]Ga-DOTATATE in neuroendocrine tumour patients. *Eur J Nucl Med Mol Imaging* **2020**, *47* (13), 3033-3046.

[45] Gower-Fry L., Kronemann T., Dorian A., Pu Y., Jaworski C., Wängler C., Bartenstein P., Beyer L., Lindner S., Jurkschat K., Recent Advances in the Clinical Translation of Silicon Fluoride Acceptor (SiFA) 18F-Radiopharmaceuticals. *Pharmaceuticals* **2021**, *14* (7), 701.

[46] Schirrmacher R., Bradtmöller G., Schirrmacher E., Thews O., Tillmanns J., Siessmeier T., Buchholz H. G., Bartenstein P., Wängler B., Niemeyer C. M., 18F-labeling of peptides by means of an organosilicon-based fluoride acceptor. *Angew Chem Int Ed* **2006**, *45* (36), 6047-6050.

[47] Gens T. A., Wethongton J. A., Brosi A. R., The Exchange of F18 between Metallic Fluorides and Silicon Tetrafluoride. *J Phys Chem* **1958**, *62* (12), 1593.

[48] Rosenthal M. S., Bosch A. L., Nickles R. J., Gatley S. J., Synthesis and some characteristics of no-carrier added [18F]fluorotrimethylsilane. *Int J Appl Radiat Isot* **1985**, *36* (4), 318-319.

[49] Hutchins L. G., Bosch A. L., Rosenthal M. S., Nickles R. J., Gatley S. J., Synthesis of [18F]2-deoxy-2-fluoro-D-glucose from highly reactive [18F]tetraethylammonium fluoride prepared by hydrolysis of [18F]fluorotrimethylsilane. *Int J Appl Radiat Isot* **1985**, *36* (5), 375-378.

[50] Choudhry U., Martin K. E., Biagini S., Blower P. J., Alkoxysilane groups for instant labelling of biomolecules with 18F. *Nucl Med Commun* **2006**, *27* (3), 293.

[51] Choudhry U., Paul R., Blower P. J., Biagini S. C. G., Rapid reaction of alkoxysilanes with [F-18]-Fluoride as a basis for biomolecule labelling for PET. *Eur J Nucl Med Mol Imaging* **2007**, *34* (Suppl), S332.

[52] Höhne A., Mu L., Honer M., Schubiger P. A., Ametamey S. M., Graham K., Stellfeld T., Borkowski S., Berndorff D., Klar U., Synthesis, 18F-labeling, and in vitro and in vivo studies of bombesin peptides modified with silicon-based building blocks. *Bioconjug Chem* **2008**, *19* (9), 1871-1879.

[53] Mu L., Höhne A., Schubiger P. A., Ametamey S. M., Graham K., Cyr J. E., Dinkelborg L., Stellfeld T., Srinivasan A., Voigtmann U., Silicon-based building blocks for one-step 18F-radiolabeling of peptides for PET imaging. *Angew Chem Int Ed* **2008**, *47* (26), 4922-4925.

[54] Schirrmacher E., Wängler B., Cypryk M., Bradtmöller G., Schäfer M., Eisenhut M., Jurkschat K., Schirrmacher R., Synthesis of p-(di-tert-butyl[18F]fluorosilyl)benzaldehyde ([18F]SiFA-A) with high specific activity by isotopic exchange: a convenient labeling synthon for the 18F-labeling of N-amino-oxy derivatized peptides. *Bioconjug Chem* **2007**, *18* (6), 2085-2089.

[55] Wängler C., Kostikov A., Zhu J., Chin J., Wängler B., Schirrmacher R., Silicon-[18F]fluorine radiochemistry: basics, applications and challenges. *Appl Sci* **2012**, *2* (2), 277-302.

[56] Höhne A., Yu L., Mu L., Reiher M., Voigtmann U., Klar U., Graham K., Schubiger P. A., Ametamey S. M., Organofluorosilanes as model compounds for 18F-labeled silicon-based PET tracers and their hydrolytic stability: Experimental data and theoretical calculations (PET = positron emission tomography). *Chem Eur J* **2009**, *15* (15), 3736-3743.

[57] Bohn P., Deyine A., Azzouz R., Bailly L., Fiol-Petit C., Bischoff L., Fruit C., Marsais F., Vera P., Design of silicon-based misonidazole analogues and 18F-radiolabelling. *Nucl Med Biol* **2009**, *36* (8), 895-905.

[58] Balentova E., Collet C., Lamandé-Langle S., Chretien F., Thonon D., Aerts J., Lemaire C., Luxen A., Chapleur Y., Synthesis and hydrolytic stability of novel 3-[18F]fluoroethoxybis(1-methylethyl)silyl]propanamine-based prosthetic groups. *J Fluor Chem* **2011**, *132* (4), 250-257.

[59] Joyard Y., Azzouz R., Bischoff L., Papamicaël C., Labar D., Bol A., Bol V., Vera P., Grégoire V., Levacher V., Synthesis of new 18F-radiolabeled silicon-based nitroimidazole compounds. *Biorg Med Chem* **2013**, *21* (13), 3680-3688.

[60] Dialer L. O., Selivanova S. V., Müller C. J., Müller A., Stellfeld T., Graham K., Dinkelborg L. M., Krämer S. D., Schibli R., Reiher M., Studies toward the development of new silicon-containing building blocks for the direct 18F-labeling of peptides. *J Med Chem* **2013**, *56* (19), 7552-7563.

[61] Wängler B., Quandt G., Iovkova L., Schirrmacher E., Wängler C., Boening G., Hacker M., Schmoeckel M., Jurkschat K., Bartenstein P., Kit-like 18F-labeling of proteins: synthesis of 4-(di-tert-butyl[18F]fluorosilyl)benzenethiol (Si[18F]FA-SH) labeled rat serum albumin for blood pool imaging with PET. *Bioconjug Chem* **2009**, *20* (2), 317-321.

[62] Zhu J., Li S., Wängler C., Wängler B., Lennox R. B., Schirrmacher R., Synthesis of 3-chloro-6-((4-(di-tert-butyl[18F]fluorosilyl)-benzyl)oxy)-1,2,4,5-tetrazine ([18F]SiFA-OTz) for rapid tetrazine-based 18F-radiolabeling. *Chem Commun* **2015**, *51* (62), 12415-12418.

[63] Rosa-Neto P., Wängler B., Iovkova L., Boening G., Reader A., Jurkschat K., Schirrmacher E., [18F]SiFA-isothiocyanate: A new highly effective radioactive labeling agent for lysine-containing proteins. *ChemBioChem* **2009**, *10* (8), 1321-1324.

[64] Wängler B., Kostikov A. P., Niedermoser S., Chin J., Orchowski K., Schirrmacher E., Iovkova-Berends L., Jurkschat K., Wängler C., Schirrmacher R., Protein labeling with the labeling precursor [18F]SiFA-SH for positron emission tomography. *Nat Protoc* **2012**, *7* (11), 1964-1969.

[65] Iovkova L., Wängler B., Schirrmacher E., Schirrmacher R., Quandt G., Boening G., Schürmann M., Jurkschat K., para-Functionalized Aryl-di-tert-butylfluorosilanes as Potential Labeling Synthons for 18F Radiopharmaceuticals. *Chemistry (Easton)* **2009**, *15* (9), 2140-2147.

[66] Tietze L. F., Schmuck K., SiFA azide: A new building block for PET imaging using click chemistry. *Synlett* **2011**, *2011* (12), 1697-1700.

[67] Hazari P. P., Schulz J., Vimont D., Chadha N., Allard M., Szlosek-Pinaud M., Fouquet E., Mishra A. K., A new SiF–dipropargyl glycerol scaffold as a versatile prosthetic group to design dimeric radioligands: Synthesis of the [18F]BMPPSiF tracer to image serotonin receptors. *ChemMedChem* **2014**, *9* (2), 337-349.

[68] Glaser M., Iveson P., Hoppmann S., Indrevoll B., Wilson A., Arukwe J., Danikas A., Bhalla R., Hiscock D., Three methods for 18F labeling of the HER2-binding affibody molecule Z(HER2:2891) including preclinical assessment. *J Nucl Med* **2013**, *54* (11), 1981-1988.

[69] Iovkova L., Könning D., Wängler B., Schirrmacher R., Schoof S., Arndt H. D., Jurkschat K., SiFA-Modified Phenylalanine: A Key Compound for the Efficient Synthesis of 18F-Labelled Peptides. *Eur J Inorg Chem* **2011**, *14* (2011), 2238-2246.

[70] Rugeri B., Audi H., Jewula P., Koudih R., Malacea-Kabbara R., Vimont D., Schulz J., Fernandez P., Jugé S., Designing Silylated L-Amino Acids using a Wittig Strategy: Synthesis of Peptide Derivatives and 18F-Labelling. *Eur J Org Chem* **2017**, *2017* (36), 5399-5409.

[71] Wängler C., Waser B., Alke A., Iovkova L., Buchholz H.-G., Niedermoser S., Jurkschat K., Fottner C., Bartenstein P., Schirrmacher R., One-step 18F-labeling of carbohydrate-conjugated octreotate-derivatives containing a silicon-fluoride-acceptor (SiFA): in vitro and in vivo evaluation as tumor imaging agents for positron emission tomography (PET). *Bioconjug Chem* **2010**, *21* (12), 2289-2296.

[72] Lindner S., Michler C., Leidner S., Rensch C., Wängler C., Schirrmacher R., Bartenstein P., Wängler B., Synthesis and in vitro and in vivo evaluation of SiFA-tagged bombesin and RGD peptides as tumor imaging probes for positron emission tomography. *Bioconjug Chem* **2014**, *25* (4), 738-749.

[73] Niedermoser S., Chin J., Wängler C., Kostikov A., Bernard-Gauthier V., Vogler N., Soucy J.-P., McEwan A. J., Schirrmacher R., Wängler B., In vivo evaluation of 18F-SiFAlin–modified TATE: a potential challenge for 68Ga-DOTATATE, the clinical gold standard for somatostatin receptor imaging with PET. *J Nucl Med* **2015**, *56* (7), 1100-1105.

[74] Litau S., Niedermoser S., Vogler N., Roscher M., Schirrmacher R., Fricker G., Wangler B., Wangler C., Next Generation of SiFAlin-Based TATE Derivatives for PET Imaging of SSTR-Positive Tumors: Influence of Molecular Design on In Vitro SSTR Binding and In Vivo Pharmacokinetics. *Bioconjug Chem* **2015**, *26* (12), 2350-2359.

[75] Wiegand A., Wiese V., Glowacki B., Iovkova L., Schirrmacher R., Jurkschat K., Krause N., GlucoSiFA and LactoSiFA: New Types of Carbohydrate-Tagged Silicon-Based Fluoride Acceptors for 18F-Positron Emission Tomography (PET). *Synthesis* **2019**, *51* (5), 1196-1206.

[76] Wurzer A., Di Carlo D., Schmidt A., Beck R., Eiber M., Schwaiger M., Wester H.-J., Radiohybrid Ligands: A Novel Tracer Concept Exemplified by 18F- or 68Ga-Labeled rhPSMA Inhibitors. *J Nucl Med* **2020**, *61* (5), 735-742.

[77] Kostikov A. P., Iovkova L., Chin J., Schirrmacher E., Wängler B., Wängler C., Jurkschat K., Cosa G., Schirrmacher R., N-(4-(di-tert-butyl[18F]fluorosilyl)benzyl)-2-hydroxy-N,N-dimethylethylammonium bromide ([18F]SiFAN+Br−): A novel lead compound for the development of hydrophilic SiFA-based prosthetic groups for 18F-labeling. *J Fluor Chem* **2011**, *132* (1), 27-34.

[78] Iovkova-Berends L., Wängler C., Zöller T., Höfner G., Wanner K. T., Rensch C., Bartenstein P., Kostikov A., Schirrmacher R., Jurkschat K., t-Bu2SiF-derivatized D2-receptor ligands: The first SiFA-containing small molecule radiotracers for target-specific PET-imaging. *Molecules* **2011**, *16* (9), 7458-7479.

[79] Holzleitner N., Günther T., Beck R., Lapa C., Wester H.-J., Introduction of a SiFA moiety into the D-glutamate chain of DOTA-PP-F11N results in radiohybrid-based CCK-2R-targeted compounds with improved pharmacokinetics in vivo. *Pharmaceuticals* **2022**, *15* (12), 1467.

[80] Wängler C., Niedermoser S., Chin J., Orchowski K., Schirrmacher E., Jurkschat K., Iovkova-Berends L., Kostikov A. P., Schirrmacher R., Wängler B., One-step 18F-labeling of peptides for positron emission tomography imaging using the SiFA methodology. *Nat Protoc* **2012**, *7* (11), 1946-1955.

[81] Connolly D., Bailey J. J., Ilhan H., Bartenstein P., Wängler C., Wängler B., Wuest M., Wuest F., Schirrmacher R., 18F-Labeling of Radiotracers Functionalized with a Silicon Fluoride Acceptor (SiFA) for Positron Emission Tomography. *J Vis Exp* **2020**, (155), e60623.

[82] Wurzer A., Di Carlo D., Herz M., Richter A., Robu S., Schirrmacher R., Mascarin A., Weber W., Eiber M., Schwaiger M., Wester H.-J., Automated synthesis of [18F]Ga-rhPSMA-7/-7.3: results, quality control and experience from more than 200 routine productions. *EJNMMI Radiopharm Chem* **2021**, *6* (1), 1-15.

[83] Lindner S., Simmet M., Gildehaus F. J., Jurkschat K., Wängler C., Wängler B., Bartenstein P., Schirrmacher R., Ilhan H., Automated production of [18F]SiTATE on a Scintomics GRP™ platform for PET/CT imaging of neuroendocrine tumors. *Nucl Med Biol* **2020**, *88*, 86-95.

[84] Eiber M., Kroenke M., Wurzer A., Ulbrich L., Jooß L., Maurer T., Horn T., Schiller K., Langbein T., Buschner G., 18F-rhPSMA-7 PET for the detection of biochemical recurrence of prostate cancer after radical prostatectomy. *J Nucl Med* **2020**, *61* (5), 696-701.

[85] Langbein T., Rauscher I., Kroenke M., Wurzer A., Schwamborn K., Worther H., Franz C., Maurer T., Horn T., Wester H.-J., Preliminary data on the diagnostic efficacy of F-18-rhPSMA-7.3 PET imaging for N-staging of Patients with Intermediate and High Risk Prostate Cancer compared to histopathology. *J Nucl Med* **2020**, *61* (Suppl 1), 1267.

[86] Ilhan H., Lindner S., Todica A., Cyran C., Tiling R., Auernhammer C. J., Spitzweg C., Boeck S., Unterrainer M., Gildehaus F. J., Biodistribution and first clinical results of 18F-SiFAlin-TATE PET: A novel 18F-labeled somatostatin analog for imaging of neuroendocrine tumors. *Eur J Nucl Med Mol Imaging* **2020**, *47* (4), 870-880.

[87] Prasad V., Di Carlo D., Miksch J., Fischer G., Zengerling F., Solbach C., Wester H.-J., Beer A. J., Novel F-18-siPSMA-14 shows favourable tracer kinetics for staging and restaging of prostate cancer patients. *Eur J Nucl Med Mol Imaging* **2019**, *46* (Suppl 1), 592-593.

[88] Tolvanen T., Kalliokoski K. K., Malaspina S., Kuisma A., Lahdenpohja S., Postema E. J., Miller M. P., Scheinin M., Safety, biodistribution and radiation dosimetry of 18F-rhPSMA-7.3 in healthy adult volunteers. *J Nucl Med* **2020**, *62* (5), 679-684.

[89] Robert Koch-Institut und die Gesellschaft der epidemiologischen Krebsregister in Deutschland e.V., *Krebs in Deutschland 2017/2018*. 13 ed., Robert Koch-Institut, Berlin, **2021**, 106-109.

[90] Kyle K. Y., Hricak H., Imaging prostate cancer. *Radiol Clin North Am* **2000**, *38* (1), 59-85.

[91] Levran Z., Gonzalez J. A., Diokno A. C., Jafri S. Z. H., Steinert B. W., Are pelvic computed tomography, bone scan and pelvic lymphadenectomy necessary in the staging of prostatic cancer? *Br J Urol* **1995**, *75* (6), 778-781.

[92] Jadvar H., Prostate cancer: PET with 18F-FDG, 18F- or 11C-acetate, and 18F- or 11C-choline. *J Nucl Med* **2011**, *52* (1), 81-89.

[93] Wester H.-J., Schottelius M., PSMA-targeted radiopharmaceuticals for imaging and therapy. *Semin Nucl Med* **2019**, *49* (4), 302-312.

[94] Horoszewicz J., Kawinski E., Murphy G., Monoclonal antibodies to a new antigenic marker in epithelial prostatic cells and serum of prostatic cancer patients. *Anticancer Res* **1987**, *7* (5B), 927-935.

[95] Schülke N., Varlamova O. A., Donovan G. P., Ma D., Gardner J. P., Morrissey D. M., Arrigale R. R., Zhan C., Chodera A. J., Surowitz K. G., The homodimer of prostate-specific membrane antigen is a functional target for cancer therapy. *Proc Natl Acad Sci USA* **2003**, *100* (22), 12590-12595.

[96] Israeli R. S., Powell C. T., Fair W. R., Heston W. D. W., Molecular cloning of a complementary DNA encoding a prostate-specific membrane antigen. *Cancer Res* **1993**, *53* (2), 227-230.

[97] Rawlings N. D., Barrett A. J., Structure of membrane glutamate carboxypeptidase. *BBA-Protein Struct M* **1997**, *1339* (2), 247-252.

[98] Holmes E. H., Greene T. G., Tino W. T., Boynton A. L., Aldape H. C., Misrock S. L., Murphy G. P., Analysis of glycosylation of prostate-specific membrane antigen derived from LNCaP cells, prostatic carcinoma tumors, and serum from prostate cancer patients. *Prostate* **1996**, *29* (S7), 25-29.

[99] Ghosh A., Heston W. D. W., Effect of carbohydrate moieties on the folate hydrolysis activity of the prostate specific membrane antigen. *Prostate* **2003**, *57* (2), 140-151.

[100] Barinka C., Šácha P., Sklenář J., Man P., Bezouška K., Slusher B. S., Konvalinka J., Identification of the N-glycosylation sites on glutamate carboxypeptidase II necessary for proteolytic activity. *Protein Sci* **2004**, *13* (6), 1627-1635.

[101] Barinka C., Rojas C., Slusher B., Pomper M., Glutamate carboxypeptidase II in diagnosis and treatment of neurologic disorders and prostate cancer. *Curr Med Chem* **2012**, *19* (6), 856-870.

[102] Barrett A. J., Nomenclature Committee of the International Union of Biochemistry and Molecular Biology (NC-IUBMB). Enzyme Nomenclature. Recommendations 1992. Supplement 4: corrections and additions (1997). *Eur J Biochem* **1997**, *250* (1), 1-6.

[103] Robinson M. B., Blakely R. D., Coyle J. T., Quisqualate selectively inhibits a brain peptidase which cleaves N-acetyl-L-aspartyl-L-glutamate in vitro. *Eur J Pharmacol* **1986**, *130* (3), 345-347.

[104] Robinson M. B., Blakely R. D., Couto R., Coyle J. T., Hydrolysis of the brain dipeptide N-acetyl-L-aspartyl-L-glutamate. Identification and characterization of a novel N-acetylated alpha-linked acidic dipeptidase activity from rat brain. *J Biol Chem* **1987**, *262* (30), 14498-14506.

[105] Carter R. E., Feldman A. R., Coyle J. T., Prostate-specific membrane antigen is a hydrolase with substrate and pharmacologic characteristics of a neuropeptidase. *Proc Natl Acad Sci USA* **1996**, *93* (2), 749-753.

[106] Tiffany C. W., Lapidus R. G., Merion A., Calvin D. C., Slusher B. S., Characterization of the enzymatic activity of PSM: comparison with brain NAALADase. *Prostate* **1999**, *39* (1), 28-35.

[107] Halsted C. H., Ling E. H., Luthi-Carter R., Villanueva J. A., Gardner J. M., Coyle J. T., Folylpoly-γ-glutamate carboxypeptidase from pig jejunum: molecular characterization and relation to glutamate carboxypeptidase II. *J Biol Chem* **1998**, *273* (32), 20417-20424.

[108] Pinto J. T., Suffoletto B. P., Berzin T. M., Qiao C. H., Lin S., Tong W. P., May F., Mukherjee B., Heston W., Prostate-specific membrane antigen: a novel folate hydrolase in human prostatic carcinoma cells. *Clin Cancer Res* **1996**, *2* (9), 1445-1451.

[109] Silver D. A., Pellicer I., Fair W. R., Heston W., Cordon-Cardo C., Prostate-specific membrane antigen expression in normal and malignant human tissues. *Clin Cancer Res* **1997**, *3* (1), 81-85.

[110] Sweat S. D., Pacelli A., Murphy G. P., Bostwick D. G., Prostate-specific membrane antigen expression is greatest in prostate adenocarcinoma and lymph node metastases. *Urology* **1998**, *52* (4), 637-640.

[111] Slusher B. S., Robinson M. B., Tsai G., Simmons M. L., Richards S. S., Coyle J. T., Rat brain N-acetylated alpha-linked acidic dipeptidase activity. Purification and immunologic characterization. *J Biol Chem* **1990**, *265* (34), 21297-21301.

[112] Halsted C. H., Jejunal brush-border folate hydrolase. A novel enzyme. *West J Med* **1991**, *155* (6), 605.

[113] Šácha P., Zámečník J., Barinka C., Hlouchova K., Vicha A., Mlčochová P., Hilgert I., Eckschlager T., Konvalinka J., Expression of glutamate carboxypeptidase II in human brain. *Neuroscience* **2007**, *144* (4), 1361-1372.

[114] Berger U. V., Carter R. E., McKee M., Coyle J. T., N-acetylated alpha-linked acidic dipeptidase is expressed by non-myelinating Schwann cells in the peripheral nervous system. *J Neurocytol* **1995**, *24* (2), 99-109.

[115] Trover J. K., Beckett M. L., Wright Jr G. L., Detection and characterization of the prostate-specific membrane antigen (PSMA) in tissue extracts and body fluids. *Int J Cancer* **1995**, *62* (5), 552-558.

[116] Kinoshita Y., Kuratsukuri K., Landas S., Imaida K., Rovito P. M., Wang C. Y., Haas G. P., Expression of prostate-specific membrane antigen in normal and malignant human tissues. *World J Surg* **2006**, *30* (4), 628-636.

[117] O'Keefe D. S., Bacich D. J., Heston W. D. W., Comparative analysis of prostate-specific membrane antigen (PSMA) versus a prostate-specific membrane antigen-like gene. *Prostate* **2004**, *58* (2), 200-210.

[118] Bostwick D. G., Pacelli A., Blute M., Roche P., Murphy G. P., Prostate specific membrane antigen expression in prostatic intraepithelial neoplasia and adenocarcinoma: a study of 184 cases. *Cancer* **1998**, *82* (11), 2256-2261.

[119] Chang S. S., Reuter V. E., Heston W. D. W., Bander N. H., Grauer L. S., Gaudin P. B., Five different anti-prostate-specific membrane antigen (PSMA) antibodies confirm PSMA expression in tumor-associated neovasculature. *Cancer Res* **1999**, *59* (13), 3192-3198.

[120] Ross J. S., Sheehan C. E., Fisher H. A., Kaufman R. P., Kaur P., Gray K., Webb I., Gray G. S., Mosher R., Kallakury B. V. S., Correlation of primary tumor prostate-specific membrane antigen expression with disease recurrence in prostate cancer. *Clin Cancer Res* **2003**, *9* (17), 6357-6362.

[121] Mhawech-Fauceglia P., Zhang S., Terracciano L., Sauter G., Chadhuri A., Herrmann F. R., Penetrante R., Prostate-specific membrane antigen (PSMA) protein expression in normal and neoplastic tissues and its sensitivity and specificity in prostate adenocarcinoma: an immunohistochemical study using mutiple tumour tissue microarray technique. *Histopathology* **2007**, *50* (4), 472-483.

[122] Davis M. I., Bennett M. J., Thomas L. M., Bjorkman P. J., Crystal structure of prostate-specific membrane antigen, a tumor marker and peptidase. *Proc Natl Acad Sci USA* **2005**, *102* (17), 5981-5986.

[123] Mesters J. R., Barinka C., Li W., Tsukamoto T., Majer P., Slusher B. S., Konvalinka J., Hilgenfeld R., Structure of glutamate carboxypeptidase II, a drug target in neuronal damage and prostate cancer. *EMBO J* **2006**, *25* (6), 1375-1384.

[124] Barinka C., Rovenská M., Mlcochová P., Hlouchová K., Plechanovová A., Majer P., Tsukamoto T., Slusher B. S., Konvalinka J., Lubkowski J., Structural insight into the pharmacophore pocket of human glutamate carboxypeptidase II. *J Med Chem* **2007**, *50* (14), 3267-3273.

[125] Barinka C., Hlouchova K., Rovenska M., Majer P., Dauter M., Hin N., Ko Y.-S., Tsukamoto T., Slusher B. S., Konvalinka J., Structural basis of interactions between human glutamate carboxypeptidase II and its substrate analogs. *J Mol Biol* **2008**, *376* (5), 1438-1450.

[126] Barinka C., Byun Y., Dusich C. L., Banerjee S. R., Chen Y., Castanares M., Kozikowski A. P., Mease R. C., Pomper M. G., Lubkowski J., Interactions between human glutamate carboxypeptidase II and urea-based inhibitors: structural characterization. *J Med Chem* **2008**, *51* (24), 7737-7743.

[127] Zhang A. X., Murelli R. P., Barinka C., Michel J., Cocleaza A., Jorgensen W. L., Lubkowski J., Spiegel D. A., A remote arene-binding site on prostate specific membrane antigen revealed by antibody-recruiting small molecules. *J Am Chem Soc* **2010**, *132* (36), 12711-12716.

[128] Sgouros G., Bodei L., McDevitt M. R., Nedrow J. R., Radiopharmaceutical therapy in cancer: clinical advances and challenges. *Nat Rev Drug Discov* **2020**, *19* (9), 589-608.

[129] Ganguly T., Dannoon S., Hopkins M. R., Murphy S., Cahaya H., Blecha J. E., Jivan S., Drake C. R., Barinka C., Jones E. F., A high-affinity [18F]-labeled phosphoramidate peptidomimetic PSMA-targeted inhibitor for PET imaging of prostate cancer. *Nucl Med Biol* **2015**, *42* (10), 780-787.

[130] Majer P., Jackson P. F., Delahanty G., Grella B. S., Ko Y.-S., Li W., Liu Q., Maclin K. M., Poláková J., Shaffer K. A., Synthesis and biological evaluation of thiol-based inhibitors of glutamate carboxypeptidase II: discovery of an orally active GCP II inhibitor. *J Med Chem* **2003**, *46* (10), 1989-1996.

[131] Jackson P. F., Cole D. C., Slusher B. S., Stetz S. L., Ross L. E., Donzanti B. A., Trainor D. A., Design, synthesis, and biological activity of a potent inhibitor of the neuropeptidase N-acetylated α-linked acidic dipeptidase. *J Med Chem* **1996**, *39* (2), 619-622.

[132] Jackson P. F., Tays K. L., Maclin K. M., Ko Y.-S., Li W., Vitharana D., Tsukamoto T., Stoermer D., Lu X.-C. M., Wozniak K., Design and pharmacological activity of phosphinic acid based NAALADase inhibitors. *J Med Chem* **2001**, *44* (24), 4170-4175.

[133] Kozikowski A. P., Nan F., Conti P., Zhang J., Ramadan E., Bzdega T., Wroblewska B., Neale J. H., Pshenichkin S., Wroblewski J. T., Design of remarkably simple, yet potent urea-based inhibitors of glutamate carboxypeptidase II (NAALADase). *J Med Chem* **2001**, *44* (3), 298-301.

[134] Wu L. Y., Anderson M. O., Toriyabe Y., Maung J., Campbell T. Y., Tajon C., Kazak M., Moser J., Berkman C. E., The molecular pruning of a phosphoramidate peptidomimetic inhibitor of prostate-specific membrane antigen. *Biorg Med Chem* **2007**, *15* (23), 7434-7443.

[135] Kiess A. P., Banerjee S. R., Mease R. C., Rowe S. P., Rao A., Foss C. A., Chen Y., Yang X., Cho S. Y., Nimmagadda S., Prostate-specific membrane antigen as a target for cancer imaging and therapy. *Q J Nucl Med Mol Imaging* **2015**, *59* (3), 241.

[136] Wester H.-J., Schmidt A., Parzinger M., PSMA ligands for imaging and endoradiotherapy. Patent WO2019/115547A1, **2020**.

[137] Wurzer A., Wester H.-J., Eiber M. J., PSMA binding dual mode radiotracer and-therapeutics. Patent WO2020/157177A1, **2020**.

[138] Wirtz M., Schmidt A., Schottelius M., Robu S., Günther T., Schwaiger M., Wester H.-J., Synthesis and in vitro and in vivo evaluation of urea-based PSMA inhibitors with increased lipophilicity. *EJNMMI Res* **2018**, *8* (1), 1-11.

[139] Mease R. C., Dusich C. L., Foss C. A., Ravert H. T., Dannals R. F., Seidel J., Prideaux A., Fox J. J., Sgouros G., Kozikowski A. P., N-[N-[(S)-1,3-Dicarboxypropyl]carbamoyl]-4-[18F]fluorobenzyl-L-cysteine, [18F]DCFBC: a new imaging probe for prostate cancer. *Clin Cancer Res* **2008**, *14* (10), 3036-3043.

[140] Cho S. Y., Gage K. L., Mease R. C., Senthamizhchelvan S., Holt D. P., Jeffrey-Kwanisai A., Endres C. J., Dannals R. F., Sgouros G., Lodge M., Biodistribution, tumor detection, and radiation dosimetry of 18F-DCFBC, a low-molecular-weight inhibitor of prostate-specific membrane antigen, in patients with metastatic prostate cancer. *J Nucl Med* **2012**, *53* (12), 1883-1891.

[141] Rowe S. P., Gage K. L., Faraj S. F., Macura K. J., Cornish T. C., Gonzalez-Roibon N., Guner G., Munari E., Partin A. W., Pavlovich C. P., 18F-DCFBC PET/CT for PSMA-based detection and characterization of primary prostate cancer. *J Nucl Med* **2015**, *56* (7), 1003-1010.

[142] Rowe S. P., Macura K. J., Ciarallo A., Mena E., Blackford A., Nadal R., Antonarakis E. S., Eisenberger M. A., Carducci M. A., Ross A. E., Comparison of prostate-specific membrane antigen–based 18F-DCFBC PET/CT to conventional imaging modalities for detection of hormone-naïve and castration-resistant metastatic prostate cancer. *J Nucl Med* **2016**, *57* (1), 46-53.

[143] Mena E., Lindenberg M. L., Shih J. H., Adler S., Harmon S., Bergvall E., Citrin D., Dahut W., Ton A. T., McKinney Y., Clinical impact of PSMA-based 18F-DCFBC PET/CT imaging in patients with biochemically recurrent prostate cancer after primary local therapy. *Eur J Nucl Med Mol Imaging* **2018**, *45* (1), 4-11.

[144] Chen Y., Pullambhatla M., Foss C. A., Byun Y., Nimmagadda S., Senthamizhchelvan S., Sgouros G., Mease R. C., Pomper M. G., 2-(3-{1-Carboxy-5-[(6-[18F]fluoro-pyridine-3-carbonyl)-amino]-pentyl}-ureido)-pentanedioic acid, [18F]DCFPyL, a PSMA-based PET imaging agent for prostate cancer. *Clin Cancer Res* **2011**, *17* (24), 7645-7653.

[145] Szabo Z., Mena E., Rowe S. P., Plyku D., Nidal R., Eisenberger M. A., Antonarakis E. S., Fan H., Dannals R. F., Chen Y., Initial evaluation of [18F]DCFPyL for prostate-specific membrane antigen (PSMA)-targeted PET imaging of prostate cancer. *Mol Imaging Biol* **2015**, *17* (4), 565-574.

[146] Dietlein M., Kobe C., Kuhnert G., Stockter S., Fischer T., Schomäcker K., Schmidt M., Dietlein F., Zlatopolskiy B. D., Krapf P., Comparison of [18F]DCFPyL and [68Ga]Ga-PSMA-HBED-CC for PSMA-PET imaging in patients with relapsed prostate cancer. *Mol Imaging Biol* **2015**, *17* (4), 575-584.

[147] Rowe S. P., Macura K. J., Mena E., Blackford A. L., Nadal R., Antonarakis E. S., Eisenberger M., Carducci M., Fan H., Dannals R. F., PSMA-based [18F]DCFPyL PET/CT is superior to conventional imaging for lesion detection in patients with metastatic prostate cancer. *Mol Imaging Biol* **2016**, *18* (3), 411-419.

[148] Giesel F. L., Will L., Lawal I., Lengana T., Kratochwil C., Vorster M., Neels O., Reyneke F., Haberkon U., Kopka K., Intraindividual comparison of 18F-PSMA-1007 and 18F-DCFPyL PET/CT in the prospective evaluation of patients with newly diagnosed prostate carcinoma: a pilot study. *J Nucl Med* **2018**, *59* (7), 1076-1080.

[149] Bouvet V., Wuest M., Jans H.-S., Janzen N., Genady A. R., Valliant J. F., Benard F., Wuest F., Automated synthesis of [18F]DCFPyL via direct radiofluorination and validation in preclinical prostate cancer models. *EJNMMI Res* **2016**, *6* (1), 1-15.

[150] Ravert H. T., Holt D. P., Chen Y., Mease R. C., Fan H., Pomper M. G., Dannals R. F., An improved synthesis of the radiolabeled prostate-specific membrane antigen inhibitor, [18F]DCFPyL. *J Label Compd Radiopharm* **2016**, *59* (11), 439-450.

[151] SNMMI Newsline, FDA approves 18F-DCFPyL PET agent in prostate cancer. *J Nucl Med* **2021**, *62*, 11N.

[152] Malik N., Baur B., Winter G., Reske S. N., Beer A. J., Solbach C., Radiofluorination of PSMA-HBED via Al18F2+ chelation and biological evaluations in vitro. *Mol Imaging Biol* **2015**, *17* (6), 777-785.

[153] Lütje S., Franssen G. M., Herrmann K., Boerman O. C., Rijpkema M., Gotthardt M., Heskamp S., In vitro and in vivo characterization of an 18F-AlF-labeled PSMA ligand for imaging of PSMA-expressing xenografts. *J Nucl Med* **2019**, *60* (7), 1017-1022.

[154] Giglio J., Zeni M., Savio E., Engler H., Synthesis of an Al18F radiofluorinated GLU-UREA-LYS(AHX)-HBED-CC PSMA ligand in an automated synthesis platform. *EJNMMI Radiopharm Chem* **2018**, *3* (1), 1-12.

[155] Al-Momani E., Israel I., Samnick S., Validation of a [Al18F]PSMA-11 preparation for clinical applications. *Appl Radiat Isot* **2017**, *130*, 102-108.

[156] Kersemans K., De Man K., Courtyn J., Van Royen T., Piron S., Moerman L., Brans B., De Vos F., Automated radiosynthesis of Al[18F]PSMA-11 for large scale routine use. *Appl Radiat Isot* **2018**, *135*, 19-27.

[157] Piron S., De Man K., Van Laeken N., D'Asseler Y., Bacher K., Kersemans K., Ost P., Decaestecker K., Deseyne P., Fonteyne V., Radiation dosimetry and biodistribution of 18F-PSMA-11 for PET imaging of prostate cancer. *J Nucl Med* **2019**, *60* (12), 1736-1742.

[158] Alonso O., dos Santos G., Giglio J., Savio E., Engler H., PET/CT evaluation of prostate cancer patients with Al18F-PSMA-HBED-CC: a head-to-head comparison with 68Ga-PSMA-HBED-CC. *J Nucl Med* **2018**, *59* (Suppl 1), 1499.

[159] Harada N., Kimura H., Onoe S., Watanabe H., Matsuoka D., Arimitsu K., Ono M., Saji H., Synthesis and biologic evaluation of novel 18F-labeled probes targeting prostate-specific membrane antigen for PET of prostate cancer. *J Nucl Med* **2016**, *57* (12), 1978-1984.

[160] Tang G., Zeng W., Yu M., Kabalka G., Facile synthesis of N-succinimidyl 4-[18F]fluorobenzoate ([18F]SFB) for protein labeling. *J Label Compd Radiopharm* **2008**, *51* (1), 68-71.

[161] Harada N., Kimura H., Ono M., Saji H., Preparation of asymmetric urea derivatives that target prostate-specific membrane antigen for SPECT imaging. *J Med Chem* **2013**, *56* (20), 7890-7901.

[162] Saga T., Nakamoto Y., Ishimori T., Inoue T., Shimizu Y., Kimura H., Akamatsu S., Goto T., Watanabe H., Kitaguchi K., Initial evaluation of PET/CT with 18F-FSU-880 targeting prostate-specific membrane antigen in prostate cancer patients. *Cancer Sci* **2019**, *110* (2), 742-750.

[163] Cardinale J., Schäfer M., Benešová M., Bauder-Wüst U., Leotta K., Eder M., Neels O. C., Haberkorn U., Giesel F. L., Kopka K., Preclinical evaluation of 18F-PSMA-1007, a new prostate-specific membrane antigen ligand for prostate cancer imaging. *J Nucl Med* **2017**, *58* (3), 425-431.

[164] Giesel F. L., Cardinale J., Schäfer M., Neels O., Benešová M., Mier W., Haberkorn U., Kopka K., Kratochwil C., 18F-Labelled PSMA-1007 shows similarity in structure, biodistribution and tumour uptake to the theragnostic compound PSMA-617. *Eur J Nucl Med Mol Imaging* **2016**, *43* (10), 1929-1930.

[165] Giesel F. L., Hadaschik B., Cardinale J., Radtke J., Vinsensia M., Lehnert W., Kesch C., Tolstov Y., Singer S., Grabe N., F-18 labelled PSMA-1007: biodistribution, radiation dosimetry and histopathological validation of tumor lesions in prostate cancer patients. *Eur J Nucl Med Mol Imaging* **2017**, *44* (4), 678-688.

[166] Giesel F. L., Knorr K., Spohn F., Will L., Maurer T., Flechsig P., Neels O., Schiller K., Amaral H., Weber W. A., Detection efficacy of 18F-PSMA-1007 PET/CT in 251 patients with biochemical recurrence of prostate cancer after radical prostatectomy. *J Nucl Med* **2019**, *60* (3), 362-368.

[167] Hartrampf P. E., Seitz A. K., Krebs M., Buck A. K., Lapa C., False-negative 18F-PSMA-1007 PET/CT in metastatic prostate cancer related to high physiologic liver uptake. *Eur J Nucl Med Mol Imaging* **2020**, *47* (8), 2044-2046.

[168] Wurzer A., Parzinger M., Konrad M., Beck R., Günther T., Felber V., Färber S., Di Carlo D., Wester H.-J., Preclinical comparison of four [18F, natGa]rhPSMA-7 isomers: influence of the stereoconfiguration on pharmacokinetics. *EJNMMI Res* **2020**, *10* (1), 149.

[169] Rauscher I., Karimzadeh A., Schiller K., Horn T., D'Alessandria C., Franz C., Wörther H., Nguyen N., Combs S. E., Weber W. A., Detection efficacy of 18F-rhPSMA-7.3 PET/CT and impact on patient management in patients with biochemical recurrence of prostate cancer after radical prostatectomy and prior to potential salvage treatment. *J Nucl Med* **2021**, *62* (12), 1719-1726.

[170] Malaspina S., Oikonen V., Kuisma A., Ettala O., Mattila K., Boström P. J., Minn H., Kalliokoski K., Postema E. J., Miller M. P., Kinetic analysis and optimisation of 18F-rhPSMA-7.3 PET imaging of prostate cancer. *Eur J Nucl Med Mol Imaging* **2021**, *48* (11), 3723-3731.

[171] Malaspina S., Taimen P., Kallajoki M., Oikonen V., Kuisma A., Ettala O., Mattila K., Boström P. J., Minn H., Kalliokoski K., Uptake of 18F-rhPSMA-7.3 in Positron Emission Tomography Imaging of Prostate Cancer: A Phase 1 Proof-of-Concept Study. *Cancer Biother Radiopharm* **2022**, *37* (3), 205-213.

[172] Langbein T., Wang H., Rauscher I., Krönke M., Knorr K., Wurzer A., Schwamborn K., Maurer T., Horn T., Haller B., Utility of 18F-rhPSMA-7.3 positron emission tomography for imaging of primary prostate cancer and pre-operative efficacy in N-staging of unfavorable intermediate to very high-risk patients validated by histopathology. *J Nucl Med* **2022**, *63* (9), 1334-1342.

[173] Damaraju V. L., Cass C. E., Sawyer M. B., Folic acid and folates - Renal Conservation of Folates: Role of Folate Transport Proteins. In *Vitamins and Hormones*, Litwack G., Vol. 79, Academic Press, Cambridge, **2008**, 185-192.

[174] Ifergan I., Assaraf Y. G., Folic acid and folates - Molecular Mechanisms of Adaptation to Folate Deficiency. In *Vitamins and Hormones*, Litwack G., Vol. 79, Academic Press, Cambridge, **2008**, 99-143.

[175] Mitchell H. K., Snell E. E., Williams R. J., The concentration of "folic acid". *J Am Chem Soc* **1941**, *63* (8), 2284.

[176] Hines J. D., Halsted C. H., Griggs R. C., Harris J. W., Megaloblastic anemia secondary to folate deficiency associated with hypothyroidism. *Ann Intern Med* **1968**, *68* (4), 792-805.

[177] Boushey C. J., Beresford S. A. A., Omenn G. S., Motulsky A. G., A quantitative assessment of plasma homocysteine as a risk factor for vascular disease: probable benefits of increasing folic acid intakes. *JAMA* **1995**, *274* (13), 1049-1057.

[178] Corrada M. M., Kawas C. H., Hallfrisch J., Muller D., Brookmeyer R., Reduced risk of Alzheimer's disease with high folate intake: the Baltimore Longitudinal Study of Aging. *Alzheimers Dement* **2005**, *1* (1), 11-18.

[179] Czeizel A. E., Dudás I., Prevention of the first occurrence of neural-tube defects by periconceptional vitamin supplementation. *N Engl J Med* **1992**, *327* (26), 1832-1835.

[180] Matherly L. H., Hou Z., Structure and function of the reduced folate carrier: a paradigm of a major facilitator superfamily mammalian nutrient transporter. In *Vitamins and Hormones*, Litwack G., Vol. 79, Academic Press, Cambridge, **2008**, 144-184.

[181] Ghitis J., Lora C., The folate binding in milk. *Am J Clin Nutr* **1967**, *20* (1), 1-4.

[182] Salter D. N., Ford J. E., Scott K. J., Andrews P., Isolation of the folate-binding protein from cow's milk by the use of affinity chromatography. *FEBS Lett* **1972**, *20* (3), 302-306.

[183] Ratnam M., Marquardt H., Duhring J. L., Freisheim J. H., Homologous membrane folate binding proteins in human placenta: cloning and sequence of a cDNA. *Biochemistry* **1989**, *28* (20), 8249-8254.

[184] Shen F., Ross J. F., Wang X., Ratnam M., Identification of a novel folate receptor, a truncated receptor, and receptor type beta in hematopoietic cells: cDNA cloning, expression, immunoreactivity, and tissue specificity. *Biochemistry* **1994**, *33* (5), 1209-1215.

[185] Spiegelstein O., Eudy J. D., Finnell R. H., Identification of two putative novel folate receptor genes in humans and mouse. *Gene* **2000**, *258* (1-2), 117-125.

[186] Cheung A., Bax H. J., Josephs D. H., Ilieva K. M., Pellizzari G., Opzoomer J., Bloomfield J., Fittall M., Grigoriadis A., Figini M., Targeting folate receptor alpha for cancer treatment. *Oncotarget* **2016**, *7* (32), 52553.

[187] Lacey S. W., Sanders J. M., Rothberg K. G., Anderson R. G., Kamen B. A., Complementary DNA for the folate binding protein correctly predicts anchoring to the membrane by glycosyl-phosphatidylinositol. *J Clin Invest* **1989**, *84* (2), 715-720.

[188] Kamen B. A., Capdevila A., Receptor-mediated folate accumulation is regulated by the cellular folate content. *Proc Natl Acad Sci USA* **1986**, *83* (16), 5983-5987.

[189] Rijnboutt S., Jansen G., Posthuma G., Hynes J. B., Schornagel J. H., Strous G. J., Endocytosis of GPI-linked membrane folate receptor-alpha. *J Cell Biol* **1996**, *132* (1), 35-47.

[190] Mantovani L. T., Miotti S., Menard S., Canevari S., Raspagliesi F., Bottini C., Bottero F., Colnaghi M. I., Folate binding protein distribution in normal tissues and biological fluids from ovarian carcinoma patients as detected by the monoclonal antibodies MOv18 and MOv19. *Eur J Cancer* **1994**, *30* (3), 363-369.

[191] Holm J., Hansen S. I., Høier-Madsen M., Bostad L., High-affinity folate binding in human choroid plexus. Characterization of radioligand binding, immunoreactivity, molecular heterogeneity and hydrophobic domain of the binding protein. *Biochem J* **1991**, *280* (1), 267-271.

[192] Antony A. C., Utley C., Van Horne K. C., Kolhouse J. F., Isolation and characterization of a folate receptor from human placenta. *J Biol Chem* **1981**, *256* (18), 9684-9692.

[193] Weitman S. D., Weinberg A. G., Coney L. R., Zurawski V. R., Jennings D. S., Kamen B. A., Cellular localization of the folate receptor: potential role in drug toxicity and folate homeostasis. *Cancer Res* **1992**, *52* (23), 6708-6711.

[194] Ross J. F., Wang H., Behm F. G., Mathew P., Wu M., Booth R., Ratnam M., Folate receptor type β is a neutrophilic lineage marker and is differentially expressed in myeloid leukemia. *Cancer* **1999**, *85* (2), 348-357.

[195] Mayanil C. S., Siddiqui M. R., Tomita T., Novel functions of folate receptor alpha in CNS development and diseases. *Neurosci Discov* **2014**, *2*, 5-11.

[196] Shen F., Wu M., Ross J. F., Miller D., Ratnam M., Folate receptor type gamma is primarily a secretory protein due to lack of an efficient signal for glycosylphosphatidylinositol modification: Protein characterization and cell type specificity. *Biochemistry* **1995**, *34* (16), 5660-5665.

[197] Tian Y., Wu G., Xing J.-C., Tang J., Zhang Y., Huang Z.-M., Jia Z.-C., Zhao R., Tian Z.-Q., Wang S.-F., A novel splice variant of folate receptor 4 predominantly expressed in regulatory T cells. *BMC Immunol* **2012**, *13* (1), 1-8.

[198] Garin-Chesa P., Campbell I., Saigo P. E., Lewis Jr J. L., Old L. J., Rettig W. J., Trophoblast and ovarian cancer antigen LK26. Sensitivity and specificity in immunopathology and molecular identification as a folate-binding protein. *Am J Pathol* **1993**, *142* (2), 557.

[199] Coney L. R., Tomassetti A., Carayannopoulos L., Frasca V., Kamen B. A., Colnaghi M. I., Zurawski V. R., Cloning of a tumor-associated antigen: MOv18 and MOv19 antibodies recognize a folate-binding protein. *Cancer Res* **1991**, *51* (22), 6125-6132.

[200] Parker N., Turk M. J., Westrick E., Lewis J. D., Low P. S., Leamon C. P., Folate receptor expression in carcinomas and normal tissues determined by a quantitative radioligand binding assay. *Anal Biochem* **2005**, *338* (2), 284-293.

[201] Hartmann L. C., Keeney G. L., Lingle W. L., Christianson T. J. H., Varghese B., Hillman D., Oberg A. L., Low P. S., Folate receptor overexpression is associated with poor outcome in breast cancer. *Int J Cancer* **2007**, *121* (5), 938-942.

[202] Siu M. K. Y., Kong D. S. H., Chan H. Y., Wong E. S. Y., Ip P. P. C., Jiang L., Ngan H. Y. S., Le X.-F., Cheung A. N. Y., Paradoxical impact of two folate receptors, FRα and RFC, in ovarian cancer: effect on cell proliferation, invasion and clinical outcome. *PLoS One* **2012**, *7* (11), e47201.

[203] Zhang Z., Wang J., Tacha D. E., Li P., Bremer R. E., Chen H., Wei B., Xiao X., Da J., Skinner K., Folate receptor α associated with triple-negative breast cancer and poor prognosis. *Arch Pathol Lab Med* **2014**, *138* (7), 890-895.

[204] Müller C., Schibli R., Prospects in folate receptor-targeted radionuclide therapy. *Front Oncol* **2013**, *3*, 249.

[205] Boss S. D., Ametamey S. M., Development of Folate Receptor-Targeted PET Radiopharmaceuticals for Tumor Imaging—A Bench-to-Bedside Journey. *Cancers (Basel)* **2020**, *12* (6), 1508.

[206] Chen C., Ke J., Zhou X. E., Yi W., Brunzelle J. S., Li J., Yong E.-L., Xu H. E., Melcher K., Structural basis for molecular recognition of folic acid by folate receptors. *Nature* **2013**, *500* (7463), 486-489.

[207] Bettio A., Honer M., Müller C., Brühlmeier M., Müller U., Schibli R., Groehn V., Schubiger A. P., Ametamey S. M., Synthesis and preclinical evaluation of a folic acid derivative labeled with 18F for PET imaging of folate receptor–positive tumors. *J Nucl Med* **2006**, *47* (7), 1153-1160.

[208] Al Jammaz I., Al-Otaibi B., Okarvi S., Amartey J., Novel synthesis of [18F]-fluorobenzene and pyridinecarbohydrazide-folates as potential PET radiopharmaceuticals. *J Label Compd Radiopharm* **2006**, *49* (2), 125-137.

[209] Al Jammaz I., Al-Otaibi B., Amer S., Okarvi S. M., Rapid synthesis and in vitro and in vivo evaluation of folic acid derivatives labeled with fluorine-18 for PET imaging of folate receptor-positive tumors. *Nucl Med Biol* **2011**, *38* (7), 1019-1028.

[210] Ross T. L., Honer M., Lam P. Y. H., Mindt T. L., Groehn V., Schibli R., Schubiger P. A., Ametamey S. M., Fluorine-18 click radiosynthesis and preclinical evaluation of a new 18F-labeled folic acid derivative. *Bioconjug Chem* **2008**, *19* (12), 2462-2470.

[211] Schieferstein H., Betzel T., Fischer C. R., Ross T. L., 18F-click labeling and preclinical evaluation of a new 18F-folate for PET imaging. *EJNMMI Res* **2013**, *3* (1), 1-10.

[212] Kettenbach K., Reffert L. M., Schieferstein H., Pektor S., Eckert R., Miederer M., Rösch F., Ross T. L., Comparison study of two differently clicked 18F-folates - Lipophilicity plays a key role. *Pharmaceuticals* **2018**, *11* (1), 30.

[213] Boss S. D., Müller C., Siwowska K., Büchel J. I., Schmid R. M., Groehn V., Schibli R., Ametamey S. M., Reduced 18F-folate conjugates as a new class of PET tracers for folate receptor imaging. *Bioconjug Chem* **2018**, *29* (4), 1119-1130.

[214] Chen Q., Meng X., McQuade P., Rubins D., Lin S.-A., Zeng Z., Haley H., Miller P., González Trotter D., Low P. S., Synthesis and preclinical evaluation of folate-NOTA-Al18F for PET imaging of folate-receptor-positive tumors. *Mol Pharm* **2016**, *13* (5), 1520-1527.

[215] Chen Q., Meng X., McQuade P., Rubins D., Lin S.-A., Zeng Z., Haley H., Miller P., González Trotter D., Low P. S., Folate-PEG-NOTA-Al18F: A new folate based radiotracer for PET imaging of folate receptor-positive tumors. *Mol Pharm* **2017**, *14* (12), 4353-4361.

[216] Ross T. L., Honer M., Müller C., Groehn V., Schibli R., Ametamey S. M., A New 18F-Labeled Folic Acid Derivative with Improved Properties for the PET Imaging of Folate Receptor–Positive Tumors. *J Nucl Med* **2010**, *51* (11), 1756-1762.

[217] Betzel T., Müller C., Groehn V., Müller A., Reber J., Fischer C. R., Krämer S. D., Schibli R., Ametamey S. M., Radiosynthesis and preclinical evaluation of 3'-Aza-2'-[18F]fluorofolic acid: a novel PET radiotracer for folate receptor targeting. *Bioconjug Chem* **2013**, *24* (2), 205-214.

[218] Boss S. D., Müller C., Siwowska K., Schmid R. M., Groehn V., Schibli R., Ametamey S. M., Diastereomerically Pure 6R- and 6S-3'-Aza-2'-18F-Fluoro-5-Methyltetrahydrofolates Show Unprecedentedly High Uptake in Folate Receptor–Positive KB Tumors. *J Nucl Med* **2019**, *60* (1), 135-141.

[219] Gnesin S., Müller J., Burger I. A., Meisel A., Siano M., Früh M., Choschzick M., Müller C., Schibli R., Ametamey S. M., Radiation dosimetry of 18F-AzaFol: A first in-human use of a folate receptor PET tracer. *EJNMMI Res* **2020**, *10*, 1-12.

[220] Smith D. P., Anderson J., Plante J., Ashcroft A. E., Radford S. E., Wilson A. J., Parker M. J., Trifluoromethyldiazirine: an effective photo-induced cross-linking probe for exploring amyloid formation. *Chem Commun* **2008**, (44), 5728-5730.

[221] Maresca K. P., Hillier S. M., Femia F. J., Keith D., Barone C., Joyal J. L., Zimmerman C. N., Kozikowski A. P., Barrett J. A., Eckelman W. C., A series of halogenated heterodimeric inhibitors of prostate specific membrane antigen (PSMA) as radiolabeled probes for targeting prostate cancer. *J Med Chem* **2009**, *52* (2), 347-357.

[222] Nomura M., Shuto S., Matsuda A., Development of an efficient intermediate, alpha-[2-(trimethylsilyl)ethoxy]-2-N-[2-(trimethylsilyl)ethoxycarbonyl]folic acid, for the synthesis of folate (gamma)-conjugates, and its application to the synthesis of folate-nucleoside conjugates. *J Org Chem* **2000**, *65* (16), 5016.

[223] Amblard M., Fehrentz J.-A., Martinez J., Subra G., Methods and protocols of modern solid phase peptide synthesis. *Mol Biotechnol* **2006**, *33* (3), 239-254.

[224] Chan W. C., Bycroft B. W., Evans D. J., White P. D., A novel 4-aminobenzyl ester-based carboxy-protecting group for synthesis of atypical peptides by Fmoc-Bu^t solid-phase chemistry. *J Chem Soc Chem Commun* **1995**, (21), 2209-2210.

[225] Díaz-Mochón J. J., Bialy L., Bradley M., Full orthogonality between Dde and Fmoc: the direct synthesis of PNA−peptide conjugates. *Org Lett* **2004**, *6* (7), 1127-1129.

[226] Lopez S. E., Salazar J., Trifluoroacetic acid: Uses and recent applications in organic synthesis. *J Fluor Chem* **2013**, *156*, 73-100.

[227] Bollhagen R., Schmiedberger M., Barlos K., Grell E., A new reagent for the cleavage of fully protected peptides synthesised on 2-chlorotrityl chloride resin. *J Chem Soc Chem Commun* **1994**, (22), 2559-2560.

[228] Weineisen M., Simecek J., Schottelius M., Schwaiger M., Wester H.-J., Synthesis and preclinical evaluation of DOTAGA-conjugated PSMA ligands for functional imaging and endoradiotherapy of prostate cancer. *EJNMMI Res* **2014**, *4* (1), 63.

[229] Reber J., Struthers H., Betzel T., Hohn A., Schibli R., Müller C., Radioiodinated folic acid conjugates: evaluation of a valuable concept to improve tumor-to-background contrast. *Mol Pharm* **2012**, *9* (5), 1213-1221.

[230] Schottelius M., Konrad M., Osl T., Poschenrieder A., Wester H.-J., An optimized strategy for the mild and efficient solution phase iodination of tyrosine residues in bioactive peptides. *Tetrahedron Lett* **2015**, *56* (47), 6602-6605.

[231] Chen Y., Foss C. A., Byun Y., Nimmagadda S., Pullambhatla M., Fox J. J., Castanares M., Lupold S. E., Babich J. W., Mease R. C., Radiohalogenated prostate-specific membrane antigen (PSMA)-based ureas as imaging agents for prostate cancer. *J Med Chem* **2008**, *51* (24), 7933-7943.

[232] Schottelius M., Ludescher M., Richter F., Kapp T. G., Kessler H., Wester H.-J., Validation of [125I]CPCR4.3 as an investigative tool for the sensitive and specific detection of hCXCR4 and mCXCR4 expression in vitro and in vivo. *EJNMMI Res* **2019**, *9* (1), 1-9.

[233] Valko K., Nunhuck S., Bevan C., Abraham M. H., Reynolds D. P., Fast gradient HPLC method to determine compounds binding to human serum albumin. Relationships with octanol/water and immobilized artificial membrane lipophilicity. *J Pharm Sci* **2003**, *92* (11), 2236-2248.

[234] Horoszewicz J. S., Leong S. S., Chu T. M., Wajsman Z. L., Friedman M., Papsidero L., Kim U., Chai L. S., Kakati S., Arya S. K., Sandberg A. A., The LNCaP cell line-a new model for studies on human prostatic carcinoma. *Prog Clin Biol Res* **1980**, *37*, 115-132.

[235] Jiang L., Zeng X., Wang Z., Chen Q., Cell line cross-contamination: KB is not an oral squamous cell carcinoma cell line. *Eur J Oral Sci* **2009**, *117* (1), 90-91.

[236] Miksch J., Prasad V., Di Carlo D., Zengerling F., Bolenz C., Solbach C., Beer M., Wiegel T., Wester H.-J., Beer A. J., Novel [F18]siPSMA14 biodistribution at 60, 90 and 120 min p.i. showing most favourable kinetics at 90 min p.i. for staging and restaging of prostate cancer patients. *Eur J Nucl Med Mol Imaging* **2020**, *47* (Suppl 1), 456.

[237] Miksch J., Strauß A. S., Di Carlo D., Bolenz C., Wiegel T., Solbach C., Prasad V., Wester H.-J., Eiber M., Beer A. J., [F-18]siPSMA14 zeigt 90min p.i. ohne forcierte Diurese eine hohe Untersucherübereinstimmung in Primär- und Re-Staging von Prostatakarzinom Patienten. *Nuklearmedizin* **2021**, *60* (2), 20.

[238] Miksch J., Prasad V., Di Carlo D., Zengerling F., Bolenz C., Solbach C., Beer M., Wiegel T., Wester H.-J., Beer A. J., Diagnostic performance of the novel PSMA-specific PET radiotracer [F-18]siPSMA-14 in staging and restaging of prostate cancer. *Eur J Nucl Med Mol Imaging* **2020**, *47* (Suppl 1), 460-461.

[239] Wessmann S., Henriksen G., Wester H.-J., Cryptate mediated nucleophilic 18F-fluorination without azeotropic drying. *Nuklearmedizin* **2012**, *51* (1), 1-8.

[240] Wurzer A., Di Carlo D., Schmidt A., Beck R., Schwaiger M., Herz M., Eiber M., Wester H.-J., PSMA-targeted 18F-labeled Radiohybrid Inhibitors: Labeling chemistry and automated GMP production of 18F-rhPSMA-7. *J Nucl Med* **2019**, *60* (Suppl 1), 342.

[241] Atkins P., De Paula J., *Physical chemistry for the life sciences*. 2 ed., Oxford University Press, Oxford, **2006**, 238-259.

[242] Chun J.-H., Lu S., Lee Y.-S., Pike V. W., Fast and high-yield microreactor syntheses of ortho-substituted [18F]fluoroarenes from reactions of [18F]fluoride ion with diaryliodonium salts. *J Org Chem* **2010**, *75* (10), 3332-3338.

[243] Cacace F., Speranza M., Wolf A. P., Macgregor R. R., Nucleophilic aromatic substitution; kinetics of fluorine-18 substitution reactions in polyfluorobenzenes. Isotopic exchange between 18F− and polyfluorobenzenes in dimethylsulfoxide. A kinetic study. *J Fluor Chem* **1982**, *21* (2), 145-158.

[244] Kuntzsch M., Lamparter D., Brüggener N., Müller M., Kienzle G. J., Reischl G., Development and successful validation of simple and fast TLC spot tests for determination of Kryptofix® 2.2.2 and tetrabutylammonium in 18F-labeled radiopharmaceuticals. *Pharmaceuticals* **2014**, *7* (5), 621-633.

[245] Brichard L., Aigbirhio F. I., An Efficient method for enhancing the reactivity and flexibility of [18F]fluoride towards nucleophilic substitution using tetraethylammonium bicarbonate. *Eur J Org Chem* **2014**, *2014* (28), 6145-6149.

[246] Inkster J. A. H., Akurathi V., Sromek A. W., Chen Y., Neumeyer J. L., Packard A. B., A non-anhydrous, minimally basic protocol for the simplification of nucleophilic 18F-fluorination chemistry. *Sci Rep* **2020**, *10* (1), 1-9.

[247] Telix Pharmaceuticals, FDA Approves New 68Ga Kit for Prostate Cancer PET. *J Nucl Med* **2022**, *63* (2), 26N.

[248] U.S. Food and Drug Administration, FDA Approves Pluvicto/Locametz for Metastatic Castration-Resistant Prostate Cancer. *J Nucl Med* **2022**, *63* (5), 13N.

[249] Kuo H.-T., Lepage M. L., Lin K.-S., Pan J., Zhang Z., Liu Z., Pryyma A., Zhang C., Merkens H., Roxin A., One-step 18F-labeling and preclinical evaluation of prostate-specific membrane antigen trifluoroborate probes for cancer imaging. *J Nucl Med* **2019**, *60* (8), 1160-1166.

[250] Robu S., Schmidt A., Eiber M., Schottelius M., Günther T., Yousefi B. H., Schwaiger M., Wester H.-J., Synthesis and preclinical evaluation of novel 18F-labeled Glu-urea-Glu-based PSMA inhibitors for prostate cancer imaging: a comparison with 18F-DCFPyl and 18F-PSMA-1007. *EJNMMI Res* **2018**, *8* (1), 30.

[251] Deberle L. M., Benešová M., Umbricht C. A., Borgna F., Büchler M., Zhernosekov K., Schibli R., Müller C., Development of a new class of PSMA radioligands comprising ibuprofen as an albumin-binding entity. *Theranostics* **2020**, *10* (4), 1678.

[252] Ghuman J., Zunszain P. A., Petitpas I., Bhattacharya A. A., Otagiri M., Curry S., Structural basis of the drug-binding specificity of human serum albumin. *J Mol Biol* **2005**, *353* (1), 38-52.

[253] Reddy J. A., Nelson M., Xu L., Westrick E., Vetzel M., Wheeler L., Felten A., Santhapuram H., Vlahov I., Leamon C. P., Abstract 852: Specificity of PSMA-617 radiotherapy for prostate cancer. *Cancer Res* **2018**, *78* (13_Suppl), 852.

[254] Kwon H., Lim H., Ha H., Choi D., Son S.-H., Nam H., Minn I., Byun Y., Structure-activity relationship studies of prostate-specific membrane antigen (PSMA) inhibitors derived from α-amino acid with (S)- or (R)-configuration at P1' region. *Bioorg Chem* **2020**, *104*, 104304.

[255] Wurzer A., Pollmann J., Schmidt A., Reich D., Wester H.-J., Notni J., Molar activity of Ga-68 labeled PSMA inhibitor conjugates determines PET imaging results. *Mol Pharm* **2018**, *15* (9), 4296-4302.

[256] Dornan M. H., Simard J. M., Leblond A., Juneau D., Delouya G., Saad F., Ménard C., DaSilva J. N., Simplified and robust one-step radiosynthesis of [18F]DCFPyL via direct radiofluorination and cartridge-based purification. *J Label Compd Radiopharm* **2018**, *61* (10), 757-763.

[257] Naka S., Watabe T., Kurimoto K., Uemura M., Soeda F., Neels O. C., Kopka K., Tatsumi M., Kato H., Nonomura N., Automated [18F]PSMA-1007 production by a single use cassette-type synthesizer for clinical examination. *EJNMMI Radiopharm Chem* **2020**, *5* (1), 1-17.

[258] Cardinale J., Martin R., Remde Y., Schäfer M., Hienzsch A., Hübner S., Zerges A.-M., Marx H., Hesse R., Weber K., Procedures for the GMP-compliant production and quality control of [18F]PSMA-1007: a next generation radiofluorinated tracer for the detection of prostate cancer. *Pharmaceuticals* **2017**, *10* (4), 77.

[259] Oh S. W., Wurzer A., Teoh E. J., Oh S., Langbein T., Krönke M., Herz M., Kropf S., Wester H.-J., Weber W. A., Quantitative and qualitative analyses of biodistribution and PET image quality of a novel radiohybrid PSMA, 18F-rhPSMA-7, in patients with prostate cancer. *J Nucl Med* **2020**, *61* (5), 702-709.

[260] Wondergem M., van der Zant F. M., Roeleveld T. A., Srbljin S., Kartachova M. S., van Dongen A., Franken V., Knol R. J. J., 18F-DCFPyL PET/CT in primary staging of prostate cancer. *Eur J Hybrid Imaging* **2018**, *2* (1), 1-14.

[261] Wondergem M., Jansen B. H. E., van der Zant F. M., van der Sluis T. M., Knol R. J. J., van Kalmthout L. W. M., Hoekstra O. S., van Moorselaar R. J. A., Oprea-Lager D. E., Vis A. N., Early lesion detection with 18F-DCFPyL PET/CT in 248 patients with biochemically recurrent prostate cancer. *Eur J Nucl Med Mol Imaging* **2019**, *46* (9), 1911-1918.

[262] Hofman M. S., Iravani A., Nzenza T., Murphy D. G., Advances in urologic imaging: prostate-specific membrane antigen ligand PET imaging. *Urol Clin North Am* **2018**, *45* (3), 503-524.

[263] Müller C., Mindt T. L., de Jong M., Schibli R., Evaluation of a novel radiofolate in tumour-bearing mice: promising prospects for folate-based radionuclide therapy. *Eur J Nucl Med Mol Imaging* **2009**, *36* (6), 938-946.

[264] Müller C., Struthers H., Winiger C., Zhernosekov K., Schibli R., DOTA conjugate with an albumin-binding entity enables the first folic acid–targeted 177Lu-radionuclide tumor therapy in mice. *J Nucl Med* **2013**, *54* (1), 124-131.

[265] Reber J., Haller S., Leamon C. P., Müller C., 177Lu-EC0800 combined with the antifolate pemetrexed: preclinical pilot study of folate receptor targeted radionuclide tumor therapy. *Mol Cancer Ther* **2013**, *12* (11), 2436-2445.

[266] Müller C., Reber J., Haller S., Dorrer H., Bernhardt P., Zhernosekov K., Türler A., Schibli R., Direct in vitro and in vivo comparison of 161Tb and 177Lu using a tumour-targeting folate conjugate. *Eur J Nucl Med Mol Imaging* **2014**, *41* (3), 476-485.

[267] Müller C., Reber J., Haller S., Dorrer H., Köster U., Johnston K., Zhernosekov K., Türler A., Schibli R., Folate receptor targeted alpha-therapy using terbium-149. *Pharmaceuticals* **2014**, *7* (3), 353-365.

[268] Haller S., Reber J., Brandt S., Bernhardt P., Groehn V., Schibli R., Müller C., Folate receptor-targeted radionuclide therapy: preclinical investigation of anti-tumor effects and potential radionephropathy. *Nucl Med Biol* **2015**, *42* (10), 770-779.

[269] Siwowska K., Haller S., Bortoli F., Benešová M., Groehn V., Bernhardt P., Schibli R., Müller C., Preclinical comparison of albumin-binding radiofolates: Impact of linker entities on the in vitro and in vivo properties. *Mol Pharm* **2017**, *14* (2), 523-532.

[270] Müller C., Guzik P., Siwowska K., Cohrs S., Schmid R. M., Schibli R., Combining albumin-binding properties and interaction with pemetrexed to improve the tissue distribution of radiofolates. *Molecules* **2018**, *23* (6), 1465.

[271] Figliola C., Marchal E., Groves B. R., Thompson A., A step-wise synthetic approach is necessary to access γ-conjugates of folate: folate-conjugated prodigiosenes. *RSC Adv* **2019**, *9* (25), 14078-14092.

[272] Siwowska K., Schmid R. M., Cohrs S., Schibli R., Müller C., Folate receptor-positive gynecological cancer cells: In vitro and in vivo characterization. *Pharmaceuticals* **2017**, *10* (3), 72.

[273] Fischer C. R., Müller C., Reber J., Müller A., Krämer S. D., Ametamey S. M., Schibli R., [18F]fluoro-deoxy-glucose folate: a novel PET radiotracer with improved in vivo properties for folate receptor targeting. *Bioconjug Chem* **2012**, *23* (4), 805-813.

[274] Curry S., Lessons from the crystallographic analysis of small molecule binding to human serum albumin. *Drug Metab Pharmacokinet* **2009**, *24* (4), 342-357.

[275] Fischer C. R., Groehn V., Reber J., Schibli R., Ametamey S. M., Müller C., Improved PET imaging of tumors in mice using a novel 18F-folate conjugate with an albumin-binding entity. *Mol Imaging Biol* **2013**, *15* (6), 649-654.

[276] Boss S. D., Betzel T., Müller C., Fischer C. R., Haller S., Reber J., Groehn V., Schibli R., Ametamey S. M., Comparative studies of three pairs of α- and γ-conjugated folic acid derivatives labeled with fluorine-18. *Bioconjug Chem* **2016**, *27* (1), 74-86.

The cover image was created based on Novartis AG **2023**, *Radioligand Therapy*, accessed 5th March 2023, <https://www.novartis.com/research-development/technology-platforms/radioligand-therapy>.

6 Supplementary Information

6.1 Abbreviations and Symbols

× g	times gravity
%IA/g	% injected activity per gram of tissue
%ID/g	% injected dose per gram of tissue
2-CT	2-chlorotrityl
2-CTC	2-chlorotrityl chloride
2-PMPA	2-(phosphonomethyl)pentanedioic acid
8-Aoc	8-amino-octanoic acid
β-Ala	β-alanine
δ	chemical shift
λ	wavelength
abs.	absolute
add.	additional
AEEAc	8-amino-3,6-dioxaoctanoic acid
Ahx	6-aminohexanoic acid
A_m	molar activity
$AMBF_3$	*N,N*-dimethyl-ammoniomethyltrifluoroborate
anal.	analytical
anhyd.	anhydrous
approx.	approximately
aq.	aqueous
Asp	aspartic acid
Bn	benzyl
Boc	*tert*-butyloxycarbonyl
BSA	bovine serum albumin
calc.	calculated
Cbz	benzyloxycarbonyl
CDI	*N,N'*-carbonyldiimidazole
Cit	citrulline
CT	X-ray computed tomography
d	doublet
Dap	2,3-diaminopropionic acid
DCE	1,2-dichloroethane
DCM	dichloromethane
Dde	1-(4,4-dimethyl-2,6-dioxocyclohex-1-ylidene)ethyl
DIPEA	*N,N*-diisopropylethylamine
DMEM/F-12	Dulbecco's Modified Eagle Medium/Nutrient Mixture F-12
DMF	*N,N*-dimethylformamide
DMSO	dimethyl sulfoxide

DOTA	1,4,7,10-tetraazacyclododecane-1,4,7,10-tetraacetic acid
EDTA	ethylenediaminetetraacetic acid
ESI	electrospray ionization
Et_2O	diethyl ether
EtOAc	ethyl acetate
EtOH	ethanol
FAP	fibroblast activation protein
FCS	fetal calf serum
FFRPMI	folate-free RPMI medium without folic acid, vitamin B12, and phenol red
Fmoc	9-fluorenylmethoxycarbonyl
FR	folate receptor
Glu	glutamic acid
Gly	glycine
GPI	glycosylphosphatidylinositol
GRPR	gastrin-releasing peptide receptor
HBBS	Hanks' Balanced Salt Solution
HOAt	1-hydroxy-7-azabenzotriazole
HOBt	hydroxybenzotriazole
HPLC	high-performance liquid chromatography
HSA	human serum albumin
IC_{50}	half maximal inhibitory concentration
J	coupling constant
K'	capacity factor
$\log D_{7.4}$	logarithmic *n*-octanol-PBS partition coefficient at pH 7.4
Lys	lysine
m.i.	monoisotopic
m/z	mass-to-charge ratio
MeCN	acetonitrile
MeOH	methanol
MS	mass spectrometry
NaAsc	sodium ascorbate
NMP	*N*-methyl-2-pyrrolidone
NMR	nuclear magnetic resonance
NOTA	1,4,7-triazacyclononane-1,4,7-triacetic acid
Orn	ornithine
p.i.	post-injection
PBS	phosphate-buffered saline
PE	petroleum ether
PEG	poly(ethylene glycol)
PET	positron emission tomography
Phe	phenylalanine
Pip	piperidine
PKM	pharmacokinetic modifier

ppm	parts per million
prep.	preparative
PSA	prostate-specific antigen
PSMA	prostate-specific membrane antigen
PyBOP	benzotriazol-1-yl-oxytripyrrolidinophosphonium hexafluorophosphate
RCC	radiochemical conversion
RCP	radiochemical purity
RCY	radiochemical yield
R_f	retention factor
RP	reversed-phase
rpm	revolutions per minute
rt	room temperature
s	singlet
sat.	saturated
SD	standard deviation
SiFA-BnBr	(4-(bromomethyl)phenyl)di-*tert*-butylfluorosilane
SiFA-BzA	4-(di-*tert*-butylfluorosilyl)benzoic acid
SiFAN$^+$Br$^-$	*N*-(4-(di-*tert*-butylfluorosilyl)benzyl)-2-hydroxy-*N*,*N*-dimethylethylammonium bromide
S_N2	bimolecular nucleophilic substitution
S_NAr	nucleophilic aromatic substitution
SPE	solid-phase extraction
SPPS	solid-phase peptide synthesis
SSTR	somatostatin receptor
SUV_{mean}	mean standardized uptake values
TBDMS	*tert*-butyldimethylsilyl
TBTU	*N*,*N*,*N*',*N*'-tetramethyl-*O*-(benzotriazol-1-yl)uronium tetrafluoroborate
*t*Bu	*tert*-butyl
*t*BuLi	*tert*-butyllithium
*t*BuOH	*tert*-butanol
TEA	triethylamine
Teoc	2-(trimethylsilyl)ethoxycarbonyl
TFA	trifluoroacetic acid
THF	tetrahydrofuran
Thr	threonine
TIPS	triisopropylsilane
TLC	thin-layer chromatography
t_R	retention time
TRIS	tris(hydroxymethyl)aminomethane
Tyr	tyrosine
UV	ultraviolet

6.2 Indices

6.2.1 Figure Index

6.2.2 Formula Index

6.2.3 Scheme Index

6.2.4 Table Index

6.3 Publication List

6.3.1 Peer-reviewed Journal Articles

[1] Günther T., Holzleitner N., Di Carlo D., Urtz-Urban N., Lapa C., Wester H.-J., Development of the First 18F-Labeled Radiohybrid-based Minigastrin Derivative with high Target Affinity and Tumor Accumulation by Substitution of the Chelating Moiety. *Pharmaceutics* **2023**, *15* (3), 826.

[2] Löffler J., Hamp C., Scheidhauer E., Di Carlo D., Solbach C., Abaei A., Hao L., Glatting G., Beer A. J., Rasche V., Winter G., Comparison of Quantification of Target-Specific Accumulation of [18F]F-siPSMA-14 in the HET-CAM Model and in Mice Using PET/MRI. *Cancers* **2021**, *13* (16), 4007.

[3] Wurzer A., Di Carlo D., Herz M., Richter A., Robu S., Schirrmacher R., Mascarin A., Weber W., Eiber M., Schwaiger M., Wester H.-J., Automated synthesis of [18F]Ga-rhPSMA-7/-7.3: results, quality control and experience from more than 200 routine productions. *EJNMMI Radiopharm Chem* **2021**, *6* (1), 1-15.

[4] Wurzer A., Parzinger M., Konrad M., Beck R., Günther T., Felber V., Färber S., Di Carlo D., Wester H.-J., Preclinical comparison of four [18F, natGa]rhPSMA-7 isomers: influence of the stereoconfiguration on pharmacokinetics. *EJNMMI Res* **2020**, *10* (1), 149.

[5] Wurzer A., Di Carlo D., Schmidt A., Beck R., Eiber M., Schwaiger M., Wester H.-J., Radiohybrid Ligands: A Novel Tracer Concept Exemplified by 18F- or 68Ga-Labeled rhPSMA Inhibitors. *J Nucl Med* **2020**, *61* (5), 735-742.

6.3.2 Conference Abstracts

[1] Miksch J., Prasad V., Di Carlo D., Strauss A.-S., Grunert M., Steinacker J. P., Thaiss W. M., Solbach C., Bolenz C., Beer M., Wiegel T., Wester H.-J., Eiber M., Beer A. J., Novel [F-18]siPSMA-14 shows favourable kinetics and high interobserver agreement in staging of prostate cancer patients. Annual Meeting of the Society of Nuclear Medicine and Molecular Imaging, June 11 – 15, 2021, Virtual. *J Nucl Med* **2021**, *62* (Suppl 1), 1328.

[2] Miksch J., Strauß A. S., Di Carlo D., Bolenz C., Wiegel T., Solbach C., Prasad V., Wester H.-J., Eiber M., Beer A. J., [F-18]siPSMA14 zeigt 90min p.i. ohne forcierte Diurese eine hohe Untersucherübereinstimmung in Primär- und Re-Staging von Prostatakarzinom Patienten. Jahrestagung der Deutschen Gesellschaft für Nuklearmedizin, April 14 – 17, 2021, Virtual. *Nuklearmedizin* **2021**, *60* (2), 20.

[3] Miksch J., Prasad V., Di Carlo D., Zengerling F., Bolenz C., Solbach C., Beer M., Wiegel T., Wester H.-J., Beer A. J., [F-18]siPSMA-14 PET/CT Acquired at 90 Minutes p.i. Without Forced Diuresis Provides Optimal Contrast for Staging and Restaging of Prostate Cancer Patients. Annual Meeting of the Radiological Society of North America, November 29 – December 5, 2020, Virtual. *Unpublished.*

[4] Miksch J., Prasad V., Di Carlo D., Zengerling F., Bolenz C., Solbach C., Beer M., Wiegel T., Wester H.-J., Beer A. J., Diagnostic performance of the novel PSMA-specific PET radiotracer [F-18]siPSMA-14 in staging and restaging of prostate cancer. Annual Congress of the European Association of Nuclear Medicine, October 22 – 30, 2020, Virtual. *Eur J Nucl Med Mol Imaging* **2020**, *47* (Suppl 1), 460-461.

[5] Miksch J., Prasad V., Di Carlo D., Zengerling F., Bolenz C., Solbach C., Beer M., Wiegel T., Wester H.-J., Beer A. J., Novel [F18]siPSMA14 biodistribution at 60, 90 and 120 min p.i. showing most favourable kinetics at 90 min p.i. for staging and restaging of prostate cancer patients. Annual Congress of the European Association of Nuclear Medicine, October 22 – 30, 2020, Virtual. *Eur J Nucl Med Mol Imaging* **2020**, *47* (Suppl 1), 456.

[6] Prasad V., Di Carlo D., Miksch J., Fischer G., Zengerling F., Solbach C., Wester H.-J., Beer A. J., Novel F-18-siPSMA-14 shows favourable tracer kinetics for staging and restaging of prostate cancer patients. Annual Congress of the European Association of Nuclear Medicine, October 12 – 16, 2019, Barcelona, Spain. *Eur J Nucl Med Mol Imaging* **2019**, *46* (Suppl 1), 592-593.

[7] Di Carlo D., Prasad V., Beer A. J., Wester H.-J., 18F-siPSMAs: A Novel Class of Radiofluorinated PSMA Inhibitors. Annual Congress of the European Association of Nuclear Medicine, October 12 – 16, 2019, Barcelona, Spain. *Eur J Nucl Med Mol Imaging* **2019**, *46* (Suppl 1), 16.

[8] Wurzer A., Di Carlo D., Schmidt A., Beck R., Eiber M., Schwaiger M., Wester H.-J., PSMA-targeted 18F-labeled Radiohybrid Inhibitors: Concept, preclinical evaluation and first proof of concept study in men. Annual Meeting of the Society of Nuclear Medicine and Molecular Imaging, June 22 – 25, 2019, Anaheim, California, United States. *J Nucl Med* **2019**, *60* (Suppl 1), 344.

[9] Wurzer A., Di Carlo D., Schmidt A., Beck R., Schwaiger M., Herz M., Eiber M., Wester H.-J., PSMA-targeted 18F-labeled Radiohybrid Inhibitors: Labeling chemistry and automated GMP production of 18F-rhPSMA-7. Annual Meeting of the Society of Nuclear Medicine and Molecular Imaging, June 22 – 25, 2019, Anaheim, California, United States. *J Nucl Med* **2019**, *60* (Suppl 1), 342.

6.3.3 Patents

[1] Di Carlo D., Wester H.-J., Method for the preparation of a composition comprising dissolved [18F]fluoride and composition obtainable by the method. Patent WO2023/088671A1, **2023**.

[2] Di Carlo D., Wester H.-J., Silicon-fluoride acceptor substituted radiopharmaceuticals and precursors thereof. Patent WO2020/157128A1, **2020**.

6.4 Spectral Data of prepared Building Blocks

((4-Bromobenzyl)oxy)(*tert*-butyl)dimethylsilane (**I**)

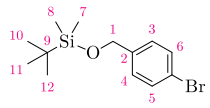

I

Chemical Formula: $C_{13}H_{21}BrOSi$
Molecular Weight: 301.30 g/mol

^{1}H-NMR (300.13 MHz, $CDCl_3$): δ [ppm] = 0.11 (s, 6 H, C7-H_3, C8-H_3), 0.96 (s, 9 H, C10-H_3, C11-H_3, C12-H_3), 4.77 (s, 2 H, C1-H_2), 7.34 (d, J = 7.9 Hz, 2 H, C3-H, C4-H), 7.57 (d, J = 8.0 Hz, 2 H, C5-H, C6-H).

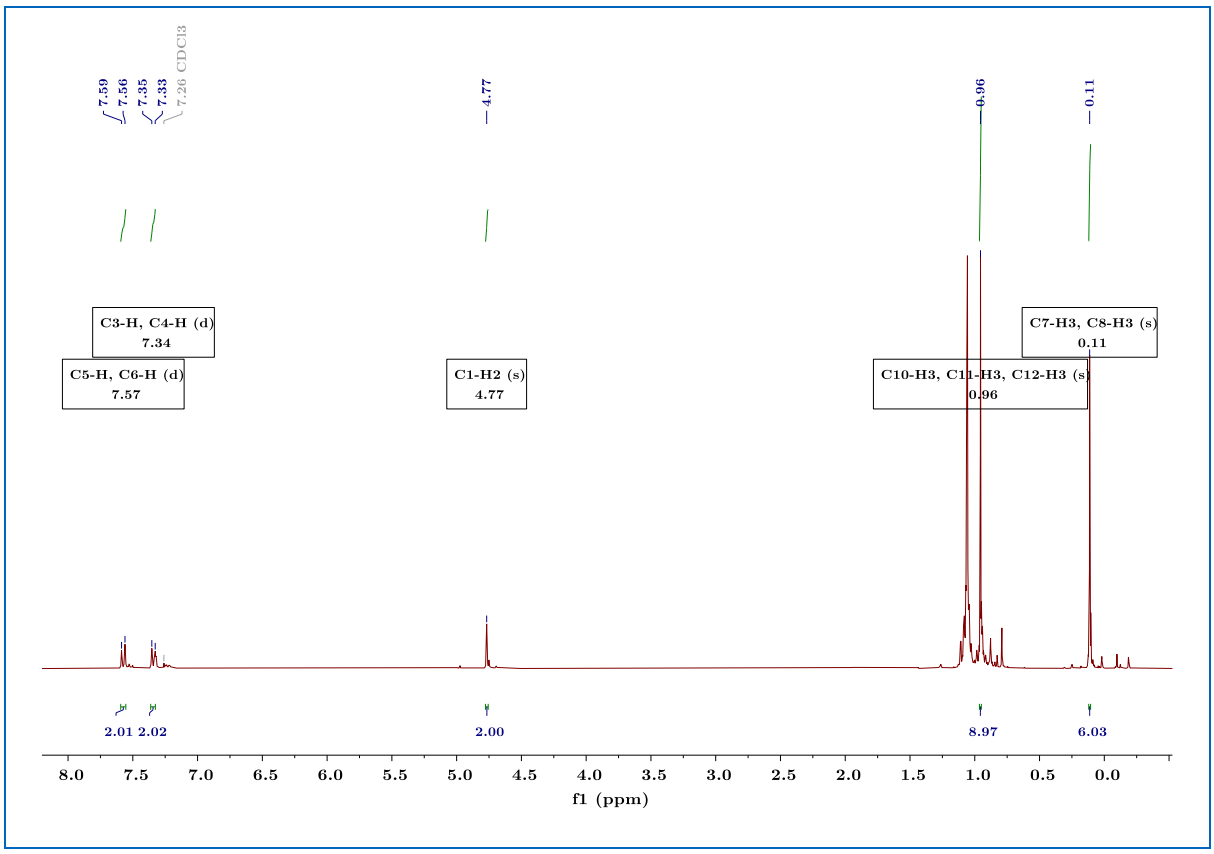

(4-(Di-*tert*-butylfluorosilyl)phenyl)methanol (**III**)

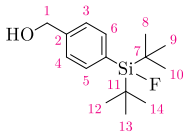

III

Chemical Formula: $C_{15}H_{25}FOSi$
Molecular Weight: 268.45 g/mol

^{1}H-NMR (300.13 MHz, $CDCl_3$): δ [ppm] = 1.06 (s, 18 H, C8-H_3, C9-H_3, C10-H_3, C12-H_3, C13-H_3, C14-H_3), 4.71 (s, 2 H, C1-H_2), 7.38 (d, 2 H, J = 7.8 Hz, C5-H, C6-H), 7.61 (d, 2 H, J = 8.0 Hz, C3-H, C4-H).

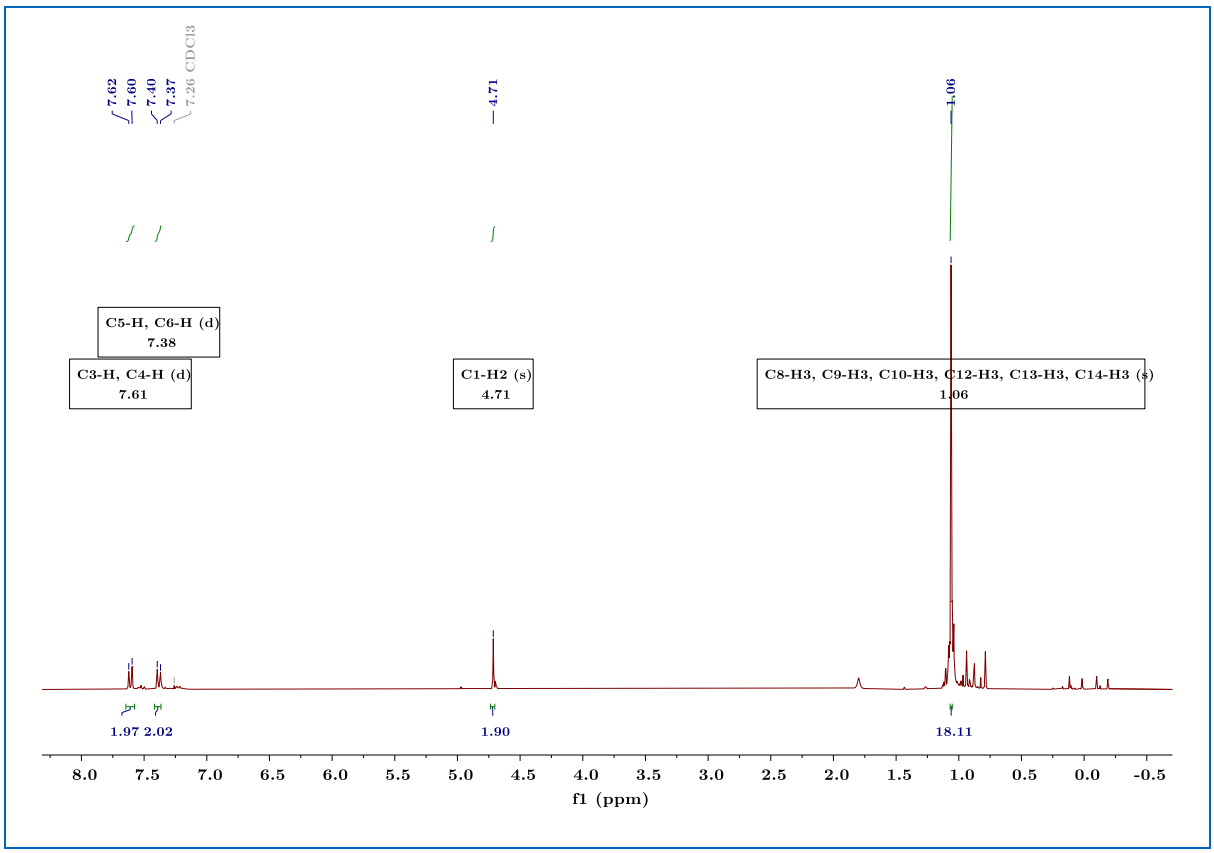

(4-(Bromomethyl)phenyl)di-*tert*-butylfluorosilane (SiFA-BnBr, **IV**)

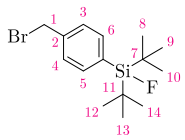

IV

Chemical Formula: $C_{15}H_{24}BrFSi$
Molecular Weight: 331.34 g/mol

^{1}H-NMR (300.13 MHz, $CDCl_3$): δ [ppm] = 1.00 (s, 18 H, C8-H_3, C9-H_3, C10-H_3, C12-H_3, C13-H_3, C14-H_3), 4.71 (s, 2 H, C1-H_2), 7.28 (d, J = 7.8 Hz, 2 H, C5-H, C6-H), 7.51 (d, J = 8.0 Hz, 2 H, C3-H, C4-H).

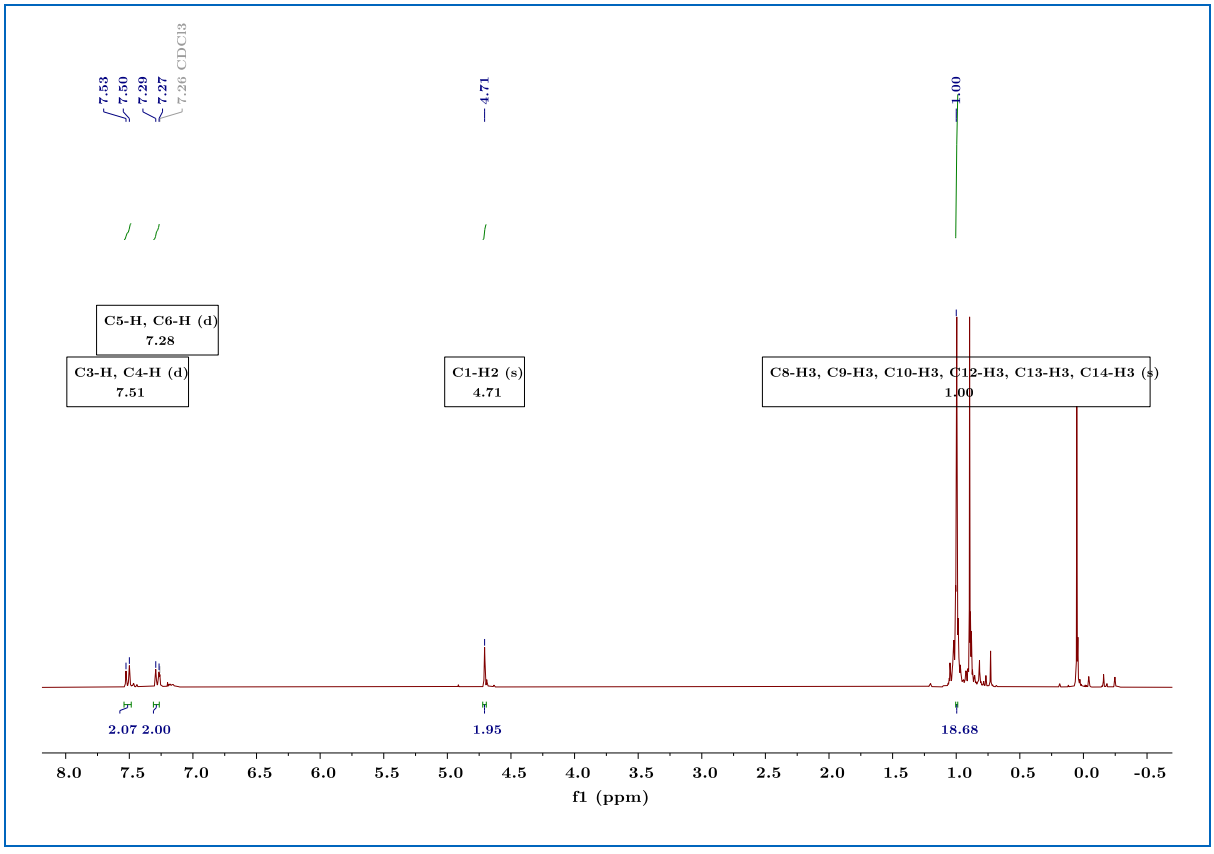

4-(Di-*tert*-butylfluorosilyl)benzoic acid (SiFA-BzA, **V**)

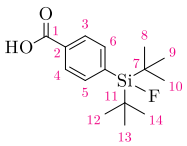

V

Chemical Formula: $C_{15}H_{23}FO_2Si$
Molecular Weight: 282.43 g/mol

^{1}H-NMR (500.13 MHz, $CDCl_3$): δ [ppm] = 1.07 (s, 18 H, C8-H_3, C9-H_3, C10-H_3, C12-H_3, C13-H_3, C14-H_3), 7.74 (d, J = 8.2 Hz, 2 H, C5-H, C6-H), 8.10 (d, J = 8.2 Hz, 2 H, C3-H, C4-H).